frontiers | Research Topics

Recent advances on renoprotection and kidney regeneration

Edited by
Vladimir T. Todorov, Ignacio Gimenez and Christian Hugo

Published in
Frontiers in Physiology

ISSN 1664-8714
ISBN 978-2-8325-2399-5
DOI 10.3389/978-2-8325-2399-5

About Frontiers

Frontiers is more than just an open access publisher of scholarly articles: it is a pioneering approach to the world of academia, radically improving the way scholarly research is managed. The grand vision of Frontiers is a world where all people have an equal opportunity to seek, share and generate knowledge. Frontiers provides immediate and permanent online open access to all its publications, but this alone is not enough to realize our grand goals.

Frontiers journal series

The Frontiers journal series is a multi-tier and interdisciplinary set of open-access, online journals, promising a paradigm shift from the current review, selection and dissemination processes in academic publishing. All Frontiers journals are driven by researchers for researchers; therefore, they constitute a service to the scholarly community. At the same time, the *Frontiers journal series* operates on a revolutionary invention, the tiered publishing system, initially addressing specific communities of scholars, and gradually climbing up to broader public understanding, thus serving the interests of the lay society, too.

Dedication to quality

Each Frontiers article is a landmark of the highest quality, thanks to genuinely collaborative interactions between authors and review editors, who include some of the world's best academicians. Research must be certified by peers before entering a stream of knowledge that may eventually reach the public - and shape society; therefore, Frontiers only applies the most rigorous and unbiased reviews. Frontiers revolutionizes research publishing by freely delivering the most outstanding research, evaluated with no bias from both the academic and social point of view. By applying the most advanced information technologies, Frontiers is catapulting scholarly publishing into a new generation.

What are Frontiers Research Topics?

Frontiers Research Topics are very popular trademarks of the *Frontiers journals series*: they are collections of at least ten articles, all centered on a particular subject. With their unique mix of varied contributions from Original Research to Review Articles, Frontiers Research Topics unify the most influential researchers, the latest key findings and historical advances in a hot research area.

Find out more on how to host your own Frontiers Research Topic or contribute to one as an author by contacting the Frontiers editorial office: frontiersin.org/about/contact

Recent advances on renoprotection and kidney regeneration

Topic editors

Vladimir T. Todorov — Technical University Dresden, Germany
Ignacio Gimenez — University of Zaragoza, Spain
Christian Hugo — University Hospital Carl Gustav Carus, Germany

Citation

Todorov, V. T., Gimenez, I., Hugo, C., eds. (2023). *Recent advances on renoprotection and kidney regeneration*. Lausanne: Frontiers Media SA. doi: 10.3389/978-2-8325-2399-5

Table of contents

frontiers | Frontiers in Physiology

TYPE Editorial
PUBLISHED 27 April 2023
DOI 10.3389/fphys.2023.1204789

OPEN ACCESS

EDITED BY
Carolyn Mary Ecelbarger,
Georgetown University, United States

REVIEWED BY
Peter R. Corridon,
Khalifa University, United Arab Emirates

*CORRESPONDENCE
Vladimir T. Todorov,
vladimir.todorov@ukdd.de

RECEIVED 12 April 2023
ACCEPTED 18 April 2023
PUBLISHED 27 April 2023

CITATION
Gimenez I, Hugo C and Todorov VT (2023), Editorial: Recent advances on renoprotection and kidney regeneration. *Front. Physiol.* 14:1204789. doi: 10.3389/fphys.2023.1204789

Editorial: Recent advances on renoprotection and kidney regeneration

Ignacio Gimenez[1,2,3], Christian Hugo[4] and Vladimir T. Todorov[4,5]*

[1]Renal and Cardiovascular Physiopathology (FISIOPREN), Aragon's Health Sciences Institute, Zaragoza, Spain, [2]Institute for Health Research Aragon (IIS Aragon), Zaragoza, Spain, [3]School of Medicine, University of Zaragoza, Zaragoza, Spain, [4]Experimental Nephrology, Division of Nephrology, Department of Internal Medicine III, University Hospital and Medical Faculty Carl Gustav Carus, Technische Universität Dresden, Dresden, Germany, [5]Institute of Physiology, Medical Faculty Carl Gustav Carus, Technische Universität Dresden, Dresden, Germany

KEYWORDS

kidney damage, renal regeneration, kidney imaging, diagnostic markers, organ perfusion, ex vivo models

Editorial on the Research Topic
Recent advances on renoprotection and kidney regeneration

Although several modes of renal replacement therapy have been co-existing for decades, end-stage renal disease (ESRD) represents a huge global healthcare burden. ESRD prevalence increased by over 40% between 2003 and 2016 (Thurlow et al., 2021). Pandemic diseases such as hypertension, obesity, and diabetes where ESRD is a frequent co-morbidity essentially contribute to this increase. Therefore, the demand for a better understanding of the underlying mechanisms of kidney damage and regeneration, for improving the current therapies as well as for the development of novel organoprotective and regenerative strategies in nephrology is bigger than ever.

The *Frontiers in Physiology* Research Topic collection "*Recent advances on renoprotection and kidney regeneration*" provides insight into several aspects of acute kidney damage and into the role of fibroblast growth factor 21 in chronic kidney disease. It also reports intriguing new findings on the function of the renin cells as a progenitor cell niche, on the therapeutic modulation of glomerular hemodynamics in the diabetic kidney, and on a kidney machine perfusion-based renoprotective drug discovery platform. Last but not least, an in-depth review focuses on the use of materials mimicking renal extracellular matrix in new kidney models.

Acute kidney injury (AKI) is a common disease that associates not only with high short-term mortality but also with long-term adverse outcomes including chronic kidney disease (CKD) and cardiovascular complications (Lameire et al., 2008; Mehta et al., 2015; Teo and Endre, 2017). AKI is also particularly interesting with regard to regeneration because it could be completely reversed by modern therapy (Legendre et al., 2013) thus underscoring the high regenerative capacity of the kidney. Yet renal functional and structural integrity could not always be restored after AKI, resulting in loss of kidney function and CKD. Therefore ongoing efforts focus on better understanding the molecular mechanisms of AKI and the development of novel regenerative and protective therapeutic approaches.

In this Research Topic collection, Buse et al. provide an overview of whole-cell sequencing findings in AKI. Particularly single-cell transcriptome sequencing represents a powerful new tool for studying in detail the global organ expression landscape. It is also a

technique with immense diagnostic potential that heralds new therapeutic strategies for AKI and AKI to CKD transition. This technology will help to clarify the fundamental question regarding the pre-existence of an intratubular progenitor cell population such as the "scattered" tubular cells (Lindgren et al., 2011) being required for tubular cell repair or whether all surviving cells are able to acquire regenerative potential via dedifferentiation. Results from the studies being discussed in this mini-review suggest the latter mechanism. Single-cell sequencing experiments also provide additional insights into the sex-specific differences of AKI after ischemia-reperfusion, a phenomenon that has been consistently demonstrated clinically in many animal models.

The diagnosis of AKI relies currently on measuring serum creatinine and urine production. However, these functional parameters only indirectly reflect the underlying tissue damage (and regeneration) in AKI. Zou et al. tackle this issue by reviewing novel subclinical biomarkers of AKI. The authors address the problem of AKI as a hospitalization complication, which is usually associated with renal tubule injury. They focus on the issue of subclinical AKI, characterized by structural renal damage in the absence or minor changes in functional markers: serum creatinine, glomerular filtration rate, and urinary output. This review provides a critical assessment of a comprehensive list of markers of renal tissue damage. The development of renal tubule injury markers aims to remedy the lack of specificity, sensitivity, and timeliness of functional markers for the diagnosis of structural damage in AKI. The review summarizes the molecular nature, physiology, analytics, preclinical studies, and clinical performance as subclinical AKI markers for cystatin C, NGAL, KIM-1, IL-18, LFBAP, and TIMP2/IGFBP7. Two recent candidates, clusterin and PenKid are reviewed in more detail. Performance appears to be conditioned to the clinical setting and the major limitation for most biomarkers is the lack of specificity. Thus, the value of measuring AKI biomarkers still resides in their integration with clinical assessment.

Corridon addresses the therapeutic potential of transient overexpression of the mitochondrial enzyme isocitrate dehydrogenase 2 (IDH2) in a rodent AKI model using plasmid-based hydrodynamic gene delivery. IDH2 is the primary enzyme maintaining the mitochondrial antioxidant system, which is markedly altered in tubular epithelial cells after AKI and may be responsible for successful ischemic pre-conditioning. In these experiments, the author demonstrates successful renal gene delivery as well as upregulated expression of IDH2 after early hydrodynamic gene transfer. Being executed 1 h after AKI induction, IDH2 gene transfer ameliorated AKI-mediated increases in serum creatinine and urea nitrogen levels, while urine output increased as well as the mitochondrial membrane potential. Apparently, still many hurdles have to be overcome to provide a successful transition of these experimental results to the clinic.

Using an acute glomerulonephritis model Labes et al. study the role of inflammation because it is thought to be crucial for the transition from acute injury to CKD. This group studies the renoprotection conferred by Annexin A1, a glucocorticoid inducible protein. They employ an animal model of Annexin A1 deficiency to show its role as a mediator of the resolution phase of rapidly progressive crescent glomerulonephritis. Deficiency of Annexin A1 led to an aggravated course of the disease with a phenotype of severe non-resolving inflammation and accelerated fibrosis. Annexin A1-deficient mice exposed to the nephrotoxic serum model exhibited a larger number of damaged glomeruli, increased abundance of inflammatory cells (neutrophils, macrophages, and leukocytes), and alteration of renal lipid levels towards a pro-inflammatory profile. Transcriptome analysis revealed upregulation of pathways related to leukocyte activation and cytokine production and secretion in Annexin A1 deficient mice at day 10 after induction of nephritis. Finally, augmented expression of fibrotic markers was demonstrated by qPCR and tissue staining for collagen. These results are in good agreement with previous observations on the anti-inflammatory and anti-fibrotic roles of Annexin A1 in the kidney. The upregulation of Annexin A1 or its downstream effectors may represent a new target for renoprotective strategies.

Zhou et al. summarize the accumulating evidence for the role of Fibroblast Growth Factor 21 (FGF21) in CKD. FGF21 serum levels increase in CKD. Importantly these could be used as a predictor for declining kidney function. Particularly in diabetic nephropathy, FGF21 appears to be a very precise prognostic marker. FGF21 is produced by the liver and is upregulated in states of cellular energy deficit. In the diabetic kidney FGF21 appears to work protectively by improving lipid metabolism and alleviating oxidative stress, thus essentially limiting renal injury and fibrosis. It is still to be discovered why FGF21 increases in the non-diabetic forms of CKD. Another interesting aspect to be addressed by future studies is why if FGF21 works protectively in CKD it is not sufficient to halt disease progression. With this regard, there are already promising findings showing that therapy with FGF21 analogs exerts beneficial metabolic effects (for more detail see review references).

The juxtaglomerular renin-producing cells in the afferent arterioles (termed hereafter renin cells) have been known for a long time as the primary source of renin in circulation. Renin is the central regulatory factor within the plasma renin-angiotensin-system, which plays a fundamental role in the control of arterial blood pressure. However, in the last several years these cells were reproducibly found to have also progenitor and protective functions in the kidney (Pippin et al., 2013; Starke et al., 2015; Lachmann et al., 2017; Steglich et al., 2020). Arndt et al. expanded the knowledge on the progenitor role of the renin cells by demonstrating that there is a seningle-nephron feedback system, which drives the movement of the renin cells into the glomerulus where they change their phenotype to replace damaged glomerular cells. The authors used longitudinal intravital microscopy and 3D image reconstruction to quantify the injury-directed renin cell migration in laser-irradiated glomeruli of mouse kidneys. Interestingly the directed migration of renin cells starts almost 3 days after the initial glomerular damage. At the same time, the intraglomerular renin cell descendants remain in spatial contact with the juxtaglomerular renin cell niche. While providing extensive quantification of the migration process for the first time, the authors only speculate about the signal mediating the feedback between glomerulus and extraglomerular renin cells. Thus, the

exact nature of the signal(s) driving the renin cell migration and differentiation after glomerular injury remains to be resolved.

The intravital imaging technique was used by the same group to study the therapeutic effects of renoprotective drugs on glomerular hemodynamics in a mouse model of diabetic kidney disease. Diabetes mellitus is the primary cause of irreversible loss of kidney function and renal replacement therapy (Tziomalos and Athyros, 2015; Alicic et al., 2017). Glomerular hyperfiltration is a major pathophysiological factor, particularly in the early phase of diabetic kidney disease. Counteracting the increase of glomerular filtration rate (GFR) is a standard renoprotective therapy in diabetic patients. Kroeger et al. studied the effects of angiotensin-converting enzyme (ACE) inhibitor enalapril or/and sodium glucose cotransporter 2 (SGLT2) inhibitor empagliflozin on single nephron GFR (snGFR) in diabetic mice using intravital imaging. Treatment with enalapril, empagliflozin, or a combination of both decreased snGFR. While the effect on snGFR was uniform, the different treatment modes induced distinct changes in the resistance of the corresponding afferent and efferent arterioles, which consistently resulted in decreased filtration. These findings demonstrated that the complexity of the pathophysiologic mechanisms causing glomerular hyperfiltration in diabetic patients offers also multiple options for beneficial modulation by renoprotective treatment regimens.

Allogeneic kidney transplantation is considered the most advanced present-day renal replacement therapy. A major limitation therein is the low number of donors available compared to the number of patients with ESRD. Therefore, transplant tissue care is decisive for increasing the number of transplantable kidneys. A modern approach in preserving transplant integrity is normothermic machine perfusion (NMP). Although still limitedly tested with human kidneys, NMP is expected to alleviate tissue ischemia and allow organ preconditioning. In this Research Topic collection, Hofmann et al. describe an *ex vivo* kidney slice perfusion as a further development of a rodent NMP technique previously reported by the same group (Czogalla et al., 2021). The novel perfusion method is based on a 3D-printed kidney slice incubator (KSI) with slots for up to nine kidney mouse slices. With this device, a high-throughput pipeline for drug testing was established. Since the testing conditions are very similar to the whole organ perfusion, coupling KSI to NMP would dramatically accelerate the preclinical studies on potential applications of NMP in human kidney allotransplantations. In support of this exciting perspective, the authors report the identification of β-nicotinamide-adenine-dinucleotide as an agent reducing endoplasmic reticulum stress in perfused kidneys through their rodent KSI-NMP pipeline.

Preclinical animal models fail to reproduce all the characteristics of AKI and CKD in humans. This is particularly evident and relevant in the field of nephrotoxicity. However, there is not a good alternative because traditional *in vitro* models based on the bi-dimensional culture of renal cells lack many of the biochemical and biomechanical stimuli present *in vivo*. Lacueva-Aparicio et al. summarize different strategies for improving *in vitro* models, based on the incorporation of biochemical and biomechanical properties of extracellular matrix (ECM) surrogates. Their thorough but concise review covers 2D, 2.5D, and 3D architecture models and discusses how biological and synthetic ECM influence renal phenotype and response to damage. Recent advances in the fields of organoids, decellularized ECM, bioprinting, and microfluidics are presented, to stress the need of incorporating complex architectures and biochemical ECM stimuli. The combination of these techniques will result in complex models close enough to *in vivo* kidney function and disease to allow for the substitution of animal preclinical models, facilitating the evaluation of nephroprotection, kidney damage, and regeneration.

In conclusion, the papers in this Research Topic collection not only summarize modern aspects of renoprotection but also report original findings on the regenerative capacity of the kidney and inspiring therapeutic approaches with strategic potential.

Author contributions

IG - contributed to the work, revised and approved the manuscript; CH - contributed to the work, revised and approved the manuscript; VT - drafted the work, revised and approved the manuscript.

Funding

The research of the authors is funded by the Government of Spain, fund number RTI 2018-0099946-B-100 (to IG) and Deutsche Forschungsgemeinschaft, grant numbers 310297900, 399229660, 426572058 (to CH); 399229660, 470138795 (to VT).

Conflict of interest

The authors declare that the research was conducted in the absence of any commercial or financial relationships that could be construed as a potential conflict of interest.

Publisher's note

References

Alicic, R. Z., Rooney, M. T., and Tuttle, K. R. (2017). Diabetic kidney disease: Challenges, progress, and possibilities. *Clin. J. Am. Soc. Nephrol.* 12 (12), 2032–2045. doi:10.2215/CJN.11491116

Czogalla, J., Grahammer, F., Puelles, V. G., and Huber, T. B. (2021). A protocol for rat kidney normothermic machine perfusion and subsequent transplantation. *Artif. Organs.* 45 (2), 168–174. doi:10.1111/aor.13799

Lachmann, P., Hickmann, L., Steglich, A., Al-Mekhlafi, M., Gerlach, M., Jetschin, N., et al. (2017). Interference with gsα-coupled receptor signaling in renin-producing cells leads to renal endothelial damage. *J. Am. Soc. Nephrol.* 28 (12), 3479–3489. doi:10.1681/ASN.2017020173

Lameire, N., Biesen, W. V., and Vanholder, R. (2008). Acute kidney injury. *Lancet* 372 (9653), 1863–1865. doi:10.1016/S0140-6736(08)61794-8

Legendre, C. M., Licht, C., Muus, P., Greenbaum, L. A., Babu, S., Bedrosian, C., et al. (2013). Terminal complement inhibitor eculizumab in atypical hemolytic-uremic syndrome. *N. Engl. J. Med.* 368 (23), 2169–2181. doi:10.1056/NEJMoa1208981

Lindgren, D., Boström, A. K., Nilsson, K., Hansson, J., Sjölund, J., Möller, C., et al. (2011). Isolation and characterization of progenitor-like cells from human renal proximal tubules. *Am. J. Pathol.* 178 (2), 828–837. doi:10.1016/j.ajpath.2010.10.026

Mehta, R. L., Cerdá, J., Burdmann, E. A., Tonelli, M., García-García, G., Jha, V., et al. (2015). International society of nephrology's 0by25 initiative for acute kidney injury (zero preventable deaths by 2025): A human rights case for nephrology. *Lancet* 385 (9987), 2616–2643. doi:10.1016/S0140-6736(15)60126-X

Pippin, J. W., Sparks, M. A., Glenn, S. T., Buitrago, S., Coffman, T. M., Duffield, J. S., et al. (2013). Cells of renin lineage are progenitors of podocytes and parietal epithelial cells in experimental glomerular disease. *Am. J. Pathol.* 183 (2), 542–557. doi:10.1016/j.ajpath.2013.04.024

Starke, C., Betz, H., Hickmann, L., Lachmann, P., Neubauer, B., Kopp, J. B., et al. (2015). Renin lineage cells repopulate the glomerular mesangium after injury. *J. Am. Soc. Nephrol.* 26 (1), 48–54. doi:10.1681/ASN.2014030265

Steglich, A., Hickmann, L., Linkermann, A., Bornstein, S., Hugo, C., and Todorov, V. T. (2020). Beyond the paradigm: Novel functions of renin-producing cells. *Rev. Physiol. Biochem. Pharmacol.* 177, 53–81. doi:10.1007/112_2020_27

Teo, S. H., and Endre, Z. H. (2017). Biomarkers in acute kidney injury (AKI). *Best. Pract. Res. Clin. Anaesthesiol.* 31 (3), 331–344. doi:10.1016/j.bpa.2017.10.003

Thurlow, J. S., Joshi, M., Yan, G., Norris, K. C., Agodoa, L. Y., Yuan, C. M., et al. (2021). Global epidemiology of end-stage kidney disease and disparities in kidney replacement therapy. *Am. J. Nephrol.* 52 (2), 98–107. doi:10.1159/000514550

Tziomalos, K., and Athyros, V. G. (2015). Diabetic nephropathy: New risk factors and improvements in diagnosis. *Rev. Diabet. Stud.* 12 (1-2), 110–118. doi:10.1900/RDS.2015.12.110

frontiers in Physiology

MINI REVIEW
published: 05 October 2021
doi: 10.3389/fphys.2021.764503

Regulation and Potential Biological Role of Fibroblast Growth Factor 21 in Chronic Kidney Disease

Xue Zhou[1], *Yuefeng Zhang*[1] *and Ning Wang*[2]*

[1] Department of Nephrology, Tianjin Haihe Hospital, Tianjin, China, [2] Tianjin Third Central Hospital, Tianjin, China

Chronic kidney disease (CKD) is an incurable progressive disease with the progressive impairment of kidney function, which can accelerate the progression of cardiovascular disease, increase the risk of infection, and lead to related complications such as anemia and bone disease. CKD is to a great extent preventable and treatable, and it is particularly important to improve the early diagnosis, strengthen the research underlying the mechanism of disease occurrence and development, and innovate new intervention measures. Fibroblast growth factor 21 (FGF21) belongs to one of members of endocrine FGF subfamily with evolutionarily conserved functions and performs a vital role in the regulation of energy balance and adipose metabolism. FGF21 needs to rely on β-Klotho protein to specifically bind to FGF receptor (FGFR), which activates the FGF21 signaling exerting the biological function. FGF21 is deemed as an important regulatory factor extensively modulating many cellular functions under physiologic and pathologic conditions. Although the metabolic effect of FGF21 has been extensively studied, its potential biological role in the kidney has not been generally investigated. In this review, we summarize the biological characteristics, regulation and biological function of FGF21 based on the current studies, and briefly discuss the potential relationship with chronic kidney disease.

Keywords: fibroblast growth factor 21, biomarker, chronic kidney disease, diabetic nephropathy, cardiovascular disease

OPEN ACCESS

Edited by:
Belisario Enrique Fernandez, University Institute of Health Sciences, Argentina

Reviewed by:
Carolina Susana Cerrudo, Universidad Nacional de Quilmes (UNQ), Argentina
Ana Maria Balaszczuk, University of Buenos Aires, Argentina
Elsa Zotta, University of Buenos Aires, Argentina

***Correspondence:**
Ning Wang
wn20121004@126.com

Specialty section:
This article was submitted to Renal and Epithelial Physiology, a section of the journal Frontiers in Physiology

Received: *26 August 2021*
Accepted: *15 September 2021*
Published: *05 October 2021*

Citation:
Zhou X, Zhang Y and Wang N (2021) Regulation and Potential Biological Role of Fibroblast Growth Factor 21 in Chronic Kidney Disease. Front. Physiol. 12:764503. doi: 10.3389/fphys.2021.764503

INTRODUCTION

Chronic kidney disease (CKD) is a progressive disease characterized by high morbidity and mortality, which is characterized by the changes in the structure and function of the kidney owing to various reasons (Kalantar-Zadeh et al., 2021). With the high and still increasing global burden of CKD, approximately 10% of adults are affected by CKD (GBD Chronic Kidney Disease Collaboration, 2020). Overall speaking, the incidence of CKD increases with age, especially in patients with obesity, diabetes and hypertension (Silverwood et al., 2013;

Abbreviations: CAG, coronary angiography; CIN, contrast-induced nephropathy; CKD, chronic kidney disease; eGFR, estimated glomerular filtration rate; ESRD, end-stage renal disease; FGF21, fibroblast growth factor 21; FGFR, fibroblast growth factor receptor; GLP-1, glucagon-like peptide-1; NAFLD, non-alcoholic fatty liver disease; NASH, non-alcoholic steatohepatitis; PPARα, peroxisome proliferator-activated receptor-α; ROS, reactive oxygen species; SGLT2, sodium glucose cotransporter 2; UGE, urinary glucose excretion.

Cockwell and Fisher, 2020). CKD can accelerate the progression of cardiovascular disease, increase the risk of infection, and lead to anemia and bone disease, as well as other complications that increase the risk of premature death. Since the progression of CKD usually takes several years and the symptoms remain not obvious, early detection of the disease is particularly important. Non-drug strategies such as diet and lifestyle adjustments, and specific drug interventions can be adopted to improve the clinical outcomes of the patients with CKD.

In the past few decades, some new biomarkers have been discovered, which contributes to recognizing renal function impairment earlier. Fibroblast growth factor 21 (FGF21), one of the emerging biomarkers, has been associated with CKD (Kondo et al., 2020). Studies have verified that serum FGF21 levels in patients with CKD increase progressively and reach 20 times over the normal range (Hindricks et al., 2014). Moreover, in type 2 diabetes patients, the level of serum FGF21 is significantly linked to the occurrence of nephropathy, proteinuria, and the progression of end-stage renal disease (ESRD) (Jian et al., 2012; Lee et al., 2015). This article will review the biological characteristics, regulation and biological function of FGF21 in the onset and development of CKD, and finally evaluate the underlying role as a therapeutic target.

BIOLOGICAL CHARACTERISTICS OF FIBROBLAST GROWTH FACTOR 21

Molecular Structure of Fibroblast Growth Factor 21

As a member of the superfamily of fibroblast growth factors, FGF21 is composed of similar structure containing 150–300 amino acids (Itoh and Ornitz, 2011). FGF21, initially discovered in 2000, was most similar to FGF19 with approximately 35% similarity in the members of human FGFs (Nishimura et al., 2000). FGF21 precursor is composed of 209 amino acids encoded by 4 exons. Next, undergoing cleavage of a signal peptide, FGF21 precursor is converted into mature FGF21 containing 181 amino acids with molecular weight of approximately 20 kDa (Zhang et al., 2015).

Fibroblast Growth Factor 21 Related Receptors

Studies have found that FGF exerts biological functions by binding to FGF receptors (FGFRs) belonging to tyrosine kinase receptors. However, the endocrine FGF (FGF19, FGF21, and FGF23) has a low affinity with FGFRs, and requires the participation of specific transmembrane glycoproteins (α or β-klotho) in the target organs. Klotho protein is an important part of the endocrine FGF receptor complex and is indispensable to the high-affinity binding between FGF and FGFR (Fernandes-Freitas and Owen, 2015; Kuro-O, 2019b). In recent years, a growing body of researches have revealed that the FGF-Klotho complex also participates in the pathophysiology of some diseases, involving CKD, diabetes, arteriosclerosis and cancer (Kuro-o, 2012). Consequently, through the thorough research on the FGF-Klotho-FGFR complex, the development of drugs targeting the FGF-Klotho endocrine axis may bring clinical benefits in multiple systems.

The specific binding between FGF21 and corresponding FGFR relies on β-Klotho protein (Ding et al., 2012). β-Klotho protein preferentially combines with FGFR for inhibiting paracrine FGFs signaling (Goetz et al., 2007), which helps endocrine FGFs to specifically bind to FGFRs in target cells avoiding the interference of paracrine FGFs. FGF signaling pathway with abundant structural information extensively modulates distinct biological process in development, tissue homeostasis and metabolism (Goetz and Mohammadi, 2013). In liver, FGF21 participates in regulating carbohydrate and fatty acid metabolism, including fatty acid oxidation and gluconeogenesis (Potthoff et al., 2009). In addition, FGF21 increases glucose uptake and lipolysis through converting white fat into brown fat for increasing energy metabolism (Emanuelli et al., 2014).

Regulation and Function of Fibroblast Growth Factor 21

FGF21, a hormone mainly produced in liver, is induced directly by peroxisome proliferator-activated receptor-α (PPARα) (Inagaki et al., 2007). In the fasting or starvation state, PPAR mediates the increase in the expression of FGF21 in the liver, leading to gluconeogenesis, fatty acid oxidation and ketone body production as an adaptive response to hunger (Woo et al., 2013). PPARα agonists, such as bezafibrate and a novel drug MHY2013, can significantly increase the expression of FGF21 for alleviating obesity-induced insulin resistance, dyslipidemia and hepatic steatosis (An et al., 2017). The regulatory process of FGF21 expression can be exhibited utilizing a diagram (**Figure 1**).

Recently, the biological characteristics of FGF have been extensively studied. The endocrine FGFs play multifaceted roles in the treatment of many chronic diseases involving in kidney disease, cardiovascular disease, obesity, type 2 diabetes, and cancer (Degirolamo et al., 2016). The abnormal signal of FGF is significantly linked to the development of cancer and metabolic diseases. The function of FGF21 was originally discovered in 2005 when looking for new drugs for the treatment of diabetes. FGF21 metabolic axes extensively participates in regulating the metabolic homeostasis (Li, 2019). FGF21 can improve glucose uptake by fibroblasts and adipocytes showing the characteristics of effective treatment of diabetes (Kharitonenkov et al., 2005). At present, FGF21, deemed as a metabolism-related hormone, is an emerging therapeutic target for metabolic diseases (Angelin et al., 2012; Lancha et al., 2012; Reitman, 2013). Furthermore, FGF21 can improve tissue damage caused by the harmful effects of metabolic abnormalities, including oxidative, inflammatory, and immune stress state (Luo et al., 2017). Consequently, some targeting FGF21 analogs have been developed for the treatment of metabolic disorders (Zhang and Li, 2015).

The latest research evidence confirms that FGF21 can improve metabolic status with anti-fibrotic effects and has the potential treatment for non-alcoholic steatohepatitis (NASH) (Harrison et al., 2021). A new type of long-acting FGF21 (LAPS-FGF21) has been developed for potential therapeutic effects on obesity.

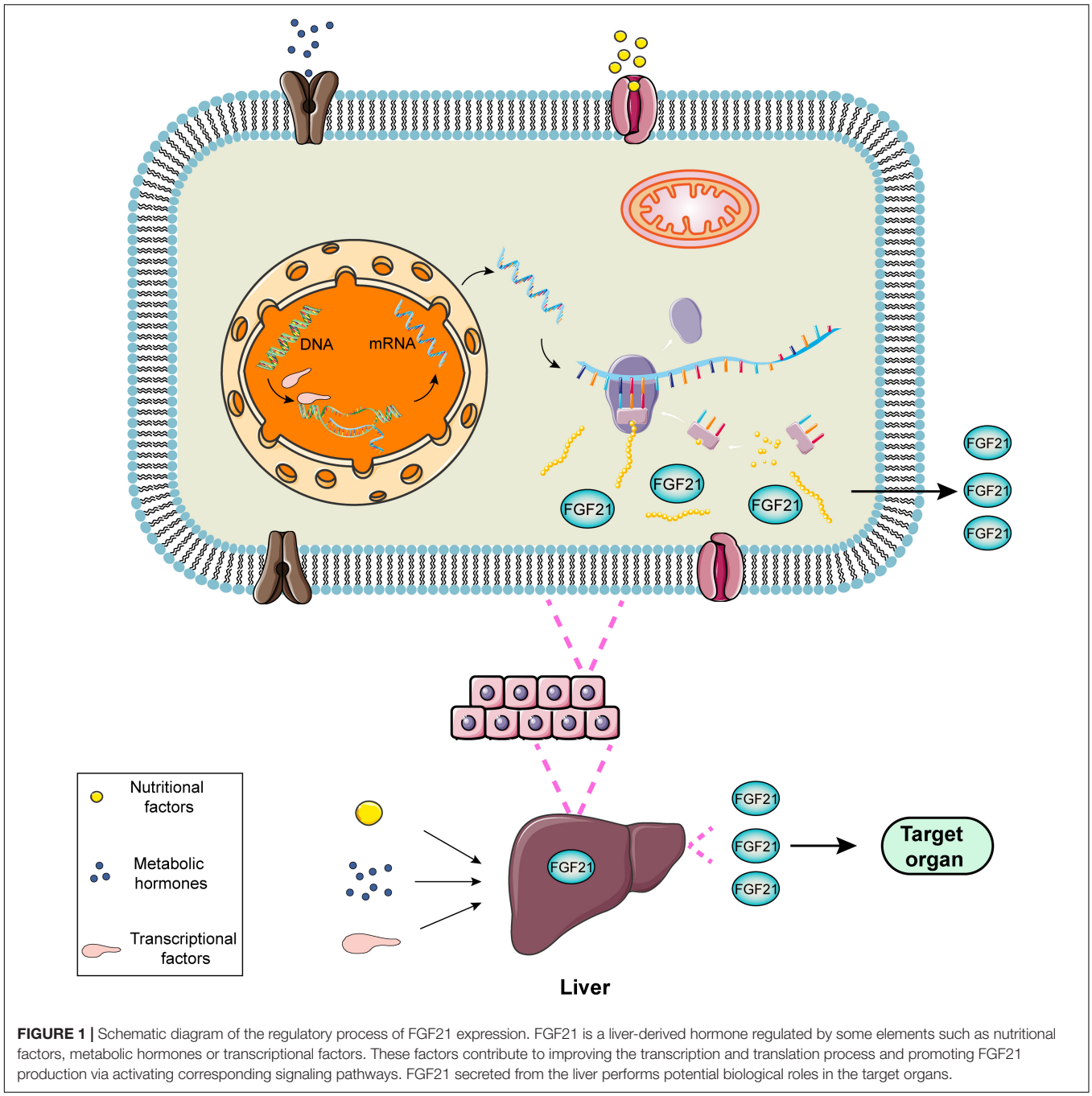

FIGURE 1 | Schematic diagram of the regulatory process of FGF21 expression. FGF21 is a liver-derived hormone regulated by some elements such as nutritional factors, metabolic hormones or transcriptional factors. These factors contribute to improving the transcription and translation process and promoting FGF21 production via activating corresponding signaling pathways. FGF21 secreted from the liver performs potential biological roles in the target organs.

LAPS-FGF21 is chemically coupled with human IgG4 Fc fragment for a longer half-life in the serum, which can effectively reduce body weight and improve glucose tolerance in a dose-dependent manner at the same time (Kim et al., 2021). FGF21 is highly expressed in the exocrine glands of the pancreas, the mechanism of which requires the FGFR-Klotho signaling transduction (Coate et al., 2017). Under physiological conditions, acute exercise can upregulate the expression level of FGF21 in skeletal muscle (Di Raimondo et al., 2016; Tanimura et al., 2016). At the same time, FGF21 has a higher level in patients with mitochondrial diseases affecting skeletal muscle, which can be used as a biomarker for mitochondrial respiratory chain defects in muscles (Suomalainen et al., 2011; Suomalainen, 2013; Nohara et al., 2019).

FGF21 is released by cardiomyocytes for avoiding hypertrophy, and also participates in regulating the expression of antioxidant pathway genes for reducing reactive oxygen species (ROS) mediated oxidative stress in cardiomyocytes, and acting as an antioxidant factor in the heart to control inflammation and cardiac hypertrophy (Planavila et al., 2013, 2015). Moreover, FGF21 can prevent atherosclerosis by regulating the interconnection among adipose tissue, liver and

blood vessels (Lin et al., 2015), and activating the angiotensin converting enzyme 2-angiotensin axis for preventing angiotensin II-induced hypertension and vascular damage (Pan et al., 2018). In addition, FGF21 can also play a therapeutic effect on atherosclerosis through the NF-κB pathway (Zhang et al., 2018). During cardiac remodeling in uremic cardiomyopathy, the effect of increased FGF21 expression on cardioprotective is needed to be further clarified (Suassuna et al., 2020). FGF21 partially ameliorates hyperglycemia by reducing renal glucose reabsorption based on the sodium glucose cotransporter 2 (SGLT2) pathway (Li et al., 2018b).

Since FGF21 is mainly excreted by the kidney (He et al., 2018), it can be predicted by the relative change of creatinine. The estimated glomerular filtration rate (eGFR) is a strong independent negative predictor of FGF21. Synergistic therapy of glucagon-like peptide-1 (GLP-1) and glucagon receptors can upregulate the expression of FGF21 and abate renal insufficiency induced by diabetes (Patel et al., 2018). Furthermore, one study has found that FGF21 has a protective effect on kidney against low protein diet-induced renal damage and inflammation (Fang et al., 2021). It has been reported that the level of circulating FGF21 is independently correlated with the occurrence of contrast-induced nephropathy (CIN) and corresponding kidney injury in patients receiving coronary angiography (CAG) (Wu et al., 2018).

FIBROBLAST GROWTH FACTOR 21 AND DIABETIC NEPHROPATHY

FGF21 is closely related to metabolic disorders including diabetes. In order to clarify the relationship between FGF21 and blood glucose, the results of a cohort study demonstrated that the level of FGF21 in the plasma of diabetic patients significantly increased, and was identified as an independent predictor of type 2 diabetes predicting the development of diabetes (Chen et al., 2011). A study has found that the high serum FGF21 level is correlated with low urinary glucose excretion (UGE) in type 2 diabetes patients (Zhang et al., 2021). Moreover, a meta-analysis found that FGF21 level in the plasma of type 2 diabetes patients significantly increased compared with the control group, which was affected by the variables of body mass index (BMI), total cholesterol and triglycerides (Wang et al., 2019). There is evidence existing to support that genetic variation in the FGF21 gene region is related to the renal function of type 2 diabetes patients and affects the eGFR of diabetic patients (Yu et al., 2019).

Studies have found that FGF21 levels can be used as a biomarker related to the prognosis of patients with diabetic nephropathy (El-Saeed and El-Mohasseb, 2017; Chang et al., 2021). Serum FGF21 levels are closely associated with early diabetic nephropathy in high-risk groups of type 2 diabetes patients, especially the circulating FGF21 value increasing more than 181 pg/mL, so that effectively targeting FGF21 therapy may contribute to early detection and prevention of diabetic microvessels complication (Esteghamati et al., 2017). A cross-sectional study also confirmed that elevated serum FGF21 level may be a useful biomarker for predicting the progression of kidney disease, especially in the early stage of diabetic nephropathy. Additionally, a recombinant human FGF21, PEGylated rhFGF21 (PEG-rhFGF21), has been developed for the treatment effect on diabetic nephropathy in diet induced obesity animal model (Zhao et al., 2017).

Insulin resistance is a pivotal process in the occurrence and development of diabetic nephropathy. Studies have found that alprostadil (prostaglandin E1) can reduce the insulin resistance via the autophagy-dependent FGF21 pathway for preventing the progression of diabetic nephropathy (Wei et al., 2018). FGF21 can negatively regulate TGF-β-p53-Smad2/3-mediated epithelial-to-mesenchymal transition by activating AKT for reducing diabetes-induced renal fibrosis (Lin et al., 2020). Based on the db/db mouse model research, targeting FGF21 treatment could function as a potential therapeutic strategy in type 2 diabetic nephropathy for significantly down-regulating FGF21 receptor components, activating ERK phosphorylation, reducing the excretion of urinary albumin and mesangial expansion, inhibiting the synthesis of pro-fibrotic molecules, and improving renal lipid metabolism and oxidative stress damage (Kim et al., 2013). FGF21 protects kidney from damage by alleviating renal lipid accumulation and inhibiting inflammation, and fibrosis effects in diabetic nephropathy (Zhang et al., 2013). Through upregulating the expression of FGF21 and activating Akt2/GSK-3β/Fyn/Nrf2 antioxidants and the AMPK pathway, fenofibrate can exert a role in preventing diabetic nephropathy in the patients with type 1 diabetes (Cheng et al., 2020). In addition, activation of FGF21 pathway may correlate with the effect of SGLT2 inhibitors on protecting the renal function in type 2 diabetes and delaying progression of CKD (Packer, 2020).

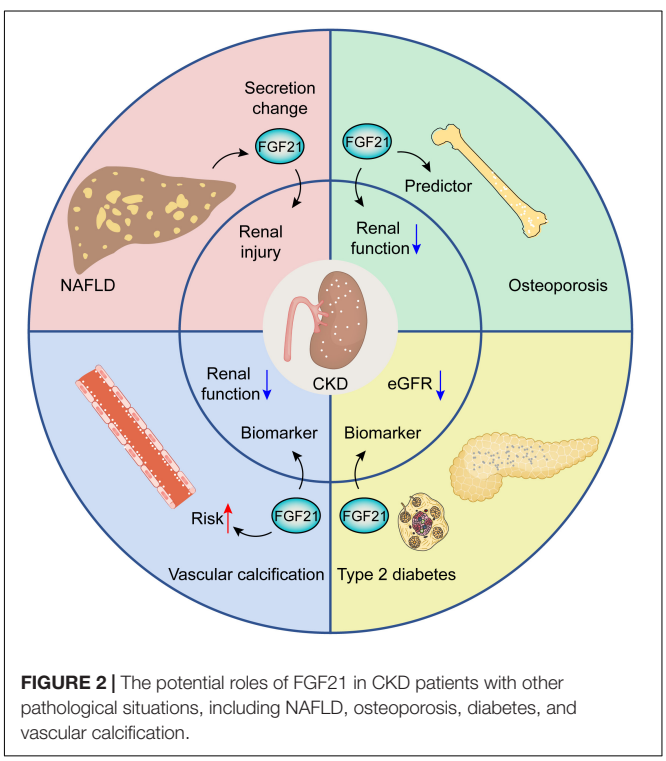

FIGURE 2 | The potential roles of FGF21 in CKD patients with other pathological situations, including NAFLD, osteoporosis, diabetes, and vascular calcification.

FIBROBLAST GROWTH FACTOR 21 AND CHRONIC KIDNEY DISEASE

In 2009, Stein et al. (2009) reported the correlation between FGF21 and kidney disease for the first time, and found that the circulating FGF21 level of chronic hemodialysis patients increased by 15 times compared with the control group based on Caucasian population in a study from Germany. Subsequently, some studies have found an 8-fold increase of FGF21 in peritoneal dialysis patients compared to normal subjects according to a study from Korean (Han et al., 2010). In clinical practice, multiple studies have shown that the level of serum FGF21 is correlated with renal function of the patients with CKD (Crasto et al., 2012). Furthermore, the elevated plasma FGF21 level in the Chinese population significantly correlated with the state of CKD progression, and is independently linked to renal function and poor blood lipid levels (Lin et al., 2011).

The determination of FGF21 may help evaluate CKD and its complications, which is expected to become a relevant biomarker of CKD (Kuro-O, 2019a; Yamamoto et al., 2020). Serum FGF21 levels in CKD patients are positively associated with oxidative stress, and negatively associated with eGFR based on a cross-sectional study from Mexico (Ángel et al., 2021). The increase in FGF21 concentration in CKD patients may be related to the metabolism of lipids and carbohydrates, and FGF21 levels in CKD patients can be reduced through hemodialysis and transplantation from a Poland study (Marchelek-Myśliwiec et al., 2019). In peritoneal dialysis patients, FGF21 can be used as a hormone signal exerting a protective role in maintaining blood glucose homeostasis and preventing potential insulin resistance (González et al., 2016).

There exert potential roles of FGF21 in CKD patients with other pathological situations (**Figure 2**). Growing evidence points to the potential interplay between non-alcoholic fatty liver disease (NAFLD) and CKD, the patients with NAFLD can result in renal injury by means of the alterations of FGF21 secretion (Musso et al., 2015). Similar findings have uncovered that FGF21 can serve as a biomarker for CKD progression and is

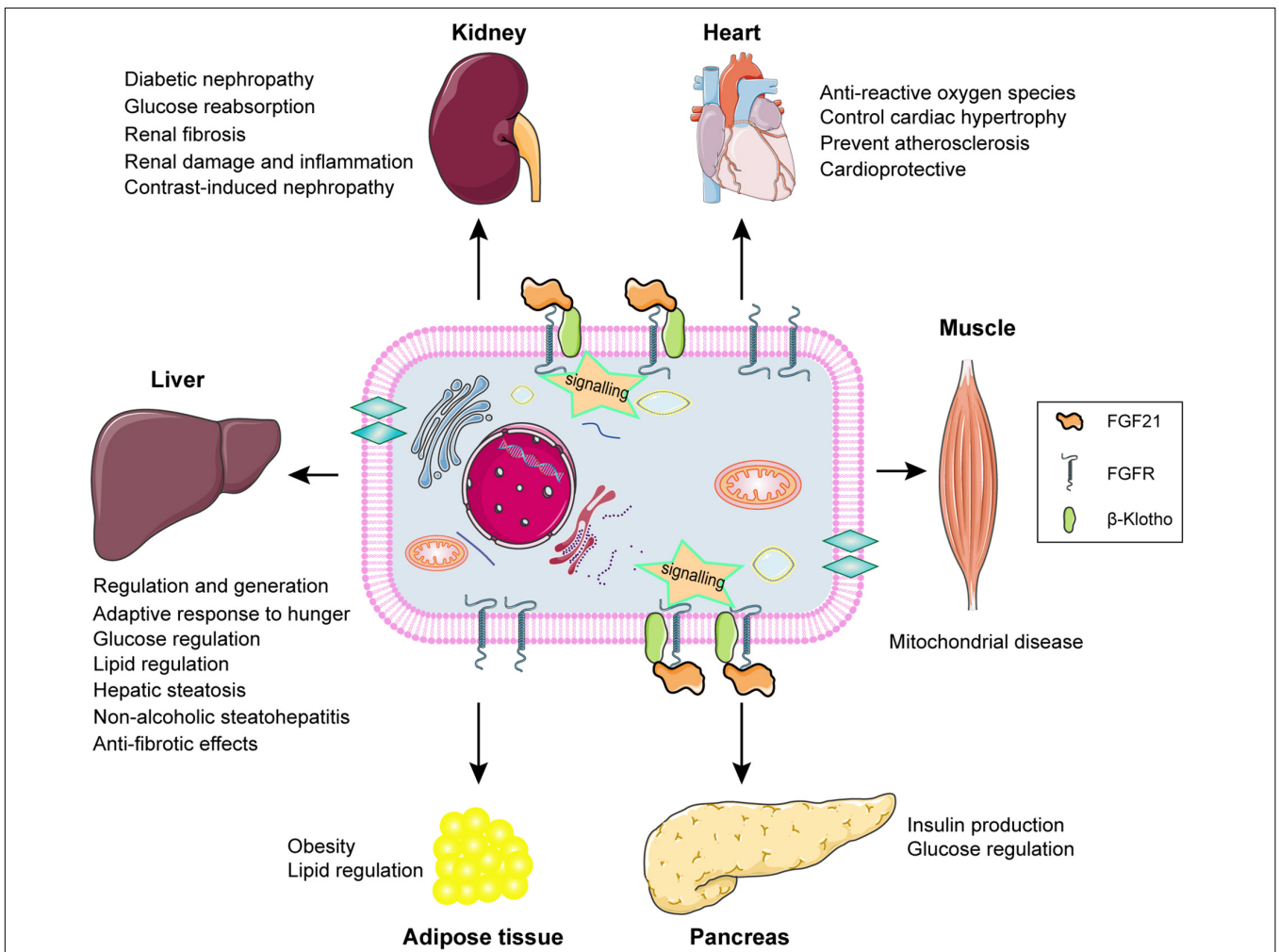

FIGURE 3 | Schematic diagram of FGF21 signaling and the potential biological role of FGF21 in different types of tissue. FGF21 exerts potential biological roles in target organs, including liver, kidney, heart, muscle, pancreas, and adipose tissue, through binding to the βKlotho-FGFR complex achieving the signal transduction.

associated with an increased risk of vascular calcification in CKD patients (Kuro-O, 2019a). FGF21 can be deemed as a sensitive predictor associated with osteoporosis in hemodialysis patients with worse renal function (Zhu et al., 2021). Serum FGF21 has been confirmed as a biomarker for predicting rapid progression of CKD patients with type 2 diabetes through eGFR decline (Looker et al., 2015).

Some studies have shown that acute kidney injury may accelerate the progression of CKD. Therefore, prevention of acute kidney injury is an important part of the treatment for CKD. In a mouse model of acute kidney injury induced by cisplatin, the application of recombinant FGF21 can remarkably downregulate the relevant protein levels of kidney injury (Li et al., 2018a; Chen et al., 2020). Additionally, another study demonstrates that the protective role of FGF21 in kidney injury can be induced by vascular calcification (Shi et al., 2018). Higher circulating FGF21 levels in patients with ESRD, but not with cardiovascular events, are associated with high mortality, which indicates that circulating FGF21 level can be used as a predictor for the prognosis of patients with CKD (Kohara et al., 2017). Although the metabolic disorder in CKD is usually thought to be the cause of the elevated FGF21, its precise mechanism has not been illustrated so far.

FIBROBLAST GROWTH FACTOR 21 AS A POTENTIAL THERAPEUTIC TARGET

FGF21 has been clarified to have the effect on lowering blood sugar and lipids, so it is expected to be a potential candidate for development of CKD therapeutic. However, short half-life and poor stability are the bottleneck of clinical application of natural FGF21 protein. By constructing a stable mutant FGF21 (mFGF21) and then genetically fusing it with human albumin through a polypeptide to form HSA-mFGF21, whose half-life is 20 times higher than that of FGF21. It can enter the body to play a continuous inhibitory effect on blood glucose, which is expected to become a new biological therapy for metabolic disorders including diabetes (Watanabe et al., 2020). In addition, the FGF21 analog LY2405319 (LY) with the half-life improving exerts an inhibitory effect on blood sugar and lipids, which indicates that the FGF21 pathway may be an ideal candidate for the treatment of metabolic diseases (Adams et al., 2013). The new long-acting FGF21 analog PF-05231023 is a promising potential drug for the treatment of type 2 diabetes, obesity and obesity-related diseases (Weng et al., 2015; Thompson et al., 2016). The current research on targeting FGF21 therapy in CKD has certain limitations with a lack of corresponding clinical trials. At the same time, the current research results of some animal models may not be applicable to humans.

CONCLUSION

FGF21 signaling and the potential biological role of FGF21 in different types of tissue are summarized and displayed by the schematic diagram (**Figure 3**). FGF21 regulation performs the potential biological roles in different tissues based on FGFR-βklotho signaling transduction, including participating in the glucose and lipid regulation, the improvement of hepatic steatosis, and anti-fibrotic effects in liver, improving damage and fibrosis in kidney, preventing ROS, cardiac hypertrophy, and atherosclerosis in heart, predicting mitochondrial disease in muscles, regulating insulin production in pancreas, and lipid regulation in adipose tissue. The increase of FGF21 levels in CKD patients is influenced by a number of factors, and the pathophysiological significance and its positive or negative impact on patients have not been fully determined. It is possible to speculate that the level of FGF21 is adaptively increased in the early stages of CKD, which contributes to alleviate the metabolic disorders. As the severity of the continuous progress of CKD, the level of FGF21 is also rising correspondingly without more active role. Later the chronically elevated FGF21 may have adverse consequences for the patients with CKD. Consequently, FGF21 may become a potential target and blocking the effect of FGF21-βklotho endocrine axis may improve the curative effects on CKD patients. However, this needs more researches and clinical trials to further confirm.

AUTHOR CONTRIBUTIONS

XZ and NW contributed to the conception and design of the review article. XZ and YZ prepared the manuscript. NW revised the manuscript. All authors approved the final draft of the manuscript.

REFERENCES

Adams, A. C., Halstead, C. A., Hansen, B. C., Irizarry, A. R., Martin, J. A., Myers, S. R., et al. (2013). LY2405319, an engineered FGF21 variant. *PLoS One* 8:e65763. doi: 10.1371/journal.pone.0065763

An, H. J., Lee, B., Kim, D. H., Lee, E. K., Chung, K. W., Park, M. H., et al. (2017). Physiological characterization of a novel PPAR pan agonist, 2-(4-(5,6-methylenedioxybenzo[d]thiazol-2-yl)-2-methylphenoxy)-2-methylpropanoic acid (MHY2013). *Oncotarget* 8, 16912–16924. doi: 10.18632/oncotarget.14818

Ángel, G. M., Paola, V. V., Froylan David, M. S., Lucía, P. B., Juan Mauricio, V. Z., María Fernanda, N. F., et al. (2021). Fibroblast growth factor 21 is associated with increased serum total antioxidant capacity and oxidized lipoproteins in humans with different stages of chronic kidney disease. *Ther. Adv. Endocrinol. Metab.* 12:20420188211001160.

Angelin, B., Larsson, T. E., and Rudling, M. (2012). Circulating fibroblast growth factors as metabolic regulators–a critical appraisal. *Cell Metab.* 16, 693–705. doi: 10.1016/j.cmet.2012.11.001

Chang, L. H., Hwu, C. M., Chu, C. H., Lin, Y. C., Huang, C. C., You, J. Y., et al. (2021). The combination of soluble tumor necrosis factor receptor type 1 and fibroblast growth factor 21 exhibits better prediction of renal outcomes in patients with type 2 diabetes mellitus. *J. Endocrinol. Invest.*

Chen, C., Cheung, B. M., Tso, A. W., Wang, Y., Law, L. S., Ong, K. L., et al. (2011). High plasma level of fibroblast growth factor 21 is an Independent predictor of type 2 diabetes: a 5.4-year population-based prospective study in Chinese subjects. *Diabetes Care* 34, 2113–2115. doi: 10.2337/dc11-0294

Chen, Q., Ma, J., Yang, X., Li, Q., Lin, Z., and Gong, F. (2020). SIRT1 mediates effects of FGF21 to ameliorate cisplatin-induced acute kidney injury. *Front. Pharmacol.* 11:241. doi: 10.3389/fphar.2020.00241

Cheng, Y., Zhang, X., Ma, F., Sun, W., Wang, W., Yu, J., et al. (2020). The role of Akt2 in the protective effect of fenofibrate against diabetic nephropathy. *Int. J. Biol. Sci.* 16, 553–567. doi: 10.7150/ijbs.40643

Coate, K. C., Hernandez, G., Thorne, C. A., Sun, S., Le, T. D. V., Vale, K., et al. (2017). FGF21 is an exocrine pancreas secretagogue. *Cell Metab.* 25, 472–480. doi: 10.1016/j.cmet.2016.12.004

Cockwell, P., and Fisher, L. A. (2020). The global burden of chronic kidney disease. *Lancet* 395, 662–664. doi: 10.1016/s0140-6736(19)32977-0

Crasto, C., Semba, R. D., Sun, K., and Ferrucci, L. (2012). Serum fibroblast growth factor 21 is associated with renal function and chronic kidney disease in community-dwelling adults. *J. Am. Geriatr. Soc.* 60, 792–793. doi: 10.1111/j.1532-5415.2011.03879.x

Degirolamo, C., Sabbà, C., and Moschetta, A. (2016). Therapeutic potential of the endocrine fibroblast growth factors FGF19. *Nat. Rev. Drug Discov.* 15, 51–69. doi: 10.1038/nrd.2015.9

Di Raimondo, D., Tuttolomondo, A., Musiari, G., Schimmenti, C., D'Angelo, A., Pinto, A., et al. (2016). Are the myokines the mediators of physical activity-induced health benefits. *Curr. Pharm. Des.* 22, 3622–3647. doi: 10.2174/1381612822666160429121934

Ding, X., Boney-Montoya, J., Owen, B. M., Bookout, A. L., Coate, K. C., Mangelsdorf, D. J., et al. (2012). βKlotho is required for fibroblast growth factor 21 effects on growth and metabolism. *Cell Metab.* 16, 387–393. doi: 10.1016/j.cmet.2012.08.002

El-Saeed, A. M., and El-Mohasseb, G. F. (2017). Circulating fibroblast growth factors 21 and 23 as biomarkers of progression in diabetic nephropathy in type 2 diabetes with normoalbuminuria. *Egypt J. Immunol.* 24, 93–99.

Emanuelli, B., Vienberg, S. G., Smyth, G., Cheng, C., Stanford, K. I., Arumugam, M., et al. (2014). Interplay between FGF21 and insulin action in the liver regulates metabolism. *J. Clin. Invest.* 124, 515–527. doi: 10.1172/jci67353

Esteghamati, A., Khandan, A., Momeni, A., Behdadnia, A., Ghajar, A., Nikdad, M. S., et al. (2017). Circulating levels of fibroblast growth factor 21 in early-stage diabetic kidney disease. *Ir. J. Med. Sci.* 186, 785–794. doi: 10.1007/s11845-017-1554-7

Fang, H., Ghosh, S., Sims, L., Stone, K. P., Hill, C. M., Spires, D., et al. (2021). FGF21 prevents low protein diet-induced renal inflammation in aged mice. *Am. J. Physiol. Renal Physiol.* 321, F356–F368.

Fernandes-Freitas, I., and Owen, B. M. (2015). Metabolic roles of endocrine fibroblast growth factors. *Curr. Opin. Pharmacol.* 25, 30–35. doi: 10.1016/j.coph.2015.09.014

GBD Chronic Kidney Disease Collaboration (2020). Global, regional, and national burden of chronic kidney disease1990-2017: a systematic analysis for the global burden of disease study 2017. *Lancet* 395, 709-733.

Goetz, R., Beenken, A., Ibrahimi, O. A., Kalinina, J., Olsen, S. K., Eliseenkova, A. V., et al. (2007). Molecular insights into the klotho-dependent, endocrine mode of action of fibroblast growth factor 19 subfamily members. *Mol. Cell Biol.* 27, 3417–3428. doi: 10.1128/mcb.02249-06

Goetz, R., and Mohammadi, M. (2013). Exploring mechanisms of FGF signalling through the lens of structural biology. *Nat. Rev. Mol. Cell Biol.* 14, 166–180. doi: 10.1038/nrm3528

González, E., Díez, J. J., Bajo, M. A., Del Peso, G., Grande, C., Rodríguez, O., et al. (2016). Fibroblast growth factor 21 (FGF-21) in peritoneal dialysis patients: natural history and metabolic implications. *PLoS One* 11:e0151698. doi: 10.1371/journal.pone.0151698

Han, S. H., Choi, S. H., Cho, B. J., Lee, Y., Lim, S., Park, Y. J., et al. (2010). Serum fibroblast growth factor-21 concentration is associated with residual renal function and insulin resistance in end-stage renal disease patients receiving long-term peritoneal dialysis. *Metabolism* 59, 1656–1662. doi: 10.1016/j.metabol.2010.03.018

Harrison, S. A., Ruane, P. J., Freilich, B. L., Neff, G., Patil, R., Behling, C. A., et al. (2021). Efruxifermin in non-alcoholic steatohepatitis: a randomized, double-blind, placebo-controlled, phase 2a trial. *Nat. Med.* 27, 1262–1271. doi: 10.1038/s41591-021-01425-3

He, Y., Li, Y., Wei, Z., Zhang, X., Gao, J., Wang, X., et al. (2018). Pharmacokinetics, tissue distribution, and excretion of FGF-21 following subcutaneous administration in rats. *Drug Test Anal.* 10, 1061–1069. doi: 10.1002/dta.2365

Hindricks, J., Ebert, T., Bachmann, A., Kralisch, S., Lössner, U., Kratzsch, J., et al. (2014). Serum levels of fibroblast growth factor-21 are increased in chronic and acute renal dysfunction. *Clin. Endocrinol. (Oxf.)* 80, 918–924. doi: 10.1111/cen.12380

Inagaki, T., Dutchak, P., Zhao, G., Ding, X., Gautron, L., Parameswara, V., et al. (2007). Endocrine regulation of the fasting response by PPARalpha-mediated induction of fibroblast growth factor 21. *Cell Metab.* 5, 415–425. doi: 10.1016/j.cmet.2007.05.003

Itoh, N., and Ornitz, D. M. (2011). Fibroblast growth factors: from molecular evolution to roles in development, metabolism and disease. *J. Biochem.* 149, 121–130. doi: 10.1093/jb/mvq121

Jian, W. X., Peng, W. H., Jin, J., Chen, X. R., Fang, W. J., Wang, W. X., et al. (2012). Association between serum fibroblast growth factor 21 and diabetic nephropathy. *Metabolism* 61, 853–859. doi: 10.1016/j.metabol.2011.10.012

Kalantar-Zadeh, K., Jafar, T. H., Nitsch, D., Neuen, B. L., and Perkovic, V. (2021). Chronic kidney disease. *Lancet*

Kharitonenkov, A., Shiyanova, T. L., Koester, A., Ford, A. M., Micanovic, R., Galbreath, E. J., et al. (2005). FGF-21 as a novel metabolic regulator. *J. Clin. Invest.* 115, 1627–1635.

Kim, D., Lee, J., Bae, I., Kim, M., Huh, Y., Choi, J., et al. (2021). Preparation, characterization, and pharmacological study of a novel long-acting FGF21 with a potential therapeutic effect in obesity. *Biologicals* 69, 49–58. doi: 10.1016/j.biologicals.2020.11.005

Kim, H. W., Lee, J. E., Cha, J. J., Hyun, Y. Y., Kim, J. E., Lee, M. H., et al. (2013). Fibroblast growth factor 21 improves insulin resistance and ameliorates renal injury in db/db mice. *Endocrinology* 154, 3366–3376. doi: 10.1210/en.2012-2276

Kohara, M., Masuda, T., Shiizaki, K., Akimoto, T., Watanabe, Y., Honma, S., et al. (2017). Association between circulating fibroblast growth factor 21 and mortality in end-stage renal disease. *PLoS One* 12:e0178971. doi: 10.1371/journal.pone.0178971

Kondo, Y., Komaba, H., and Fukagawa, M. (2020). Endocrine fibroblast growth factors as potential biomarkers for chronic kidney disease. *Expert Rev. Mol. Diagn.* 20, 715–724. doi: 10.1080/14737159.2020.1780918

Kuro-o, M. (2012). Klotho and βKlotho. *Adv. Exp. Med. Biol.* 728, 25–40.

Kuro-O, M. (2019b). The Klotho proteins in health and disease. *Nat. Rev. Nephrol.* 15, 27–44. doi: 10.1038/s41581-018-0078-3

Kuro-O, M. (2019a). Klotho and endocrine fibroblast growth factors: markers of chronic kidney disease progression and cardiovascular complications. *Nephrol. Dial. Transplant.* 34, 15–21. doi: 10.1093/ndt/gfy126

Lancha, A., Frühbeck, G., and Gómez-Ambrosi, J. (2012). Peripheral signalling involved in energy homeostasis control. *Nutr. Res. Rev.* 25, 223–248. doi: 10.1017/s0954422412000145

Lee, C. H., Hui, E. Y., Woo, Y. C., Yeung, C. Y., Chow, W. S., Yuen, M. M., et al. (2015). Circulating fibroblast growth factor 21 levels predict progressive kidney disease in subjects with type 2 diabetes and normoalbuminuria. *.J Clin. Endocrinol. Metab.* 100, 1368–1375. doi: 10.1210/jc.2014-3465

Li, S., Wang, N., Guo, X., Li, J., Zhang, T., Ren, G., et al. (2018b). Fibroblast growth factor 21 regulates glucose metabolism in part by reducing renal glucose reabsorption. *Biomed. Pharmacother.* 108, 355–366. doi: 10.1016/j.biopha.2018.09.078

Li, F., Liu, Z., Tang, C., Cai, J., and Dong, Z. (2018a). FGF21 is induced in cisplatin nephrotoxicity to protect against kidney tubular cell injury. *FASEB J.* 32, 3423–3433. doi: 10.1096/fj.201701316r

Li, X. (2019). The FGF metabolic axis. *Front. Med.* 13:511–530. doi: 10.1007/s11684-019-0711-y

Lin, S., Yu, L., Ni, Y., He, L., Weng, X., Lu, X., et al. (2020). fibroblast growth factor 21 attenuates diabetes-induced renal fibrosis by negatively regulating TGF-β-p53-Smad2/3-mediated epithelial-to-mesenchymal transition via activation of AKT. *Diabetes Metab. J.* 44, 158–172. doi: 10.4093/dmj.2018.0235

Lin, Z., Pan, X., Wu, F., Ye, D., Zhang, Y., Wang, Y., et al. (2015). Fibroblast growth factor 21 prevents atherosclerosis by suppression of hepatic sterol regulatory element-binding protein-2 and induction of adiponectin in mice. *Circulation* 131, 1861–1871. doi: 10.1161/circulationaha.115.015308

Lin, Z., Zhou, Z., Liu, Y., Gong, Q., Yan, X., Xiao, J., et al. (2011). Circulating FGF21 levels are progressively increased from the early to end stages of chronic kidney diseases and are associated with renal function in Chinese. *PLoS One* 6:e18398. doi: 10.1371/journal.pone.0018398

Looker, H. C., Colombo, M., Hess, S., Brosnan, M. J., Farran, B., Dalton, R. N., et al. (2015). Biomarkers of rapid chronic kidney disease progression in type 2 diabetes. *Kidney Int.* 88, 888–896. doi: 10.1038/ki.2015.199

Luo, Y., Ye, S., Chen, X., Gong, F., Lu, W., and Li, X. (2017). Rush to the fire: FGF21 extinguishes metabolic stress, metaflammation and tissue damage. *Cytokine Growth Factor Rev.* 38, 59–65. doi: 10.1016/j.cytogfr.2017.08.001

Marchelek-Myśliwiec, M., Dziedziejko, V., Nowosiad-Magda, M., Dołęgowska, K., Dołęgowska, B., Pawlik, A., et al. (2019). chronic kidney disease is associated with increased plasma levels of fibroblast growth factors 19 and 21. *Kidney Blood Press Res.* 44, 1207–1218. doi: 10.1159/000502647

Musso, G., Cassader, M., Cohney, S., Pinach, S., Saba, F., and Gambino, R. (2015). Emerging liver-kidney interactions in nonalcoholic fatty liver disease. *Trends Mol. Med.* 21, 645–662. doi: 10.1016/j.molmed.2015.08.005

Nishimura, T., Nakatake, Y., Konishi, M., and Itoh, N. (2000). Identification of a novel FGF. *Biochim. Biophys. Acta.* 1492, 203–206. doi: 10.1016/s0167-4781(00)00067-1

Nohara, S., Ishii, A., Yamamoto, F., Yanagiha, K., Moriyama, T., Tozaka, N., et al. (2019). GDF-15, a mitochondrial disease biomarker, is associated with the severity of multiple sclerosis. *J. Neurol. Sci.* 405:116429. doi: 10.1016/j.jns.2019.116429

Packer, M. (2020). Role of ketogenic starvation sensors in mediating the renal protective effects of SGLT2 inhibitors in type 2 diabetes. *J. Diabetes Complications* 34:107647. doi: 10.1016/j.jdiacomp.2020.107647

Pan, X., Shao, Y., Wu, F., Wang, Y., Xiong, R., Zheng, J., et al. (2018). FGF21 prevents angiotensin II-induced hypertension and vascular dysfunction by activation of ACE2/angiotensin-(1-7) axis in mice. *Cell Metab.* 27, 1323.e–1337.e.

Patel, V. J., Joharapurkar, A. A., Kshirsagar, S. G., Sutariya, B. K., Patel, M. S., Patel, H. M., et al. (2018). Coagonist of glucagon-like peptide-1 and glucagon receptors ameliorates kidney injury in murine models of obesity and diabetes mellitus. *World J. Diabetes* 9, 80–91. doi: 10.4239/wjd.v9.i6.80

Planavila, A., Redondo, I., Hondares, E., Vinciguerra, M., Munts, C., Iglesias, R., et al. (2013). Fibroblast growth factor 21 protects against cardiac hypertrophy in mice. *Nat. Commun.* 4:2019.

Planavila, A., Redondo-Angulo, I., Ribas, F., Garrabou, G., Casademont, J., Giralt, M., et al. (2015). Fibroblast growth factor 21 protects the heart from oxidative stress. *Cardiovasc. Res.* 106, 19–31. doi: 10.1093/cvr/cvu263

Potthoff, M. J., Inagaki, T., Satapati, S., Ding, X., He, T., Goetz, R., et al. (2009). FGF21 induces PGC-1alpha and regulates carbohydrate and fatty acid metabolism during the adaptive starvation response. *Proc. Natl. Acad. Sci. U.S.A.* 106, 10853–10858. doi: 10.1073/pnas.0904187106

Reitman, M. L. (2013). FGF21 mimetic shows therapeutic promise. *Cell Metab.* 18, 307–309. doi: 10.1016/j.cmet.2013.08.014

Shi, Y. C., Lu, W. W., Hou, Y. L., Fu, K., Gan, F., Cheng, S. J., et al. (2018). protection effect of exogenous fibroblast growth factor 21 on the kidney injury in vascular calcification rats. *Chin. Med. J. (Engl.)* 131, 532–538. doi: 10.4103/0366-6999.226065

Silverwood, R. J., Pierce, M., Thomas, C., Hardy, R., Ferro, C., Sattar, N., et al. (2013). Association between younger age when first overweight and increased risk for CKD. *J. Am. Soc. Nephrol.* 24, 813–821. doi: 10.1681/asn.2012070675

Stein, S., Bachmann, A., Lössner, U., Kratzsch, J., Blüher, M., Stumvoll, M., et al. (2009). Serum levels of the adipokine FGF21 depend on renal function. *Diabetes Care* 32, 126–128. doi: 10.2337/dc08-1054

Suassuna, P. G. A., Cherem, P. M., de Castro, B. B., Maquigussa, E., Cenedeze, M. A., Lovisi, J. C. M., et al. (2020). αKlotho attenuates cardiac hypertrophy and increases myocardial fibroblast growth factor 21 expression in uremic rats. *Exp. Biol. Med. (Maywood)* 245, 66–78. doi: 10.1177/1535370219894302

Suomalainen, A. (2013). Fibroblast growth factor 21: a novel biomarker for human muscle-manifesting mitochondrial disorders. *Expert Opin. Med. Diagn.* 7, 313–317. doi: 10.1517/17530059.2013.812070

Suomalainen, A., Elo, J. M., Pietiläinen, K. H., Hakonen, A. H., Sevastianova, K., Korpela, M., et al. (2011). FGF-21 as a biomarker for muscle-manifesting mitochondrial respiratory chain deficiencies: a diagnostic study. *Lancet Neurol.* 10, 806–818. doi: 10.1016/s1474-4422(11)70155-7

Tanimura, Y., Aoi, W., Takanami, Y., Kawai, Y., Mizushima, K., Naito, Y., et al. (2016). Acute exercise increases fibroblast growth factor 21 in metabolic organs and circulation. *Physiol. Rep.* 4:e12828.

Thompson, W. C., Zhou, Y., Talukdar, S., and Musante, C. J. (2016). PF-05231023, a long-acting FGF21 analogue, decreases body weight by reduction of food intake in non-human primates. *J. Pharmacokinet. Pharmacodyn.* 43, 411–425. doi: 10.1007/s10928-016-9481-1

Wang, Y. S., Ye, J., Cao, Y. H., Zhang, R., Liu, Y., Zhang, S. W., et al. (2019). Increased serum/plasma fibroblast growth factor 21 in type 2 diabetes mellitus: a systematic review and meta-analysis. *Postgrad. Med. J.* 95, 134–139. doi: 10.1136/postgradmedj-2018-136002

Watanabe, H., Miyahisa, M., Chikamatsu, M., Nishida, K., Minayoshi, Y., Takano, M., et al. (2020). Development of a long acting FGF21 analogue-albumin fusion protein and its anti-diabetic effects. *J. Control. Release* 324, 522–531.

Wei, W., An, X. R., Jin, S. J., Li, X. X., and Xu, M. (2018). Inhibition of insulin resistance by PGE1 via autophagy-dependent FGF21 pathway in diabetic nephropathy. *Sci. Rep.* 8:9.

Weng, Y., Chabot, J. R., Bernardo, B., Yan, Q., Zhu, Y., Brenner, M. B., et al. (2015). Pharmacokinetics (PK), pharmacodynamics (PD) and integrated PK/PD modeling of a novel long acting FGF21 clinical candidate PF-05231023 in diet-induced obese and leptin-deficient obese mice. *PLoS One* 10:e0119104. doi: 10.1371/journal.pone.0119104

Woo, Y. C., Xu, A., Wang, Y., and Lam, K. S. (2013). Fibroblast growth factor 21 as an emerging metabolic regulator: clinical perspectives. *Clin. Endocrinol. (Oxf.)* 78, 489–496. doi: 10.1111/cen.12095

Wu, C. H., Chou, R. H., Kuo, C. S., Huang, P. H., Chang, C. C., Leu, H. B., et al. (2018). Circulating fibroblast growth factor 21 is associated with subsequent renal injury events in patients undergoing coronary angiography. *Sci. Rep.* 8:12425.

Yamamoto, S., Koyama, D., Igarashi, R., Maki, T., Mizuno, H., Furukawa, Y., et al. (2020). Serum endocrine fibroblast growth factors as potential biomarkers for chronic kidney disease and various metabolic dysfunctions in aged patients. *Intern. Med.* 59, 345–355. doi: 10.2169/internalmedicine.3597-19

Yu, W., Zhu, H., Chen, X., Gu, X., Zhang, X., Shen, F., et al. (2019). Genetic variants flanking the FGF21 gene were associated with renal function in chinese patients with type 2 diabetes. *J Diabetes Res.* 2019:9387358.

Zhang, C., Shao, M., Yang, H., Chen, L., Yu, L., Cong, W., et al. (2013). Attenuation of hyperlipidemia- and diabetes-induced early-stage apoptosis and late-stage renal dysfunction via administration of fibroblast growth factor-21 is associated with suppression of renal inflammation. *PLoS One* 8:e82275. doi: 10.1371/journal.pone.0082275

Zhang, F., Yu, L., Lin, X., Cheng, P., He, L., Li, X., et al. (2015). Minireview: roles of fibroblast growth factors 19 and 21 in metabolic regulation and chronic diseases. *Mol. Endocrinol.* 29, 1400–1413. doi: 10.1210/me.2015-1155

Zhang, J., and Li, Y. (2015). Fibroblast growth factor 21 analogs for treating metabolic disorders. *Front. Endocrinol. (Lausanne)* 6:168. doi: 10.3389/fendo.2015.00168

Zhang, R., Cai, X., Du, Y., Li, W., Liu, L., and Lin, Q. (2021). Association of serum fibroblast growth factor 21 and urinary glucose excretion in hospitalized patients with type 2 diabetes. *J. Diabetes Complications* 35:107750. doi: 10.1016/j.jdiacomp.2020.107750

Zhang, Y., Liu, Z., Zhou, M., and Liu, C. (2018). Therapeutic effects of fibroblast growth factor-21 against atherosclerosis via the NF-κB pathway. *Mol. Med. Rep.* 17, 1453–1460.

Zhao, L., Wang, H., Xie, J., Chen, Z., Li, X., and Niu, J. (2017). Potent long-acting rhFGF21 analog for treatment of diabetic nephropathy in db/db and DIO mice. *BMC Biotechnol.* 17:58. doi: 10.1186/s12896-017-0368-z

Zhu, L., Li, M., Zha, Q., Yang, M., Yu, J., Pan, M., et al. (2021). Fibroblast growth factor 21 (FGF21) is a sensitive marker of osteoporosis in haemodialysis patients: a cross-sectional observational study. *BMC Nephrol.* 22:183. doi: 10.1186/s12882-021-02393-z

Conflict of Interest: The authors declare that the research was conducted in the absence of any commercial or financial relationships that could be construed as a potential conflict of interest.

Publisher's Note: All claims expressed in this article are solely those of the authors and do not necessarily represent those of their affiliated organizations, or those of the publisher, the editors and the reviewers. Any product that may be evaluated in this article, or claim that may be made by its manufacturer, is not guaranteed or endorsed by the publisher.

frontiers | Frontiers in Physiology

MINI REVIEW
published: 08 June 2022
doi: 10.3389/fphys.2022.933677

What We Have Learned so far From Single Cell Sequencing in Acute Kidney Injury

*Marc Buse, Marcus J. Moeller and Eleni Stamellou**

Division of Nephrology and Clinical Immunology, RWTH Aachen University Hospital, Aachen, Germany

Acute Kidney injury is a major clinical problem associated with increased morbidity and mortality. Despite, intensive research the clinical outcome remains poor and apart from supportive therapy no other specific therapy exists. Single cell technologies have enabled us to get deeper insights into the transcriptome of individual cells in complex tissues like the kidney. With respect to kidney injury, this would allow us to better define the unique role of individual cell populations in the pathophysiology of acute kidney injury and progression to chronic kidney disease. In this mini review, we would like to give an overview and discuss the current major findings in the field of acute kidney injury through Single-Cell technologies.

Keywords: tubular regeneration, acute kidney injury, single cell sequencing, chronic kidney disease, transcriptomics

OPEN ACCESS

Edited by:
Christian Hugo,
University Hospital Carl Gustav Carus, Germany

Reviewed by:
Emmanuelle Charrin,
Karolinska Institutet (KI), Sweden

****Correspondence:***
Eleni Stamellou
estamellou@ukaachen.de

Specialty section:
This article was submitted to Renal Physiology and Pathophysiology, a section of the journal Frontiers in Physiology

Received: *01 May 2022*
Accepted: *25 May 2022*
Published: *08 June 2022*

Citation:
Buse M, Moeller MJ and Stamellou E (2022) What We Have Learned so far From Single Cell Sequencing in Acute Kidney Injury. Front. Physiol. 13:933677. doi: 10.3389/fphys.2022.933677

INTRODUCTION

Acute kidney injury (AKI) is a major clinical problem and one of the most serious complications in hospitalized patients. It affects about two percent of all hospitalized patients and up to 35–57% patients in intensive care unit (Liangos et al., 2006; Ostermann and Chang, 2007; Bagshaw et al., 2008; Hoste et al., 2015). Additionally, its incidence has increased substantially over the last years due to the growing ageing population and increased prevalence of comorbidities such as diabetes or obesity (Susantitaphong et al., 2013; Hoste et al., 2015).

It is associated with high costs, prolonged hospital stays, and most important with a higher mortality (Hoste et al., 2015). Furthermore, acute kidney injury increases the risk of developing a chronic kidney disease (CKD) and end stage-renal-disease (Coca et al., 2012).

Despite a better understanding of the pathophysiology of AKI over the last years, still no specific therapy, apart from supportive measurements and dialysis, exist. Therefore, there is an urgent unmet need to better diagnose and treat AKI.

Pathophysiology

AKI is a heterogeneous disease with various causes mainly including transient ischemia and/or toxic injury. Acute tubular injury accounts for the most common intrinsic cause for AKI. The main site of injury is the proximal tubule due to its high workload and energy demand. Upon injury, an intratubular subpopulation of proximal epithelial cells proliferates and restores tubular integrity. However, the origin of these cells still remains a controversy and so far, two hypotheses exist. One argues for the existence of a stable progenitor population (Sagrinati et al., 2006; Lazzeri et al., 2007; Ronconi et al., 2009; Angelotti et al., 2012) and the second supports that any tubular cell can adapt a transient regenerative phenotype as a common reaction to injury (Smeets et al., 2013; Berger et al., 2014; Kusaba et al., 2014; Stamellou et al., 2021). Nevertheless, despite its strong regenerative capacity, the kidney does not always achieve its former integrity and function and incomplete

TABLE 1 | IRI and scRNA seq platforms.

	IRI-Time (min)	Type of IRI	Time Points	Sex	Age	scRNA Platform
Gerhard et al	18	bilateral	7 and 28 d	male	11–19 w	10X Genomics
Rudman-Melnick et al	30	unilateral	1, 2, 4, 7, 11, and 14 d	male	4 and 10 w	DropSeq
Kirita et al	18	bilateral	4 h, 12 h, 2 d, 14 d, 42 d	male	8–10 w	10X Genomics
Dixon et al	34	Bilateral	4 h, 12 h, 2 d, 6 w	female	8–10 w	10X Genomics Visium

h, denotes hours; d, denotes days and w, denotes weeks.

recovery leads to persistent and progressive CKD. (Yang et al., 2010; Chawla and Kimmel, 2012; Liu et al., 2017). The remaining nephrons then have to carry a higher workload leading to pathological hyperfiltration, hypertrophy and further fibrosis due to secondary glomerulosclerosis, ending in a vicious circle.

The New Area of Single Cell Sequencing

Since the appearance of Next-Generation-Sequencing, it has been become possible to get deeper insights into the transcriptome. Even though bulk-RNA-Sequencing was a powerful resource, enabling to understand diseases at molecular level, it is limited in that relevant cell-specific gene expression signatures may be lost within the integrated expression profiles of the other cell types in the sample. Techniques for high throughput RNA-sequencing of individual single cells, so called single cell RNA-sequencing (scRNA-seq), introduced in 2009, have allowed to dissect the genetic program of single cells at very high resolution, enabling detection of heterogeneity among individual cells and characterization of rare cell population. While the evolution to spatial gene expression or ATAC-Sequencing have enabled individual cell resolution incorporated with spatial information and exploration of epigenetic modifications (Hwang et al., 2018).

Cell Sequencing in Acute Kidney Injury

In the last 2 years (2020/21), three studies appeared which investigated acute kidney injury using Single-Cell-Sequencing technologies (Kirita et al., 2020; Rudman-Melnick et al., 2020; Gerhardt et al., 2021) and one using spatial transcriptomics (Dixon et al., 2022). In all of these, the Ischemia-Reperfusion-model (IRI) was used as an injury model (**Table 1**).

The first study appeared in 2020 from Humphrey's group (Kirita et al., 2020). In this study, single cell profiles were generated 4 h, 12 h, 2 days, 14 days, 6 weeks after injury in C57BL/6J wildtype mice. Early after induction of the injury (4 and 12 h), the authors could identify different clusters which contain healthy and injured proximal tubular cells (PTs) and were able to annotate them according to their origin (injured S1/2, injured S3) and the magnitude of injury (severe injured vs injured S1/2, S3). All injured clusters upregulated KIM-1 and share similarities with each other as well as with healthy PTs. Severe injured PT upregulated Keratin 20 and genes encoding heat shock proteins, proposing a stronger damage to these cells, and showed a cell cycle arrest. Interestingly the injured and severely injured clusters upregulated the myc gene, which encodes c-Myc and plays a role in cell cycle progression.

The injured and severely injured clusters almost disappeared 2 days after AKI, while another cluster which exhibited upregulation of cell cycle genes (i.e Top2a) appeared. Since this cluster had the highest proportion of proliferating cells, it was annotated as "repairing PT" cluster. In addition, by 2 days a new distinct cell cluster appeared, reaching almost 30% of all PTs by 14 days. These cells shared a unique transcriptional profile, characterized by the down-regulation of terminal differentiation markers and the up-regulation of a distinct set of genes i. e Vcam1, Sema5a, Dcdc2. This cluster was annotated as 'failed repair proximal tubule cells. Gene set enrichment analysis revealed pathways related to inflammation. Immunofluorescence staining could confirm the presence of these cells in further injury models (folic acid nephropathy) and in human kidney allografts.

Finally, the authors investigated the intercellular communication within the kidney by performing ligand-receptor analysis and particularly they quantified Ccl2-Ccr2 signaling across all time points. Ccl2 and its receptor Ccr2 are important in the pathophysiology of AKI by recruiting T-cells and monocytes (Xu et al., 2019). Fibroblasts and endothelial cells signaled leucocytes first, followed by leucocyte-leucocyte signaling, whereas failed repair cells appeared at last to induce an increased signal.

Next, Gerhardt et al. from McMahon group, employed genetic labeling strategies focused on PTs using single nuclei RNA sequencing (Gerhardt et al., 2021). In this study mice were sacrificed 7 days (designated as early time point) and 28 days (designated as late time point) after induction of the injury. Based on the notion that keratin 20 represent an injury marker of PTs, in order to enable the isolation and tracing of $Krt20^{+}$ cells, the authors generated a *Krt20* mouse line (Liu et al., 2017), which enabled irreversible tamoxifen-dependent labeling of nuclei in injured PTs.

Analysis revealed 7PT clusters which appear in both the control and Ischemia-reperfusion (IR) dataset and 5 clusters appearing only in IRI, annotated by the authors as IRI-clusters. Within these IRI-clusters there were two clusters which emerge mainly during the early time point (7 days) after AKI. One of these clusters exhibits exclusively a strong upregulation of cell-cycling genes like Mki67 and Top2a indicating a proliferative response to ischemia, similar as observed by Kirita et al. (Kirita et al., 2020). During the late time point these proliferative cells almost disappeared and another cluster related to inflammation and fibrosis appeared. These cells upregulated Pdgfd, Kcnip4, Vcam1 and Ccl2, all

known markers for fibrosis and inflammation (Seron et al., 1991; Ostendorf et al., 2012; Kirita et al., 2020), while pathway analysis showed activation of AP-1 and NF-kB pathways, both pathways that have been identified previously to play an important role in driving kidney fibrosis after AKI (Liu et al., 2014; Ferenbach and Bonventre, 2015; Nakagawa et al., 2016; Kitani et al., 2022). Based on that, these cells were named maladaptive PTs. Next, in order to decipher the origin of these cells, the authors used a *Ki67* mouse line, which enabled tamoxifen-dependent labeling of proliferating cells. They assumed that these cells arise from proliferating cells which failed to repair. Intriguingly 89% of the maladaptive cells in the cortico-medullary boundary were GFP positive, whereas in the cortex only 27% of the maladaptive cells were GFP positive. Based on these results, the authors proposed that most cortical Vcam1$^+$/*Ccl2*$^+$ cells either originate from cells that were injured during the initial IRI, but did not initiate replication or show obvious injury responses at this time, or from a secondary spread of the injury within the cortico-medullary boundary to the cortex, presumptively by paracrine signaling.

In the study of Rudman-Melnick et al. from Potter's group, single cell profiles were generated 1, 2, 4, 7, 11 and 14 days after injury in Swiss-Webster (CFW) mice (Rudman-Melnick et al., 2020). Again, a cluster exhibiting a strong upregulation of cell-cycling could be identified, as observed in the above discussed studies (Kirita et al., 2020; Gerhardt et al., 2021). In addition, they identified a novel cell phenotype named as "mixed identity cells", as these cells expressed ectopic markers of different cell types, i. e Umod (marker of loop of Henle), Lrp2 (marker for PT) and Nephrin (podocyte marker), while they down-regulate terminal differentiation markers. This cluster appeared directly after induction of the injury and it was no longer present at day 7. Next the authors, try to describe the gene expression patterns of injured tubule cells. Injured tubule cells were characterized by the downregulation of terminal differentiation proximal tubular markers, suggesting a dedifferentiation-process. Parallelly, they observed in these cells an elevation of genes implicated in nephrogenesis, i. e Sox4, Cd24, Hes1, Puuf3f3 and Hox genes. They focused mainly on Sox4, a transcription factor mainly expressed in the developing kidney (Yu et al., 2012) and Cd24, which encodes for a cell-surface sialoglycoprotein expressed during nephrogenesis (Challen et al., 2004). By studying Sox4 expression pattern in the injured kidney, interestingly they found an opposite relationship of Sox4 to terminal differentiation proximal tubule markers, i. e when resolution of injury began, Sox4 returned gradually to its original expression level and differentiation markers were upregulated, suggesting that Sox4 expression labels proximal tubule dedifferentiation. However, this was not the case in a subpopulation cell with a proinflammatory and profibrotic behavior, which showed prolonged elevated expression of Sox4 and no differentiation into PT. Furthermore, they observed that despite Cd24 is elevated in injured proximal tubule cells, its upregulation was more prominent in injured distal tubule. In addition, Spp1, which encodes secreted phophoprotein 1, and Cytokeratins (Krt7, Krt8, Krt18), both implicated in several kidney pathologies, among them renal cell carcinoma (RCC), found also to increase immediately after induction of the injury and remained upregulated till day 4, when they lowered to the normal levels. While later (by day 4), genes related to fibrosis, i. e Vim and Col18a1 upregulated in both injured and mixed identity cells. Finally, the authors compare the regenerative capacity of young to older mice (10 weeks) and they proposed an increased maladaptive response, estimated by a sustained expression of Sox4/Cd24a and missed upregulation of differentiation markers.

Dixon et al. from Humprhey's group applied spatial transcriptomics during AKI and repair (Dixon et al., 2022). In this study, tissues were collected at early acute (4 and 12 h), early (2 days) and late (6 weeks) time points, while for the first time female C57BL6/J mice were used. The authors could identify several patterns of gene expression during injury and repair, i. e up-regulation of injury markers and down-regulation of proximal tubular markers. While, genes implicated in fibrosis or inflammation were rather upregulated only at late time points. Furthermore, they observed increased T cell and macrophage interactions with injured proximal tubular cells later on the course of injury retained up to 6 weeks, suggesting ongoing injury and inflammation. This work provides some additional findings regarding the molecular evidence and the cellular crosstalk of AKI to CKD transition.

DISCUSSION

Here, we describe the findings of four recently published works on AKI, through which it became possible to define better the cells implicated in the pathophysiology of AKI. Kirita et al. (Kirita et al., 2020) and Gerhardt et al. (Gerhardt et al., 2021) both describe a tubule cell population that fails to repair named either as failed-repair or maladaptive. These cells appear late in the course of injury and are characterized by the up-regulation of a new distinct set of genes, i. e Vcam-1, Ccl2, Pdgfd and by the down-regulation of terminal differentiation markers. According to the authors these cells are acquiring a proinflammatory and profibrotic phenotype, and it was suggested that they are implicated in the progression to CKD. Additionally, Rudman-Melnick et al. described a cell subpopulation with a proinflammatory and profibrotic phenotype, characterized by the prolonged elevated expression of Sox4 and Cd24, both genes associated with nephrogenesis and a later up-regulation of Vimentin. Interestingly most of the above-mentioned genes have been associated with a distinct proximal cell tubule phenotype, known as scattered tubular cells. Scattered tubular cells were firstly described by Lindgren et al. as a distinct cell subpopulation of cells acquiring a unique phenotype; smaller, with less cytoplasm, fewer mitochondria and less pronounced brush border (Lindgren et al., 2011). These cells are characterized by the expression of Cd24, Cd133, Vimentin, Vcam-1, Kim-1 and several other marker proteins (Sagrinati et al., 2006; Smeets et al., 2013; Kusaba et al., 2014). While, additionally they show down-regulation of terminal differentiation proximal tubule markers. However, as already mentioned above, there is a disagreement whether they represent a pre-existing intratubular cell population or whether all surviving cells acquire an equivalent regenerative

capacity through dedifferentiation (Kramann et al., 2015; Stamellou et al., 2021).

To our opinion, the findings from the above discussed studies even though they do not exclude the existence of an intratubular progenitor population, they demonstrate that these cells rather represent damaged epithelial cells that have dedifferentiated and lost their epithelial characteristics than progenitor cells. If the highly cycling cells identified in all three studies represent progenitor cells remains still unclear and has still to be elucidated.

Finally, the study from Dixon et al. re-introduces a variable that is often disregarded which is the sex of the studied model. Animal models have consistently demonstrated that female sex is protective in the development of AKI after ischemia-reperfusion injury (Wyatt et al., 2016; Hosszu et al., 2020). Dixon et al. confirmed previous observations that there is a difference in male/female regarding the time of ischemia to induce similar extent of injury and identified some sex-specific differentially expressed genes.

Overall, we believe that these studies contribute significantly to solving the puzzle around AKI and AKI to CKD transition enabling us to understand the role of individual cells, with the overall aim to develop new strategies to treat AKI and prevent progression to CKD.

AUTHOR CONTRIBUTIONS

MB and ES wrote the manuscript. MM and ES revised the manuscript.

FUNDING

This research was supported by the consortium STOP-FSGS by the German Ministry for Science and Education (BMBF 01GM1518A to MM), and by the clinical research unit InteraKD consortium CRU 5011: Project ID: 445703531 (SP03 to ES, SP05 to MM) and by the German Research Foundation (DFG, MO 1802/7-1, 8-1, 11-1 to MM). ES is supported by a START grant (19/21 to ES) and by a clinician scientist-program of the Faculty of Medicine of the RWTH Aachen University. ES has received a research grant of the German Society of Nephrology (DGfN).

REFERENCES

Angelotti, M. L., Ronconi, E., Ballerini, L., Peired, A., Mazzinghi, B., Sagrinati, C., et al. (2012). Characterization of Renal Progenitors Committed toward Tubular Lineage and Their Regenerative Potential in Renal Tubular Injury. *Stem Cells* 30 (8), 1714–1725. doi:10.1002/stem.1130

Bagshaw, S. M., George, C., Dinu, I., and Bellomo, R. (2008). A Multi-Centre Evaluation of the RIFLE Criteria for Early Acute Kidney Injury in Critically Ill Patients. *Nephrol. Dial. Transplant.* 23 (4), 1203–1210. doi:10.1093/ndt/gfm744

Berger, K., Bangen, J.-M., Hammerich, L., Liedtke, C., Floege, J., Smeets, B., et al. (2014). Origin of Regenerating Tubular Cells after Acute Kidney Injury. *Proc. Natl. Acad. Sci. U.S.A.* 111 (4), 1533–1538. doi:10.1073/pnas.1316177111

Challen, G. A., Martinez, G., Davis, M. J., Taylor, D. F., Crowe, M., Teasdale, R. D., et al. (2004). Identifying the Molecular Phenotype of Renal Progenitor Cells. *J. Am. Soc. Nephrol.* 15 (9), 2344–2357. doi:10.1097/01.ASN.0000136779.17837.8F

Chawla, L. S., and Kimmel, P. L. (2012). Acute Kidney Injury and Chronic Kidney Disease: an Integrated Clinical Syndrome. *Kidney Int.* 82 (5), 516–524. doi:10.1038/ki.2012.208

Coca, S. G., Singanamala, S., and Parikh, C. R. (2012). Chronic Kidney Disease after Acute Kidney Injury: a Systematic Review and Meta-Analysis. *Kidney Int.* 81 (5), 442–448. doi:10.1038/ki.2011.379

Dixon, E. E., Wu, H., Muto, Y., Wilson, P. C., and Humphreys, B. D. (2022). Spatially Resolved Transcriptomic Analysis of Acute Kidney Injury in a Female Murine Model. *J. Am. Soc. Nephrol.* 33 (2), 279–289. doi:10.1681/ASN.2021081150

Ferenbach, D. A., and Bonventre, J. V. (2015). Mechanisms of Maladaptive Repair after AKI Leading to Accelerated Kidney Ageing and CKD. *Nat. Rev. Nephrol.* 11 (5), 264–276. doi:10.1038/nrneph.2015.3

Gerhardt, L. M. S., Liu, J., Koppitch, K., Cippà, P. E., and McMahon, A. P. (2021). Single-nuclear Transcriptomics Reveals Diversity of Proximal Tubule Cell States in a Dynamic Response to Acute Kidney Injury. *Proc. Natl. Acad. Sci. U.S.A.* 118 (27), e2026684118. doi:10.1073/pnas.2026684118

Hosszu, A., Fekete, A., and Szabo, A. J. (2020). Sex Differences in Renal Ischemia-Reperfusion Injury. *Am. J. Physiol.-Renal Physiol.* 319 (2), F149–F154. doi:10.1152/ajprenal.00099.2020

Hoste, E. A. J., Bagshaw, S. M., Bellomo, R., Cely, C. M., Colman, R., Cruz, D. N., et al. (2015). Epidemiology of Acute Kidney Injury in Critically Ill Patients: the Multinational AKI-EPI Study. *Intensive Care Med.* 41 (8), 1411–1423. doi:10.1007/s00134-015-3934-7

Hwang, B., Lee, J. H., and Bang, D. (2018). Single-cell RNA Sequencing Technologies and Bioinformatics Pipelines. *Exp. Mol. Med.* 50 (8), 1–14. doi:10.1038/s12276-018-0071-8

Kirita, Y., Wu, H., Uchimura, K., Wilson, P. C., and Humphreys, B. D. (2020). Cell Profiling of Mouse Acute Kidney Injury Reveals Conserved Cellular Responses to Injury. *Proc. Natl. Acad. Sci. U.S.A.* 117 (27), 15874–15883. doi:10.1073/pnas.2005477117

Kitani, T., Kidokoro, K., Nakata, T., Kirita, Y., Nakamura, I., Nakai, K., et al. (2022). Kidney Vascular Congestion Exacerbates Acute Kidney Injury in Mice. *Kidney Int.* 101 (3), 551–562. doi:10.1016/j.kint.2021.11.015

Kramann, R., Kusaba, T., and Humphreys, B. D. (2015). Who Regenerates the Kidney Tubule? *Nephrol. Dial. Transplant.* 30 (6), 903–910. doi:10.1093/ndt/gfu281

Kusaba, T., Lalli, M., Kramann, R., Kobayashi, A., and Humphreys, B. D. (2014). Differentiated Kidney Epithelial Cells Repair Injured Proximal Tubule. *Proc. Natl. Acad. Sci. U.S.A.* 111 (4), 1527–1532. doi:10.1073/pnas.1310653110

Lazzeri, E., Crescioli, C., Ronconi, E., Mazzinghi, B., Sagrinati, C., Netti, G. S., et al. (2007). Regenerative Potential of Embryonic Renal Multipotent Progenitors in Acute Renal Failure. *J. Am. Soc. Nephrol.* 18 (12), 3128–3138. doi:10.1681/ASN.2007020210

Liangos, O., Wald, R., O'Bell, J. W., Price, L., Pereira, B. J., and Jaber, B. L. (2006). Epidemiology and Outcomes of Acute Renal Failure in Hospitalized Patients: a National Survey. *Clin. J. Am. Soc. Nephrol.* 1 (1), 43–51. doi:10.2215/CJN.00220605

Lindgren, D., Boström, A.-K., Nilsson, K., Hansson, J., Sjölund, J., Möller, C., et al. (2011). Isolation and Characterization of Progenitor-like Cells from Human Renal Proximal Tubules. *Am. J. Pathol.* 178 (2), 828–837. doi:10.1016/j.ajpath.2010.10.026

Liu, J., Krautzberger, A. M., Sui, S. H., Hofmann, O. M., Chen, Y., Baetscher, M., et al. (2014). Cell-specific Translational Profiling in Acute Kidney Injury. *J. Clin. Invest.* 124 (3), 1242–1254. doi:10.1172/JCI72126

Liu, J., Kumar, S., Dolzhenko, E., Alvarado, G. F., Guo, J., Lu, C., et al. (2017). Molecular Characterization of the Transition from Acute to Chronic Kidney Injury Following Ischemia/reperfusion. *JCI Insight* 2 (18), e94716. doi:10.1172/jci.insight.94716

Nakagawa, N., Barron, L., Gomez, I. G., Johnson, B. G., Roach, A. M., Kameoka, S., et al. (2016). Pentraxin-2 Suppresses C-Jun/AP-1 Signaling to Inhibit Progressive Fibrotic Disease. *JCI Insight* 1 (20), e87446. doi:10.1172/jci.insight.87446

Ostendorf, T., Eitner, F., and Floege, J. (2012). The PDGF Family in Renal Fibrosis. *Pediatr. Nephrol.* 27 (7), 1041–1050. doi:10.1007/s00467-011-1892-z

Ostermann, M., and Chang, R. W. S. (2007). Acute Kidney Injury in the Intensive Care Unit According to RIFLE. *Crit. Care Med.* 35 (8), 1837–1843. quiz 1852. doi:10.1097/01.CCM.0000277041.13090.0A

Ronconi, E., Sagrinati, C., Angelotti, M. L., Lazzeri, E., Mazzinghi, B., Ballerini, L., et al. (2009). Regeneration of Glomerular Podocytes by Human Renal Progenitors. *J. Am. Soc. Nephrol.* 20 (2), 322–332. doi:10.1681/ASN.2008070709

Rudman-Melnick, V., Adam, M., Potter, A., Chokshi, S. M., Ma, Q., Drake, K. A., et al. (2020). Single-Cell Profiling of AKI in a Murine Model Reveals Novel Transcriptional Signatures, Profibrotic Phenotype, and Epithelial-To-Stromal Crosstalk. *J. Am. Soc. Nephrol.* 31 (12), 2793–2814. doi:10.1681/ASN.2020010052

Sagrinati, C., Netti, G. S., Mazzinghi, B., Lazzeri, E., Liotta, F., Frosali, F., et al. (2006). Isolation and Characterization of Multipotent Progenitor Cells from the Bowman's Capsule of Adult Human Kidneys. *J. Am. Soc. Nephrol.* 17 (9), 2443–2456. doi:10.1681/ASN.2006010089

Seron, D., Cameron, J. S., and Haskard, D. O. (1991). Expression of VCAM-1 in the Normal and Diseased Kidney. *Nephrol. Dial. Transplant.* 6 (12), 917–922. doi:10.1093/ndt/6.12.917

Smeets, B., Boor, P., Dijkman, H., Sharma, S. V., Jirak, P., Mooren, F., et al. (2013). Proximal Tubular Cells Contain a Phenotypically Distinct, Scattered Cell Population Involved in Tubular Regeneration. *J. Pathol.* 229 (5), 645–659. doi:10.1002/path.4125

Stamellou, E., Leuchtle, K., and Moeller, M. J. (2021). Regenerating Tubular Epithelial Cells of the Kidney. *Nephrol. Dial. Transpl.* 36 (11), 1968–1975. doi:10.1093/ndt/gfaa103

Susantitaphong, P., Cruz, D. N., Cerda, J., Abulfaraj, M., Alqahtani, F., Koulouridis, I., et al. (2013). World Incidence of AKI: a Meta-Analysis. *Clin. J. Am. Soc. Nephrol.* 8 (9), 1482–1493. doi:10.2215/CJN.00710113

Wyatt, C. M., Coates, P. T., and Reeves, W. B. (2016). Of Mice and Women: Do Sex-dependent Responses to Ischemia-Reperfusion Injury in Rodents Have Implications for Delayed Graft Function in Humans? *Kidney Int.* 90 (1), 10–13. doi:10.1016/j.kint.2016.05.008

Xu, L., Sharkey, D., and Cantley, L. G. (2019). Tubular GM-CSF Promotes Late MCP-1/CCR2-Mediated Fibrosis and Inflammation after Ischemia/Reperfusion Injury. *J. Am. Soc. Nephrol.* 30 (10), 1825–1840. doi:10.1681/ASN.2019010068

Yang, L., Besschetnova, T. Y., Brooks, C. R., Shah, J. V., and Bonventre, J. V. (2010). Epithelial Cell Cycle Arrest in G2/M Mediates Kidney Fibrosis after Injury. *Nat. Med.* 16 (5), 535–543. 531p following 143. doi:10.1038/nm.2144

Yu, J., Valerius, M. T., Duah, M., Staser, K., Hansard, J. K., Guo, J.-j., et al. (2012). Identification of Molecular Compartments and Genetic Circuitry in the Developing Mammalian Kidney. *Development* 139 (10), 1863–1873. doi:10.1242/dev.074005

Conflict of Interest: The authors declare that the research was conducted in the absence of any commercial or financial relationships that could be construed as a potential conflict of interest.

Publisher's Note: All claims expressed in this article are solely those of the authors and do not necessarily represent those of their affiliated organizations, or those of the publisher, the editors and the reviewers. Any product that may be evaluated in this article, or claim that may be made by its manufacturer, is not guaranteed or endorsed by the publisher.

frontiers | Frontiers in Physiology

TYPE Review
PUBLISHED 24 August 2022
DOI 10.3389/fphys.2022.960059

OPEN ACCESS

EDITED BY
Ignacio Gimenez,
University of Zaragoza, Spain

REVIEWED BY
Hasan Dursun,
Prof. Dr. Cemil Tascioglu City Hospital, Turkey
Shan Mou,
Shanghai Jiao Tong University, China

*CORRESPONDENCE
Chenchen Zou,
nlkbjyczcc@163.com
Lin Lu,
mailto:471445684@qq.com

SPECIALTY SECTION
This article was submitted to Renal Physiology and Pathophysiology, a section of the journal Frontiers in Physiology

RECEIVED 02 June 2022
ACCEPTED 27 July 2022
PUBLISHED 24 August 2022

CITATION
Zou C, Wang C and Lu L (2022), Advances in the study of subclinical AKI biomarkers.
Front. Physiol. 13:960059.
doi: 10.3389/fphys.2022.960059

Advances in the study of subclinical AKI biomarkers

Chenchen Zou[1]*, Chentong Wang[2] and Lin Lu[3]*

[1]Mudanjiang Medical College, Mudanjiang, Heilongjiang, China, [2]Mudanjiang Medical College, Mudanjiang, Heilongjiang, China, [3]Department of Integrative Medicine-Geriatrics, Hongqi Hospital, Mudanjiang Medical College, Mudanjiang, Heilongjiang, China

Acute kidney injury (AKI) is a prevalent and serious illness in all clinical departments, with a high morbidity and death rate, particularly in intensive care units, where prevention and treatment are crucial. As a result, active prevention, early detection, and timely intervention for acute kidney injury are critical. The current diagnostic criteria for acute kidney injury are an increase in serum creatinine concentration and/or a decrease in urine output, although creatinine and urine output merely reflect changes in kidney function, and AKI suggests injury or damage, but not necessarily dysfunction. The human kidney plays a crucial functional reserve role, and dysfunction is only visible when more than half of the renal mass is impaired. Tubular damage markers can be used to detect AKI before filtration function is lost, and new biomarkers have shown a new subset of AKI patients known as "subclinical AKI." Furthermore, creatinine and urine volume are only marginally effective for detecting subclinical AKI. As a result, the search for new biomarkers not only identifies deterioration of renal function but also allows for the early detection of structural kidney damage. Several biomarkers have been identified and validated. This study discusses some of the most promising novel biomarkers of AKI, including CysC, NGAL, KIM-1, IL-18, L-FABP, IGFBP7, TIMP-2, Clusterin, and Penkid. We examine their performance in the diagnosis of subclinical AKI, limitations, and future clinical practice directions.

KEYWORDS

acute kidney injury, subclinical acute kidney injury, biomarkers, early diagnosis, research progress

Introduction

Acute Kidney Injury (AKI) is a serious hospital complication that compromises crucial illness. It is related with increase rates of short-term dialysis, morbidity, death rate, and prolonged hospitalization, and long-term negative output such as cardiovascular mortality and chronic kidney disease (Teo and Endre, 2017). Although renal tubular ischemia is the predominant mechanism of damage in AKI, it is frequently caused by multiple aspects including major surgery, sepsis, hypovolemia, poor cardiac output, urinary tract obstruction, rhabdomyolysis, and drug toxicity in clinical practice (Beker et al., 2018). Despite breakthroughs in AKI management, its morbidity and mortality remain high, owing primarily to

unrecognizable kidney injury and delayed diagnosis. Relying on the patient's underlying condition, the mortality rate of AKI patients ranges from 10% in hospitalized patients to 60% in intensive care unit (ICU) patients (Bhosale and Kulkarni, 2020). AKI also lengthens hospitalization, raises medical expenditures, and places a significant financial burden on patients (Rosner et al., 2018), and the prevention and treatment form is quite severe. Therefore, active prevention, early detection and timely intervention for acute kidney injury are vital.

Limitations of creatinine (SCr) and urine output (UO)

The diagnosis of AKI remains highly complex, and multiple categorization criteria for diagnosing AKI have emerged, ranging from risk, injury, failure, renal function loss, end-stage renal disease (RIFLE), and the Acute Kidney Injury Network (AKIN) to the 2012 Kidney Disease Improving Global Outcomes (KDIGO) criteria. There are still limitations in using these criteria to diagnose AKI. Changes in SCr and UO represent only functional changes in the kidney. The increase in SCr concentration often comes after a large fall in GFR, and the renal tubular epithelium is the principal site of injury in most forms of AKI, SCr does not directly capture tubulointerstitial injury, and lacks accuracy in diagnosing structural renal damage (Moledina and Parikh, 2018). Furthermore, renal reserve, degree of tubular injury, intravascular volume status, patient muscle mass and nutrition, hemodynamic alterations, and fluid transfer all impact SCr levels (Bhosale and Kulkarni, 2020). Because creatinine accumulates in the body over time, acute alterations in GFR after renal injury do not lead in a rapid tise in SCr (Endre et al., 2011). After damage, it usually takes 24–36 h to achieve a steady-state (Waikar and Bonventre, 2009). The rise in SCr is slowed in patients with reduced GFR and associated fluid overload. Similarly, when GFR improves, SCr does not fall immediately (Chen, 2013). As a result, the lack of specificity, sensitivity, and timeliness limits serum creatinine levels. Urine output (UO) may be a time-sensitive marker of glomerular filtration rate (GFR), as it tends to decrease before serum creatinine concentrations increase (Rizvi and Kashani, 2017). However, in the absence of a catheter, UO is challenging to quantify and can be significantly affected by hypovolemic conditions and diuretics. Severe AKI can occur despite standard urine output. Fluid overflow is always seen in patients with critical AKI diagnosed by UO (Gameiro and Lopes, 2019). As a result, urine volume is insensitive, and non-oliguric AKI can develop with limited specificity (Srisawat and Kellum, 2020). Therefore, detection of AKI is greatly deferred in up to 43% of admitted patients, resulting in missed treatment windows.

Subclinical AKI

It is well known that the human kidney plays an important role as a functional reserve, and it is only when more than 50% of the kidney mass is compromised (i.e., GFR decreases by more than 50%) that dysfunction becomes apparent and SCr begins to rise. Because of this, observing changes in SCr may cause the clinical "window of opportunity" for treatment to be missed, especially in the acute stage. It is possible that the clinical "window of opportunity" for treatment will be missed if alterations in SCr are observed. This is especially during the acute tubular necrosis phase, as SCr does not differentiate between the many causes of AKI at this stage. AKI diagnosed only by elevated markers of tubular/glomerular injury is called subclinical AKI, and it is imperative to improve the recognition of subclinical AKI (Haase et al., 2012), when a clinical syndrome characterized by normal clinical SCr levels and normal or mildly decreased GFR occurs. Preclinical studies have repeatedly demonstrated that untreated acute tubular injury can lead to progression of AKI to chronic kidney injury (CKD), a finding that has been confirmed in patients with long-term follow-up AKI, and data from experimental and clinical studies have now established the role of tubular injury markers and demonstrated that these biomarkers can diagnose AKI early in the absence of other signals and clinical symptoms. This observation has also been validated in individuals with AKI who have been followed for a long time (Jones et al., 2012). Markers of renal tubular injury, particularly elevated levels of NGAL and KIM-1, which are associated with the transition from AKI to CKD, are specific indicators of high risk of progression to CKD. The study comprised of 1,635 patients from 3 centers (Nickolas et al., 2012), who were divided based on their blood creatinine level, KIM-1 level (>2.8 ng/ml) and NGAL level (>104 ng/ml). In the absence of acute renal function loss, a considerable proportion of patients (15%–20%) exhibited elevated markers of tubular injury, which increased the risk of death or requiring RRT by 2–3 times compared to patients without elevated levels of blood creatinine and markers of tubular injury (Haase et al., 2011). When patients have significant renal function loss, tubular injury marker levels can be tested to provide a prognostic assessment, with patients with two elevated tubular injury marker levels (NGAL, KIM-1) and elevated blood creatinine levels having the worst prognosis, with a 15.5%–17.5% mortality rate or need for RRT. Furthermore, some research suggests that tubular injury markers may fluctuate with time and length of injury, and that their levels represent the extent of injury. Based on these findings, ADQI proposes that the diagnosis of AKI be reformulated to include not only markers of renal function (e.g., changes in SCr and UO), but also markers of tubular injury such as NGAL, KIM-1, IL-18, and L-FABP (e.g., Figure 1), which, when combined, would not only better characterize the phenotype of AKI and enhance the diagnostic accuracy, but would also detect kidney damage prior to the rise of

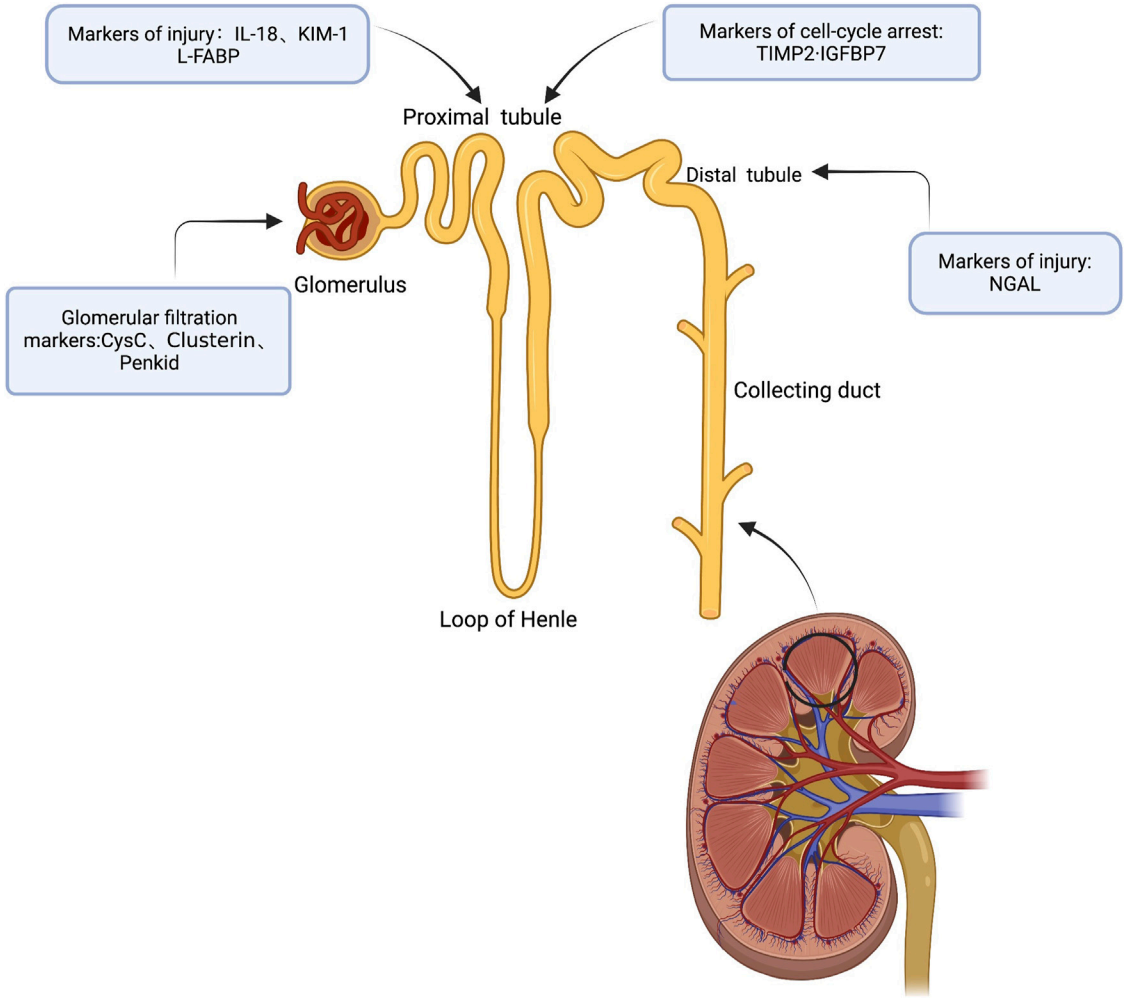

FIGURE 1
Subclinical AKI biomarkers are labeled according to anatomic location and/or production mechanism (Created with BioRender).

creatinine, which leads to the identification and treatment of subclinical AKI (Ostermann et al., 2020). In this study, we evaluate the most frequently investigated subclinical AKI biomarkers that are likely to be employed in clinical practice. We also summarize their performance in the diagnosis of subclinical AKI, as well as their current limits and future directions in clinical practice.

Subclinical AKI biomarkers

CysC

CysC is a cysteine protease inhibitor with a small molecular weight of 13 kDa, which allows it to be freely filtered in the glomerulus, disseminated on the cell surface, and about to completely reabsorbed and catabolized by proximal tubular cells (Yong et al., 2011). Given that the kidney is the sole organ capable of clearing CysC, it is a more accurate marker for determining glomerular filtration rate (GFR) than creatinine (Bhosale and Kulkarni, 2020). Compared to creatinine, CysC levels are not changed by age, sex, or muscle mass (Pozzoli et al., 2018). CysC performed substantially better than SCr and BUN in the mouse model of sepsis, with a three-fold increase in CysC at 3 h post sepsis compared to baseline (0 h) CysC. At this stage, the values of both SCr and BUN were twice as low as the baseline (Leelahavanichkul et al., 2014). It was discovered that an increase in CysC indicates tubular injury or damage and predicts AKI 24–48 h before an increase in SCr, suggesting that CysC can identify subclinical renal injury, in which renal injury occurs without a deterioration in renal function (Fang et al., 2018). In crucially ill patients, it is crucial to analyze patients with subclinical AKI who have renal damage but typical SCr levels. It is attainable to avoid the enlargement and growth of acute renal

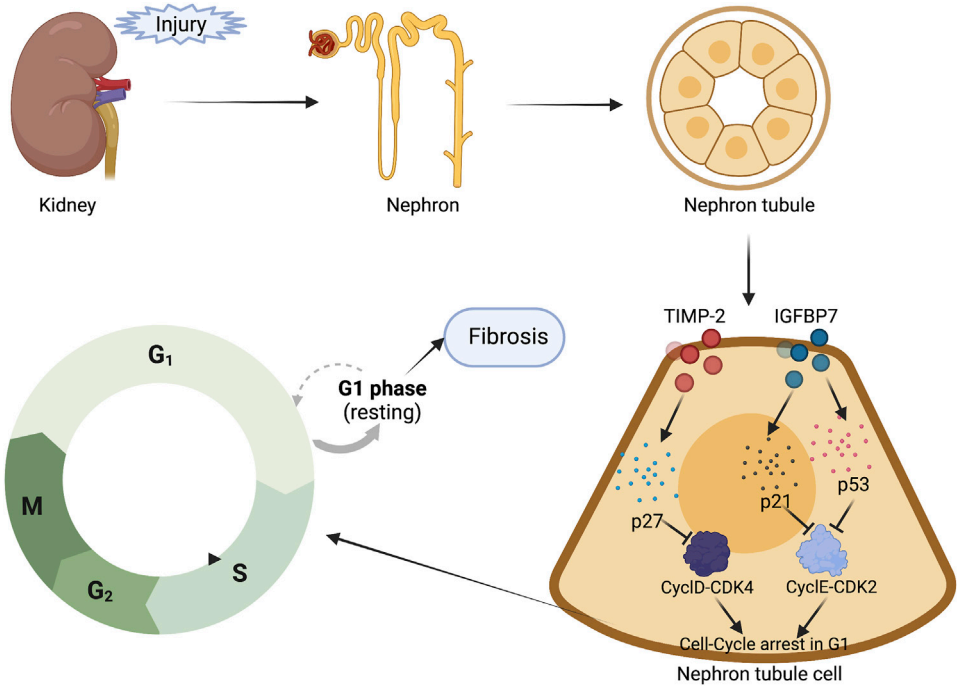

FIGURE 2
G1 Cell cycle arrest markers: TIMP-2 and IGFBP7(Created with BioRender).

insufficiency if a timely diagnosis is made and preventative measures are adopted. Among the early diagnostic markers, CysC is a promising indicator. A recent study revealed that ICU patients who presented with elevated CysC levels at admission were more likely to develop AKI during their hospitalization. ROC curve analysis revealed that the AUC of Cys-C for predicting AKI was 0.67. With a sensitivity of 63% and a specificity of 66%, 0.94 mg/L was established to be the Cys-C threshold level (Gaygısız et al., 2016). Fang et al. discovered that CysC detects subclinical AKI in critically ill infants and children with an AUC of 0.72 and a sensitivity of 61.1% and specificity of 76.0% for peak uCysC, strengthening the support link between high CysC and AKI. CysC levels are a delicate indicator of subclinical AKI, and CysC-positive subclinical AKI is related to bad clinical results in crucially ill infants and children. Additional randomized and controlled clinical tests are required to determine if treating subclinical AKI improves clinical results in this populace (Fang et al., 2018). In a study of patients over 60 years old, Dalboni et al. found a contrary conclusion that Cys-C did not predict AKI, but greater Cys-C levels were an independent risk factor for death (Dalboni et al., 2013). Several investigations have found that Cys-C levels can alter as a result of conditions other than renal filtration (e.g., use of glucocorticoids, thyroid hormones, and systemic inflammation), however, acute inflammation, especially that induced by sepsis, has no effect on it (Manetti et al., 2005; Stevens et al., 2009). These studies have significant limitations, and the idea of CysC-positive subclinical AKI has yet to be verified in other case mixes, particularly in patients with high disease severity scores. More multicenter prospective studies are also needed to corroborate CysC's age-related reference value (Fang et al., 2018).

KIM-1

KIM-1 is a 38.7 kDa type I transmembrane glycoprotein (Oh, 2020) with immunoglobulin and mucin structural domains (Ichimura et al., 1998). In recent years, KIM-1 has been utilized as a sensitive indicator for the early detection of renal tubular injury with distinct advantages: in normal renal tissues, it is hardly expressed, however, its expression is significantly increased in mouse models of ischemia-reperfusion injury and drug-induced AKI, and KIM-1 is upregulation primarily in rodent and human S3 segments, where it is inserted into the apical membrane of the proximal tubule and remains in epithelial cells present until recovery (Vaidya et al., 2008). Furthermore, it is highly specific, particularly for ischemic or nephrotoxic AKI, rarely expressed in other organs, unaffected by pre-renal azotemia, urinary tract infections and chronic kidney disease (Assadi and Sharbaf, 2019). Moreover, KIM-1 has a protein hydrolysis area. It is easily detectable in urine, where it

increases within the first hour following tubular toxicity or ischemic injury, far before serum creatinine (Lei et al., 2018; Pietrukaniec et al., 2020). Urinary KIM-1 can be used to differentiate patients with acute tubular necrosis from those with non-acute tubular necrosis, and measuring uKIM-1 levels in patients without AKI can serve as a marker of early kidney injury and predict adverse clinical outcomes, such as dialysis requirements and mortality (Kashani et al., 2017). KIM-1 can detect patients with subclinical AKI, who are at a higher risk of unfavorable consequences (Pietrukaniec et al., 2020). KIM-1 in urine has the potential to be a helpful biomarker for subclinical AKI associated with obstruction, according to Olvera-Posada et al. The significance lies not only in the ability to identify an obstruction marker in urine but also in the ability to quantify the grade of renal impairment to modify the treatment paradigm (Olvera-Posada et al., 2017). In a comparison of three promising urinary AKI biomarkers, KIM-1, NGAL, and IL-18, urinary KIM-1 had the maximal diagnostic performance in the initial diagnosis of AKI in children with hypovolemia, cardiogenic or aseptic shock before alterations in SCr became apparent (Assadi and Sharbaf, 2019). Urinary KIM-1 levels correspond with the amount of renal tissue injury and can be used to predict adverse renal outcomes in patients with acute tubular injury (ATI). Furthermore, correlating uKIM-1 and sKIM-1 can enhance the sensitivity and specificity for the detection of serious ATI, allowing clinicians to treat earlier, particularly in patients who are highly suspected of having ATI but are not appropriate for kidney biopsy (Cai et al., 2019). KIM-1 is approved in North America for preclinical monitoring of nephrotoxicity in drug development studies (Moledina et al., 2017). In a recent study, patients with mild and moderate COVID-19 who did not meet the requirement for AKI presented with findings of proximal tubular injury, particular non-albuminuria, and elevated uKIM-1 levels, indicating the emergence of subclinical AKI, in this study, the AUC was 0.830, with a sensitivity of 77% and a specificity of 76% (Yasar et al., 2022). However, some studies have found that comorbidities such as diabetes, hypertension, and atherosclerotic cerebral ischemia can have a significant impact on uKIM-1 concentrations. KIM-1 value is also susceptible to inflammatory diseases. All of these factors would reduce the specificity of AKI prediction.

NGAL

NGAL is a 25 kDa protein that belongs to the lipocalin superfamily. Human NGAL was initially recognized from the supernatant of activated neutrophils (Kjeldsen et al., 1993) that are usually the primary cellular source of circulating NGAL. Physiologically, NGAL binds to iron-siderophore complexes, limiting bacterial iron uptake, and by sequestering iron-siderophore complexes, NGAL intercede the mitogenic impact of epidermal growth factor receptor (EGFR) signaling (Flo et al., 2004; Barasch et al., 2016). EGFR activation is related with stimulation of hypoxia-inducible factor-1α (HIF-1α) and NGAL expression, resulting in increased cellular proliferation, cytogenesis, and renal injury (Viau et al., 2010). NGAL is conveyed at reduce levels in different cell types, including prostate, uterus, salivary gland, trachea, lung, stomach, kidney, and colon (Friedl et al., 1999). It is the most extremely researched AKI biomarker, which is reabsorbed by the proximal tubules and released by the damaged distal tubules in the setting of acute tubular injury and can be identified within hours of tubular injury, even in lack of functional AKI (Lupu et al., 2021). NGAL was discovered to be one of the fastest growing genes in the kidney early after tubular injury, particularly in the distal tubular segment in transcriptome analysis studies in rodent models, and there is evidence that it may be the earliest known marker of renal injury. In mice, NGAL levels in the urine are significantly higher within 2 h after renal ischemia-reperfusion injury (Zhang and Parikh, 2019), while in humans, elevated NGAL levels can increase within 3 h after tubular injury and peak around 6–12 h, depending on the severity of the injury (Parikh et al., 2011). According to new research, elevated NGAL in urine can detect AKI as early as 2 h (Karademir et al., 2016). Haase et al. discovered that high NGAL levels were related with poor results even in the lack of diagnostic SCr elevations in a pooled data analysis of 10 studies of patients hospitalized to ICU (Casas-Aparicio et al., 2022). Urine NGAL was shown to detect NSAID-mediated renal tubular injury in the initial phase of renal injury in a cohort study of children with congenital heart disease who underwent cardiopulmonary bypass (CPB), and urine NGAL had good diagnostic accuracy in identifying children receiving NSAIDs, with an AUC of 0.95–0.96 at 24–48 h after administration of NSAIDs. Continuous NGAL monitoring in children using NSAIDs would allow doctors to identify subclinical AKI and its progression as depicted by elevated NGAL levels and would offer a therapeutic time window to prevent AKI and functional impairment (Nehus et al., 2017). NGAL is by far the most extensively characterized and researched biomarker of AKI in patients undergoing cardiac surgery, and it is also the focus of current research. NGAL demonstrated good diagnostic ability in predicting pediatric (AUC:0.96) (Dent et al., 2007) and adult cardiac surgery (AUC:0.72) (Ho et al., 2015). Patients are frequently administered diuretics, angiotensin-converting enzyme inhibitors, and antibiotics as needed following cardiac surgery (CSA), which may exacerbate the identified acute tubular injury. CSA-NGAL score can help avoid this from happening. Preoperative risk assessment can be aided by baseline measurements, and an elevated NGAL value may even suggest delaying surgery until renal function can be maximized and additional injury avoided. The CSA-NGAL score, in addition to the functional score of AKI, can be used in prospective studies of patients having cardiac operations to identify subclinical AKI early and to take relevant interventions to prevent further injury

or the development of functional AKI (de Geus et al., 2016). The performance of NGAL has also been studied in other contexts, including critically ill patients (AUC: 0.80) (de Geus et al., 2011), emergency department patients (AUC: 0.95) (Nickolas et al., 2008), and renal transplant patients (AUC: 0.82) (Pajek et al., 2014). In a cohort analysis of COVID-19 patients, urinary NGAL >150 ng/ml anticipated the duration, diagnosis, and severity of AKI and acute tubular damage, and admission, dialysis, shock, and death in patients with acute COVID-19 (Xu et al., 2021). NGAL was also discovered to be an independent risk factor for COVID-19 patients (He et al., 2021). In another cohort study, those with NGAL ≥45 ng/ml had a substantially shorter time to AKI than those with <45 ng/ml, but NGAL was not a risk factor for AKI during admission, and NGAL performed considerably better on day 7 than throughout hospitalization, implying that NGAL has a limited time window for predicting AKI and that higher NGAL thresholds appear to help predict the progression of AKI rather than the onset of AKI (Casas-Aparicio et al., 2022). Because NGAL threshold value is still controversial, including NGAL in clinical prediction models to improve disease identification requires additional research.

IL-18

IL-18 is an interleukin-1 family pro-inflammatory cytokine generated by monocytes/macrophages and other antigen-presenting cells. IL-18 functions as an inactive precursor and is synthesized by a variety of tissues, such as monocytes, macrophages, proximal tubular epithelial cells, and intercalated duct cells of collecting ducts (Gauer et al., 2007). It is found intracellularly, and it is converted to the active form by caspase-1 (Schrezenmeier et al., 2017). IL-18 is an inflammatory mediator that is increased in numerous endogenous inflammatory processes, and its concentration is elevated in serum during sepsis, joint inflammation, inflammatory bowel disease syndrome, liver inflammation, and lupus (Beker et al., 2018). It is created in response to ischemia in different organs, including the kidney, heart, and brain. IL-18 levels in the kidney are enhanced in the presence of ischemia in animal experiments, and it has been demonstrated to be a mediator of acute tubular injury, inducing tubular necrosis through mediating ischemia-reperfusion injury and infiltration of neutrophils and monocytes into the renal parenchyma (Melnikov et al., 2001). IL-18 levels begin to rise roughly 6 h after kidney damage and peak between 12–18 h. Surprisingly, mice lacking IL-18 are protected from AKI caused by ischemia-reperfusion injury. Urinary IL-18 levels were considerably greater in patients with acute tubular necrosis in comparison to healthy subjects in subsequent trials (Parikh et al., 2004). According to a current systematic analysis of 11 studies in 2,796 patients, IL-18 is considered a promising biomarker with some diagnostic accuracy in the initial diagnosis of AKI, the AUC was 0.77 (95%CI 0.71–0.83) (Lin et al., 2015). In a study of AKI after CPB, urinary IL-18 levels were found to be more diagnostic than SCr and urinary NGAL in early diagnosis of AKI in clinical practice. At 2 h after CPB, the AUC was 83.25%, and when the threshold was set at 100 μg/L, the sensitivity and specificity were 90.91 and 93.83%, respectively (Wang et al., 2017). Isocyclophosphamide is a common nephrotoxic chemotherapeutic agent, and urinary IL-18 has to promise as a diagnostic test for early AKI in children treated with isocyclophosphamide and may play a possible role in drug toxicity monitoring (Sterling et al., 2017). As a result, it is an appealing target for biomarker-directed therapy for AKI, and more research on anti-IL-18 therapy is pending. Only a few clinical trials appear to have investigated the use of IL-18 as a biomarker for AKI (Lin et al., 2015). These studies have revealed acceptable outcomes in pediatric AKI patients following cardiac surgery (AUC:0.82) (Krawczeski et al., 2011; Zheng et al., 2013). Other studies, however, have found that IL-18 is not a strong predictor of AKI in ICU(AUC:0.59) or emergency department populations (AUC:0.64) (Nickolas et al., 2012; Nisula et al., 2015). According to a current systematic analysis, these inconsistencies may be resulted from the absence of clear consensus on the appropriate cutoff level of IL-18 for AKI prediction (Lin et al., 2015).

L-FABP

L-FABP is a 14 kDa protein that belongs to the fatty acid-binding protein (FABP) family (Tan et al., 2002). It was discovered in the liver, where serum L-FABP levels are elevated in liver dysfunction (Pelsers et al., 2005), and it is also expressed in the kidney, intestine, pancreas, lung, and stomach. L-FABP has a high affinity and binding capacity for long-chain fatty acid oxidation products, suggesting that it could be a potent endogenous antioxidant (Ek-Von Mentzer et al., 2001). The transcriptional regulatory region upstream of the human L-FABP gene comprise transcription aspect confining areas related to ischemia and lipid metabolism, including hypoxia-inducible factor-1 (HIF-1), hepatocyte nuclear factor (HNF-1, HNF-4) and peroxisomal response element (PPRE), and gene expression is activated in response to ischemia and oxidative stress (Divine et al., 2003; Schachtrup et al., 2004). Furthermore, L-FABP binds to fatty acids and transports them to mitochondria or peroxisomes, participates in intracellular fatty acid homeostasis, and is one of the fundamental regulators of free fatty acid (FFA) stability *in vivo* (Martin et al., 2005). Excessive aggregation of FFA in the proximal tubules of the kidney, as well as its oxidation and peroxidation products, can cause enhanced tubular damage and high expression of L-FABP in renal tubular epithelial cells under stressful conditions (McMahon and Murray, 2010). Moreover, elevated levels of L-FABP in urine and plasma have been linked to the degree of renal injury

(Kokkoris et al., 2013). In a cisplatin-induced kidney damage model in mice, urinary L-FABP levels rose before creatinine level elevation over 72 h. Noiriet revealed that urinary L-FABP increased 1 h after ischemia and that urinary L-FABP was superior to BUN and urinary NAG in initial and correct diagnosis of acute tubular necrosis in distinct AKI animal models (Noiri et al., 2009). Urinary L-FABP levels were substantially changed after cardiac catheterization in a study on contrast-induced AKI after cardiac catheterization in cardiac patients, but urinary NGAL, IL-18, and KIM-1 levels were not substantially changed, so this research determined that urinary L-FABP could be one of the helpful markers for detecting subclinical AKI due to contrast after cardiac catheterization (Hwang et al., 2014). Urinary L-FABP concentration was discovered by Portilla et al. to be utilized as an early and sensitive predictor of AKI complicating pediatric postoperative cardiac surgery, a 24-fold increase in urinary L-FABP at 4 h postoperatively, an AUC of 0.810, sensitivity of 0.714 and specificity of 0.684 (Portilla et al., 2008). Tang et al. (2017) also showed that urinary L-FABP was considerably elevated early in AKI (2 h postoperatively); utilizing SCr to diagnose AKI requires waiting until 48–72 h postoperatively, whereas applying 2-h postoperative urinary L-FABP for prediction. The utilization of Urine L-FABP at 2 h postoperatively can greatly advance the diagnosis of AKI. In predicting AKI, the AUCs of 2 and 6 h postoperative urinary L-FABP were 0.921 and 0.896, respectively. Meanwhile, urine samples were simple to collect and analyze, implying that elevated urinary L-FABP levels in the early postoperative period could better predict the occurrence of AKI. The combined application of urinary L-FABP and NGAL at 2 and 6 h postoperative cardiac surgery predicted the occurrence of AKI with AUC of 0.942 and 0.929, respectively, indicating that the combined test can more accurately predict the AKI's occurrence and has a greater clinical value in the early diagnosis of AKI after cardiac surgery in children. Urine L-FABP has also demonstrated good performance in predicting AKI after cardiac surgery in adults, AUC of 0.720, and the application of urine L-FABP/creatinine ratio can improve urine L-FABP discrimination even more. Related research has also demonstrated that using extracorporeal circulation (CPB) time can help recognize people at high risk of AKI in cardiovascular surgery. CPB time is firstly used to assess the risk of postoperative AKI, afterwards, urinary L-FABP or urinary L-FABP/creatinine ratio was used to predict and diagnose AKI early, with urinary L-FABP at 16–18 h demonstrating improved discrimination with an AUC of 0.742, enabling more cost-effective and reliable risk identification than utilizing urinary L-FABP tests (Lee et al., 2021). In addition, urinary L-FABP levels at admission are a powerful predictor of long-term negative results in medical cardiac intensive care unit (CICU) patients. Urinary L-FABP may substantially improve long-term risk stratification in patients hospitalized to the medical CICU when combined with creatinine-defined AKI (Naruse et al., 2020). Moreover, baseline urinary L-FABP levels are a reliable biomarker for predicting AKI in patients with acute decompensated heart failure (ADHF), AUC was 0.930, sensitivity was 94.2%, specificity was 87.0% (Hishikari et al., 2017). However, certain existing renal diseases, including non-diabetic chronic kidney disease, early diabetic nephropathy, polycystic kidney disease, and idiopathic focal glomerulosclerosis, may affect the diagnostic performance of urinary L-FABP. Since L-FABP is conveyed in the liver, urinary L-FABP may lose its specificity for kidney disease when liver disease is also present. To summarize, L-FABP seems to be the best biomarker for the initial prediction of AKI (Cho et al., 2013), but its potential value must be verified in large-scale research and a broader clinical setting.

TIMP-2·IGFBP7

TIMP-2 is a 21 kDa protein with anti-apoptotic and pro-proliferative properties, while IGFBP7 is a 29 kDa protein which acts as an IGF-1 receptor antagonist that causes tumor suppression and regulates cellular aging by inhibiting kinase signaling. Renal tubular cells express and secrete them (Bhosale and Kulkarni, 2020). TIMP-2 and IGFBP7 are both inducers of G1 cell cycle arrest that are produced during the early phases of cellular stress or injury (Cavalcante et al., 2022). Some tumor suppressor proteins such as p27, p53, and p21 are activated and upregulated differently after renal injury (e.g., oxidative stress, toxins, ischemia, sepsis, inflammation, etc.) (Ortega and Heung, 2018), with IGFBP7 directly increasing the expression of p53 and p21, while TIMP-2 enhances the expression of p27. These p-proteins prevent the cell cycle-dependent protease complexes (CyclD-CDK4 and CyclE-CDK2) from supporting the cell cycle progression, leading in transitory G1 cell arrest. This process inhibits cell division and apoptosis, allowing the cell to restore DNA damage and function (as shown in Figure 2) (Barnum and O'Connell, 2014). A prolonged arrest of tubular cells in G1 phase would lead in a senescent cell phenotype and fibrosis (Yang et al., 2010). TIMP-2 and IGFBP7 can signal in an autocrine and paracrine manner to send alarms from the location of injury to other sites (Ortega and Heung, 2018). The consolidation of these two biomarkers has been explored as predictors of AKI and is beneficial in identifying early structural kidney impairment, also known as subclinical kidney injury, which can indicate an increased risk of adverse outcomes. In a laboratory investigation in rats, the combination of TIMP2 and IGFBP7 was more accurate for detecting AKI than either marker alone. TIMP2-IGFBP7 was significantly raised in >10% of patients in the low-risk CI-AKI population, indicating structural kidney injury, while serum creatinine remained silent, thus revealing subclinical CI-AKI (SCI-AKI), according to a study on contrast-induced AKI (CI-AKI). The use

of appropriate biomarkers early in the diagnostic process has the potential to assist clinicians in identifying patients with renal stress and injury for early observation or preventive intervention to restrict the development of AKI (Breglia et al., 2020). A significant proportion of COVID-19 severe illness patients are admitted with subclinical symptoms of renal dysfunction that has not yet constituted AKI. This study discovered that urinary TIMP-2-IGFBP7 ≥0.2 (ng/ml) 2/1000 was a risk factor for AKI, and individuals with higher TIMP-2-IGFBP7 had a significantly shorter time to AKI. TIMP-2-IGFBP7, when combined with clinical information, was an excellent predictor of subclinical AKI in crucially ill COVID-19 patients (AUC: 0.682) (Casas-Aparicio et al. 2022). Meersch et al. measured TIMP2-IGFBP7 concentrations in serial urine samples from 50 patients undergoing cardiac surgery; changes in creatinine and urine volume did not occur until 1–3 days postoperatively, whereas TIMP2-IGFBP7 concentrations began to rise as early as 4 h postoperatively in patients who had AKI, and the 4-h postoperative cutoff value demonstrated positive sensitivity and specificity, with an area under the ROC curve of 0.81 (CI: 0.68–0.93). Furthermore, a decrease in urine [TIMP-2] and [IGFBP-7] at discharge was a strong predictor of renal recovery (Meersch et al., 2014). Oezkur et al. measured TIMP-2-IGFBP-7 in urine samples at baseline, at ICU admission and 24 h following surgery with a cutoff of 0.3. The main endpoint was the occurrence of AKI within 48 h postoperatively. [TIMP-2] x [GFBP-7] values >0.3 were highly linked with the development of AKI (OR 11.8, $p < 0.001$) upon ICU admission, with a sensitivity of 0.60 and specificity of 0.88, whereas measurements before surgery (baseline) were not associated with the risk of AKI (Oezkur et al., 2017). Meersch et al. (2017) carried out a randomized clinical test that early predictive biomarkers like [TIMP-2]x [IGFBP7] identified patients at risk for AKI and preventive treatments were used to reduce AKI occurrence. Early diagnosis of AKI using urine biomarkers after non-cardiac surgery allows for the initiation of renal protective measures, including CRRT, a new approach for assessing renal function in critically ill patients (Clark et al., 2017). Elevated TIMP-2-IGFBP-7 levels are also predictors of negative results in a variety of clinical situations, including dialysis, death, or development to severe AKI in patients with septic shock (AUC: 0.72); AKI in patients following major surgery (AUC: 0.85); and AKI in platinum-treated patients in the ICU (Casas-Aparicio et al., 2022). These findings show that IGFBP-7 and TIMP-2 have powerful diagnostic properties. The US Food and Drug Administration (FDA) has approved TIMP2-IGFBP7 to predict AKI in critically ill adults within 12 h (Guzzi et al., 2019). However, the presence of proteinuria, urinary albumin >125 mg/dl interferes with the test results, and >3,000 mg/dl negates the test results, as does a urinary bilirubin concentration >7.2 g/dl (Vijayan et al., 2016). Therefore, the approval of the new biomarker combination [TIMP-2]-[IGFBP7] represents a significant step forward in the investigation for a reliable and accurate method of identifying early kidney injury. Early kidney disease interventions will be critical in translating AKI biomarkers advances into major improvements in clinical outcomes. Additional trials are required to study the function of this biomarker in preventative efforts and interventional trials to evaluate its efficacy in enhancing AKI results.

Other novel biomarkers

Clusterin

Clusterin is a 75–80 kDa molecular weight heterodimeric glycoprotein. Clusterin is only found in trace amounts in normal kidneys, primarily in the intima of the renal arteries and renal tubules. Clusterin expression increases in acute kidney injury, mostly demonstrating anti-apoptotic effects, and is related with lipid utilization, cell aggregation and adhesion. Clusterin has been found to suppress apoptosis in human renal proximal tubular epithelial HK-2 cells via an extracellular pathway, and to protect renal cells (Wang et al., 2016). Its expression is decreased during glomerular lesions, which exacerbates post-ischemic renal injury and proteinuria. After the ischemia-reperfusion injury, mice lacking Clusterin demonstrate the development of renal inflammation and fibrosis (Guo et al., 2016). Clusterin was expressed in dedifferentiated renal tubular epithelial cells, and Clusterin levels considerably raised in the kidney and urine in an early kidney injury model, according to Vaidya et al.(2008) Gentamicin administration to Lewis mice resulted in increased urinary NAG and Clusterin on day 4, as well as a 10-, 116-, and 3-fold rise in renal tissue, urinary, and serum Clusterin on day 9, respectively (Aulitzky et al., 1992). mRNA expression of renal Clusterin was raised 8.5-fold in mice with renal lesions compared to controls, consistent with increased serum creatinine, and urinary levels correlated with the degree of toxic renal damage (Hidaka et al., 2002). Clusterin and KIM-1 are two of the earliest markers of proximal tubular injury, with levels rising within 1 h of injury, far before serum creatinine. In contrast to CysC and KIM-1, Clusterin predicts drug-induced AKI in adults well (AUC:0.86) (Da et al., 2019). Clusterin was found to be superior to conventional indices for the diagnosis of proximal tubular injury by Dieterle et al., indicating a high diagnostic value not only in severe acute kidney injury. It can also be noticed in early stages, when there is no histopathological evidence yet, showing that it can reflect early and mild lesions (Dieterle et al., 2010). Regarding the localization of urinary Clusterin injury, most research has demonstrated that Clusterin expression is higher in tubular injury but not in glomerular injury, implying that the amount of Clusterin may be quantified to detect whether the injury occurred in the tubules or glomeruli (Hidaka et al., 2002). However, in a recent study, Clusterin outperformed renal function indicators targeting both

glomeruli and tubules in the assessment of subclinical AKI, indicating that it appears to be a promising marker of renal injury, covering both tubular and glomerular injury (Musiał et al., 2020), and thus Clusterin remains relevant for the detection of not only tubular but also glomerular injury significance. Clusterin has received little attention in human, and its ability to be a marker of dual renal function and renal injury in a wider patient population has yet to be determined.

Proenkephalin a 119-159(Penkid)

Proenkephalin A 119–159(Penkid) is a 5 kDa peptide that is identical to the precursors of met-enkephalins and leu-enkephalins and is considered to be an alternative marker of the unstable endogenous opioid peptide enkephalins (Hollinger et al., 2018). Enkephalins participate in a variety of physiological processes through binding to opioid receptors, including the γ-opioid receptor, which is expressed in a number of tissues but is especially dense in renal tissues (Denning et al., 2008). Penkid has a long *in vivo* half-life, is stable after collection, is not easily catabolized, and its levels are unaffected by age or gender. Furthermore, it is not a plasma-bound protein and is only filtered solely in the glomerulus (Lima et al., 2022). Penkid plasma concentrations have been observed to correlate positively and inversely with measured glomerular filtration rate (GFR) (Beunders et al., 2020), and high Penkid values appear to represent a more important risk status than low eGFR values, as Penkid predicts 28-days mortality but eGFR does not, and it is therefore considered to be a biomarker of glomerular filtration injury or a biomarker of renal function. Penkid was found to identify AKI 48 h before serum creatinine, and its specificity remained high in the context of major inflammation-driven sepsis, since Penkid remained at very low concentrations in patients with sepsis who did not have renal failure (Rosenqvist et al., 2019). Penkid levels raised with increasing severity of sepsis in Kim et al. (2017) cohort study of 167 patients, with a cut-off value of 154.5 pmol/L with an AUC of 0.73 for the diagnosis of AKI, and Penkid was found to be significantly higher in patients with severe AKI in Camila Lima et al., 2022 study before liver transplantation. Patients had significantly higher AUC of 0.69 (CI 0.54–0.83), cut-off value of 55.30 pmol/L, sensitivity of 0.86, specificity of 0.52 and accuracy of 0.75, and at 48 h after liver transplantation, the performance of Penkid in determining severe AKI was unchanged with an AUC of 0.83 (CI 0.72–0.94), a cut-off value of 119.05 pmol/L, a sensitivity of 0.81, a specificity of 0.90 and an accuracy of 0.84 (Lima et al., 2022). Moreover, Penkid has shown promising results in monitoring renal function in acute patients, especially those with sepsis. Penkid has added value in monitoring renal function in patients with acute heart failure, in addition to reflecting cardiorenal state following acute myocardial infarction and predicting AKI after cardiac surgery (Hollinger et al., 2018). Penkid and TIMP2-IGFBP7 concentrations were measured at the time of ICU patient admission and showed a correlation with AKI severity, confirming a substantial association of PenKid as a filtration marker with AKI (AUC:0.668). When investigating renal replacement therapy (RRT) as an outcome parameter, in our standard ICU population (n = 60), elevated PenKid levels predicted RRT requirement more accurately (AUC:0.778) than elevated TIMP2-IGFBP7 (AUC: 0.678) levels (Gayat et al., 2018). Plasma Penkid concentrations on admission are related to an increased risk of death in AKI and burn patients, and predict 90-days mortality, with Penkid having stronger prognostic value than SCr and SOFA. Patients with subclinical AKI (no diagnosis of AKI but with elevated Penkid) have a higher risk of death than those with low Penkid concentrations (i.e., non-subclinical AKI). Penkid provides clinical relevance in the detection of subclinical AKI (Dépret et al., 2020). Detection of subclinical AKI using PenKid provides better phenotypic analysis of patients who do not meet the current definition of AKI. PenKid's potential utility is evidence of prognostic impact connected with its level, which would transcend the constraints of the current definition of AKI. Subclinical AKI patients have a greater fatality rate than non-subclinical AKI patients, approaching that of AKI patients. PenKid improves the prognosis of patients who were previously categorized as non-AKI (Dépret et al., 2020). However, there have been fewer studies comparing PenKid to other biomarkers, and it has to be seen whether the combination with other indicators can further improve the characterization and definition of sub-AKI and its association with prognosis.

Clinical implementation of AKI biomarkers

Although progress has been made in identifying AKI biomarkers, their use in clinical practice has not been widely accepted, and it was recommended at the 23rd ADQI Consensus Conference that injury and functional biomarkers can be combined with clinical information to improve the diagnostic performance of AKI, identify different pathophysiological processes, differentiate the etiology of AKI, and assess AKI severity. The identification of particular kidney injury biomarkers has allowed for a more accurate definition of pathophysiology, site, mechanism, and severity of injury, allowing for a more targeted and individualized treatment plan for each AKI patient. Validated biomarkers can predict the development or progression of AKI and may provide opportunities for intervention (Ostermann et al., 2020). Trials have demonstrated that timely initiation of a preventive strategy, TIMP-2-IGFBP7, after renal injury in patients with positive

TABLE 1 Comparison of characteristics of acute kidney injury biomarkers.

Biomarker	Characteristics/ functions	Expression time	Animal research	AUCs of AKI prediction	Sample collections	Limitations
CysC	A cysteine protease inhibitor with a molecular weight of 13 KDa that is freely filtered in the glomerulus and almost completely reabsorbed in the proximal tubule	12–24 h	In the mouse model of sepsis, CysC performed significantly better than SCr and BUN, with a three-fold increase in CysC at 3 h post sepsis compared to baseline (0 h) CysC	0.67 0.72	ICU Gaygısız et al. (2016) critically ill infants and children Fang et al. (2018)	Cys-C levels can alter as a result of conditions other than renal filtration (e.g.,use of glucocorticoids, thyroid hormones, and systemic inflammation)
KIM-1	A 38.7 KDa type I transmembrane glycoprotein with immunoglobulin and mucin structural domains	1–12 h	KIM-1 shows upregulation mainly in rodent and human S3 segments, inserts into the apical membrane of the proximal tubule, and persists in the epithelium until recovery	0.83	patients with mild and moderate COVID-19 Yasar et al. (2022)	Vulnerability to diabetes, hypertension and atherosclerotic cerebral ischemia, and inflammatory diseases
NGAL	A 25 KDa protein, a member of the lipocalin superfamily, binds to iron-siderophore complexes, thereby limiting iron uptake by bacteria and exerting a bactericidal effect on the innate immune system	1–12 h	In a transcriptome analysis study in a rodent model, NGAL was found to be one of the fastest-rising genes in the kidney early after tubular injury, especially in the distal tubular segment, and NGAL levels in the urine were significantly elevated within 2 h after ischemia-reperfusion injury in the murine kidney	0.95–0.96 0.96 0.72 0.80 0.95 0.77	Children with congenital heart disease on NSAIDs after CPB Nehus et al. (2017) Pediatric Cardiac Surgery Dent et al. (2007) Adult Cardiac Surgery Ho et al. (2015) critically ill patients de Geus et al. (2011) emergency department patients Nickolas et al. (2008) renal transplant patients Pajek et al. (2014)	Its threshold value is controversial
IL-18	an interleukin-1 family pro-inflammatory cytokine generated by monocytes/ macrophages and other antigen-presenting cells	1–12 h	IL-18-deficient mice are protected from AKI induced by ischemia-reperfusion injury	0.77 0.8325 0.82 0.59 0.64	systematic analysis of 11 studies in 2,796 patients Lin et al. (2015) CPB Wang et al. (2017) Pediatric Cardiac Surgery Krawczeski et al. (2011); Zheng et al. (2013) ICU Nickolas et al. (2012); Nisula et al. (2015) emergency department patients Nickolas et al. (2012); Nisula et al. (2015)	Lack of suitable cut-off values
L-FABP	It is a 14 kDa protein belonging to the fatty acid-binding protein (FABP) family, a potent endogenous antioxidant and one of the key regulators of free fatty	1–12 h	In a cisplatin-induced kidney injury model in mice, elevation of urinary L-FABP levels preceded creatinine elevation over 72 h	0.810 0.720 0.742	Pediatric Cardiac Surgery Portilla et al. (2008) Adult Cardiac Surgery Lee et al. (2021) CPB Lee et al. (2021)	Urinary L-FABP may lose its specificity for renal disease in early diabetic nephropathy, non-diabetic chronic kidney disease, polycystic kidney disease

(Continued on following page)

TABLE 1 (*Continued*) Comparison of characteristics of acute kidney injury biomarkers.

Biomarker	Characteristics/ functions	Expression time	Animal research	AUCs of AKI prediction	Sample collections	Limitations
	acid (FFA) stability in the body			0.930	ADHF Lee et al. (2021)	and idiopathic focal glomerulosclerosis, when liver disease is also present
TIMP2·IGFBP7	TIMP-2, a 21 KDa protein with anti-apoptotic and proliferative properties, and IGFBP7, a 29 KDa protein and IGF-1 receptor antagonist, cause tumor suppression and regulate cellular aging by inhibiting kinase signaling.TIMP-2 and IGFBP7 are both inducers of G1 cell cycle arrest	1–12 h	In an experimental study in rats, the combination of TIMP2 and IGFBP7 was more accurate for the diagnosis of AKI than each marker alone	0.682 0.81 0.72 0.85	ICU in COVID-19 Casas-Aparicio et al. (2022) Cardiac Surgery Meersch et al. (2014) Sepsis Casas-Aparicio et al. (2022) major surgery Casas-Aparicio et al. (2022)	The presence of proteinuria in the patient, urinary albumin >125 mg/dl will interfere with the test results, and >3000 mg/dl will invalidate the test results, as will the concentration of urinary bilirubin >7.2 g/dl
Clusterin	It is a heterodimeric glycoprotein with a molecular weight of 75–80 kDa, which exhibits anti-apoptotic effects and is associated with lipid utilization, cell aggregation and adhesion	1–12 h	In mice with renal lesions, mRNA expression of renal Clusterin was increased 8.5 times more than in controls, consistent with increased serum creatinine, and urinary levels correlated with the degree of toxic renal damage	0.86	Medicated AKI in adults Da et al. (2019)	There are relatively few human studies, and its ability to be a marker of dual kidney function and kidney injury remains to be determined in studies in larger patient populations
PenKid	A 5 kDa peptide that is identical to the precursors of met-enkephalins and leu-enkephalins and is considered to be an alternative marker of the unstable endogenous opioid peptide enkephalins	1–12 h	—	0.73 0.69 0.83 0.668	Sepsis Kim et al. (2017) Pre-operative liver Transplantation Lima et al. (2022) Post liver transplantation Lima et al. (2022) ICU Gayat et al. (2018)	There are fewer studies related to the comparison of PenKid with other biomarkers, while it remains to be explored whether the combination with other markers can further improve the definition of sub-AKI and its association with prognosis

stress biomarkers is helpful in preventing AKI. The incidence of AKI was lowered by 17% 72 h later. To improve the process of care and patient outcomes, it is also recommended to integrate clinical assessment and validated biomarkers to triage patients and optimize the timing and type of intervention. Negative outcomes are also valuable. For example, critically ill patients with oliguria and urinary TIMP-2-IGFBP7 levels less than 0.3 (ng/mL)2/1000 had no increased risk of developing more severe AKI (Ostermann et al., 2020).

Conclusion

The need to include markers of injury in AKI risk assessment is becoming more apparent, many biomarkers have been explored for their predictive value in a range of conditions, each with its unique characteristics (Table 1), and several novel biomarkers have been developed, but for the time being, none are totally specific for AKI. Therefore, it is still difficult to introduce these biomarkers into clinical practice, and the use of creatinine as a diagnostic criterion is erroneous; it does not rule out the potential of subclinical AKI. In addition, some specific markers, such as using L-FABP to predict AKI in patients with underlying metabolic syndrome or non-alcoholic hepatic steatosis, and the use of NGAL in patients with sepsis, may be influenced by specific clinical situations. Studies on AKI biomarkers have revealed significant changes in results based on different clinical situations such as cardiac surgery, sepsis, renal transplantation, and contrast nephropathy (Bennett et al., 2008). For instance, in patients undergoing cardiac surgery, NGAL is an initial AKI biomarker and IL-18 is a mid-stage AKI biomarker. In contrast, in nephropathy, IL-18 is not an important AKI biomarker, and the exact mechanisms by which each biomarker changes in different clinical situations have yet to be well revealed, and it has been

suggested that different clinical situations should identify specific AKI biomarkers to enhance the initial detection and mediation of subclinical AKI. Different AKI biomarkers can indicate different mechanisms of injury and may be able to differentiate particular aspects of renal function (e.g., tubular injury, decreased filtration rate, etc.). NGAL, a distal tubular injury marker, is elevated when tubular cell structure is injured and serves as an early biomarker of a variety of ischemic, septic, or nephrotoxic kidney ailments. IL-18 is created by proximal tubular cells during kidney damage and has shown potential in diagnosing ATI. KIM-1 is conveyed on the apical membrane of proximal tubular cells following kidney damage and is detectable in urine. Given the added diagnostic dimension that the inclusion of biomarkers may bring, it is reasonable to expect biomarkers to suggest particular therapeutic targets for intervention. As a result, future research should concentrate on mechanisms of injury to broaden understanding of AKI phenotypes based on pathophysiology. Enhanced understanding the underlying biological sequence from renal stress to subsequent subclinical or clinical AKI could lead to therapeutic interventions, drug application or suspension, and improved patient prognosis.

Author contributions

CZ: Data collection, manuscript writing. CW: Manuscript editing. LL: Data collection, manuscript writing.

Conflict of interest

The authors declare that the research was conducted in the absence of any commercial or financial relationships that could be construed as a potential conflict of interest.

Publisher's note

References

Assadi, F., and Sharbaf, F. G. (2019). Urine KIM-1 as a potential biomarker of acute renal injury after circulatory collapse in children. *Pediatr. Emerg. Care* 35 (2), 104–107. doi:10.1097/PEC.0000000000000886

Aulitzky, W. K., Schlegel, P. N., Wu, D. F., Cheng, C. Y., Chen, C. L., Li, P. S., et al. (1992). Measurement of urinary clusterin as an index of nephrotoxicity. *Proc. Soc. Exp. Biol. Med.* 199 (1), 93–96. doi:10.3181/00379727-199-43335

Barasch, J., Hollmen, M., Deng, R., Hod, E. A., Rupert, P. B., Abergel, R. J., et al. (2016). Disposal of iron by a mutant form of lipocalin 2. *Nat. Commun.* 7, 12973. doi:10.1038/ncomms12973

Barnum, K. J., and O'Connell, M. J. (2014). Cell cycle regulation by checkpoints. *Methods Mol. Biol.* 1170, 29–40. doi:10.1007/978-1-4939-0888-2_2

Beker, B. M., Corleto, M. G., Fieiras, C., and Musso, C. G. (2018). Novel acute kidney injury biomarkers: Their characteristics, utility and concerns. *Int. Urol. Nephrol.* 50, 705–713. doi:10.1007/s11255-017-1781-x

Bennett, M., Dent, C. L., Ma, Q., Dastrala, S., Grenier, F., Workman, R., et al. (2008). Urine NGAL predicts severity of acute kid-ney injury after cardiac surgery: A prospective study. *Clin. J. Am. Soc. Nephrol.* 3, 665–673. doi:10.2215/CJN.04010907

Beunders, R., van Groenendael, R., Leijte, G. P., Kox, M., and Pickkers, P. (2020). Proenkephalin Compared to Conventional Methods to Assess Kidney Function in Critically Ill Sepsis Patients *Shock* 54 (3), 308–314. doi:10.1097/SHK.0000000000001510

Bhosale, S. J., and Kulkarni, A. P. (2020). Biomarkers in acute kidney injury. *Indian J. Crit. Care Med.* 24 (3), S90–S93. doi:10.5005/jp-journals-10071-23398

Breglia, A., Godi, I., Virzì, G. M., Guglielmetti, G., Iannucci, G., De Cal, M., et al. (2020). Subclinical contrast-induced acute kidney injury in patients undergoing cerebral computed tomography. *Cardiorenal Med.* 10 (2), 125–136. doi:10.1159/000505422

Cai, J., Jiao, X., Luo, W., Chen, J., Xu, X., Fang, Y., et al. (2019). Kidney injury molecule-1 expression predicts structural damage and outcome in histological acute tubular injury. *Ren. Fail.* 41 (1), 80–87. doi:10.1080/0886022X.2019.1578234

Casas-Aparicio, G., Alvarado-de la Barrera, C., Escamilla-Illescas, D., Leon-Rodriguez, I., Del Rio-Estrada, P. M., Calderon-Davila, N., et al. (2022). Role of urinary kidney stress biomarkers for early recognition of subclinical acute kidney injury in critically ill COVID-19 patients. *Biomolecules* 12 (2), 275. doi:10.3390/biom12020275

Cavalcante, C. T. M. B., Cavalcante, M. B., Castello Branco, K. M. P., Chan, T., Maia, I. C. L., Pompeu, R. G., et al. (2022). Biomarkers of acute kidney injury in pediatric cardiac surgery. *Pediatr. Nephrol.* 37 (1), 61–78. doi:10.1007/s00467-021-05094-9

Chen, S. (2013). Retooling the creatinine clearance equation to esti-mate kinetic GFR when the plasma creatinine is changing acutely. *J. Am. Soc. Nephrol.* 24 (6), 877–888. doi:10.1681/ASN.2012070653

Cho, E., Yang, H. N., Jo, S. K., Cho, W. Y., and Kim, H. K. (2013). The role of urinary liver-type fatty acid-binding protein in critically ill patients. *J. Korean Med. Sci.* 28, 100–105. doi:10.3346/jkms.2013.28.1.100

Clark, W. R., Neri, M., Garzotto, F., Ricci, Z., Goldstein, S. L., Ding, X., et al. (2017). The future of critical care: Renal support in 2027. *Crit. Care* 21 (1), 92. doi:10.1186/s13054-017-1665-6

Da, Y., Akalya, K., Murali, T., Vathsala, A., Tan, C.-S., Low, S., et al. (2019). Serial quantification of urinary protein biomarkers to predict drug-induced acute kidney injury. *Curr. Drug Metab.* 20, 656–664. doi:10.2174/1389200220666190711114504

Dalboni, M. A., Beraldo Dde, O., Quinto, B. M., Blaya, R., Narciso, R., Oliveira, M., et al. (2013). Cystatin C atadmission in the intensive care unit predicts mortalityamong elderly patients. *ISRN Nephrol.* 24, 673795. doi:10.5402/2013/673795

de Geus, H. R., Bakker, J., Lesaffre, E. M., and le Noble, J. L. (2011). Neutrophil gelatinase-associated lipocalin at ICU admission predicts for acute kidney injury in adult patients. *Am. J. Respir. Crit. Care Med.* 183, 907–914. doi:10.1164/rccm.200908-1214OC

de Geus, H. R., Ronco, C., Haase, M., Jacob, L., Lewington, A., and Vincent, J. L. (2016). The cardiac surgery-associated neutrophil gelatinase-associated lipocalin (CSA-NGAL) score: A potential tool to monitor acute tubular damage. *J. Thorac. Cardiovasc. Surg.* 151 (6), 1476–1481. doi:10.1016/j.jtcvs.2016.01.037

Denning, G. M., Ackermann, L. W., Barna, T. J., Armstrong, J. G., Stoll, L. L., Weintraub, N. L., et al. (2008). Proenkephalin expression and enkephalin release are widelyobserved in non-neuronal tissues. *Peptides* 29 (1), 83–92. doi:10.1016/j.peptides.2007.11.004

Dent, C. L., Ma, Q., Dastrala, S., Bennett, M., Mitsnefes, M. M., Barasch, J., et al. (2007). Plasma neutrophil gelatinase-associated lipocalin predicts acute kidney injury, morbidity and mortality after pediatric car-diac surgery: A prospective uncontrolled cohort study. *Crit. Care* 11, R127. doi:10.1186/cc6192

Dépret, F., Hollinger, A., Cariou, A., Deye, N., Vieillard-Baron, A., Fournier, M. C., et al. (2020). Incidence and outcome of subclinical acute kidney injury using

penKid in critically ill patients. *Am. J. Respir. Crit. Care Med.* 202 (6), 822–829. doi:10.1164/rccm.201910-1950OC

Dieterle, F., Perentes, E., Cordier, A., Roth, D. R., Verdes, P., Grenet, O., et al. (2010). Urinary clusterin, cystatin C, beta2-microglobulin and total protein as markers to detect drug-induced kidney injury. *Nat. Biotechnol.* 28 (5), 463–469. doi:10.1038/nbt.1622

Divine, J. K., McCaul, S. P., and Simon, T. C. (2003). HNF-1alpha and endodermal transcription factors cooperatively activate fabpl: MODY3 mutations abrogate cooperativity. *Am. J. Physiol. Gastrointest. Liver Physiol.* 285 (1), G62–G72. doi:10.1152/ajpgi.00074.2003

Ek-Von Mentzer, B. A., Zhang, F., and Hamilton, J. A. (2001). Binding of 13-HODE and 15-HETE to phospholipid bilayers, albumin, and intracellular fatty acid binding proteins. implications for transmembrane and intracellular transport and for protection from lipid peroxidation. *J. Biol. Chem.* 276 (19), 15575–15580. doi:10.1074/jbc.M011623200

Endre, Z. H., Pickering, J. W., and Walker, R. J. (2011). Clearance and beyond: The complementary roles of GFR measurement and injury bio-markers in acute kidney injury (AKI). *Am. J. Physiol. Ren. Physiol.* 301 (4), F697–F707. doi:10.1152/ajprenal.00448.2010

Fang, F., Hu, X., Dai, X., Wang, S., Bai, Z., Chen, J., et al. (2018). Subclinical acute kidney injury is associated with adverse outcomes in critically ill neonates and children. *Crit. Care* 22 (1), 256. doi:10.1186/s13054-018-2193-8

Flo, T. H., Smith, K. D., Sato, S., Rodriguez, D. J., Holmes, M. A., Strong, R. K., et al. (2004). Lipocalin 2 mediates an innate immune response to bacterial infection by sequestrating iron. *Nature* 432 (7019), 917–921. doi:10.1038/nature03104

Friedl, A., Stoesz, S. P., Buckley, P., and Gould, M. N. (1999). Neutrophil gelatinase-associated lipocalin in normal and neoplastic human tissues.Cell type-specific pattern of expression. *Histochem. J.* 31, 433–441. doi:10.1023/a:1003708808934

Gameiro, J., and Lopes, J. A. (2019). Complete blood count in acute kidney injury prediction: A narrative review. *Ann. Intensive Care* 9 (1), 8761–8764. doi:10.1186/s13613-019-0561-4

Gauer, S., Sichler, O., Obermuller, N., Holzmann, Y., Kiss, E., Sobkowiak, E., et al. (2007). IL-18 is expressed in the intercalated cell of human kidney. *Kidney Int.* 72, 1081–1087. doi:10.1038/sj.ki.5002473

Gayat, E., Touchard, C., Hollinger, A., Vieillard-Baron, A., Mebazaa, A., Legrand, M., et al. (2018). Back-to-back comparison of penKID with NephroCheck® to predict acute kidney injury at admission in intensive care unit: A brief report. *Crit. Care* 22 (1), 24. doi:10.1186/s13054-018-1945-9

Gaygısız, Ü., Aydoğdu, M., Badoğlu, M., Boyacı, N., Güllü, Z., and Gürsel, G. (2016). Can admission serum cystatin C level be an early marker subclinical acute kidney injury in critical care patients? *Scand. J. Clin. Lab. Invest.* 76 (2), 143–150. doi:10.3109/00365513.2015.1126854

Guo, J., Guan, Q., Liu, X., Wang, H., Gleave, M. E., Nguan, C. Y. C., et al. (2016). Relationship of clusterin with renalinflammation and fibrosis after the recovery phase of ischemia-reperfusion injury. *BMC Nephrol.* 17, 133. doi:10.1186/s12882-016-0348-x

Guzzi, L. M., Bergler, T., Binnall, B., Engelman, D. T., Forni, L., Germain, M. J., et al. (2019). Clinical use of [TIMP-2] [IGFBP7]biomarker testing to assess risk of acute kidney injury in critical care: Guidancefrom an expert panel. *Crit. Care* 23, 225. doi:10.1186/s13054-019-2504-8

Haase, M., Devarajan, P., Hasse - Fielitz, A., Bellomo, R., Cruz, D. N., Wagener, G., et al. (2011). The outcome of neutrophil gelatinase-associated lipocalin-positive subclinical acute kidney injury: A multicenter pooled analysis of prospective studies. *J. Am. Coll. Cardiol.* 57 (17), 1752–1761. doi:10.1016/j.jacc.2010.11.051

Haase, M., Kellum, J. A., and Ronco, C. (2012). Subclinical AKI-an emerging syndrome with important consequences. *Nat. Rev. Nephrol.* 8 (12), 735–739. doi:10.1038/nrneph.2012.197

He, L., Zhang, Q., Li, Z., Shen, L., Zhang, J., Wang, P., et al. (2021). Incorporation of urinary NeutrophilGelatinase-associated lipocalin and computed tomography quantification to predict acute kidney injury and in-HospitalDeath in COVID-19 patients. *Kidney Dis.* 7, 120–130. doi:10.1159/000511403

Hidaka, S., Kränzlin, B., Gretz, N., and Witzgall, R. (2002). Urinary clusterin levels in the rat correlate with the severity of tubular damage and may help to differentiate between glomerular and tubular injuries. *Cell Tissue Res.* 310 (3), 289–296. doi:10.1007/s00441-002-0629-5

Hishikari, K., Hikita, H., Nakamura, S., Nakagama, S., Mizusawa, M., Yamamoto, T., et al. (2017). Urinary liver-type fatty acid-binding protein level as a predictive biomarker of acute kidney injury in patients with acute decompensated heart failure. *Cardiorenal Med.* 7 (4), 267–275. doi:10.1159/000476002

Ho, J., Tangri, N., Komenda, P., Kaushal, A., Sood, M., Brar, R., et al. (2015). Urinary, plasma, and serum biomarkers' utility for predicting acute kidney injury associated with cardiac surgery in adults: A meta-analysis. *Am. J. Kidney Dis.* 66, 993–1005. doi:10.1053/j.ajkd.2015.06.018

Hollinger, A., Wittebole, X., François, B., Pickkers, P., Antonelli, M., Gayat, E., et al. (2018). Proenkephalin A 119-159 (Penkid) is an early biomarker of septic acute kidney injury: The kidney in sepsis and septic shock (Kid-SSS) study. *Kidney Int. Rep.* 3 (6), 1424–1433. doi:10.1016/j.ekir.2018.08.006

Hwang, Y. J., Hyun, M. C., Choi, B. S., Chun, S. Y., and Cho, M. H. (2014). Acute kidney injury after using contrast during cardiac catheterization in children with heart disease. *J. Korean Med. Sci.* 29 (8), 1102–1107. doi:10.3346/jkms.2014.29.8.1102

Ichimura, T., Bonventre, J. V., Bailly, V., Wei, H., Hession, C. A., Cate, R. L., et al. (1998). Kidney injury molecule-1 (KIM-1), a putative epithelial cell adhesion molecule containing a novel immuno-globulin domain, is up-regulated in renal cells after injury. *J. Biol. Chem.* 273 (7), 4135–4142. doi:10.1074/jbc.273.7.4135

Jones, J., Holmen, J., De Graauw, J., Jovanovich, A., Thornton, S., and Chonchol, M. (2012). Association of complete recovery from acute kidney injury with incident CKD stage 3 and all-cause mortality. *Am. J. Kidney Dis.* 60 (3), 402–408. doi:10.1053/j.ajkd.2012.03.014

Karademir, L. D., Dogruel, F., Kocyigit, I., Yazici, C., Unal, A., Sipahioglu, M. H., et al. (2016). The efficacy of theophylline in preventingcisplatin-related nephrotoxicity in patients with cancer. *Ren. Fail.* 38, 806–814. doi:10.3109/0886022X.2016.1163154

Kashani, K., Cheungpasitporn, W., and Ronco, C. (2017). Biomarkers of acute kidney injury: The pathway from discovery to clinical adoption. *Clin. Chem. Lab. Med.* 55 (8), 1074–1089. doi:10.1515/cclm-2016-0973

Kim, H., Hur, M., Lee, S., Marino, R., Magrini, L., Cardelli, P., et al. (2017). Proenkephalin, neutrophil gelatinase-associated lipocalin, and estimated glomerular filtration rates in patients with sepsis. *Ann. Lab. Med.* 37 (5), 388–397. doi:10.3343/alm.2017.37.5.388

Kjeldsen, L., Johnsen, A. H., Sengelov, H., and Borregaard, N. (1993). Isolation and primary structure of NGAL, a novel protein associated with human neutrophil gelatinase. *J. Biol. Chem.* 268 (14), 10425–10432. doi:10.1016/s0021-9258(18)82217-7

Kokkoris, S., Pipili, C., Grapsa, E., Kyprianou, T., and Nanas, S. (2013). Novel biomarkers of acute kidney injury in theGeneral adult ICU: A review. *Ren. Fail.* 35, 579–591. doi:10.3109/0886022X.2013.773835

Krawczeski, C. D., Goldstein, S. L., Woo, J. G., Wang, Y., Piyaphanee, N., Ma, Q., et al. (2011). Temporal relationship and predictive value of urinary acute kidney injury biomarkers after pediatric cardiopulmonary bypass. *J. Am. Coll. Cardiol.* 58, 2301–2309. doi:10.1016/j.jacc.2011.08.017

Lee, T. H., Lee, C. C., Chen, J. J., Fan, P. C., Tu, Y. R., Yen, C. L., et al. (2021). Assessment of cardiopulmonary bypass duration improves novel biomarker detection for predicting postoperative acute kidney injury after cardiovascular surgery. *J. Clin. Med.* 10 (13), 2741. doi:10.3390/jcm10132741

Leelahavanichkul, A., Souza, A. C., Street, J. M., Hsu, V., Tsuji, T., Doi, K., et al. (2014). Comparison of serum creatinine and serum cystatin C as biomarkers to detect sepsis-induced acute kidney injury and to predict mortality in CD-1 mice. *Am. J. Physiol. Ren. Physiol.* 307 (8), F939–F948. doi:10.1152/ajprenal.00025.2013

Lei, L., Li, L. P., Zeng, Z., Mu, J. X., Yang, X., Zhou, C., et al. (2018). Value of urinary KIM-1 and NGAL combined with serum Cys C for predicting acute kidney injury secondary to decompensated cirrhosis. *Sci. Rep.* 8 (1), 7962. doi:10.1038/s41598-018-26226-6

Lima, C., Gorab, D. L., Fernandes, C. R., and Macedo, E. (2022). Role of proenkephalin in the diagnosis of severe and subclinical acute kidney injury during the perioperative period of liver transplantation. *Pract. Lab. Med.* 31, e00278. doi:10.1016/j.plabm.2022.e00278

Lin, X., Yuan, J., Zhao, Y., and Zha, Y. (2015). Urine interleukin-18 in prediction of acute kidney injury: A systemic review and meta-analysis. *J. Nephrol.* 28, 7–16. doi:10.1007/s40620-014-0113-9

Lupu, L., Rozenfeld, K. L., Zahler, D., Morgan, S., Merdler, I., Shtark, M., et al. (2021). Detection of renal injury following primary coronary intervention among ST-segment elevation myocardial infarction patients: Doubling the incidence using neutrophil gelatinase-associated lipocalin as a renal biomarker. *J. Clin. Med.* 10 (10), 2120. doi:10.3390/jcm10102120

Manetti, L., Pardini, E., Genovesi, M., Campomori, A., Grasso, L., Morselli, L. L., et al. (2005). Thyroid function differently affects serumcystatin C and creatinine concentrations. *J. Endocrinol. Invest.* 28, 346–349. doi:10.1007/BF03347201

Martin, G. G., Atshaves, B. P., McIntosh, A. L., Mackie, J. T., Kier, A. B., and Schroeder, F. (2005). Liver fatty-acid-binding protein (L-FABP) gene ablation alters

liver bile acid metabolism in male mice. *Biochem. J.* 391 (3), 549–560. doi:10.1042/BJ20050296

McMahon, B. A., and Murray, P. T. (2010). Urinary liver fatty acid-binding protein:another novel biomarker of acute kidney injury. *Kidney Int.* 77 (8), 657–659. doi:10.1038/ki.2010.5

Meersch, M., Schmidt, C., Hofmeier, A., Van Aken, H., Wempe, C., Gerss, J., et al. (2017). Prevention of cardiacsurgery-associated AKI by implementing the KDIGO guidelines inhigh risk patients identified by biomarkers: The PrevAKI randomized controlled trial. *Intensive Care Med.* 43, 1551–1561. doi:10.1007/s00134-016-4670-3

Meersch, M., Schmidt, C., Van Aken, H., Martens, S., Rossaint, J., Singbartl, K., et al. (2014). Urinary TIMP-2 andIGFBP7 as early biomarkers of acute kidney injury and renal recov-ery following cardiac surgery. *PLoS One* 9 (3), e93460. doi:10.1371/journal.pone.0093460

Melnikov, V. Y., Ecder, T., Fantuzzi, G., Siegmund, B., Lucia, M. S., Dinarello, C. A., et al. (2001). Impaired IL-18 processing protectscaspase-1-deficient mice from ischemic acute renalfailure. *J. Clin. Invest.* 107, 1145–1152. doi:10.1172/JCI12089

Moledina, D. G., Hall, I. E., Thiessen-Philbrook, H., Reese, P. P., Weng, F. L., Schroppel, B., et al. (2017). Performance of serum creatinine and kidney injury biomarkers for diagnosing histologic acute tubular injury. *Am. J. Kidney Dis.* 70 (6), 807–816. doi:10.1053/j.ajkd.2017.06.031

Moledina, D. G., and Parikh, C. R. (2018). Phenotyping of acute kidney injury: Beyond serum creatinine. *Semin. Nephrol.* 38 (1), 3–11. doi:10.1016/j.semnephrol.2017.09.002

Musiał, K., Augustynowicz, M., Miśkiewicz-Migoń, I., Kałwak, K., Ussowicz, M., and Zwolińska, D. (2020). Clusterin as a new marker of kidney injury in children undergoing allogeneic hematopoietic stem cell transplantation-A pilot study. *J. Clin. Med.* 9 (8), 2599. doi:10.3390/jcm9082599

Naruse, H., Ishii, J., Takahashi, H., Kitagawa, F., Nishimura, H., Kawai, H., et al. (2020). Urinary liver-type fatty-acid-binding protein predicts long-term adverse outcomes in medical cardiac intensive care units. *J. Clin. Med.* 9 (2), 482. doi:10.3390/jcm9020482

Nehus, E., Kaddourah, A., Bennett, M., Pyles, O., and Devarajan, P. (2017). Subclinical kidney injury in children receiving nonsteroidal anti-inflammatory drugs after cardiac surgery. *J. Pediatr.* 189, 175–180. doi:10.1016/j.jpeds.2017.06.045

Nickolas, T. L., O'Rourke, M. J., Yang, J., Sise, M. E., Canetta, P. A., Barasch, N., et al. (2008). Sensitivity and specificity of a single emer-gency department measurement of urinary neutrophil gelati-nase-associated lipocalin for diagnosing acute kidney injury. *Ann. Intern. Med.* 148, 810–819. doi:10.7326/0003-4819-148-11-200806030-00003

Nickolas, T. L., Schmidt-Ott, K. M., Canetta, P., Forster, C., Singer, E., Sise, M., et al. (2012). Diagnostic and prognostic stratification in the emergency department using urinary biomarkers of nephron damage: A multicenter prospective cohort study. *J. Am. Coll. Cardiol.* 59, 246–255. doi:10.1016/j.jacc.2011.10.854

Nisula, S., Yang, R., Poukkanen, M., Vaara, S. T., Kaukonen, K. M., Tallgren, M., et al. (2015). Predictive value of urine interleukin-18 in the evolution and outcome of acute kidney injury in critically ill adult patients. *Br. J. Anaesth.* 114, 460–468. doi:10.1093/bja/aeu382

Noiri, E., Doi, K., Negishi, K., Tanaka, T., Hamasaki, Y., Fujita, T., et al. (2009). Urinary fatty acid-bind-ing protein 1: An early predictive biomarker of kidneyinjury. *Am. J. Physiol. Ren. Physiol.* 296 (4), F669–F679. doi:10.1152/ajprenal.90513.2008

Oezkur, M., Magyara, A., Thomasa, P., Stork, T., Schneider, R., Bening, C., et al. (2017). TIMP-2*IGFBP7(Nephrocheck®) measurements at intensive care unit admissionafter cardiac surgery are predictive for acute kidney injury within48 hours. *Kidney Blood Press. Res.* 42 (3), 456–467. doi:10.1159/000479298

Oh, D. J. (2020). A long journey for acute kidney injury biomarkers. *Ren. Fail.* 42 (1), 154–165. doi:10.1080/0886022X.2020.1721300

Olvera-Posada, D., Dayarathna, T., Dion, M., Alenezi, H., Sener, A., Denstedt, J. D., et al. (2017). KIM-1 is a potential urinary biomarker of obstruction: Results from a prospective cohort study. *J. Endourol.* 31 (2), 111–118. doi:10.1089/end.2016.0215

Ortega, L. M., and Heung, M. (2018). The use of cell cycle arrest biomarkers in theearly detection of acute kidney injury. Is this the new renal troponin? *Nefrologia* 38 (4), 361–367. doi:10.1016/j.nefro.2017.11.013

Ostermann, M., Zarbock, A., Goldstein, S., Kashani, K., Macedo, E., Murugan, R., et al. (2020). Recommendations on Acute Kidney Injury Biomarkers From the Acute Disease Quality Initiative Consensus Conference: A Consensus Statement [published correction appears in JAMA Netw Open. 2020 Nov 2;3(11):e2029182]. *JAMA Netw. Open* 3 (10), e2019209. doi:10.1001/jamanetworkopen.2020.19209

Pajek, J., Škoberne, A., Šosterič, K., Adlesic, B., Leskosek, B., Bucar Pajek, M., et al. (2014). Non-inferiority of creatinine excretion rate to urinary L-FABP and NGAL as predictors of early renal allograft function. *BMC Nephrol.* 15, 117. doi:10.1186/1471-2369-15-117

Parikh, C. R., Coca, S. G., Thiessen-Philbrook, H., Shlipak, M. G., Koyner, J. L., Wang, Z., et al. (2011). Postoperative biomarkers predict acute kidney injury and poor outcomes after adult cardiac surgery. *J. Am. Soc. Nephrol.* 22 (9), 1748–1757. doi:10.1681/ASN.2010121302

Parikh, C. R., Jani, A., Melnikov, V. Y., Faubel, S., and Edelstein, C. L. (2004). Urinary interleukin-18 is a marker of human acute tubularnecrosis. *Am. J. Kidney Dis.* 43, 405–414. doi:10.1053/j.ajkd.2003.10.040

Pelsers, M. M., Hermens, W. T., and Glatz, J. F. (2005). Fatty acid-binding proteins as plasma markers of tissue injury. *Clin. Chim. Acta.* 352 (1-2), 15–35. doi:10.1016/j.cccn.2004.09.001

Pietrukaniec, M., Migacz, M., Żak-Gołąb, A., Olszanecka-Glinianowicz, M., Chudek, J., Dulawa, J., et al. (2020). Could KIM-1 and NGAL levels predict acute kidney injury after paracentesis? preliminary study. *Ren. Fail.* 42 (1), 853–859. doi:10.1080/0886022X.2020.1801468

Portilla, D., Dent, C., Sugaya, T., Nagothu, K. K., Kundi, I., Moore, P., et al. (2008). Liver fatty acid-binding protein as a biomarker of acute kidney injury after cardiac surgery. *Kidney Int.* 73 (4), 465–472. doi:10.1038/sj.ki.5002721

Pozzoli, S., Simonini, M., and Manunta, P. (2018). Predicting acute kidney injury: Current status and future challenges. *J. Nephrol.* 31 (2), 209–223. doi:10.1007/s40620-017-0416-8

Rizvi, M. S., and Kashani, K. B. (2017). Biomarkers for early detection of acute kidney injury. *J. Appl. Lab. Med.* 2 (3), 386–399. doi:10.1373/jalm.2017.023325

Rosenqvist, M., Bronton, K., Hartmann, O., Bergmann, A., Struck, J., and Melander, O. (2019). Proenkephalin a 119-159 (penKid) - a novel biomarker for acute kidney injury in sepsis: An observational study. *BMC Emerg. Med.* 19 (1), 75. doi:10.1186/s12873-019-0283-9

Rosner, M. H., La Manna, G., and Ronco, C. (2018). Acute kidney injury in the geriatric population. *Contrib. Nephrol.* 193, 149–160. doi:10.1159/000484971

Schachtrup, C., Emmler, T., Bleck, B., Sandqvist, A., and Spener, F. (2004). Functional analysis of peroxisome-proliferator-responsive element motifs in genes of fatty acid-binding proteins. *Biochem. J.* 382 (1), 239–245. doi:10.1042/BJ20031340

Schrezenmeier, E. V., Barasch, J., Budde, K., Westhoff, T., and Schmidt-Ott, K. M. (2017). Biomarkers in acute kidneyinjury—Pathophysiological basis and clinical performance. *Acta Physiol.* 219, 554–572. doi:10.1111/apha.12764

Srisawat, N., and Kellum, J. A. (2020). The role of biomarkers in acute kidney injury. *Crit. Care Clin.* 36 (1), 125–140. doi:10.1016/j.ccc.2019.08.010

Sterling, M., Al-Ismaili, Z., McMahon, K. R., Piccioni, M., Pizzi, M., Mottes, T., et al. (2017). Urine biomarkers of acute kidney injury in noncritically ill, hospitalized children treated with chemotherapy. *Pediatr. Blood Cancer* 64 (10), e26538. doi:10.1002/pbc.26538

Stevens, L. A., Schmid, C. H., Greene, T., Li, L., Beck, G. J., Joffe, M. M., et al. (2009). Factors other than glomerular filtration rate affect serumcystatin C levels. *Kidney Int.* 75, 652–660. doi:10.1038/ki.2008.638

Tan, N. S., Shaw, N. S., Vinckenbosch, N., Liu, P., Yasmin, R., Desvergne, B., et al. (2002). Selective cooperation between fatty acid binding proteins and peroxisome proliferator-activated receptors in regulating transcription. *Mol. Cell. Biol.* 22, 5114–5127. doi:10.1128/MCB.22.14.5114-5127.2002

Tang, R., Ao, X., Zhong, Y., Wang, R. L., and Zhou, Q. L. (2017). Values of combination of urinary L-FABP and NGAL in early diagnosis of acute kidney injury after cardiac surgery in children. *Zhongguo Dang Dai Er Ke Za Zhi* 19 (7), 770–775. doi:10.7499/j.issn.1008-8830.2017.07.008

Teo, S. H., and Endre, Z. H. (2017). Biomarkers in acute kidney injury (AKI). *Best. Pract. Res. Clin. Anaesthesiol.* 31 (3), 331–344. doi:10.1016/j.bpa.2017.10.003

Vaidya, V. S., Ferguson, M. A., and Bonventre, J. V. (2008). Biomarkers of acute kidney injury. *Annu. Rev. Pharmacol. Toxicol.* 48, 463–493. doi:10.1146/annurev.pharmtox.48.113006.094615

Viau, A., El Karoui, K., Laouari, D., Burtin, M., Nguyen, C., Mori, K., et al. (2010). Lipocalin 2 is essential for chronic kidney disease progression in mice and humans. *J. Clin. Invest.* 120 (11), 4065–4076. doi:10.1172/JCI42004

Vijayan, A., Faubel, S., Askenazi, D. J., Cerda, J., Fissell, W. H., Heung, M., et al. (2016). Clinical use of the urine biomarker [TIMP-2] × [IGFBP7] for acute kidney injury risk assessment. *Am. J. Kidney Dis.* 68 (1), 19–28. doi:10.1053/j.ajkd.2015.12.033

Waikar, S. S., and Bonventre, J. V. (2009). Creatinine kinetics and the defi-nition of acute kidney injury. *J. Am. Soc. Nephrol.* 20 (3), 672–679. doi:10.1681/ASN.2008070669

Wang, C., Zhang, J., Han, J., Yang, Q., Liu, J., and Liang, B. (2017). The level of urinary IL-18 in acute kidney injury after cardiopulmonary bypass. *Exp. Ther. Med.* 14 (6), 6047–6051. doi:10.3892/etm.2017.5317

Wang, C. F., Ma, L., Feng, L., Yin, M. R., Gu, J. F., and Jia, X. B. (2016). Evaluation of nephrotoxicity induced by total terpenoids from Alismatis Rhizoma on HK-2 cells *in vitro* and its induction of apoptosis. *Zhongguo Zhong Yao Za Zhi* 41 (3), 490–497. doi:10.4268/cjcmm20160322

Xu, K., Shang, N., Levitman, A., Corker, A., Kudose, S., Yaeh, A., et al. (2021). Urine test predicts kidney injury and death in COVID-19. medRxiv.2021.06.10.21258638. doi:10.1101/2021.06.10.21258638

Yang, L., Besschetnova, T. Y., Brooks, C. R., Shah, J. V., and Bonventre, J. V. (2010). Epithelial cell cycle arrest in G2/M mediates kidneyfibrosis afterinjury. *Nat. Med.* 16 (5), 535–543. doi:10.1038/nm.2144

Yasar, E., Ozger, H. S., Yeter, H. H., Yildirim, C., Osmanov, Z., Cetin, T. E., et al. (2022). Could urinary kidney injury molecule-1 be a good marker in subclinical acute kidney injury in mild to moderate COVID-19 infection? *Int. Urol. Nephrol.* 54 (3), 627–636. doi:10.1007/s11255-021-02937-0

Yong, K., Dogra, G., Boudville, N., Pinder, M., and Lim, W. (2011). Acute kidney injury: Controversies revisited. *Int. J. Nephrol.* 2011, 762634. doi:10.4061/2011/762634

Zhang, W. R., and Parikh, C. R. (2019). Biomarkers of acute and chronic kidney disease. *Annu. Rev. Physiol.* 81, 309–333. doi:10.1146/annurev-physiol-020518-114605

Zheng, J., Xiao, Y., Yao, Y., Xu, G., Li, C., Zhang, Q., et al. (2013). Comparison of urinary biomarkers for early detection of acute kidney injury after cardiopulmonary bypass surgery in infants and young children. *Pediatr. Cardiol.* 34, 880–886. doi:10.1007/s00246-012-0563-6

frontiers | Frontiers in Physiology

TYPE Original Research
PUBLISHED 12 September 2022
DOI 10.3389/fphys.2022.982722

OPEN ACCESS

EDITED BY
Ignacio Gimenez,
University of Zaragoza, Spain

REVIEWED BY
Diego Orlando Pastene,
University of Heidelberg, Germany
Andrew Hall,
University of Zurich, Switzerland

*CORRESPONDENCE
Christian Hugo,
christian.hugo@uniklinikum-dresden.de

†These authors have contributed equally to this work and share last authorship

SPECIALTY SECTION
This article was submitted to Renal Physiology and Pathophysiology, a section of the journal Frontiers in Physiology

RECEIVED 30 June 2022
ACCEPTED 19 August 2022
PUBLISHED 12 September 2022

CITATION
Kroeger H, Kessel F, Sradnick J, Todorov V, Gembardt F and Hugo C (2022), Intravital imaging of hemodynamic glomerular effects of enalapril or/and empagliflozin in STZ-diabetic mice.
Front. Physiol. 13:982722.
doi: 10.3389/fphys.2022.982722

Intravital imaging of hemodynamic glomerular effects of enalapril or/and empagliflozin in STZ-diabetic mice

Hannah Kroeger, Friederike Kessel, Jan Sradnick, Vladimir Todorov, Florian Gembardt† and Christian Hugo*†

Experimental Nephrology and Division of Nephrology, Department of internal Medicine III, University Hospital Carl Gustav Carus at the Technische Universität Dresden, Dresden, Germany

Background: Diabetic kidney disease is the leading cause of end-stage renal disease. Administration of ACE inhibitors or/and SGLT2 inhibitors show renoprotective effects in diabetic and other kidney diseases. The underlying renoprotective mechanisms of SGLT2 inhibition, especially in combination with ACE inhibition, are incompletely understood. We used longitudinal intravital microscopy to directly elucidate glomerular hemodynamics on a single nephron level in response to the ACE inhibitor enalapril or/and the SGLT2 inhibitor empagliflozin.

Methods: Five weeks after the induction of diabetes by streptozotocin, male C57BL/6 mice were treated with enalapril, empagliflozin, enalapril/empagliflozin or placebo for 3 days. To identify hemodynamic regulation mechanisms, longitudinal intravital multiphoton microscopy was employed to measure single nephron glomerular filtration rate (snGFR) and afferent/efferent arteriole width.

Results: Diabetic mice presented a significant hyperfiltration. Compared to placebo treatment, snGFR was reduced in response to enalapril, empagliflozin, or enalapril/empagliflozin administration under diabetic conditions. While enalapril treatment caused significant dilation of the efferent arteriole (12.55 ± 1.46 µm vs. control 11.92 ± 1.04 µm, $p < 0.05$), empagliflozin led to a decreased afferent arteriole diameter (11.19 ± 2.55 µm vs. control 12.35 ± 1.32 µm, $p < 0.05$) in diabetic mice. Unexpectedly under diabetic conditions, the combined treatment with enalapril/empagliflozin had no effects on both afferent and efferent arteriole diameter change.

Conclusion: SGLT2 inhibition, besides ACE inhibition, is an essential hemodynamic regulator of glomerular filtration during diabetes mellitus. Nevertheless, additional mechanisms—independent from hemodynamic regulation—are involved in the nephroprotective effects especially of the combination therapy and should be further explored in future studies.

KEYWORDS

SGLT2 inhbition, ACE inhibition, single nephron GFR, hemodynamic, intravital 2-photon microscopy, Type 1 diabetes mellitus, STZ (streptozocin)

Introduction

Diabetes mellitus is the main reason for end-stage renal disease (ESRD) in the Western world (Kovesdy, 2022). The number of patients with ESRD is expected to double in the next 10-15 years further increasing treatment costs. Despite tremendous efforts and ongoing research, until recently there was no specific therapy for diabetic nephropathy (DN) or other chronic progressive kidney diseases (CKD) besides angiotensin-converting enzyme (ACE) inhibition (Joannidis and Hoste, 2018; Kovesdy, 2022). One characteristic of early stage changes of DN is the activation of the renin-angiotensin system (RAS), resulting in vasoconstriction of the efferent arteriole and increasing intraglomerular pressure (Giani et al., 2021). RAS blockade with angiotensin-converting enzyme inhibitors (ACEi) or angiotensin-receptor blockers (ARBs) was the gold standard to slow down the development and progression of any CKD, including DN (Joannidis and Hoste, 2018).

Sodium-glucose cotransporter 2 (SGLT2) inhibitors are a new, recently approved therapy for diabetes mellitus type 2 (Wanner et al., 2016), also with beneficial effects in type 1 diabetes (Henry et al., 2015). SGLT2 inhibitors (SGLT2i) are the first class of antidiabetic drugs directly acting on the kidney and exhibiting nephroprotective effects (Zinman et al., 2015; Wanner et al., 2016). Additionally, recent clinical trials in different cardiovascular/diabetic high risk patient groups have demonstrated that SGLT2i such as empagliflozin, dapagliflozin, or canagliflozin reduce the risk for death, as well as cardiac and renal outcomes (Zinman et al., 2015; Wanner et al., 2016; Neal et al., 2017; Wiviott et al., 2019).

The tubuloglomerular feedback (TGF) plays an important role in maintaining intraglomerular pressure and glomerular filtration rate (GFR) (Vallon, 2003). TGF is a negative feedback loop at the juxtaglomerular apparatus that stabilizes GFR and distal salt delivery at the *macula densa* (Vallon, 2003; Schnermann and Castrop, 2013). Under diabetic conditions, high amounts of glucose are reabsorbed by SGLT2 in the early proximal tubule. The subsequent increase in Na^+-reabsorption lowers its distal delivery at the *macula densa*. Consequently, activation of TGF leads to vasodilation of the afferent arteriole, thus increasing intraglomerular pressure and GFR (Heerspink et al., 2016). Considering that SGLT2 is solely expressed within the proximal tubules (Chen et al., 2010), overall- and nephroprotective effects in humans are likely to be mediated via the kidneys (Zinman et al., 2015; Wanner et al., 2016). Furthermore, recent results demonstrated that the concurrent administration of ACEi and SGLT2i improves renal outcomes synergistically (Kojima et al., 2015; Wanner et al., 2016). The underlying mechanisms, linking arteriole width alterations, intraglomerular pressure regulation, and sodium delivery to the *macula densa* - subsequently slowing down the progression of CKD - are not fully understood. SGLT2i alone may normalize GFR under diabetic conditions by restoring the TGF mechanism (Nespoux and Vallon, 2018). Consistent with this hypothesis, we and others have shown that SGLT2 inhibition reduced renal and glomerular hypertrophy and kidney injury in experimental diabetic nephropathy (Gembardt et al., 2014).

Based on the modes of action, simultaneous ACE and SGLT2 inhibition may have synergistic effects regarding restoration of TGF under diabetic conditions. While synergistic hemodynamic effects by combination therapy of nonsteroidal anti-inflammatory drugs (NSAIDs) and ACEi/ARBs are known to frequently cause severe tubular necrosis and compromised renal function via glomerular hypotension (Seelig, Maloley and Campbell, 1990), it remains unclear why SGLT2i together with ACEi/ARBs prevents from acute renal failure and are especially effective in reno- and cardioprotection (Kojima et al., 2015; Zhang et al., 2018; Sridhar, Tuttle and Cherney, 2020).

Therefore, our experimental study for the first time investigates glomerular hemodynamic regulation of ACE inhibition with enalapril or/and SGLT2 inhibition with empagliflozin at the single nephron level in mice *in vivo*. Hereby, we used sophisticated intravital multiphoton imaging techniques to directly visualize glomerular hemodynamics by longitudinal, repetitive assessment of single nephron GFR (snGFR) and afferent as well as efferent arteriole width in STZ-induced type 1 diabetic mice at baseline conditions and in response to ACEi or/and SGLT2i within the same animals.

Material and methods

Animals

Diabetes was induced in male C57BL/6 (Janvier) mice at 6-7 weeks of age by intraperitoneal injections of streptozotocin (STZ; Sigma-Aldrich) in sodium citrate buffer (pH 4.5) at a dose of 50 mg/kg for five consecutive days. Non-diabetic controls received equal amounts of buffer alone. Blood glucose levels were determined 1 week after the last injection of STZ. Mice with blood glucose level above 20 mmol/l were considered as diabetic. Healthy controls and STZ-diabetic mice were randomly divided into four groups (1. Control; 2. 50 mg/l enalapril in drinking water; 3. 300 mg/kg empagliflozin in chow; 4. co-treatment with enalapril and empagliflozin; 50 mg/l enalapril and 300 mg/kg empagliflozin) 5 weeks later. The control group (placebo) received standard chow and drinking water without any drugs.

For urine collection, mice were housed individually in metabolic cages for 24 h. The mice had free access to food and water in the metabolic cages. Blood samples were obtained from non-fasting animals after 16 days of treatment. Blood samples were centrifuged for 15 min at 2.500 × *g*, and the collected serum was stored at -20°C for further analysis. Urinary and serum samples were analyzed at the Clinical Chemistry at the University Hospital Carl Gustav Carus (Dresden, Germany) using standard laboratory methods to determine different parameters such as serum glucose, serum ACE activity, and urinary glucose.

Transdermal measurement of glomerular filtration rate (GFR) was performed as described previously using FITC-sinistrin (Schreiber et al., 2012).

All animal experiments were performed in accordance with the Federal Law on the Use of Experimental Animals in Germany and were approved by local authorities (Az. 25-5131/496/48 and Az. 24-9168.11/1/380).

Intravital multiphoton microscopy

For intravital microscopy, only STZ-diabetic mice were used. First, the mice were anesthetized with isoflurane (0.8 l/min, 2.5%, Baxter Deutschland GmbH), and an abdominal body window was implanted for repeated kidney imaging as previously described (Schiessl et al., 2019).

The next day, mice were anesthetized with isoflurane (0.8 l/min, 1.5%), intubated, and catheterized into the lateral tail vein. To maintain body temperature during intravital microscopy, the mice were kept on a heating plate.

Image acquisition was performed using an upright Leica SP8 multiphoton laser scanning microscope with a 40x/1.1 NA water immersion objective at the Core Facility Cellular Imaging at the Technical University Dresden. Multiphoton imaging was performed with 860 nm laser excitation to visualize Angiospark680® (Perkin&Elmer, 30 µl), Hoechst 33,342 (Thermo Fischer, 50 µl of 2 mg/ml stock), and Lucifer Yellow (LY; Sigma-Aldrich).

Single nephron GFR measurement

snGFR measurement in living mice was measured as previously described (Kang et al., 2006). In brief, superficial glomeruli with a subsequent proximal tubule (PT; minimum 45 µm length) were used for analysis. An automated syringe pump injected the freely filtering LY (15 µl of 5 mg/ml stock) into the lateral tail vein. A time series (6 frames/s) was acquired during the application of LY and was used to calculate snGFR as we previously described (Kessel et al., 2021).In short, semi-automatic image analysis was programmed using FIJI (Schindelin et al., 2012) and data analysis using R (R Core Team, 2017) with RStudio (RStudio Team, 2019). For image analysis, the position and direction of the flow along the proximal tubule had to be manually set. Afterwards, LY intensity was measured over time in every frame automatically. The selection further provides PT length and mean PT diameter to calculate PT volume. Finally, snGFR is automatically calculated as volume change over time. Number of animals/number of snGFR measurements: *n* (Placebo) = 8/13, *n* (Enalapril) = 5/9, n (Empagliflozin) = 5/9, *n* (Enalapril/Empagliflozin) = 5/7. The number of measurement is limited to three nephrons per animal.

Measurement of arteriole diameter and glomerular volume

For measurement of afferent and efferent arteriole diameter in living mice, a z-stack (1 µm z-size over 120 µm length) of superficial glomeruli was captured. The repeated measurement of arteriole diameter was performed without a cortical slice as mentioned in other experimental setups (Satoh et al., 2010; Kidokoro et al., 2019). Further analysis was performed in Imaris (version 9.5.0, Bitplane). The afferent and efferent arteriole were identified by the direction of blood flow. Afterwards, the arterioles were marked in every plane of the z-stack, three-dimensionally reconstructed, and the mean diameter was calculated automatically. For glomerular volume, the glomerulus was three-dimensional reconstructed by identification of the glomerular capillaries in every plane of the z-stack. Afterwards, the glomerular volume was automatically calculated. Number of animals/number of afferent arteriole measurements: *n* (animals/AA): *n* (Placebo) = 5/11, *n* (Enalapril) = 2/5, *n* (Empagliflozin) = 5/7, *n* (Enalapril/Empagliflozin) = 8/14. Number of animals/number of efferent arteriole measurements: n (animals/EA): *n* (Placebo) = 4/7, *n* (Enalapril) = 2/4, *n* (Empagliflozin) = 4/6, *n* (Enalapril/Empagliflozin) = 6/14. The number of animals for arteriole width measurements varies between the individual groups, because depending on the orientation of the glomeruli to the microscope objective, the measurement of the afferent and efferent arteriole diameter is not possible in all glomeruli at each time point.

Statistical analysis

Data are shown as dot plot ± standard deviation (SD). The data were visualized and analyzed using R (version 4.0.2.) (R Core Team, 2017) with RStudio (version 1.2.5033) (RStudio Team, 2019). Comparison between multiple groups was performed by using one-way ANOVA followed by the Šídák's multiple comparison test. Comparison between two groups was performed using an unpaired or paired 2-tailed Student t-test. p values < 0.05 were considered statistically significant.

10.3389/fphys.2022.982722

TABLE 1 Basic parameters of non-diabetic control mice and STZ-diabetic mice. Values are shown before mice were randomly divided into groups (at randomisation) and after treatment with placebo, enalapril, empagliflozin, and enalapril/empagliflozin. BW indicates bodyweight, KW/BW, kidney weight to body weight ratio, s-Glucose, serum-Glucose, ACE-Angiotensin Converting Enzyme, and u-Glucose, urinary Glucose, nd, not detected. At randomisation an unpaired *t*-test was performed for statistical difference. For comparison between the treatment groups an one-way ANOVA was performed, *n* (non-diabetic controls) = 10-22, except for ACE activity in the enalapril group (*n* = 3), *n* (diabetic) = 5-16. All values are expressed as mean ± SD.

	Non-diabetic control					Diabetic				
Group	**At randomisation**	**Placebo**	**Enalapril**	**Empagliflozin**	**Enalapril/ Empagliflozin**	**At randomisation**	**Placebo**	**Enalapril**	**Empagliflozin**	**Enalapril/ Empagliflozin**
BW [g]	25.5 ± 2.0	26.4 ± 2.5	26.1 ± 1.3	25.0 ± 1.5	24.1 ± 2.3	21.6 ± 2.6§	20.9 ± 2.2	21.2 ± 2.1	20.4 ± 1.1	22.5 ± 2.6
KW/BW [mg/g]	-	6.5 ± 1.1	5.8 ± 0.7	6.9 ± 0.8	6.3 ± 1.0	-	8.2 ± 1.0*	7.1 ± 0.7	8.1 ± 0.9	7.9 ± 1.0
u-Glucose [mmol/24 h]	nd	nd	nd	1.8 ± 0.6	1.9 ± 0.5	6.6 ± 3.4§	8.0 ± 3.8	5.9 ± 1.9	7.0 ± 2.7	4.3 ± 1.7
ACE [U/L]	-	404.5 ± 71.7	117.7 ± 27.7*	409.8 ± 50.3	71.1 ± 28.2*	-	437.6 ± 52.4	74.7 ± 34.6#	415.3 ± 54.1	55.4 ± 32.2#
Urine volume [ml/24 h]	1.0 ± 0.6	0.9 ± 0.4	1.1 ± 0.4	2.0 ± 0.9	2.1 ± 1.3	11.2 ± 5.2§	13.8 ± 5.8	13.5 ± 3.8	11.9 ± 6.8	7.1 ± 4.0

*$p < 0.05$ vs. non-diabetic control-placebo, #$p < 0.05$ vs. diabetic-placebo, §$p < 0.05$ vs. non-diabetic control-at randomisation.

Results

Basic parameters

First, we analyzed the clinical changes in non-diabetic control and STZ-diabetic mice. Before the mice were randomly divided into treatment groups, diabetic mice had a significantly lower body weight (Table 1), higher serum glucose levels (data not shown), and higher amounts of urinary glucose (Table 1) than the non-diabetic controls. Treatment with enalapril, empagliflozin, and enalapril/empagliflozin itself had no impact on body weight or kidney weight. However, diabetic mice had significantly higher kidney weights than the controls without an impact of the different treatments (Table 1).

Treatment of non-diabetic mice with empagliflozin or enalapril/empagliflozin reduced slightly serum glucose levels compared to the control/placebo group (Figure 1A, 11.5 ± 2.4 mmol control/empagliflozin or 12.6 ± 2.3 mmol control/enalapril/empagliflozin vs. 14.9 ± 3.4 mmol control/placebo). In diabetic mice, treatment with empagliflozin numerically reduced blood glucose levels compared to the placebo group without reaching significance (Figure 1A, diabetic/empagliflozin 33.3 ± 4.6 mmol/l vs. diabetic/placebo 39.0 ± 6.6 mmol/l). In the combined treatment group of enalapril/empagliflozin, a significant blood glucose-lowering effect was noted (Figure 1A, diabetic/enalapril/empagliflozin 28.1 ± 9.2 mmol vs. diabetic/placebo 39.0 ± 6.6 mmol, $p = 0.001$). Furthermore, empagliflozin treatment induced pronounced glucosuria in non-diabetic animals (Table 1). Without empagliflozin treatment no urinary glucose was detectable in non-diabetic controls. In diabetic mice, urinary glucose levels were significantly higher than in the non-diabetic groups without differences between the treatment groups. Empagliflozin and enalapril/empagliflozin treatments increased urinary volume significantly in the control group. Similar to glucosuria, urinary volume was already increased under diabetic conditions without any impact of the different treatments. The urine osmolality was not influenced by enalapril or/and empagliflozin in the diabetic animals (Supplementary Figure S1). Measurement of serum angiotensin-converting enzyme (ACE) activity showed a significant reduction after enalapril or enalapril/empagliflozin treatment in both, the non-diabetic controls and diabetic groups.

Hemodynamic changes in snGFR by enalapril or/and empagliflozin treatment

First, we confirmed the expected glomerular hyperfiltration in kidneys of diabetic mice compared to non-diabetic controls by transdermal GFR measurements (Figure 1B). To analyze hemodynamic changes in glomerular filtration in response to enalapril, empagliflozin, and enalapril/empagliflozin treatment, we measured the acute effects on snGFR longitudinally within the

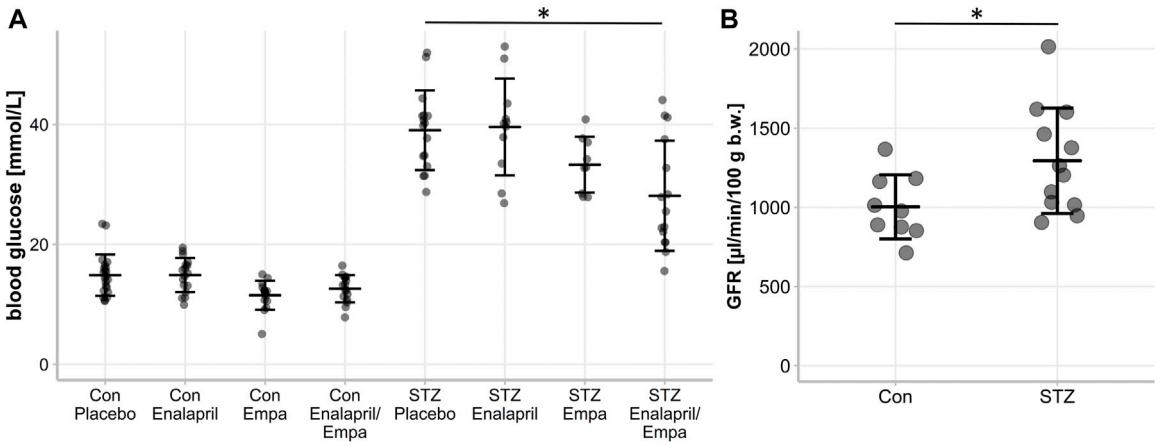

FIGURE 1
Blood glucose level and glomerular filtration rate (GFR) of non-diabetic control mice and STZ-diabetic mice. Effect of enalapril, empagliflozin (Empa), and enalapril/empagliflozin (Enalapril/Empa) treatment on **(A)** blood glucose and **(B)** glomerular filtration rate (GFR) in controls (Con) and diabetic (STZ) mice. For statistical differences an one-way ANOVA was performed in **(A)**, n = 9-22, and an unpaired t-test in **(B)**, n = 9-13.Values are expressed as mean ± SD. $p < 0.05$.

same nephrons of diabetic mice. The experimental setup and a representative measurement is shown in Figures 2A–C and the supplementary material (Supplementary Figure S2). As expected, snGFR remained unaltered in placebo-treated diabetic mice (Figure 2D). In contrast, treatment with the ACEi enalapril reduced snGFR by ~44% (Figure 2D; treated 2.36 ± 1.0 nl/min vs. control 4.24 ± 1.28 nl/min, p = 0.014). Empagliflozin treatment reduced snGFR by ~61% (Figure 2D; treated 1.6 ± 0.55 nl/min vs. control 4.12 ± 1.5 nl/min, p = 0.0006). The combination therapy with enalapril and empagliflozin reduced snGFR by ~65% (Figure 2D; treated 2.07 ± 0.84 nl/min vs. control 6.03 ± 3.17 nl/min, p = 0.014).

Alterations in afferent and efferent arteriole diameter by enalapril or/and empagliflozin treatment

Beside snGFR, the width of glomerular afferent and efferent arterioles can be captured intravitally in single glomeruli and measured longitudinally via three-dimensional reconstruction. Three-dimensional images were obtained on the same days as snGFR measurements were performed (Figure 3A). The three-dimensional reconstruction of the afferent and efferent arteriole was performed afterwards (Figure 3B). Inhibition of SGLT2 with empagliflozin for 3 days led to a significant diameter reduction of the afferent arteriole (Figure 3C; treated 11.19 ± 2.55 µm vs. control 12.35 ± 1.32 µm, p = 0.044) in diabetic mice. Treatment with either placebo (Figure 3C; treated 11.4 ± 1.83 µm vs. control 12.09 ± 1.56 µm), enalapril (Figure 3C; treated 12.44 ± 1.70 µm vs. control 12.46 ± 1.51 µm), or enalapril/empagliflozin (Figure 3C; 10.97 ± 2.00 µm vs. control 10.42 ± 2.03 µm) had no influence on afferent arteriole width compared to the same glomeruli before treatment. In contrast, enalapril treatment led to a significant relaxation of efferent arterioles in the same glomeruli (Figure 3D; treated 12.55 ± 1.46 µm vs. control 11.92 ± 1.04 µm, p = 0.022). Neither placebo (Figure 3D; treated 11.06 ± 1.40 vs. control 11.18 ± 1.50), nor empagliflozin treatment alone (Figure 3D; treated 12.02 ± 1.96 µm vs. control 12.04 ± 1.79 µm), nor the combination therapy with enalapril/empagliflozin (Figure 3D; 11.03 ± 0.79 µm to 10.75 ± 1.61 µm) had an effect on the diameter of the efferent arterioles. The glomerular volume was not influenced by either enalapril or empagliflozin treatment. The combination therapy with enalapril and empagliflozin also did not change the glomerular volume (Supplementary Figure S3).

Discussion

SGLT2i treatment reduces hyperglycemia in diabetic patients (Zinman et al., 2015) and in animal models (Vallon et al., 2013). Additionally, SGLT2i were the first class of antidiabetic drugs significantly reducing mortality, cardiovascular and renal events in diabetic patients (Wanner et al., 2016; Neal et al., 2017). Meanwhile, these beneficial effects of SGLT2i have been equally demonstrated in patients without diabetes but with cardiovascular and renal diseases suggesting a pronounced generalized mode of action that is even independent on hyperglycemia and diabetes mellitus as a disease per se (Teo et al., 2021). Considering that SGLT2 is solely expressed within the proximal tubules (Chen et al., 2010), overall- and

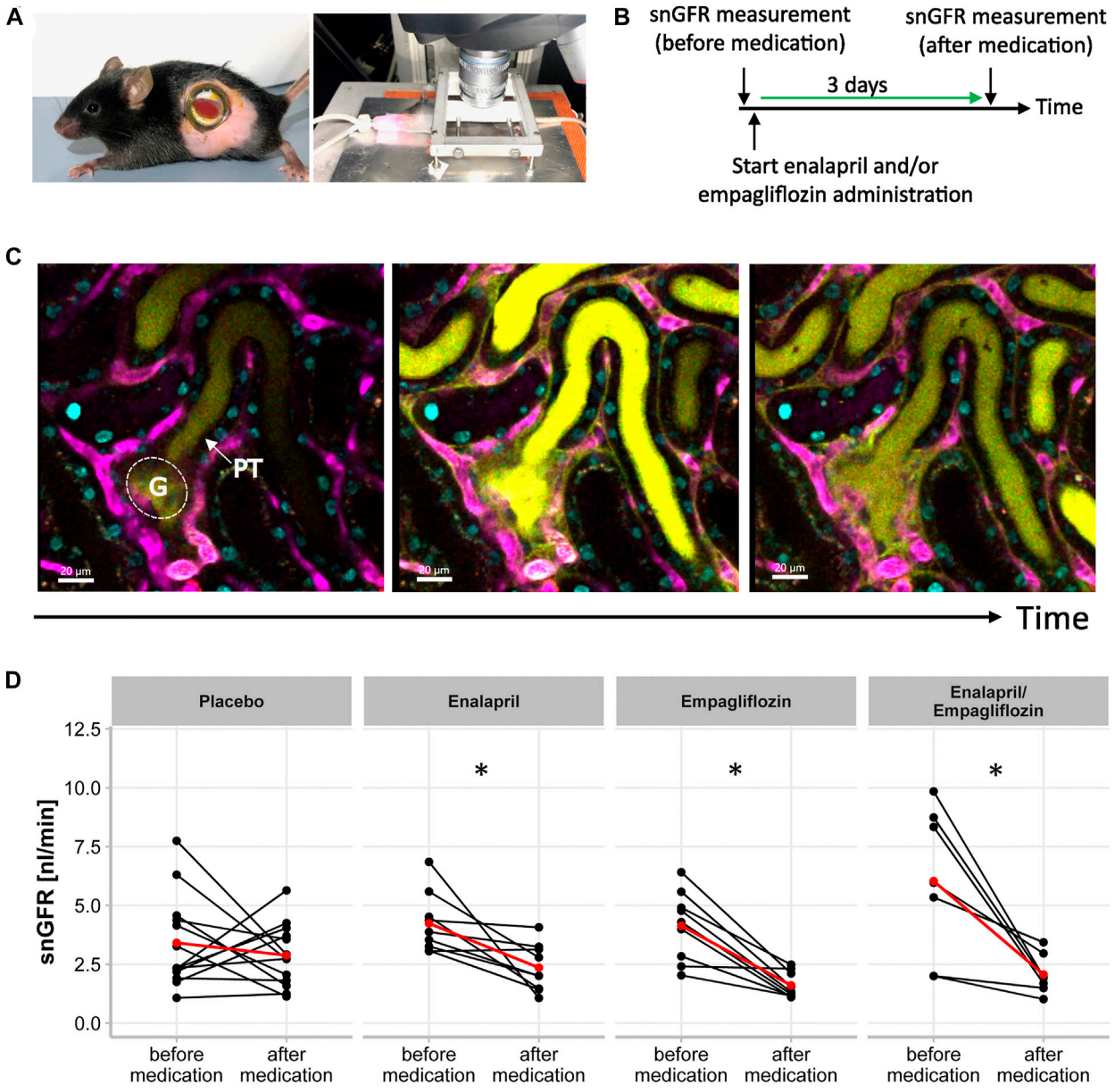

FIGURE 2
Single Nephron Glomerular Filtration Rate in STZ-diabetic mice. **(A)** Experimental setup for intravital microscopy. Mouse with an abdominal body window for repetitive imaging (right) and anesthetized mouse (endotracheal intubation) with extoriorized and stabilizied kidney for use in upright-imaging systems (left). **(B)** Timeline of snGFR measurement in the same nephrons of STZ-diabetic mice. After first snGFR measurement (before medication) administration of placebo, enalapril, empagliflozin, and enalapril/empagliflozin started. Three days later (after medication) the snGFR of the same nephron is measured again. **(C)** Beginning of filtration of the freely filtered Lucifer Yellow of one single glomerulus (G) with its subsequent proximal tubule (PT). The middle picture displays the completely filled proximal tubule and in the left picture, the filtration process is completed. The blood vessels are fluorescently labeled in magenta and the nuclei in cyan. **(D)** Alterations of snGFR in the same nephrons before and after 3 days of placebo, enalapril, empagliflozin and enalapril/empagliflozin administration in STZ-diabetic mice. Each point connected by a line represents the effect on GFR of one single nephron by the mentioned medication. The red point connected by a line indicates the mean value each before and after medication. A paired *t*-test was performed for statistical differences before and after medication in the same nephron. $*p < 0.05$ before vs. after medication.

nephroprotective effects in humans are likely to be mediated via the kidneys, but the exact mechanisms and the role of hemodynamic effects especially in combination therapy with ACEi/ARBs are controversially discussed. While RAS inhibition was the standard nephroprotective therapy in DN for many years, in recent studies SGLT2i were beneficial despite

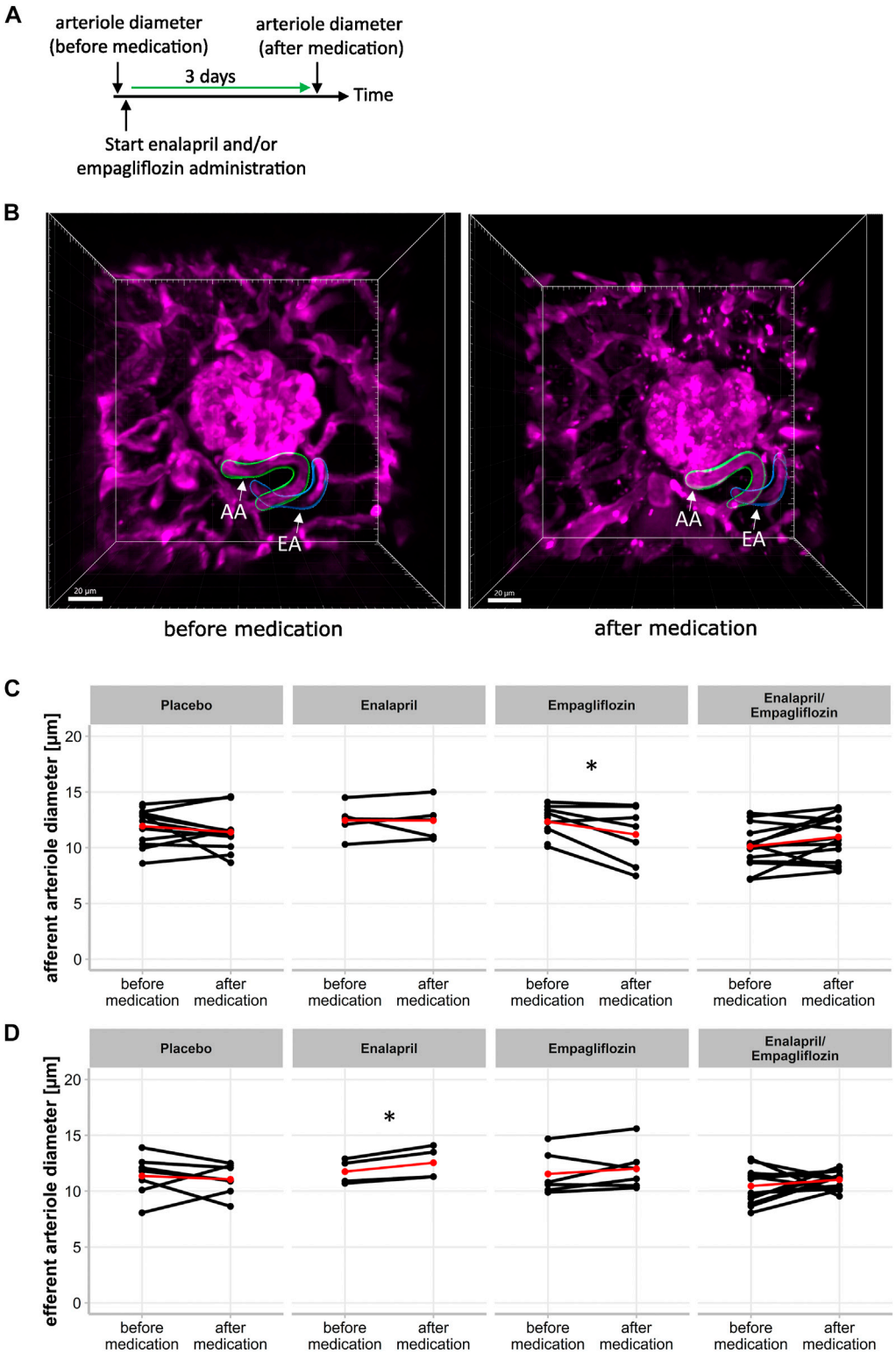

FIGURE 3
Effect of enalapril, empagliflozin and enalapril/empagliflozin on afferent and efferent arteriole alterations in STZ-diabetic mice. **(A)** Timeline of experimetal setup for afferent and efferent arteriole diameter measurement. First measurement (before medication) of arteriole diameter was obtained before the start of placebo, enalapril, empagliflozin and enalapril/empagliflozin administration. The second measurement was performed after 3 days of the respective drug treatment (after medication). **(B)** Three dimensional image of afferent (AA) and efferent (EA) arteriole of one

(*Continued*)

FIGURE 3 (Continued)
glomerulus before medication (left) with three dimensional reconstructed afferent (green) and efferent (blue) arteriole for mean diameter calculation. The right image shows the same afferent and efferent arteriole after 3 days of either placebo, enalapril, empagliflozin, or enalapril/empagliflozin treatment (after medication). **(C)** Afferent and **(D)** efferent arteriole diameter. Same glomeruli are measured before and after respective medication. Each point connected with a line indicates the same afferent or efferent arteriole of one glomerulus on both days. The red point connected by a line indicates the mean value each before and after medication. *$p < 0.05$ before vs. after medication.

80% or more of all patients that were already on ACEi/ARB medication (Zinman et al., 2015; Wanner et al., 2016). Recent experimental studies even showed that the simultaneous administration prevented the development of renal injury more than SGLT2i or ACEi alone (Kojima et al., 2015). To compare the hemodynamic mechanisms of single and combined ACEi/SGLT2i therapy, we measured snGFR and arteriole width regulation in response to enalapril, empagliflozin, and enalapril/empagliflozin administration in the same nephrons on different days via longitudinal intravital microscopy.

Enalapril treatment significantly reduced snGFR in the diabetic group compared to placebo treated animals. The snGFR reduction by enalapril was accompanied and likely caused by efferent arteriole dilation, while no effect was seen regarding width regulation of the afferent arteriole. This interpretation of our findings fits the paradigm that the angiotensin type 1 receptors are expressed stronger in the efferent arteriole than in the afferent arteriole. (Hall et al., 1977; Schrankl et al., 2021). Another intravital microscopy study in STZ-diabetic rats showed restored arteriole width regulation and diminished hyperfiltration in response to ARBs (Satoh et al., 2010). In diabetic patients, hypertension is a relevant comorbidity. ACEi/ARBs are effective drugs to regulate hypertension by efferent vasodilation with a fall in filtration pressure. Long term clinical trials showed slower renal function loss in CDK and lower cardiovascular mortality (Perico, Ruggenenti and Remuzzi, 2017).

In contrast to enalapril, successful snGFR reduction by SGLT2i seems to be promoted by afferent arteriole vasoconstriction but not via width regulation of the efferent arteriole as supported by our *in vivo* study results in type 1 diabetic mice. SGLT2i are shown to activate the production of the TGF mediator adenosine, causing vasoconstriction of the afferent arteriole by binding to the adenosine A1 receptor (Alicic, Johnson and Tuttle, 2018). In humans little is known about the correlation of TGF, adenosine and SGLT2 inhibition. Patients with type 1 diabetes showed increased urinary adenosine production in response to empagliflozin treatment, suggesting that reduced GFR and afferent arteriole constriction was related to increased adenosine production by *macula densa* (Rajasekeran et al., 2017). Kidokoro et al. (2019) showed afferent arteriole vasoconstriction in type 1 diabetes Akita mice in response to SGLT2i *in vivo*, which was abolished by A1 adenosine receptor antagonist. This data further promotes the importance of the adenosine signaling pathway for TGF regulation (Kidokoro et al., 2019). The opposite was shown in patients with type 2 diabetes, here preliminary data supported that SGLT2 inhibition by dapagliflozin may also lower GFR by vasodilation of the efferent arteriole (van Bommel et al., 2020). These controversial results of SGLT2 inhibition in type 1 versus type 2 diabetes models needs further investigation to clarify the arteriole tone regulation in response to SGLT2i *in vivo*.

The combination therapy of ACEi/SGLT2i did reduce snGFR equally to SGLT2i alone. Unexpectedly, in the combined ACEi/SGLT2i therapy approach, snGFR was lowered without any obvious afferent or efferent arteriole width regulation. Currently, we cannot provide a clear explanation for this finding. The reduction of snGFR was not accompanied by osmotic changes in the urine. The snGFR changes were also not related to changes in the glomerular volume most probably because of the short period of treatment. Interestingly, simultaneous administration of both ACEi/SGLT2i drugs does not synergistically reduce intraglomerular pressure as with ACEi and NSAIDs (Lapi et al., 2013; Joannidis and Hoste, 2018). In this context, combination therapy of ACEi with NSAIDs but not together with SGLT2i increases the risk of acute renal failure suggesting a specific interacting or novel regulatory mechanism preserving renal function with combined ACEi/SGLT2i therapy. Hereby, adenosine, as a TGF mediator and angiotensin II, the main effector of the RAS are known to interact to regulate glomerular hemodynamics. Low concentration of the afferent arteriole vasoconstrictor adenosine increases the response to angiotensin II on the efferent arteriole. In contrast, physiological concentration of angiotensin II increases the contractility as response to adenosine. Moreover, the addition of nitric oxide abolished both modulating effects regulating TGF responses (Persson et al., 2013). Additional investigations are needed to clarify the involved mechanisms of a combined therapy in detail. Besides hemodynamic regulation, alternative renoprotective mechanisms may become increasingly important especially under combination therapy. SGLT2i also inhibits proximal tubular reabsorption reducing active tubular transport work. This may redistribute energy demand and oxygen consumption in the kidney, thereby upregulating erythropoietin production with potential protective effects (Nespoux and Vallon, 2020). We and others showed that SGLT2i ameliorated also inflammation and mesangial matrix expansion in a mouse model of DN. Future studies need to investigate, whether RASi or SGLT2i may regulate juxtaglomerular (next to the afferent arteriole) renin-lineage cell phenotype and recruitment as a well described regenerative response to injury mechanism besides the known classical hemodynamic TGF pathway connection (Sequeira López et al., 2004).

Overall, it also needs to be considered that slight differences exist between SGLT2 regulation in mice and humans. While

SGLT2 seems to be usually upregulated in diabetic kidney disease in man, in our STZ-induced kidney model as well as in many other experimental diabetic disease models renal SGLT2 expression is not upregulated which limits the SGLT2i-mediated increase in urinary glucose levels in diabetic mice (Albertoni Borghese et al., 2009; Vallon et al., 2013).

Despite the strength of the *in vivo* visualization of direct effects on renal hemodynamics, our study has also limitations. We cannot exclude any dose-dependent effects of ACEi and/or SGLT2i, especially in the combined treatment group. Furthermore, the direct effect of ACEi and/or SGLT2i was only measured shortly after start of treatment within the same nephron. Combined therapy with ACEi and SGLT2i showed better outcomes in clinical trials compared to each treatment alone (Kojima et al., 2015). Visualization of single glomeruli with a subsequent proximal tubule in mice with the used age is very challenging. Next to the limited number of glomeruli suitable for measuring snGFR and arteriole width, the visualization of nephrons deeper than 100 µm is technically not possible. Therefore, all studies concerning snGFR and arteriole width regulation were performed on superficial glomeruli. This, together with the general functional heterogeneity within the glomeruli represents a major limiting factor of our study. Further investigation of long-term effects regarding snGFR and arteriole width would help to understand the renoprotective effects in more detail.

In conclusion, we directly visualized the hemodynamic actions of RAS or SGLT2 inhibition on single glomeruli in type 1 diabetic mice. Therein, snGFR was reduced via either efferent arteriole vasodilation (ACEi) or afferent arteriole vasoconstriction (SGLT2i), which might be responsible for long term renoprotective effects. The decreased snGFR without changes in arteriole width in diabetic mice with combined ACEi and SGLT2i therapy suggests unknown interactions of both drug groups potentially at the level of *macula densa* cell regulation as well as additional renoprotective mechanisms.

Data availability statement

The original contributions presented in the study are included in the article/supplementary material, further inquiries can be directed to the corresponding author.

Ethics statement

The animal study was reviewed and approved by Landesdirektion Sachsen.

Author contributions

HK did the data aquisition and data analysis. HK and CH wrote the manuscript. FK helped with data analysis. JS, FG, VT, and CH provided assistance in the design of the experiments. JS, FG, VT helped with manuscript preparation. CH and FG contributed equally. All authors have approved the manuscript.

Funding

This work was funded by Böhringer Ingelheim Pharma (BI #418981).

Acknowledgments

We highly acknowledge the technical assistance of Anika Wirth, Andrea Angermann and Maria Schuster. We thank the Core Facility Cellular Imaging (CFCI) and the Institute of Clinical Chemistry at the Medical Faculty Carl Gustav Carus of the Technical University Dresden for their support.

Conflict of interest

The author declares that the research was conducted in the absence of any commercial or financial relationships that could be construed as a potential conflict of interest.

Publisher's note

Supplementary material

The Supplementary Material for this article can be found online at: https://www.frontiersin.org/articles/10.3389/fphys.2022.982722/full#supplementary-material

References

Albertoni Borghese, M. F., Majowicz, M. P., Ortiz, M. C., Passalacqua, M. d. R., Sterin Speziale, N. B., and Vidal, N. A. (2009). Expression and activity of SGLT2 in diabetes induced by streptozotocin: Relationship with the lipid environment. *Nephron. Physiol.* 112 (3), p45–p52. doi:10.1159/000214214

Alicic, R. Z., Johnson, E. J., and Tuttle, K. R. (2018). SGLT2 inhibition for the prevention and treatment of diabetic kidney disease: A review. *Am. J. Kidney Dis.* 72 (2), 267–277. doi:10.1053/j.ajkd.2018.03.022

Chen, J., Williams, S., Ho, S., Loraine, H., Hagan, D., Whaley, J. M., et al. (2010). Quantitative PCR tissue expression profiling of the human SGLT2 gene and related family members. *Diabetes Ther.* 1 (2), 57–92. doi:10.1007/s13300-010-0006-4

Gembardt, F., Bartaun, C., Jarzebska, N., Mayoux, E., Todorov, V. T., Hohenstein, B., et al. (2014). The SGLT2 inhibitor empagliflozin ameliorates early features of diabetic nephropathy in BTBR ob/ob type 2 diabetic mice with and without hypertension. *Am. J. Physiol. Ren. Physiol.* 307 (3), F317–F325. doi:10.1152/ajprenal.00145.2014

Giani, J. F., Veiras, L. C., Shen, J. Z. Y., Bernstein, E. A., Cao, D., Okwan-Duodu, D., et al. (2021). Novel roles of the renal angiotensin-converting enzyme. *Mol. Cell. Endocrinol.* 529, 111257. doi:10.1016/j.mce.2021.111257

Hall, J. E., Guyton, A. C., Jackson, T. E., Coleman, T. G., Lohmeier, T. E., and Trippodo, N. C. (1977) "Control of glomerular filtration rate by renin-angiotensin system," 2(5). doi:10.1152/AJPRENAL.1977.233.5.F366

Heerspink, H. J. L., Perkins, B. A., Fitchett, D. H., Husain, M., and Cherney, D. Z. I. (2016). Sodium glucose cotransporter 2 inhibitors in the treatment of diabetes mellitus cardiovascular and kidney effects, potential mechanisms, and clinical applications. *Circulation* 134, 752–772. doi:10.1161/CIRCULATIONAHA.116.021887

Henry, R. R., Thakkar, P., Tong, C., Polidori, D., and Alba, M. (2015). Efficacy and safety of canagliflozin, a sodium–glucose cotransporter 2 inhibitor, as add-on to insulin in patients with type 1 diabetes. *Diabetes Care* 38 (12), 2258–2265. doi:10.2337/dc15-1730

Joannidis, M., and Hoste, E. (2018). Angiotensin inhibition in patients with acute kidney injury: Dr. Jekyll or Mr. Hyde? *Intensive Care Med.* 44, 1159–1161. doi:10.1007/s00134-018-5223-8

Kang, J. J., Toma, I., Sipos, A., McCulloch, F., and Peti-Peterdi, J. (2006). Quantitative imaging of basic functions in renal (patho)physiology. *Am. J. Physiol. Ren. Physiol.* 291 (2), 495–502. doi:10.1152/ajprenal.00521.2005

Kessel, F., Kroger, H., Gerlach, M., Sradnick, J., Gembardt, F., Todorov, V., et al. (2021). A new analysis approach for single nephron GFR in intravital microscopy of mice. *F1000Res.* (9), 1372. doi:10.12688/f1000research.26888.3

Kidokoro, K., Cherney, D. Z. I., Bozovic, A., Nagasu, H., Satoh, M., Kanda, E., et al. (2019). Evaluation of glomerular hemodynamic function by empagliflozin in diabetic mice using *in vivo* imaging. *Circulation* 140 (4), 303–315. doi:10.1161/CIRCULATIONAHA.118.037418

Kojima, N., Williams, J. M., Slaughter, T. N., Kato, S., Takahashi, T., Miyata, N., et al. (2015). Renoprotective effects of combined SGLT2 and ACE inhibitor therapy in diabetic Dahl S rats. *Physiol. Rep.* 3 (7), e12436. doi:10.14814/phy2.12436

Kovesdy, C. P. (2022). Epidemiology of chronic kidney disease: An update 2022. *Kidney Int. Suppl.* 12 (1), 7–11. doi:10.1016/j.kisu.2021.11.003

Lapi, F., Azoulay, L., Yin, H., Nessim, S. J., and Suissa, S. (2013). Concurrent use of diuretics, angiotensin converting enzyme inhibitors, and angiotensin receptor blockers with non-steroidal anti-inflammatory drugs and risk of acute kidney injury: Nested case-control study. *BMJ* 346, e8525. doi:10.1136/bmj.e8525

Neal, B., Perkovic, V., Mahaffey, K. W., de Zeeuw, D., Fulcher, G., Erondu, N., et al. (2017). Canagliflozin and cardiovascular and renal events in type 2 diabetes. *N. Engl. J. Med.* 377 (7), 644–657. doi:10.1056/NEJMoa1611925

Nespoux, J., and Vallon, V. (2020). Renal effects of SGLT2 inhibitors: An update. *Curr. Opin. Nephrol. Hypertens.* 29 (2), 190–198. doi:10.1097/MNH.0000000000000584

Nespoux, J., and Vallon, V. (2018). *SGLT2 inhibition and kidney protection*, Clinical Science. London: Portland Press Ltd, 1329–1339. doi:10.1042/CS20171298

Perico, N., Ruggenenti, P., and Remuzzi, G. (2017). ACE and SGLT2 inhibitors: The future for non-diabetic and diabetic proteinuric renal disease. *Curr. Opin. Pharmacol.* 33, 34–40. doi:10.1016/j.coph.2017.03.006

Persson, A. E. G., Lai, E. Y., Gao, X., Carlstrom, M., and Patzak, A. (2013). Interactions between adenosine, angiotensin II and nitric oxide on the afferent arteriole influence sensitivity of the tubuloglomerular feedback. *Front. Physiol.* 4, 187. doi:10.3389/fphys.2013.00187

R Core Team (2017). *R: A language and environment for statistical computing*. Vienna, Austria. Available at: https://www.r-project.org/ (Accessed March 22, 2022).

Rajasekeran, H., Lytvyn, Y., Bozovic, A., Lovshin, J. A., Diamandis, E., Cattran, D., et al. (2017) "Urinary adenosine excretion in type 1 diabetes, " *Am. J. Physiol. Ren. Physiol.*, 313, pp. F184–F191. doi:10.1152/ajprenal.00043.2017

RStudio Team (2019). *RStudio*. Boston, MA: Integrated DEvelopment Environment for R. Available at: https://www.rstudio.com/ (Accessed March 22, 2022).

Satoh, M., Kobayashi, S., Kuwabara, A., Tomita, N., Sasaki, T., and Kashihara, N. (2010). *In vivo* visualization of glomerular microcirculation and hyperfiltration in streptozotocin-induced diabetic rats. *Microcirculation* 17 (2), 103–112. doi:10.1111/j.1549-8719.2009.00010.x

Schiessl, I. M., and Fremter, K, Burford, J. L., Castrop, H, and Peti-Peterdi, J. (2019). Long-term cell fate tracking of individual renal cells using serial intravital microscopy, *Imaging and Tracking Stem Cells,Methods in Molecular Biology*, 79–81. doi:10.1007/7651_2019_232

Schindelin, J., Arganda-Carreras, I., Frise, E., Kaynig, V., Longair, M., Pietzsch, T., et al. (2012). Fiji: An open-source platform for biological-image analysis. *Nat. Methods* 9 (7), 676–682. doi:10.1038/nmeth.2019

Schnermann, J. B., and Castrop, H. (2013). "Function of the juxtaglomerular apparatus," in *Seldin and giebisch's the kidney* (Elsevier), 757–801. doi:10.1016/B978-0-12-381462-3.00023-9

Schrankl, J., Fuchs, M., Broeker, K., Daniel, C., Kurtz, A., and Wagner, C. (2021). Localization of angiotensin II type 1 receptor gene expression in rodent and human kidneys. *Am. J. Physiol. Ren. Physiol.* 320 (4), F644–F653. doi:10.1152/AJPRENAL.00550.2020

Schreiber, A., Shulhevich, Y., Geraci, S., Hesser, J., Stsepankou, D., Neudecker, S., et al. (2012). Transcutaneous measurement of renal function in conscious mice. *Am. J. Physiol. Ren. Physiol.* 303 (5), F783–F788. doi:10.1152/ajprenal.00279.2012

Seelig, C. B., Maloley, P. A., and Campbell, J. R. (1990). Nephrotoxicity associated with concomitant ACE inhibitor and NSAID therapy. *South. Med. J.* 83 (10), 1144–1148. doi:10.1097/00007611-199010000-00007

Sequeira López, M. L. S., Pentz, E. S., Nomasa, T., Smithies, O., and Gomez, R. (2004). Renin cells are precursors for multiple cell types that switch to the renin phenotype when homeostasis is threatened. *Dev. Cell* 6 (5), 719–728. doi:10.1016/S1534-5807(04)00134-0

Sridhar, V. S., Tuttle, K. R., and Cherney, D. Z. I. (2020). We can finally stop worrying about SGLT2 inhibitors and acute kidney injury. *Am. J. Kidney Dis.* 76 (4), 454–456. doi:10.1053/j.ajkd.2020.05.014

Teo, Y. H., Syn, N. L., Kow, C. S., Yoong, C. S. Y., Tan, B. Y. Q., Yeo, T.-C., et al. (2021). Effects of sodium/glucose cotransporter 2 (Sglt2) inhibitors on cardiovascular and metabolic outcomes in patients without diabetes mellitus: A systematic review and meta-analysis of randomized-controlled trials. *J. Am. Heart Assoc.* 10 (5), e019463–18. doi:10.1161/JAHA.120.019463

Vallon, V., Rose, M., Gerasimova, M., Satriano, J., Platt, K. A., Koepsell, H., et al. (2013). Knockout of Na-glucose transporter SGLT2 attenuates hyperglycemia and glomerular hyperfiltration but not kidney growth or injury in diabetes mellitus. *Am. J. Physiol. Ren. Physiol.* 304 (2), F156–F167. doi:10.1152/AJPRENAL.00409.2012

Vallon, V. (2003). Tubuloglomerular feedback and the control of glomerular filtration rate. *News Physiol. Sci.* 18 (4), 169–174. doi:10.1152/nips.01442.2003

van Bommel, E. J. M., Muskiet, M. H. A., van Baar, M. J. B., Tonneijck, L., Smits, M. M., Emanuel, A. L., et al. (2020). The renal hemodynamic effects of the SGLT2 inhibitor dapagliflozin are caused by post-glomerular vasodilatation rather than pre-glomerular vasoconstriction in metformin-treated patients with type 2 diabetes in the randomized, double-blind RED trial. *Kidney Int.* 97 (1), 202–212. doi:10.1016/J.KINT.2019.09.013

Wanner, C., Inzucchi, S. E., Lachin, J. M., Fitchett, D., von Eynatten, M., Mattheus, M., et al. (2016). Empagliflozin and progression of kidney disease in type 2 diabetes. *N. Engl. J. Med.* 375 (4), 323–334. doi:10.1056/NEJMOA1515920

Wiviott, S., Raz, I., Bonaca, M., Mosenzon, O., Kato, E., Cahn, A., et al. (2019). Dapagliflozin and cardiovascular outcomes in type 2 diabetes. *N. Engl. J. Med.* 380 (4), 347–357. doi:10.1056/NEJMOA1812389/SUPPL_FILE/NEJMOA1812389_DATA-SHARING

Zhang, Y., Nakano, D., Guan, Y., Hitomi, H., Uemura, A., Masaki, T., et al. (2018). A sodium-glucose cotransporter 2 inhibitor attenuates renal capillary injury and fibrosis by a vascular endothelial growth factor–dependent pathway after renal injury in mice. *Kidney Int.* 94 (3), 524–535. doi:10.1016/j.kint.2018.05.002

Zinman, B., Wanner, C., Lachin, J. M., Fitchett, D., Bluhmki, E., Hantel, S., et al. (2015). Empagliflozin, cardiovascular outcomes, and mortality in type 2 diabetes. *N. Engl. J. Med.* 373 (22), 2117–2128. doi:10.1056/NEJMoa1504720

frontiers | Frontiers in Physiology

TYPE Original Research
PUBLISHED 26 September 2022
DOI 10.3389/fphys.2022.974615

OPEN ACCESS

EDITED BY
Vladimir T. Todorov,
Technical University Dresden, Germany

REVIEWED BY
Peter R. Corridon,
Khalifa University, United Arab Emirates
James Hunter,
University of Oxford, United Kingdom

*CORRESPONDENCE
Tobias B. Huber,
t.huber@uke.de
Jan Czogalla,
j.czogalla@uke.de

SPECIALTY SECTION
This article was submitted to Renal Physiology and Pathophysiology, a section of the journal Frontiers in Physiology

RECEIVED 21 June 2022
ACCEPTED 07 September 2022
PUBLISHED 26 September 2022

CITATION
Hofmann S, Grahammer F, Edenhofer I, Puelles VG, Huber TB and Czogalla J (2022), A high-throughput drug discovery pipeline to optimize kidney normothermic machine perfusion. *Front. Physiol.* 13:974615. doi: 10.3389/fphys.2022.974615

A high-throughput drug discovery pipeline to optimize kidney normothermic machine perfusion

Smilla Hofmann[1], Florian Grahammer[1,2], Ilka Edenhofer[1], Victor G. Puelles[1,3], Tobias B. Huber[1]* and Jan Czogalla[1,2]*

[1]III. Department of Medicine, University Medical Center Hamburg-Eppendorf UKE, Hamburg, Germany, [2]University Transplant Center, University Medical Center Hamburg-Eppendorf UKE, Hamburg, Germany, [3]Department of Clinical Medicine, Division of Pathology, Aarhus University, Aarhus, Denmark

Kidney transplantation is the only definitive therapy for end-stage kidney disease. The shortage of organs for transplantation is the main limitation of this life-saving treatment. Normothermic machine perfusion (NMP) is a novel preservation technique with the potential to increase the number of transplantable kidneys through reducing delayed graft function and organ evaluation under physiological conditions. To date, the cellular effects and possible pharmacological interventions during machine perfusion are incompletely understood. A major limitation is the technically complex, time-consuming, and small-scale replication of NMP in rodent models. To overcome this, we developed a 3D-printed, high throughput *ex-vivo* mouse kidney slice incubator (KSI) mimicking mouse kidney NMP by working under closely resembling conditions. KSI significantly reduced the time per experiment and increased the sample throughput (theoretical: 54 incubations with n = 500/day). The model recapitulated the cellular responses during NMP, namely increased endoplasmic reticulum stress (ER stress). Using KSI, five pharmacological interventions against ER stress taken from the literature were tested. While four were ineffective and excluded, one, β-Nicotinamide-adenine-dinucleotide (NADH), ameliorated ER stress significantly during KSI. The test of NADH in mouse kidney NMP replicated the positive effects against ER stress. This suggests that testing the addition of NADH during clinical kidney NMP might be warranted.

KEYWORDS

normothermic machine perfusion, kidney transplantation, kidney regeneration, er stress, NADH, upr, AKI

1 Introduction

End-stage kidney disease (ESKD) is a global health burden with four to seven million estimated patients in need of renal replacement therapy worldwide. The increasing prevalence of risk factors for ESKD, such as hypertension, diabetes mellitus, obesity, and general aging of the population, further drives the incidence of ESKD (Lv and Zhang, 2019). Kidney

transplantation is the gold standard for the treatment of ESKD, as the mortality of patients who receive a renal transplant is lower and the quality of life is greater compared to dialysis patients (Tonelli et al., 2011; Wyld et al., 2012). A growing organ shortage, resulting from fewer donations and increased incidence of ESKD, presents a major problem in the field of kidney transplantation (Liyanage et al., 2015). One solution may be increased use of marginal organs, organs in less than an optimal condition that would normally not be transplanted (Noble et al., 2019). However, these organs are more prone to ischemic injury, delayed graft function, and associated long-term complications (Giraud et al., 2020).

Kidney normothermic machine perfusion (NMP) has gained attention as a promising preservation technique during transplantation due to the theoretical advantages it offers in improving ischemic damage, as well as organ conditioning, analysis, and treatment (Hosgood et al., 2021). NMP for human kidneys has only been tested in-depth in a small number of studies. However, the molecular readout analyzed in these studies unequivocally suggested cytokine release and metabolic- and ER stress during perfusion, revealing the importance of further improvement of the buffer before routine clinical application (Hameed et al., 2019; Ferdinand et al., 2021).

We have recently established a cell-free rodent NMP model for the rigorous preclinical study of potential interventions during NMP (Czogalla et al., 2021). However, the complexity and time-consuming nature of rodent NMP models only allows small-scale sample generation, resulting in slow progress. Here, we describe the generation of a novel, high-throughput *ex-vivo* mouse kidney slice incubation model (KSI) working under "NMP-like" conditions, which recapitulates ER stress as seen during NMP and can be used for drug pre-screening before the time-consuming testing in NMP.

2 Methods

2.1 Animals

Animal experiments were carried out with the approval of the Hamburg University Hospital-Eppendorf and the Hamburg State Department for Animal Welfare (Ethics Approval No. N002/2020). Age- and weight-matched male wildtype C57/Bl6 mice were housed under a 12-h light-dark pattern in an accredited animal facility at UKE Hamburg with free access to chow and water.

2.2 Mouse kidney slice incubator

KSI consists of a beaker with an inset 3D printed chamber, with slots for up to nine kidney slices. Please see Supplementary Figure S2 for dimensions and attached. stl files for 3D-printables. For 3D printing, Extrudr GreenTec Pro natur was used (Extrudr, Austria) based on the basis of excellent oil and salt resistance. Gey's Balanced Salt Solution (GBSS, G9779-6X500ML, Sigma-Aldrich) was used as incubation buffer. Silicon tubing connected to a standard aquarium bubble air stone was used to enrich the buffer with carbogen, a mixture of 95% O2 and 5% CO2, until saturation was reached. The beaker including the 3D-printed chamber was placed in a water bath heated to reach a constant temperature of 33°C. Decapsulated mouse kidneys were cut into 1-mm-sized slices with a homemade razorblade-based tissue chopper and got either incubated in drug solutions (GBSS + added drugs) or in control solution (GBSS + diluent, where used) for 30 min. After incubation, tissue was snap-frozen in liquid nitrogen, placed in 4% PFA for diffusion fixation, or RNAlater (AM7021, Qiagen) for mRNA analysis. Experiments were repeated in at least three animals. No further repeats were performed to satisfy animal ethics concerns.

2.3 Mouse kidney normothermic machine perfusion

Mouse kidney NMP was performed as previously described (Czogalla et al., 2016). After median laparotomy, ligatures were placed around aorta, kidney arteries and vena cava. The kidney artery and vein were cannulated and the kidney removed from the animal. The kidney was connected to a pressure-controlled perfusion circuit and perfusion was carried out for 1 h at 100 mmHg. The kidney was placed in a moist chamber (TYPE 834/8, 73-2901, Hugo Sachs, Germany) and the lid closed. Perfusion flow was continuously recorded at the arterial tip using a pressure transducer (APT300, Hugo Sachs, Germany), a three-channel cannula (73-3309, Hugo Sachs, Germany), a TAM-D Plugsys transducer (73-1793, Hugo Sachs, Germany) and recording software (HSE BDAS 73-4796, Hugo Sachs, Germany) (Supplementary Figure S3). The pump used was a Reglo Digital 4-Channel pump (75-1004, Hugo Sachs, Germany). Buffer reservoirs used were jacketed and filled with 37°C (73-3440). For further surgical and technical details, please refer to: (Czogalla et al., 2016). GBSS (Sigma-Aldrich, G9779) was used as perfusate, kept at 37°C and continuously enriched via dialysis with 95% O_2 and 5% CO_2. For the intervention, b-nicotinamide adenine dinucleotide (Sigma-Aldrich, N8129) was dissolved in GBSS to a concentration of 0.07 mM. Perfusion flow was continuously recorded at the arterial tip using a pressure transducer (APT300, Hugo Sachs, Germany), a three-channel cannula (73-3309, Hugo Sachs, Germany), a TAM-D plugsys transducer (73-1793, Hugo Sachs, Germany) and recording software (HSE BDAS 73-4796, Hugo Sachs,

List of incubation drugs

Drug	Company	Article number	Concentration
Salubrinal	Sigma Aldrich	SML0951	37.42 µM
Isoproterenol	Sigma Aldrich	I5627	200 nM
Ursodeoxycholic Acid	Sigma Aldrich	U5127	100 µM
β-Nicotinamide-adenine-dinucleotide	Sigma Aldrich	N8129	0.07 mM
Roflumilast	Sigma Aldrich	SML1099	49.6 µM

List of components for KSI

Components	Company	Article number
Glass beaker	Th. Geyer	7690006
3D printed chamber	Self-made	Design in Supplement
Gey's Balanced Salt Solution	Sigma Aldrich	G9779-6X500 ML
Printing material (GREENTEC PRO natur)	Extrudr	2286
Bubble air stone	Aipaide	APD-Stone-063
Water bath	Julabo	CD-BT19

List of antibodies

Target	Company	Article number	Dilution
BiP	Cell Signaling	3183	1:500
pS51-eIF2α	Cell Signaling	9721	1:250
total eIF2α	Cell Signaling	2103S	1:500
alpha-tubulin	Sigma-Aldrich	T9026	1:5.000
beta-actin	Sigma-Aldrich	A5441	1:10.000

Germany) (Supplementary Figure S3). After perfusion, tissue was either snap-frozen in liquid nitrogen, placed in 4% PFA for diffusion-fixation, or RNAlater (AM7021, Qiagen) for mRNA analysis. Experiments were repeated in six animals.

2.4 Immunoblotting

For Western blot analysis, kidney samples were lysed for 30 min in 0.5–1 ml of RIPA buffer with the Minilys personal homogenizer (P000673-MLYS0-A, Bertin Technologies). Subsequently, samples were centrifuged at 4.600 rpm for 15 min, the supernatant was transferred to a new tube for the adjustment of protein concentration. Protein content was determined by a BCA assay (23227, Thermo Fisher Scientific) with a Tecan sunrise scanner (30111999, Tecan Trading AG). Before protein electrophoresis, the samples were diluted with 2x Laemmli buffer (1:1) and cooked at 95°C for 5 min. For each lane, 50 µg of protein were loaded. The sample proteins and a protein ladder in one lane were separated in pre-cast gels of 4%–20% (4561096EDU, BioRad) for 20 min at 80 V and 1 h at 120 V. Immunoblotting was performed with Trans-Blot Turbo Mini 0.2 µm PVDF transfer packs (704156, BioRad) for 7 min at 25 V, 1.3 A, using a Trans-Blot Turbo Transfer System (1704150, BioRad). Blocking was performed with a 5% bovine-serum-albumin- (BSA, A9430, Sigma-Aldrich) PBST solution (0.1% Tween) for 1 h. The membranes were incubated with a primary antibody solution at 4°C overnight. Incubation with horseradish peroxidase-conjugated secondary antibodies was performed at room temperature for 1 h. Imaging was performed after incubation of the membranes with ECL Western Blot Substrate (32209, Thermo Scientific) with a chemiluminescence detector (Amersham Imager 600). Analysis was performed with ImageJ [2.3.0/1.53 f (64-bit), US National Institutes of Health].

2.5 Quantitative real-time RT-PCR

Total RNA was extracted with QIAzol Lysis Reagent (79306, Qiagen) and the isolation was performed with the miRNeasy Plus Universal Mini Kit (217084, Qiagen). The RNase-Free DNase Set (79254, Qiagen) was used for DNA digestion. For reverse transcription, Protoscript II First Strand cDNA Synthesis Kit (E6560L, New England

List of primers

Target	Company	Article number	TaqMan Assay ID
Mouse GAPD (GAPDH)	Thermo Fisher Scientific	4352932E	Mm99999915_g1
Mouse activating transcription factor 4 (ATF4)	Thermo Fisher Scientific	4331182	Mm00515324_m1
Mouse DNA damage inducible transcript 3 (CHOP)	Thermo Fisher Scientific	4331182	Mm00492097_m1
Mouse receptor-interacting serine-threonine kinase 3 (RIPK3)	Thermo Fisher Scientific	4331182	Mm00444947_m1

BioLabs) was applied. Quantitative PCR was performed on a QuantStudio 3 System (A28566, Thermo Fisher Scientific) using 0.5 µg of cDNA, gene-specific TaqMan™ primers, and TaqMan™ Fast Universal PCR Master Mix (43-660-73, Thermo Fisher Scientific). Glyceraldehyde-3-phosphate dehydrogenase (GAPDH, Thermo Fisher Scientific) was used for normalization. The qPCR data were analyzed with the double delta CT method.

2.6 Histological analysis

Samples diffusion-fixed in 4% formaldehyde and stored at 4°C were embedded in paraffin and stained with periodic acid-Schiff (PAS) reagent following standard protocol. Incubation times were 1 hour in Schiff's reagent and staining of nuclei in hematoxylin for 3 min. Tubular damage was evaluated by two researchers. For TUNEL staining, Deadend Colorimetric TUNEL System (G7130, Promega) was used according to the manufacturer's specifications. The incubation time of proteinase K was 20 min, the staining time of DAB 12 min. PAS damage scores were graded by two researchers according to Pulskens et al. (2008). Briefly, the percentage of damaged tubules in the corticomedullary junction was estimated according to the following criteria: tubular dilatation, cast deposition, brush border loss, and necrosis. Lesions were grouped into 5 groups: involvement of less than 10% of the cortex; involvement of 10%–25% of the cortex; involvement of 25%–50% of the cortex; involvement of 50%–75% of cortex; involvement of more than 75% of the cortex. TUNEL-positive nuclei were counted by two researchers. For each condition, 3* 20x microscopic images per animal were evaluated.

2.7 Statistics

Statistical analysis was performed with GraphPad Prism. For statistics, Shapiro-Wilk test was used to ascertain normal distribution. All data passed the Shapiro-Wilk test, except when explicitly mentioned in figure legends. Following this procedure, an unpaired two-tailed *t*-test with Welch's correction or one-way ANOVA combined with Tukey's multiple comparisons test were used for determination of statistical significance when data were normally distributed (see figure legends for details). If data were not normally distributed, Mann-Whitney test was used. Data were considered statistically significant if $p < 0.05$.

3 Results

3.1 Establishment of a simple, rapid and easily replicable 3D printed kidney slice incubation setup to study drug targeting of ER stress.

Kidney slice incubation chambers were designed based on our previous experience (Penton et al., 2016). 3D printing allowed rapid prototyping and improvement until a final design was chosen based on the best handling properties (.stl files for reprinting in supplement). Using a razorblade-based tissue slicer, ~20 1 mm thick kidney slices could be generated from both kidneys of one animal. The parallel use of 6 3D printed chambers allowed the investigation of n = 54 kidney slices incubated under 6 different conditions at the same time (Figure 1). The time spent from tissue harvesting to the end of the experiment and tissue storage was 1 hour, increasing the theoretical n/day from 2 during mouse machine perfusion to 500. First, we analyzed the optimal conditions to study ER stress during KSI. As a readout, we focused on the phosphorylation of eIF2α, since the targets of phosphorylated eIF2α appeared during the sequencing of human kidneys after NMP (Hameed et al., 2019). Analysis of eIF2α phosphorylation, a hallmark of ER stress and integrated stress response, over time showed increased phosphorylation until 30 min, which then slowly faded over time, presumably due to cell death (Using the methods described here, tissue degradation cannot be ruled out). This interpretation was underlined by conjoined loss of α-tubulin, while loading of 50 µg of protein was ensured (Supplementary Figure S1A). Using the same read-out, we tested different temperatures for incubation and arrived at 33°C.

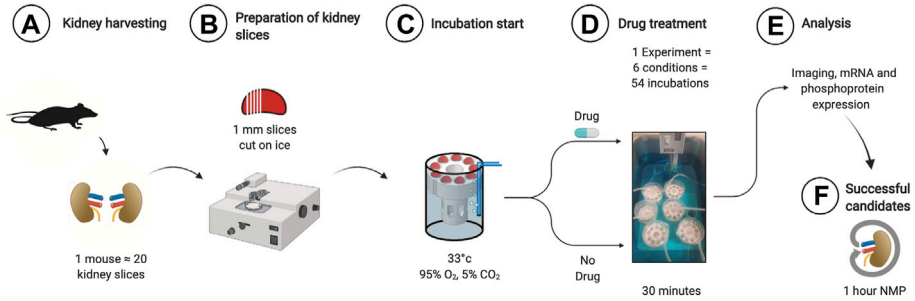

FIGURE 1
Workflow for KSI. Both kidneys are harvested and decapsulated **(A)**. On ice, ~1 mm slices are prepared using a razor-based tissue cutter **(B)**. Slices are put into KSI incubator **(C)**. Drugs are added and incubation performed for 30 min **(D)**. Material is analyzed **(E)** and successful candidates taken towards further testing in mouse NMP.

As the optimum (Supplementary Figure S1B). Buffer and carbogen were needed to activate full eIF2α phosphorylation (Supplementary Figure S1C).

3.2 Kidney slice incubator and cell-free mouse kidney normothermic machine perfusion show comparable activation of the unfolded protein response

Next, we performed a direct comparison of UPR activation in the KSI model vs the NMP model established in our laboratory (Czogalla et al., 2016). BiP expression and eIF2α phosphorylation, hallmarks of the early UPR (For an overview of the UPR, see Figure 2A), were strongly increased after both inventions (Figures 2B,D). In both models, the mRNA of ATF4 and CHOP was upregulated, which is the classical transcriptomic response to increased eIF2α phosphorylation of eIF2 (Figures 2C,E) (Iurlaro and Muñoz-Pinedo, 2016) (Lau et al., 2013). Analysis of tubular morphology and damage after interventions revealed severe damage and TUNEL positive nuclei in proximal tubuli in both models (Figure 2F and Supplementary Figures S3B,C). Luminal PAS-positive casts, most likely resembling Tamm-Horsfall protein accumulation, underline this interpretation. In summary, UPR activation and subsequent proximal tubular damage and cell death are seen to a comparable extent in both the KSI- and the NMP models.

3.3 NADH ameliorates ER stress in kidney slice incubator and mouse kidney normothermic machine perfusion

To test whether pharmacological interventions discovered during KSI can be transferred to NMP, we investigated drugs proposed to work against ER stress (Gao et al., 2013; Chen et al., 2021; Xu et al., 2021): Salubrinal, Isoproterenol, Roflumilast, UDCA and β-Nicotinamide-adenine-dinucleotide. Surprisingly, salubrinal, isoproterenol, roflumilast, and UDCA did not show significant improvements in KSI (Figure 3A) (Supplementary Table S1). β-Nicotinamide-adenine-dinucleotide, however, did show a promising decrease in the expression of ATF4 and CHOP mRNA in KSI (Figure 3C). Initiation of apoptosis was reduced in TUNEL staining of KSI (Figure 3D and Supplementary Figure S3B). We interpreted these results as promising enough to test the addition of NADH to the perfusion buffer during NMP. When NADH was added, the effects observed during KSI were found to be reproducible (Figures 3F,G and Supplementary Figure S3C). In both models, protein analysis (Figures 3B,E) showed a trend towards reduction, however, this effect was not significant. The perfusion flow was not significantly different (Supplementary Figure S3A). To test translatability of negative results during KSI towards NMP, we tested isoproterenol addition during NMP. The addition of isoproterenol did not improve markers of ER stress during NMP (Supplementary Table S1).

4 Discussion

We here describe a simple, high-throughput model for drug prescreening before the time-consuming testing during mouse kidney NMP. The model can easily be reproduced using a 3D printer, allows incubation of 54 kidney slices under six different conditions at the same time, and partially recapitulates tubular damage and ER stress seen during NMP. Application of an established pharmacological treatment, β-Nicotinamide-adenine-dinucleotide, reduced transcriptomic markers of ER stress during KSI. This

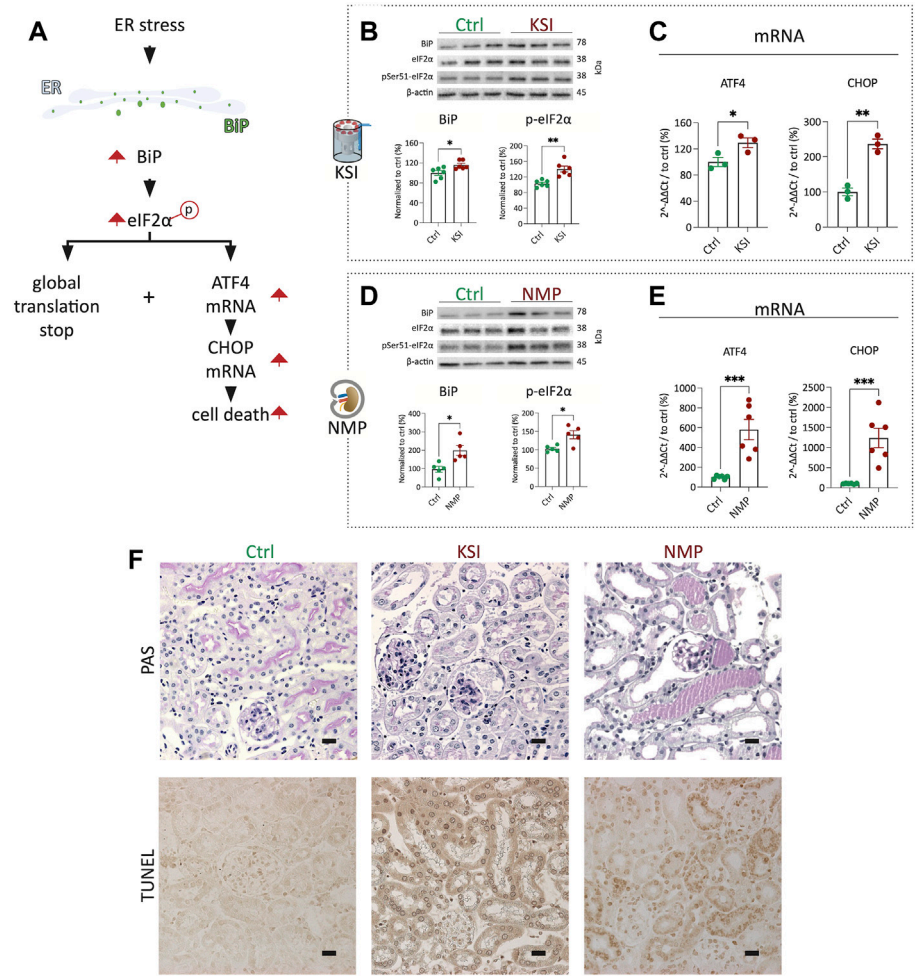

FIGURE 2
KSI and NMP exhibit broadly comparable molecular adaptions to ER stress. Pathway overview of the molecular processes of ER stress as investigated during KSI and NMP **(A)**. Western blotting reveals increased BiP release and eIF2α phosphorylation after KSI. BiP release after KSI did not pass Shapiro-Wilk test for normal distribution. **(B)**. Western blotting reveals increased BiP release and eIF2α phosphorylation after NMP **(D)**. ATF4 and CHOP mRNA are increased with KSI and NMP **(C,E)**. Increased, mainly proximal, tubular damage is seen to comparable extends after KSI and NMP using PAS- and TUNEL stainings **(F)**. Unpaired *t*-test with Welch's correction was used for all data, except 2b BiP, where Mann-Whitney test was used. *p* values: *< 0.05, ** <0.01, ***< 0.001. Scalebar: 15 μm n ≥ 3 for KSI and n = 6 for NMP.

finding was reproducible during NMP. Isoproterenol did not reduce ER stress during KSI. This negative result was replicated during NMP. Three other unsuccessful drug candidates could be excluded before the time-consuming test during NMP.

There are several arguments against the use of mouse kidney NMP for large-scale drug testing: The method requires an advanced setup with two different pumping systems, perfusion parameters constantly need to be analyzed and adjusted, and the surgery has to be performed by specifically trained investigators. Finally, one setup allows the perfusion of only two kidneys per day, including preparation- and postprocessing time. The novel KSI model, on the other hand, has a simple setup with material found in almost any laboratory. The chambers are 3D printed and can easily be reproduced. Explantation of the kidneys does not require advanced skills. Furthermore, kidney slices, as compared to cell culture, organ-on-a-chip approaches, and kidney organoids possess the advantage of the complete renal cellular architecture (Yin et al., 2020). All in all, the KSI model provides a simple and rapid means for hypothesis-testing of drug efficacy towards ER stress before their application in NMP.

Using KSI, we found one drug, β-Nicotinamide-adenine-dinucleotide, that partially reversed the maladaptations occurring during overshooting ER stress. Given these promising results, we continued to test NADH in NMP. Underlining the value of KSI, the favorable drug response was

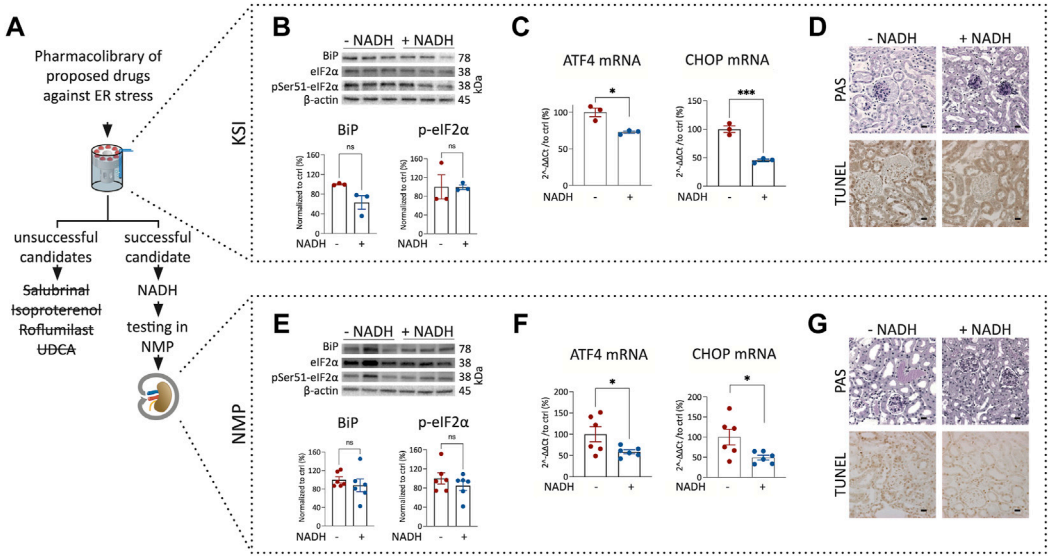

FIGURE 3
Addition of NADH reduces markers of ER stress and cell death in KSI and NMP. Workflow for drug discovery using KSI **(A)**. Western blotting reveals a nonsignificant trend towards reduced BiP release and eIF2α phosphorylation in KSI co-incubated with NADH **(B)**. ATF4 and CHOP mRNA are reduced when NADH is added to the incubation buffer **(C)** Cellular damage was less pronounced in TUNEL, but not in PAS stainings of tissue co-incubated with NADH **(D)**. BiP release and eIF2α phosphorylation in NMP co-incubated with NADH are not significantly reduced **(E)**. ATF4 and CHOP mRNA are reduced when NADH is added to the perfusion buffer **(F)** Cellular damage appears less pronounced in PAS- and TUNEL stainings of tissue coperfused with NADH **(G)**. Unpaired *t*-test with Welch's correction was used. *p* values: *< 0.05, ** <0.01, ***< 0.001. Scalebar: 15 μm $n = 3$ for KSI and $n = 6$ for NMP.

replicable during NMP. We chose to use the NADH energy-rich NAD formulation, as we hypothesized beneficial effects during acute models. To our knowledge, this is the first time the beneficial effects of the addition of NADH to NMP preparations have been shown.

Since the molecular maladaptations we observed, as well as the morphological changes, are in line with findings in acute kidney injury (AKI), and the molecular improvement with addition of NAD has also been described for AKI *in vivo* (Arykbaeva et al., 2021) (Faivre et al., 2021; Morevati et al., 2021) (Morevati et al., 2021), KSI could additionally be a model well suited to study drug treatment for the acute phases of ischemic AKI. Other *ex-vivo* techniques for the study of ischemia-reperfusion (e.g., cell culture microflow chamber) take comparable approaches (Giraud et al., 2020). Compared to these, KSI has the advantage of intact anatomy and the disadvantage of a shorter time of observation.

There are several limitations to the KSI model and this study. We found the optimal time period for analysis of the ER stress response in KSI was 30 min. This is a shorter time than used in rodent NMP models (1 hour in mice, 2 hours in rats) (Czogalla et al., 2021). Most probably, adaptions and molecular processes occurring during NMP are missed during this shorter time. Furthermore, we found the optimal temperature for the analysis of the ER stress response in KSI is 33°C, whereas mouse kidney NMP is performed at 37°C. Although the enzyme kinetics analyzed during this study of the UPR did show roughly comparable activity, the effects seemed to be more sustained with NMP. While we focused on the analysis of one single pathway of particular interest for our laboratory, we cannot rule out that other pathways might be affected as well, however, our findings cannot be extrapolated toward other signaling pathways. During KSI, drugs reach cells via passive diffusion rather than active perfusion. While this provides a minimalistic model that can be used to study molecular signaling on the cellular level without the influence of perfusion, the perfusion itself could have various effects that are not featured in the KSI model. The number of animals chosen during KSI in this study ($n = 3$) is small and does not completely rule out that results may differ when large groups of animals are used. Lastly, we did not perform testing of all drugs under both KSI- and NMP and can thus not exclude that drugs not working in KSI would have worked in NMP.

To conclude, we developed a kidney slice model that can be used to study drug targeting of ER stress signaling and associated cell death responses. Comparison to NMP suggests that successful results may, at least in part, be transferrable. KSI provides a solution for rapid large-scale drug testing and could lead the way to generating a library of promising drug candidates for clinical testing during NMP. Further testing of NADH for clinical perfusion buffers might be warranted.

Data availability statement

The original contributions presented in the study are included in the article/Supplementary Material, further inquiries can be directed to the corresponding authors.

Ethics statement

The animal study was reviewed and approved by Behörde für Justiz und Verbraucherschutz, Stadt Hamburg.

Author contributions

SH, FG, IE, VP, TH, and JC designed, executed, and analyzed the experiments. SH, VP, and JC wrote the manuscript. The manuscript was read and approved by all authors.

Funding

JC was supported by a Clinician Scientist- and a Tandemgrant from the University of Hamburg. SH was supported by an iPrime stipend (Else-Kroener-Fresenius Foundation). VP was supported by Young Investigator Award (NNF21OC0066381) by Novo Nordisk Foundation. TH was supported by the DFG (CRC1192, HU 1016/8-2, HU 1016/11-1, HU 1016/12-1) and by the BMBF (STOP-FSGS-01GM1901C).

Acknowledgments

The authors thank David Penton Ribas, University of Zurich, for multiple scientific advances in the field of tissue slice incubation and the pre-design of the incubator described in this manuscript.

Conflict of interest

The authors declare that the research was conducted in the absence of any commercial or financial relationship that could be construed as a potential conflict of interest.

Publisher's note

All claims expressed in this article are solely those of the authors and do not necessarily represent those of their affiliated organizations, or those of the publisher, the editors and the reviewers. Any product that may be evaluated in this article, or claim that may be made by its manufacturer, is not guaranteed or endorsed by the publisher.

Supplementary material

The Supplementary Material for this article can be found online at: https://www.frontiersin.org/articles/10.3389/fphys.2022.974615/full#supplementary-material

References

Arykbaeva, A. S., Vries, D. K. de, Doppenberg, J. B., Engelse, M. A., Hankemeier, T., and Harms, A. C. (2021). Metabolic needs of the kidney graft undergoing normothermic machine perfusion. *Kidney Int.* 100, 301–310. doi:10.1016/j.kint.2021.04.001

Chen, J.-H., Wu, C.-H., and Chiang, C.-K. (2021). Therapeutic approaches targeting proteostasis in kidney disease and fibrosis. *Int. J. Mol. Sci.* 22, 8674. doi:10.3390/ijms22168674

Czogalla, J., Schweda, F., and Loffing, J. (2016). The mouse isolated perfused kidney technique. 117, *J. Vis. Exp. JoVE*. doi:10.3791/54712

Czogalla, J., Grahammer, F., Puelles, V. G., and Huber, T. B. (2021). A protocol for rat kidney normothermic machine perfusion and subsequent transplantation. *Artif. organs* 45, 168–174. doi:10.1111/aor.13799

Faivre, A., Katsyuba, E., Verissimo, T., Lindenmeyer, M., Rajaram, R. D., and Naesens, M. (2021). Differential role of nicotinamide adenine dinucleotide deficiency in acute and chronic kidney disease*Nephrol. Dial. Transplant.* official publication of the European Dialysis and Transplant Association - European. Renal Association 36, 60–68. doi:10.1093/ndt/gfaa124

Ferdinand, J. R., Hosgood, S. A., Moore, T., Ferro, A., Ward, C. J., and Castro-Dopico, T. (2021). Cytokine absorption during human kidney perfusion reduces delayed graft function-associated inflammatory gene signature. *Am. J. Transplant.* 21, 2188–2199. doi:10.1111/ajt.16371

Gao, B., Zhang, X., Han, R., Zhang, T., Chen, C., and Qin, Z. (2013). The endoplasmic reticulum stress inhibitor salubrinal inhibits the activation of autophagy and neuroprotection induced by brain ischemic preconditioning. *Acta Pharmacol. Sin.* 34, 657–666. doi:10.1038/aps.2013.34

Giraud, S., Thuillier, R., Cau, J., and Hauet, T. (2020). *In vitro/ex vivo* models for the study of ischemia reperfusion injury during kidney perfusion. *Int. J. Mol. Sci.* 21. doi:10.3390/ijms21218156

Hameed, A. M., Lu, D. B., Patrick, E., Xu, B., Hu, M., and Chew, Y. V., (2019). Brief normothermic machine perfusion rejuvenates discarded human kidneys. *Transplant. direct* 5, e502. doi:10.1097/TXD.0000000000000944

Hosgood, S. A., Hoff, M., and Nicholson, M. L. (2021). Treatment of transplant kidneys during machine perfusion. *Transpl. Int. official J. Eur. Soc. Organ Transplant.* 34, 224–232. doi:10.1111/tri.13751

Iurlaro, R., and Muñoz-Pinedo, C. (2016). Cell death induced by endoplasmic reticulum stress. *FEBS J.* 283, 2640–2652. doi:10.1111/febs.13598

Lau, A., Wang, S., Jiang, J., Haig, A., Pavlosky, A., and Linkermann, A. (2013). RIPK3-mediated necroptosis promotes donor kidney inflammatory injury and reduces allograft survival. *Am. J. Transplant. official J. Am. Soc. Transplant. Am. Soc. Transpl. Surg.* 13, 2805–2818. doi:10.1111/ajt.12447

Liyanage, T., Ninomiya, T., Jha, V., Neal, B., Patrice, H. M., and Okpechi, I., (2015). Worldwide access to treatment for end-stage kidney disease: A systematic review. *Lancet* 385, 1975. doi:10.1016/S0140-6736(14)61601-9

Lv, J.-C., and Zhang, L.-X. (2019). Prevalence and disease burden of chronic kidney disease. *Adv. Exp. Med. Biol.* 1165, 3–15. doi:10.1007/978-981-13-8871-2_1

Morevati, M., Egstrand, S., Nordholm, A., Mace, M. L., Andersen, C. B., and Salmani, R. (2021). Effect of NAD+ boosting on kidney ischemia-reperfusion injury. *PloS one* 16, e0252554. doi:10.1371/journal.pone.0252554

Noble, J., Jouve, T., Malvezzi, P., Süsal, C., and Rostaing, L. (2019). Transplantation of marginal organs: Immunological aspects and therapeutic perspectives in kidney transplantation. *Front. Immunol.* 10, 3142. doi:10.3389/fimmu.2019.03142

Penton, D., Czogalla, J., Wengi, A., Himmerkus, N., Loffing-Cueni, D., and Carrel, M. (2016). Extracellular K+ rapidly controls NaCl cotransporter

phosphorylation in the native distal convoluted tubule by Cl- -dependent and independent mechanisms. *J. physiology* 594, 6319–6331. doi:10.1113/JP272504

Pulskens, W., Teske, G. J., Butter, L. M., Roelofs, J. J., van der Poll, T., and Florquin, S. (2008). Toll-Like Receptor-4 coordinates the innate immune response of the kidney to renal ischemia/reperfusion injury. *Plos One*. 1. 1. doi:10.1371/journal.pone.0003596

Tonelli, M., Wiebe, N., Knoll, G., Bello, A., Browne, S., and Jadhav, D. (2011). Systematic review: Kidney transplantation compared with dialysis in clinically relevant outcomes. *Am. J. Transplant. official J. Am. Soc. Transplant. Am. Soc. Transpl. Surg.* 11, 2093–2109. doi:10.1111/j.1600-6143.2011.03686.x

Wyld, M., Morton, R. L., Hayen, A., Howard, K., and Webster, A. C. (2012). A systematic review and meta-analysis of utility-based quality of life in chronic kidney disease treatments. *PLoS Med.* 9, e1001307. doi:10.1371/journal.pmed.1001307

Xu, B., Xu, J., Cai, N., Li, M., Liu, L., and Qin, Y., (2021). Roflumilast prevents ischemic stroke-induced neuronal damage by restricting GSK3β-mediated oxidative stress and IRE1α/TRAF2/JNK pathway. *Free Radic. Biol. Med.* 163, 281–296. doi:10.1016/j.freeradbiomed.2020.12.018

Yin, L., Du, G., Zhang, B., Zhang, H., Yin, R., and Zhang, W., (2020). Efficient drug screening and nephrotoxicity assessment on Co-culture microfluidic kidney chip. *Sci. Rep.* 10, 6568. doi:10.1038/s41598-020-63096-3

frontiers | Frontiers in Physiology

TYPE Original Research
PUBLISHED 27 September 2022
DOI 10.3389/fphys.2022.980787

OPEN ACCESS

EDITED BY
Sebastian Frische,
Aarhus University, Denmark

REVIEWED BY
Jeffrey Kopp,
National Institute of Diabetes and Digestive and Kidney Diseases (NIH), United States
Luciano D'Apolito,
BioGeM Institute, Italy

*CORRESPONDENCE
Christian Hugo,
Christian.hugo@ukdd.de

SPECIALTY SECTION
This article was submitted to Renal Physiology and Pathophysiology, a section of the journal Frontiers in Physiology

RECEIVED 29 June 2022
ACCEPTED 01 September 2022
PUBLISHED 27 September 2022

CITATION
Arndt P, Sradnick J, Kroeger H, Holtzhausen S, Kessel F, Gerlach M, Todorov V and Hugo C (2022), A quantitative 3D intravital look at the juxtaglomerular renin-cell-niche reveals an individual intra/extraglomerular feedback system. *Front. Physiol.* 13:980787. doi: 10.3389/fphys.2022.980787

A quantitative 3D intravital look at the juxtaglomerular renin-cell-niche reveals an individual intra/extraglomerular feedback system

Patrick Arndt[1], Jan Sradnick[1], Hannah Kroeger[1], Stefan Holtzhausen[2], Friederike Kessel[1], Michael Gerlach[3], Vladimir Todorov[1] and Christian Hugo[1]*

[1]Experimental Nephrology, Division of Nephrology, Department of Internal Medicine III, University Hospital Carl Gustav Carus, Dresden University of Technology, Dresden, Germany, [2]Institute of Machine Elements and Machine Design, Chair of Virtual Product Development, Dresden University of Technology, Dresden, Germany, [3]Core Facility Cellular Imaging, Experimental Center, Faculty of Medicine Carl Gustav Carus, Dresden University of Technology, Dresden, Germany

The juxtaglomerular niche occupied by renin cells (RCN) plays an important role in glomerular repair but the precise temporal and spatial interrelations remain unclear. This study proposes the hypothesis of a local intra-extraglomerular regenerative feedback system and establishes a new quantifiable system for RCN responses in individual glomeruli *in vivo*. A strictly intraglomerular two-photon laser-induced injury model was established. Labeled renin cells (RC) in transgenic renin reporter mice were fate-traced in healthy and injured glomeruli over several days by intravital microscopy and quantified via new three-dimensional image processing algorithms based on ray tracing. RC in healthy glomeruli demonstrated dynamic extraglomerular protrusions. Upon intraglomerular injury the corresponding RCN first increased in volume and then increased in area of dynamic migration up to threefold compared to their RCN. RC started migration reaching the site of injury within 3 hours and acquired a mesangial cell phenotype without losing physical RCN-contact. During intraglomerular repair only the corresponding RCN responded via stimulated neogenesis, a process of *de novo* differentiation of RC to replenish the RCN. Repeated continuous intravital microscopy provides a state-of-the-art tool to prove and further study the local intraglomerular RCN repair feedback system in individual glomeruli *in vivo* in a quantifiable manner.

KEYWORDS

intravital imaging, two-photon microscopy, renin cells, laser injury, glomerular injury, cell migration, ray tracing

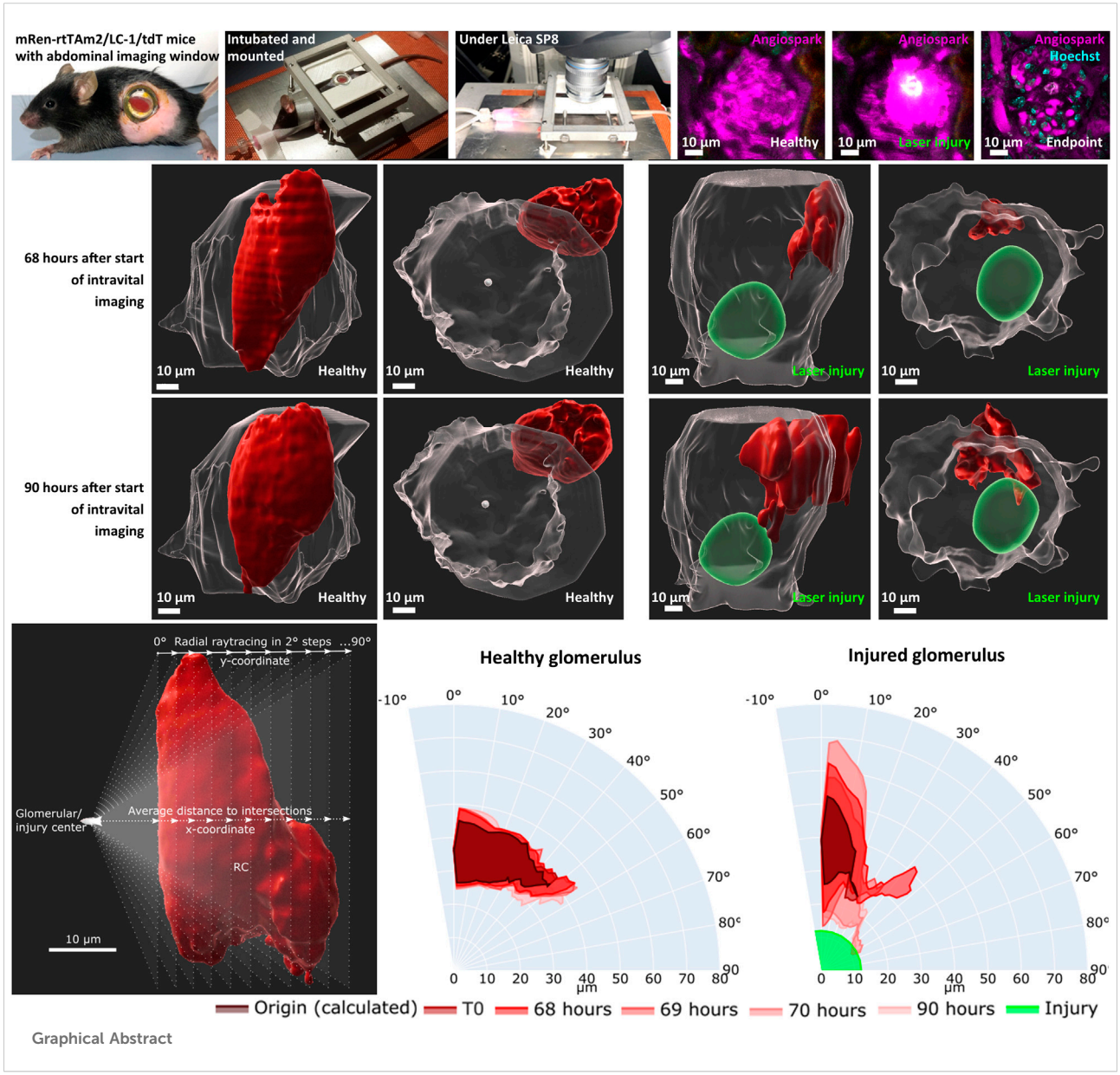

Graphical Abstract

Introduction

Specific renal progenitor cells occupy particular niches that have been identified to contribute to kidney regeneration and repair (Oliver et al., 2004; Starke et al., 2015; Andrianova et al., 2019). During nephrogenesis, stromal precursors differentiate into renal cell types that persist in the adult kidney (Sequeira Lopez and Gomez, 2011; Sequeira-Lopez and Gomez, 2021). Among them, renin cells (RC) reside in the juxtaglomerular apparatus (JGA) forming a renin cell niche (RCN) and function as pluripotent progenitors capable of migrating into the glomerulus after injury and acquiring a mesangial cell phenotype (Pippin et al., 2013; Pippin et al., 2015; Starke et al., 2015). In addition, juxtaglomerular RC are constantly replenished by neogenesis (*de novo* differentiation), a rare process of differentiation of a cell to join the renin lineage for the very first time under matured physiological conditions, that is markedly stimulated during response to injury (Hickmann et al., 2017; Steglich et al., 2020). While regulation of these complex repair processes is poorly understood, similar to the canonical tubulo-glomerular RC feedback mechanisms relating to salt-water homeostasis (Thurau and Schnermann, 1965), the authors hypothesized that these remarkable processes in adults, which resemble embryonic nephrogenesis to some extent, also underlie a local individual intraglomerular-extraglomerular feedback mechanism (Steglich et al., 2020).

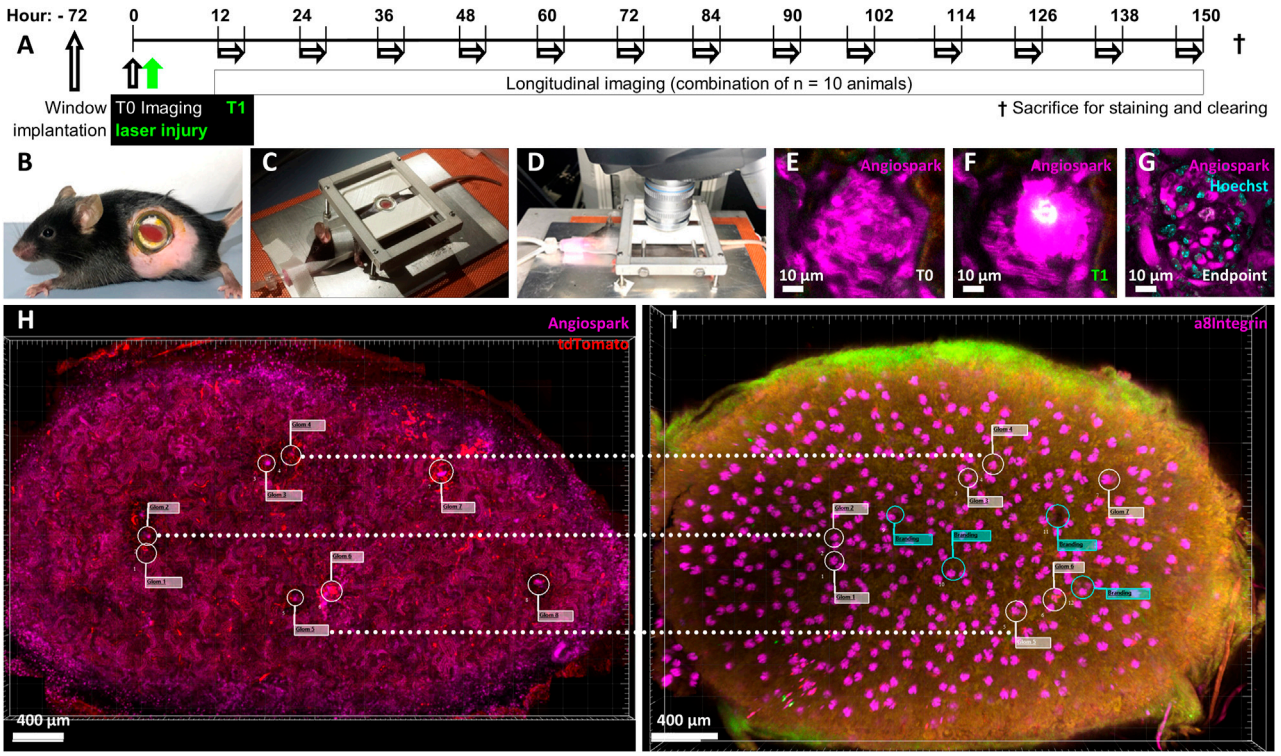

FIGURE 1
Experimental overview. Ten mRen-rtTAm2/LC-1/tdT mice underwent a 21-day pulse labelling induction period with 625 mg/kg Doxycycline and 10 mg/kg enalapril, followed by a 7-day washout period. **(A)** Timeline of experimental setup after pulse induction, washout and with abdominal imaging window implantation 72 h before baseline imaging (T0) followed by immediate laser injury irradiation (T1). Longitudinal imaging experiments from all mice were combined and overlapped to cover the entire time period according to the scheme. Each single mouse was imaged longitudinal for 3 h, always with at least 12 h recovery time and only to a maximum of 3 times. **(B)** Mouse with implanted abdominal imaging window in left flank and visible kidney (red) glued to the inside of the window. **(C)** Intubated, ventilated and anesthetized mouse on a heating plate fixed via the abdominal imaging window, **(D)** mounted for intravital two-photon microscopy. **(E)** Intravital imaged healthy glomerulus and its capillary structures made visible via **(I)** *v*. Angiospark 680 (magenta). **(F)** Laser-induced injury of the identical glomerulus with Angiospark 680 leakage and white autofluorescence of the laser-injured area. **(G)** Follow-up of the same laser-irradiated glomerulus 5 days after injury. The autofluorescent area is further visible in the still-functioning glomerulus revealed by Hoechst nuclear staining. **(H)** Kidney overview of glomeruli positions in three-dimensional intravital imaging data and **(I)** alignment to identical glomeruli after sacrifice, immunohistology staining and tissue clearing. Guiding laser brandings are marked with green flags in the overlay.

Understanding of this feedback mechanism and its mediators could open the door for new treatments for glomerular disease via stimulating endogenous renal repair mechanisms.

This hypothesis could be directly studied if a model system would be available, in which RC can be continuously visualized, individual glomeruli can be specifically injured and longitudinally imaged until an injury-directed repair process is completed and possibly quantified. In antibody mediated inflammatory glomerular injury models, systemic inflammation leads to injury and activation of a broad range of kidney cell types complicating the experimental study of the principle of cause and effect. In these models, RC-mediated repair processes occur only focally and variably up to 10 days following disease induction (Starke et al., 2015), making it impossible to study this hypothesis via intravital microscopy (Ruhnke et al., 2018).

Therefore, intravital imaging was applied in RC transgenic mice with an inducible cell type specific marker representing a state-of-the-art technique allowing the longitudinal study of complex glomerular and extraglomerular responses to injury on a cellular level (Schiessl et al., 2020; Desposito et al., 2021; Gyarmati et al., 2021). It enables spatially and temporally detailed visualization of the complex three-dimensional structure of various renal cell compartments under physiological and pathophysiological conditions (Hohne et al., 2013; Burford et al., 2014; Hickmann et al., 2017). This method can also be used to induce local injury/damage limited to very few cells by targeted laser irradiation in individual glomeruli and to observe processes longitudinally under controlled conditions (Kaverina et al., 2017; Schiessl et al., 2020). In this study, injury was chosen to be strictly intraglomerular and distant from the JGA. Three-dimensional object information could be obtained directly by

virtual reconstruction and rendering, and used for novel quantification via ray tracing techniques. Ray tracing is an established method in microscopic and optical object characterization in which the path of light through pixels is traced in individual image planes (Kostenko et al., 2013; Khitrin et al., 2017). It finds broad application in generating images in computer graphics. Combining these novel techniques would extend the current knowledge in glomerular imaging (Hackl et al., 2013; Kaverina et al., 2017). Precise intravital overview imaging can enable the rediscovery of corresponding cleared tissue areas and complement intravital imaging with fixed immunohistology to detect renin cell differentiation to mesangial cells (Renier et al., 2014; Klingberg et al., 2017).

The combination of site-specific glomerular injury induction and longitudinal observation with intravital two-photon microscopy in transgenic mice provides a direct view of the regenerative process involving site-directed RC migration and its underlying mechanisms (Zhang et al., 2020). This model system was developed to test the hypothesis of an intraglomerular-extraglomerular RC feedback system, since characterization of individual glomerular responses to injury can only be done in an artificial but timely and spatially controlled model system without broad and undefined systemically mediated injury.

Materials and methods

Animal experiments

Eight-week-old female mRen-rtTAm2/LC-1/tdT mice underwent pulse induction via recombination with 625 mg/kg Doxycycline and 10 mg/kg enalapril for 21 days, followed by 7 days of washout without Doxycycline and enalapril (see Figure 1A) and were then used for imaging of healthy and laser-injured glomeruli (Ashworth et al., 2007; Steglich et al., 2019). Female mice are smaller compared to males and the nephrons are thus closer to the renal capsule (Schiessl et al., 2013). Due to the limited optical penetration depth of the laser, small mice are more suitable for intravital multiphoton microscopy. This approach also reduced (3R) the number of experimental animals. Constitutive mice double heterozygous for mRen and tdT/GFP (mRen-Cre-mT/mG) were used for neogenesis experiments (Hickmann et al., 2017). All mice were initially implanted with an abdominal imaging window (Figure 1B) as previously described (Schiessl et al., 2020). Under anesthetic tracheal intubation (isoflurane 1.5%, 0.8 O2 L/min) and after *i. v.* Injection of fluorescent agents Angiospark 680 (30 µL, undiluted, Perkin&Elmer) and Hoechst 33,342 (50 µL of 2 mg/ml water stock, Sigma-Aldrich), all mice were prepared for upright imaging on a heating plate with a custom-made abdominal imaging window holder (Figure 1C). For the laser injury characterization experiments only, Angiospark was exchanged for propidium iodide (50 µL of 2 mg/ml water stock, Sigma-Aldrich).

The animal study was reviewed and approved by TU Dresden and Landesdirektion Sachsen.

Intravital two-photon laser scanning microscopy

Glomeruli were observed with an upright SP8 MP/OPO laser scanning microscope (Leica, Figure 1D) of the Core Facility Cellular Imaging (CFCI) for 3 hours on 3 days in different mice to cover seven consecutive days with intervals of at least 12 h each according to Figure 1A. Imaging was performed using a Leica HC PL IRAPO 40x/1.10 W (Wd = 0.65 mm) objective employing passive triggering by tracheal ventilation. Two-photon imaging was used with 860 nm/910 nm laser excitation, GFP detection at 525/50 nm, tdTomato detection at 617/81 nm and fared detection at 680/40 nm. Data was acquired with a pixel size of 0.362 µm × 0.362 µm and a Z-step size of 1 µm over a range of 120 µm. Glomeruli not deeper than 120 µm in the renal cortex (Figure 1E) were visualized in 10 mRen-rtTAm2/LC-1/tdT mice and in four mRen-Cre-mT/mG mice. The laser injury was induced by focusing 100% laser power for a maximum of 5 seconds at 48x zoom with a pixel size of 0.011 µm × 0.011 µm on one predetermined Z-plane. Individual intraglomerular Hoechst positive nuclei were carefully selected for each glomerular injury. Successful injury was characterized by strong local autofluorescence (Figure 1F). Injured glomeruli did not lose glomerular perfusion (Figure 1G). After the final imaging, a three-dimensional overview of the kidney area attached to the window was obtained (Figure 1H) and the examined kidney was removed.

Kidney clearing and immunofluorescence staining

Intravitally imaged kidneys were perfused, harvested, the sections glued to the abdominal imaging window approx. 3 mm thick were cut and then immunolabeled with antibodies against α8Integrin (R&D systems, catalog-no. BAF4076) and tdTomato (anti-RFP, Rockland, catalog-no. 600-401–379) following the iDISCO protocol (Renier et al., 2014) and cleared with ethyl cinnamate (ECi) (Klingberg et al., 2017). Briefly, perfused kidney sections were treated in the following order: Paraformaldehyde fixation, methanol dehydration, H_2O_2 bleaching, H_2O rehydration, permeabilization, blocking, antibody staining, methanol dehydration, embedding in agarose and finally ECi clearing. The cleared sample was microscoped entirely and reassessed without automation for the identical microscopic area captured prior to the final biopsy (Figure 1I). Selected glomeruli could be rediscovered by superimposed overviews, comparing landmarks such as laser brandings and identical orientations of glomeruli for

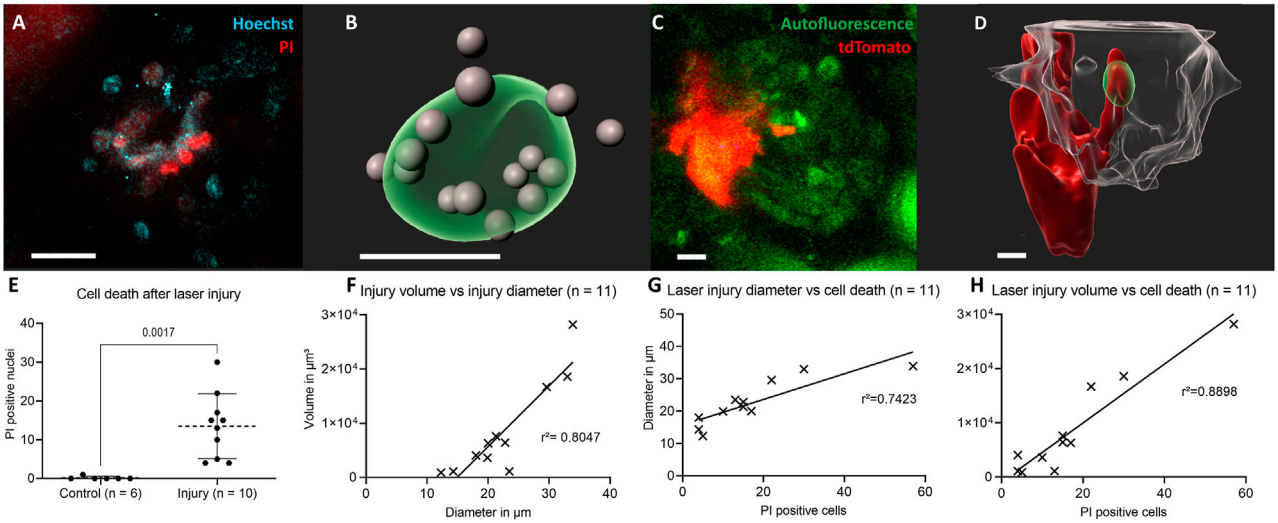

FIGURE 2
Characterization of the laser-induced injury model. **(A)** Two-dimensional slice view with Hoechst and PI stainings around the laser injury and **(B)** corresponding three-dimensional rendering of the autofluorescent area of a glomerular laser injury (green) with propidium iodide (PI) and Hoechst double positive cell nuclei in grey. **(C)** Two-dimensional slice view of renin cells (red) directly invading the laser injured area (green) and **(D)** corresponding three-dimensional rendered glomerulus (transparent-white). **(E)** Number of propidium iodide and Hoechst double positive nuclei 30 min following laser irradiation compared to control. Mean ± SD are indicated and compared with unpaired, two-tailed *t* test calculating $p = 0.017$ for statistical significance. **(F)** Positive linear correlation between laser injury volume and diameter. The geometric parameters were calculated with object statistics in Imaris 9.7.2 based on the autofluorescent area of the laser injury. The underlying geometric mean diameter amounted to 22.60 ± 7.05 µm and the volume to 8604 ± 8818 µm^3 and were normally distributed in each case. **(G)** PI positive cells and laser injury diameter of autofluorescent area. **(H)** PI and laser injury volume of autofluorescent area. White scale bars represent 10 µm.

detailed fluorescence imaging. Virtual green flags (Figure 1I) in the overlay marked laser brandings, guiding the manual rediscovery to completion.

Data analysis

Three-dimensional image processing and analysis was performed with Imaris 9.7.2 (Bitplane AG). Here, surface models of the renin cells and injured areas were created via intensity thresholds across all compared and normalized time points. Glomerular borders were generated by defining object edges in multiple z planes and then automatically extrapolated. The glomerular centers were also automatically calculated by volume statistics of the glomerular borders. All surface models and images were corrected for spatial drift and aligned to one another in image stacks.

Novel automated three-dimensional image quantification was realized by the Marching Cubes algorithm. Image stacks were used to calculate a surface model described by triangles. The calculation of the directional thickness of the JGA in relation to the glomerular center in healthy glomeruli and to the injury center in laser-injured glomeruli was based on an adapted ray tracing method. A reference coordinate system was defined in these centers and used as the basis for further calculations. In this way, the point of origin $\vec{O}$ and the orientation were determined on the basis of the initial position of the objects relative to one another. The directional thickness was determined integrally by scanning individual rays, calculating the distance between the entry point and the exit point of the JGA. The tracing rays were calculated by a spherical coordinate system, with angles phi (φ) and theta (ϑ) defining the range of values of the tracing as given in Eq. 1, 2 (see Supplementary Material). The direction vector $\vec{X}$ of the ray tracing can be described by Supplementary Material Eq 3, with $r = 1$. With vector $\vec{X}$, the ray tracing function $\overrightarrow{R(t)}$ is given in Eq 4 (see Supplementary Material). For each ray, the intersection points with the triangle mesh of the JGA were calculated. This calculation of the intersection points was carried out via a plane spanned by a triangle. This plane can be described with the normal $\vec{n}$ and the distance d to the origin as in Eq 5 (see Supplementary Material). By inserting Eq. 4, 5 and converting, the running variable t (Eq 6) was calculated (see Supplementary Material). Thus, Eq 7 (Supplementary Material) followed for the intersection point $\vec{Q}$. This also defined the intersection point $\vec{Q}$ within the plane. For a triangle with the vertices $\overrightarrow{p_1}$, $\overrightarrow{p_2}$ and $\overrightarrow{p_3}$ the intersection point $\vec{Q}$ can be determined by converting into so-called barycentric coordinates. Therefore, the intersection point $\vec{Q}$ lies within the triangle if Eqs, 8,9 are true (see Supplementary Material). The result is the first and last intersection point with the JGA for each

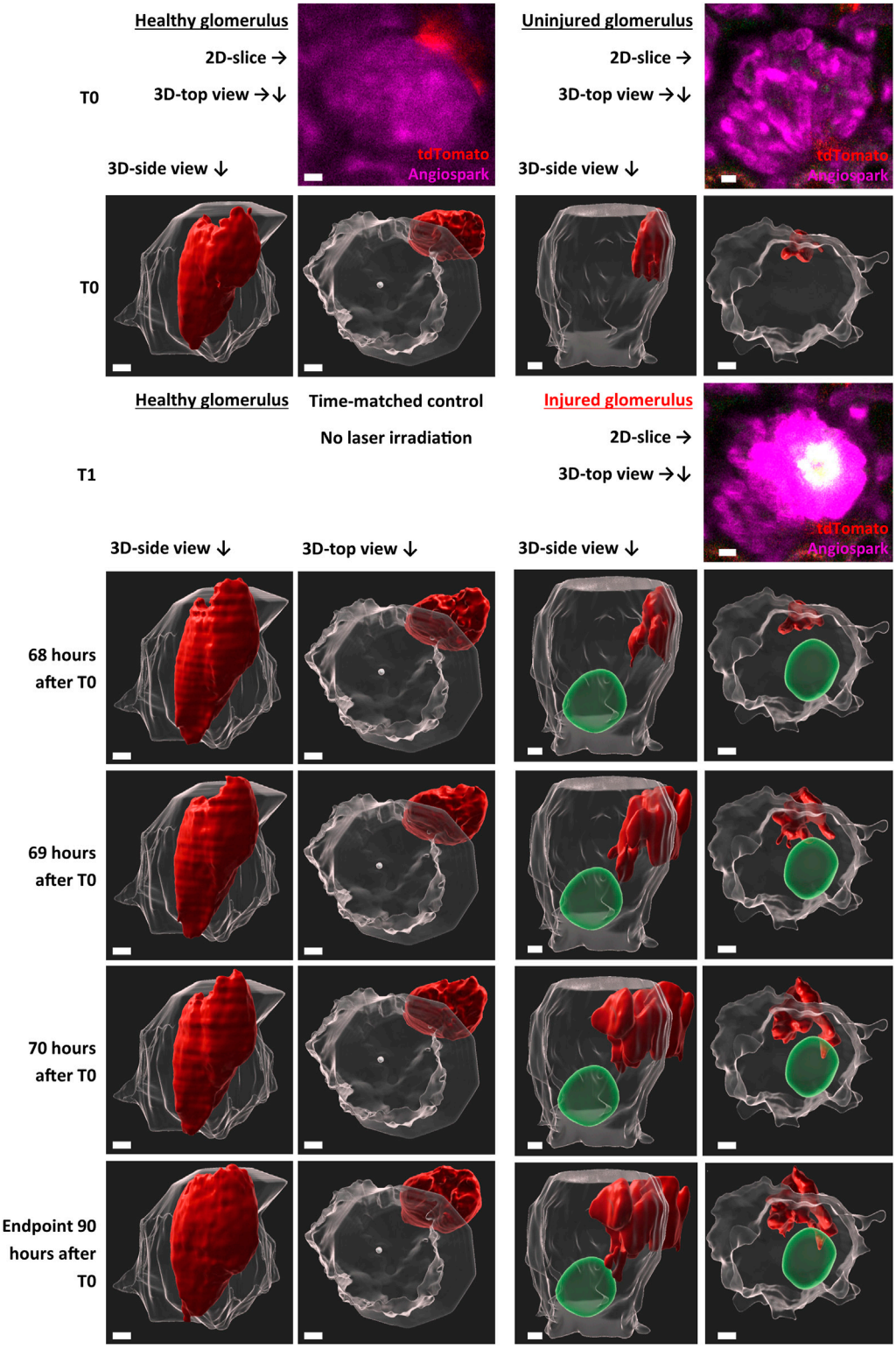

FIGURE 3
Representative intravital imaging data of physiological renin cell motion and pathophysiological migration. Z-stack imaging data of two time-matched glomeruli were rendered with Imaris 9.7.2 for the shown time points. T1 (laser irradiation) was applied in one glomerulus (right side). The individual migration in the injured glomerulus began after 68 h. Two three-dimensional-view points are given, side view of the glomeruli and top view along the *Z*-axis. TdTomato-labelled renin cells are presented in red. The autofluorescence of the laser injury was rendered in green. Glomerular border and center, automatic calculated with object statistics in Imaris 9.7.2 are marked in transparent white. White scale bars represent 10 µm.

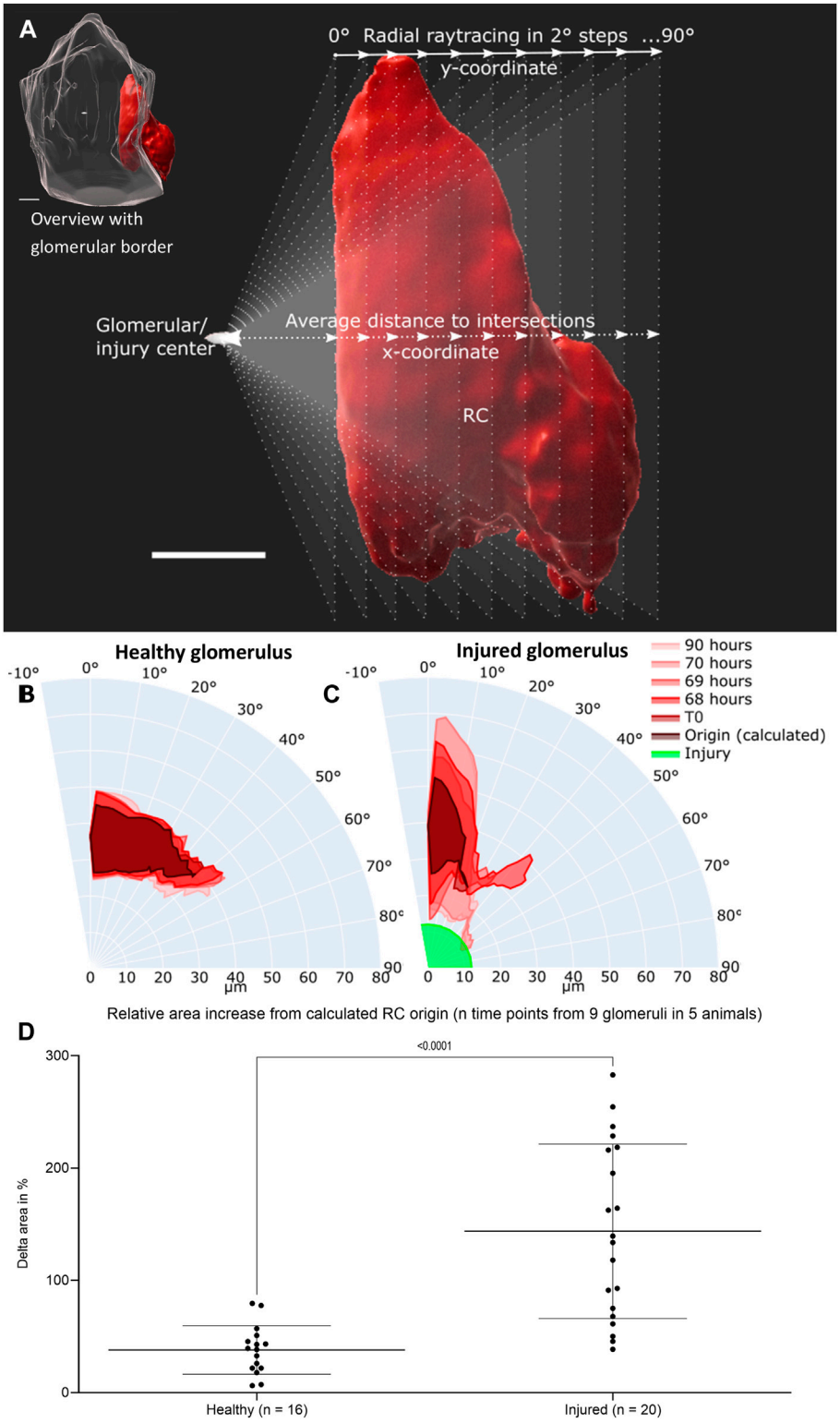

FIGURE 4
Intravital data (representative healthy and injured glomeruli) was quantified via average distance over view angles in 2-degree steps based on ray tracing. **(A)** Schematic representation of fan-like object quantification for healthy and injured glomeruli. White scale bars represent 10 µm. The origin of raytracing RC under physiological conditions were set to the center of the glomerular object and under pathophysiological conditions to the center of the autofluorescent laser injury. Resulting healthy RC motion and migration after injury are pictured in polar charts. **(B)** Quantification

(*Continued*)

FIGURE 4 (Continued)
of the representative healthy glomerulus with the given time points from Figure 3. **(C)** Quantification of representative injured glomerulus with the given time points from Figure 3. The individual origin of RC in all glomeruli were calculated by the sum of the plotted area between the maximal inner border and the minimal outer border of all time points. **(D)** Increase in relative plotted area (see Supplementary Table S1) of n time points from the calculated RC origin from nine healthy and injured glomeruli from five different animals. Mean ± SD are indicated and were compared with unpaired, two-tailed *t* test calculating a highly significant statistical difference. White scale bars represent 10 µm.

ray in the specified value range of angles. For each of these angles, 36 measurements were performed at symmetrically distributed points and the mean value was calculated. The thickness of the JGA and distance to a given center in each plane was derived from this. A schematic representation is given in Figure 4A.

This novel image quantification method was applied to all intravitally imaged time points and the data was plotted in polar charts generated with the Python package plotly, as shown in two representations (Figures 4B,C). The amounts of the plotted areas between the maximal inner border and the minimal outer border of all time points (Eq 10, Supplementary Material) were calculated and determined the individual origin of RC in each glomerulus. Further absolute and relative quantification after ray tracing was performed by subtracting the plotted area of an inner triangle from the area of an outer triangle between rays in 2° steps (Eq 11, Supplementary Material).

Quantifiable image deviation was calculated with the Python packages opencv-python and numpy and used as a representative surrogate parameter for glomerular perfusion. In brief, images were converted in two-dimensional float32 values, from which pixel standard deviations were calculated.

Statistics

Statistical data was calculated in GraphPad Prism 9.0. Linear regressions are indicated with corresponding r^2 factors. D'Agostino-Pearson omnibus normality tests confirmed Gaussian distributions. Data was compared either with Student's t test, or with two-way ANOVA tests and Tukey's multiple comparisons test calculated individual mean ± SD values. $P < 0.05$ indicates statistical significance.

Study approval

All procedures were prospectively approved by the local authorities (TU Dresden and Landesdirektion Sachsen).

Results

Figure 1 demonstrates the experimental setup, in which pulse labelled transgenic mice were baseline and then longitudinally repetitively imaged either without or with/after intraglomerular laser injury (for details see methods). Targeted use of laser irradiation established an inducible, selective and reproducible intraglomerular injury model of individual glomeruli (Figure 2). After laser irradiation, propidium iodide (PI) and Hoechst double positive dead cells appeared (Figures 2A,B,E). Injury diameter, volume and number of PI-positive cells correlated linearly (Figures 2F–H). After laser injury, site-directed migration and infiltration of RC into the injured area could be observed intravitally, as seen two-dimensionally in Figure 2C. The same set of data is presented three-dimensionally in Figure 2D with RC (red) entering the autofluorescent area (green) of laser injury, while still being connected to the RC within the JGA.

TdTomato-labelled RC of the JGA in healthy glomeruli showed a constant flux of surface motion (representative healthy glomerulus in Supplement Video one and in Figure 3) over time. This active motion consisted of reversible protrusions appearing and disappearing within minutes (Supplementary Video S1) or over several hours and days as demonstrated in Figure 3 (T0—Endpoint).

With this established laser-induced injury model, the behavior of RC under pathophysiological conditions was analyzed intravitally (Figure 3). Targeted migration towards the area of glomerular injury was observed (representative injured glomerulus in Supplementary Video S2 and in Figure 3). Starting time points of RC migration varied between glomeruli, starting after 68 h in the representative injured glomerulus (Figure 3). At these time points protrusions from the juxtaglomerular RCN began to infiltrate the intraglomerular region. These migrating RC extended during 3 h towards the injury area, infiltrating the vicinity of the injured area without losing contact to the juxtaglomerular RCN.

Using a novel quantification technique (see scheme in Figure 4A), the motion of healthy RC and their migration after glomerular injury were further characterized with larger group sizes. The majority of RC in healthy glomeruli remained in a constant position over all time points, pictured exemplary in overlays in a polar chart in Figure 4B. Numerically, the physiological motion differs from T0 to up to 156% after 90 h (Supplementary Tables 1–4).

Under pathophysiological conditions after laser irradiation, RC from injured glomeruli first broadened significantly around their origin before converging on the laser-induced injury and further infiltrating the damaged

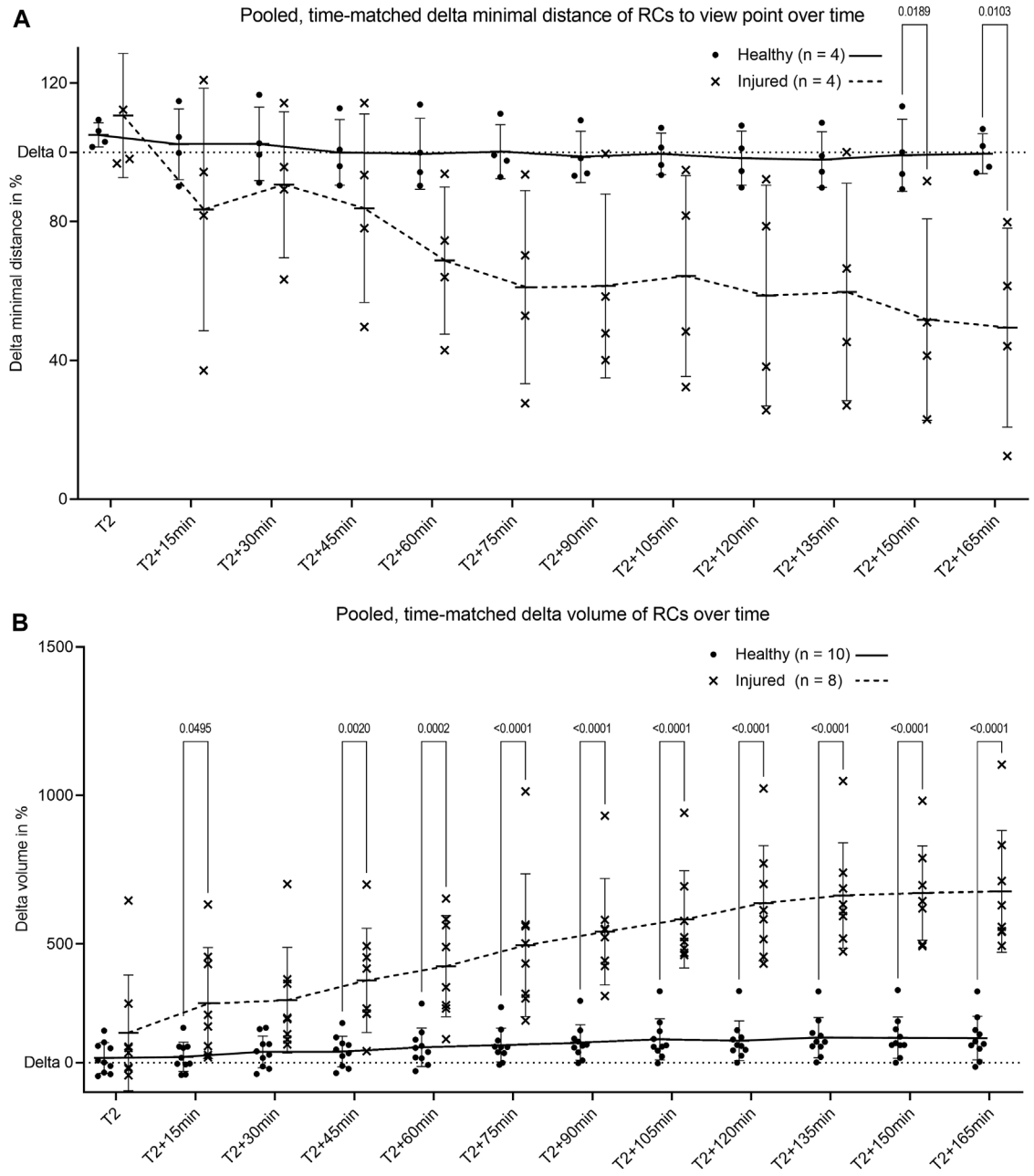

FIGURE 5
Pooled quantification of renin cell motion and migration. **(A)** Change of minimal distance between RC and their glomerular center for healthy glomeruli and between RC and the center of laser injury for injured glomeruli. The minimal distances were obtained by the novel automated three-dimensional image quantification based on ray tracing (*n* = 4 glomeruli per group each of four different animals). **(B)** Intravital change of renin cell volume over time in healthy glomeruli and in laser injured glomeruli. T2 defines begin of migration for injured glomeruli with matched time points from healthy controls. Renin cell volumes were calculated with object statistics in Imaris 9.7.2 based on the renderings of the tdTomato signal (n = 10 glomeruli per group each of 10 different animals). Healthy and injured data were compared with two-way ANOVA tests and Tukey's multiple comparisons test calculated individual mean ± SD values. The corresponding mean values are connected by trend lines.

area (representative injured glomerulus in Figure 4C). During these processes the RC area increased relatively in injured glomeruli from 100% (T1) to up to 350% (Supplementary Tables 5–8).

The calculated origin area of the juxtaglomerular RC was defined as the amount of the plotted area between the maximal inner border and the minimal outer border of all time points. This origin area from all analyzed glomeruli (healthy

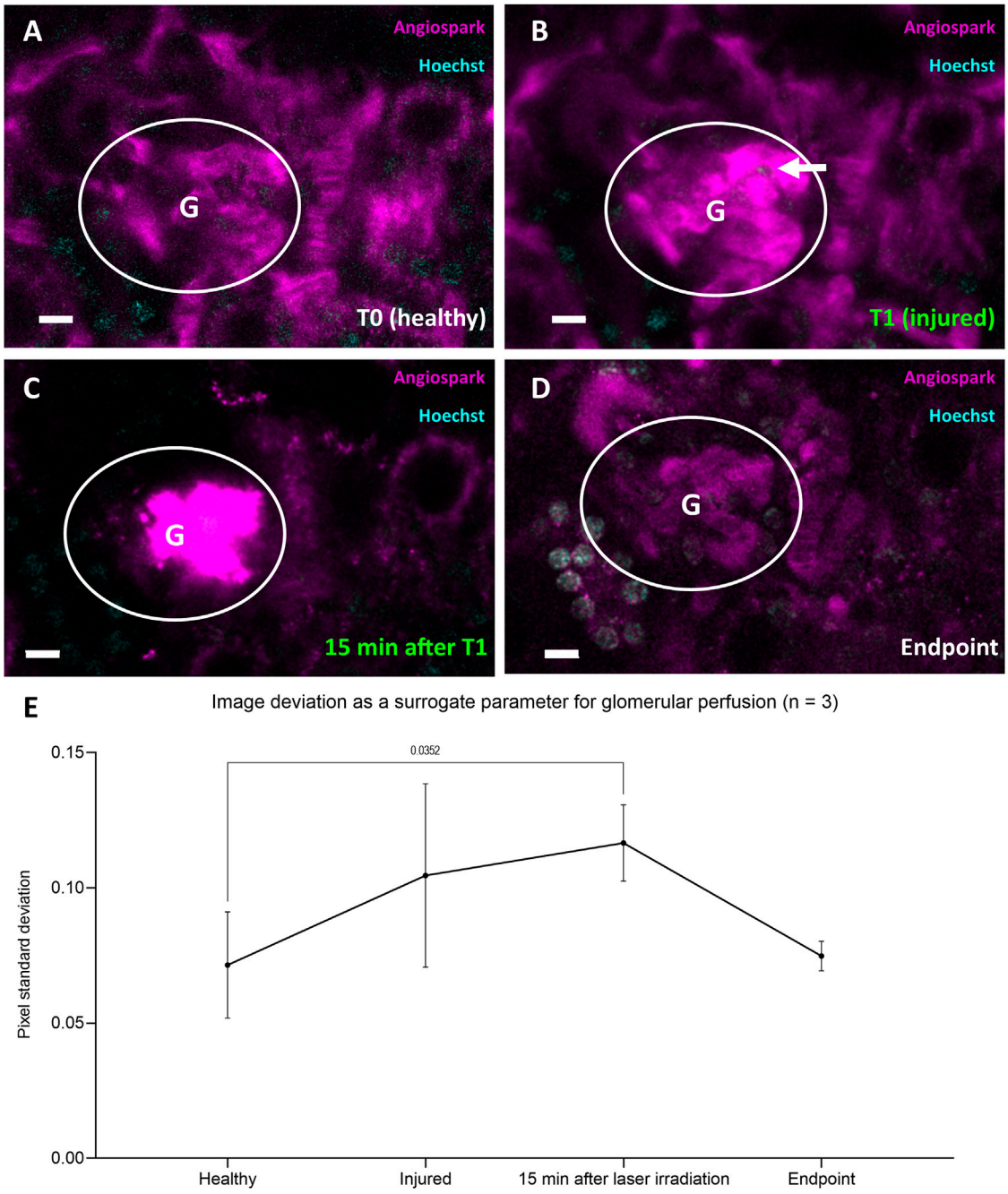

FIGURE 6
Representative data of glomerular perfusion before, during and after laser irradiation. **(A)** Representative glomerulus in white circle at four time-points healthy at T0 and **(B)** immediately after laser irradiation (white arrow) at T1. **(C)** Identical glomerulus 15 min after laser irradiation at T1 with visible Angiospark 680 leakage and **(D)** at experiment endpoint 96 h after T0. **(E)** Time-points **(A–D)** from three glomeruli of three different animals derived image deviation as a quantifiable surrogate parameter for glomerular perfusion. Image deviation data was compared with two-way ANOVA tests and Tukey's multiple comparisons test calculated individual mean ± SD values. White scale bars represent 10 µm.

glomeruli I–IV and injured glomeruli I–V) amounted to an average of 76.71 ± 16.14% of RC from the first intravitally imaged time-point (100%) of the respective glomerulus. All underlying individual glomerular origin areas are listed in Supplementary Tables 1–9. A level of dynamic change in RC was calculated by comparing the increase in relative plotted area of the RC from all time points to the corresponding calculated origin area in both groups of glomeruli (Figure 4D).

10.3389/fphys.2022.980787

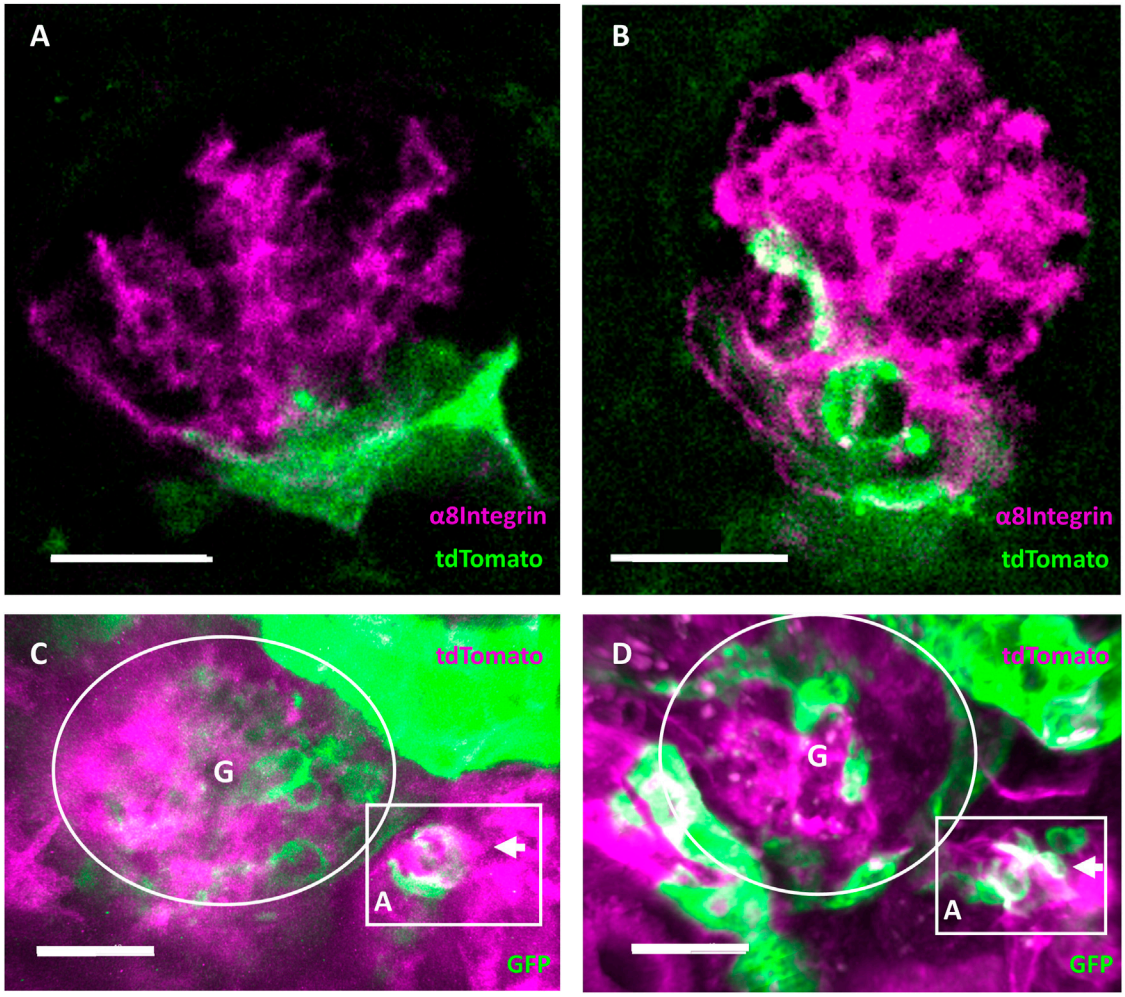

FIGURE 7
Evidence of regeneration and neogenesis during renin cell migration. **(A)** Healthy and **(B)** injured glomeruli from cleared mouse kidneys after intravital experiment endpoints. Complementary pseudocolors mark tdTomato immunohistological staining in green and α8Integrin in magenta. White areas indicate overlap in protein expression. The overlap of α8Integrin with tdTomato positive renin cell descendants after migration in injured glomeruli quantified to a mean of 32.71 ± 15.56% (n = 7). **(C)** RC neogenesis over **(D)** 6 days following renin cell migration in individually injured mRen-Cre-mT/mG mouse glomeruli demonstrated by single cell switch (arrows) from membrane-tdTomato-expressing non-RC (magenta) to membrane-GFP-expressing RC (green). Gradient tdTomato and GFP double positive signals are visible in white (magenta and green, respectively). Rectangular box highlights the neogenesis located at the JGA in three-dimensional intravital imaging data around the afferent arteriole **(A)** of one identical glomerulus **(G)**. A cluster of *de novo* differentiated RC (white and green cells in the rectangular box at d6) can be seen in the arteriole. White scale bars represent 20 µm.

This data demonstrated significant higher delta areas of migrating RC in injured glomeruli than of RC in healthy glomeruli (Figure 4F).

Comparison of pooled and time-matched RC migration based on the change of distance and volume revealed a decreased distance to the injured area (Figure 5A) and an increase in RC volume after laser-induced injury (Figure 5B). Longitudinal physiological surface motion of RC was also present, as indicated by non-significantly varying distances and RC volumes in healthy glomeruli in Figures 5A,B, respectively. RC migration processes reached the distant site of injury within the observation time of 3 hours.

To demonstrate that laser injury did not lead to global glomerular death but rather to a RC-mediated repair reaction, repetitive longitudinal perfusion of glomeruli was monitored. Healthy perfused glomerular capillaries were visible through Angiospark 680 (magenta) during intravital imaging before laser irradiation (T0, Figure 6A). The Angiospark 680 intensity started to increase locally around the laser injury immediately after laser irradiation representative of capillary leakage (T1, Figure 6B) and increased to an

overexposed intensity 15 min after laser irradiation (Figure 6C). Glomerular perfusion returned back to a physiological state after laser injury and subsequent RC migration intravitally visible at experiment endpoints, representative shown in Figure 6D. This process was quantitively assessed with the help of image deviation, a surrogate parameter for vascular perfusion in three glomeruli of three different animals (see Figure 6E). Healthy glomerular perfusion was defined as a homogeneously distributed Angiospark 680 filled vascular signal. The mean image deviation started at T0 under healthy conditions at 0.071 ± 0.019 and then increased to 0.105 ± 0.034 immediately after laser irradiation (T1) with a maximum of 0.117 ± 0.014 15 minutes after T1 (Figure 6E). The mean image deviation at the experiment endpoint returned to a similar initial value of 0.075 ± 0.005 as before laser irradiation (see also Figure 6E). A significant difference existed between healthy image deviation and image deviation 15 min after laser injury of $p = 0.0352$.

Endpoint immunohistology with complementary pseudocolors further characterized RC migration with tdTomato positive RC (green) overlapping (white) with α8Integrin (magenta) in injured glomeruli but not in healthy glomeruli (Figures 7A,B, respectively).

Using constitutive transgenic mRenCre-mT/mG mice with GFP-expressing RC (green) and tdTomato-expressing non-RC (magenta), RC neogenesis important for maintaining the RCN can be identified over time, when *de novo* differentiated RC cluster can be observed via a gradient from tdTomato (non-RC) to GFP (RC marker, see Figures 7C,D). During repetitive intravital observations in uninjured glomeruli, this physiological process of RC neogenesis apparently occurred too infrequently to be documented. In contrast, after intraglomerular injury intravital observations of neogenesis only in the corresponding RCN were consistently detected by changing colors from magenta (non-RC) towards white (magenta and green for the first time) towards solely GFP-expressing RC (green) over time in the same cells. Representatively seen in Figures 7C,D, following laser injury mediated RC migration a *de novo* differentiated RC cluster was observed via a gradient from tdTomato (non-RC) to GFP (RC marker).

Discussion

The presented novel quantifiable *in vivo* migration model system using longitudinal intravital microscopy combined with an intraglomerular laser-induced injury model allows new insights in the physiological and regenerative behavior and regulation of the RCN at the JGA. With the development of this model system, it is possible to describe and quantify fast and continuing alterations of RC protrusions under physiological conditions associated with its juxta/extraglomerular position. Applying intraglomerular injury to this model system in individual glomeruli showed that a locally acting feedback system gives notice of intraglomerular injury specifically to the associated JGA, leading to a timely (one to 3 days) and spatially coordinated repair response via directed migration of juxtaglomerular RC towards the site of injury. Hereby, the migrating RC switch their phenotype towards mesangial cells by expressing α8Integrin and during process completion continuously keep contact to the niche of origin. This repair response is also evident in the return to a physiological state of glomerular perfusion after laser injury and RC migration. The demonstrated glomerular leakage of Angiospark 680 filled vascular fluid represents a mechanical consequence of the laser irradiation and disappears a certain time after the onset of the repair response.

Besides the above described intra-/extraglomerular feedback repair mechanism, a second feedback system regulates specifically the maintenance of the RCN after intraglomerular RC migration. During the intraglomerular repair process by migrating RC, stimulation of their own replenishment via RC neogenesis was observed specifically in the corresponding RCN, a process in which nonRC switch their phenotype to a RC for the first time.

With this novel model in hand, understanding of the intra-/extraglomerular as well as RCN feedback mechanisms and its mediators could now open the door for new treatments for glomerular disease via stimulating/regulating these important endogenous renal repair mechanisms.

While laser-induced injury in individual glomeruli has been used before (Hackl et al., 2013; Zhang et al., 2020), the experimental setup was improved for reproducibility of injury areas. Treatment with enalapril was performed to induce the RC pulse labeling during induction, as previously published (Starke et al., 2015). Only an inducible reporter system ensures cell fate tracking and Ren promotor activity for a specific and short period of time, greatly reducing the risk of unwanted recombination, which is a limitation of constitutive reporter systems (Kaverina et al., 2017). The 7 day washout phase guaranteed the absence of experimental side effects because of enalapril's short half-life of 35 h (Gomez et al., 1983). Using only 1.5% isoflurane as anesthesia administered via tracheal intubation excluded cardiovascular depression and provided a quick recovery of the animal after intravital imaging. Moreover, combining tracheal intubation with passive triggering controlled by the laser scanning microscope provided stable imaging without motion artifacts. In addition, the imaging technique had to be optimized and combined with novel computational algorithms to develop for the first time a quantifiable *in vivo* migration assay to study the hypothesis of a strictly locally regulated intraglomerular-extraglomerular feedback system for a RC-mediated response to injury in such a complex environment (Steglich et al., 2020). The use of the abdominal imaging windows

markedly improves imaging conditions without pressure-induced restrictions of circulation (Schiessl et al., 2020). Intravitally imaged kidneys could be stained and cleared for translational immunohistology. Subsequent challenging but successful rediscovery of identical areas also demonstrated the mesangial phenotype switch of the migrating intraglomerular RC as a consistent finding as shown before in antibody induced systemic glomerulonephritis models (Starke et al., 2015).

Establishing an automated workflow of three-dimensional image quantification as presented here allows for unbiased and comparable analysis of cell behavior. Due to the calculation by the Marching Cubes algorithm, non-manifold, closed three-dimensional models were created, which were directly used for the semiautomated quantification of this complex three-dimensional longitudinal data. Representative shown image data was validated by statistically reliable comparisons. Cell motion and migration patterns can now be precisely calculated to detect spatial and temporal differences among glomeruli in further studies. A modest increase of relative area in healthy glomeruli over time is a limitation, but does not diminish the comparison to the results after laser-induced injury. The relative area, delta volume and delta minimal distance of RC between healthy and injured glomeruli are significant and, in several magnitudes, different. The introduction of thresholds for mathematical parameters will allow an easy distinction between fixed and dynamic cells. Interestingly, the start of visible RC recruitment occurred with some variability between one and at latest 3 days after injury, while the migrating RC frequently reached the intraglomerular site of injury within an observation time of 3 hours. The time point of RC recruitment may be influenced by the development of the injury/cell death itself, the corresponding functionality of the feedback players, of glomerular and/or tubular perfusion, or the (necro)inflammatory response (Sarhan et al., 2018). Once the feedback network and RC activation in individual glomeruli/JGA has been established, a quite uniform rapid migration of RC from the RCN towards the intraglomerular site of injury takes places with little variation in cellular speed.

This quantitative model system of the migratory response of RC after site-directed injury can now be used for comparative studies in different transgenic mouse strains or established therapies such as ACE-I, ARBs, SGLT-2 inhibitors, corticosteroids or may serve to find novel therapies.

Starting from the introduced hypothesis of a feedback system, several mechanisms may be relevant to inform the JGA about intraglomerular injury (Thurau and Schnermann, 1965). Either a chemoattractive gradient within the glomerulus towards the JGA, a cell junction mediated interconnective signaling mechanism, or an intraglomerular release of (death) molecules into Bowman space with a following interaction with the macula densa mimicking a real glomerular-tubulo-extraglomerular feedback mechanism may regulate the RCN and its responses. The model system presented here can be combined with new sophisticated technologies such as two-photon guided glomerular/tubular micropuncture and liquid chromatography/mass spectrometry of nanoliter range samples from recovered filtrates from Bowman space and segments of the nephron to answer the above questions (Matsushita et al., 2018). Subsequent studies utilizing the pluripotent (Pippin et al., 2015) potential of RC or further controlled intraglomerular (micro-)injection experiments (Ikeda et al., 2017; Saxena et al., 2021) will extend the presented research of RC-mediated repair and RCN replenishment regulation via neogenesis. In addition, the translational potential of this methodology remains high, as it can be applied to many image analysis questions.

In conclusion, repeated continuous intravital microscopy provides a state-of-the-art tool to prove and further study the local intraglomerular injury - extraglomerular RCN repair feedback system in individual glomeruli *in vivo* in a quantifiable manner. This model system may open the door for developing new treatments for glomerular disease via stimulating/regulating this important, endogenous renal repair mechanism.

Data availability statement

The original contributions presented in the study are included in the article/Supplementary Material further inquiries can be directed to the corresponding author.

Ethics statement

The animal study was reviewed and approved by the TU Dresden and Landesdirektion Sachsen.

Author contributions

PA performed experiments, analyzed data and wrote the manuscript. JS designed the study, performed experiments and analyzed data. HK and MG performed experiments. SH and FK analyzed data. VT designed the study. CH designed the study and revised the manuscript. All authors read and approved the final manuscript.

Funding

This study was funded by the German Research Foundation (DFG)—Projects HU 600/8-1, 399229660 and 426572058.

Acknowledgments

The authors thank Nicole Bunk for her technical assistance. Experimental imaging and animal care support was provided by all members of the Core Facility Cellular Imaging and the Experimental Center of the Faculty of Medicine Carl Gustav Carus, University Hospital Carl Gustav Carus, TU Dresden, respectively. Supporting work by Johannes Radde is also acknowledged.

Conflict of interest

The authors declare that the research was conducted in the absence of any commercial or financial relationships that could be construed as a potential conflict of interest.

Publisher's note

Supplementary material

The Supplementary Material for this article can be found online at: https://www.frontiersin.org/articles/10.3389/fphys.2022.980787/full#supplementary-material

References

Andrianova, N. V., Buyan, M. I., Zorova, L. D., Pevzner, I. B., Popkov, V. A., Babenko, V. A., et al. (2019). Kidney cells regeneration: Dedifferentiation of tubular epithelium, resident stem cells and possible niches for renal progenitors. *Int. J. Mol. Sci.* 20 (24), 6326. doi:10.3390/ijms20246326

Ashworth, S. L., Sandoval, R. M., Tanner, G. A., and Molitoris, B. A. (2007). Two-photon microscopy: Visualization of kidney dynamics. *Kidney Int.* 72 (4), 416–421. doi:10.1038/sj.ki.5002315

Burford, J. L., Villanueva, K., Lam, L., Riquier-Brison, A., Hackl, M. J., Pippin, J., et al. (2014). Intravital imaging of podocyte calcium in glomerular injury and disease. *J. Clin. Invest.* 124 (5), 2050–2058. doi:10.1172/JCI71702

Desposito, D., Schiessl, I. M., Gyarmati, G., Riquier-Brison, A., Izuhara, A., Kadoya, H., et al. (2021). Serial intravital imaging captures dynamic and functional endothelial remodeling with single-cell resolution. *JCI Insight* 6, 123392. doi:10.1172/jci.insight.123392

Gomez, H. J., Cirillo, V. J., and Jones, K. H. (1983). The clinical pharmacology of enalapril. *J. Hypertens. Suppl.* 1 (1), 65–70.

Gyarmati, G., Shroff, U. N., Riquier-Brison, A. D. M., Kriz, W., Kaissling, B., Neal, C. R., et al. (2021). A new view of macula densa cell microanatomy. *Am. J. Physiol. Ren. Physiol.* 320, F492–F504. doi:10.1152/ajprenal.00546.2020

Hackl, M. J., Burford, J. L., Villanueva, K., Lam, L., Suszták, K., Schermer, B., et al. (2013). Tracking the fate of glomerular epithelial cells *in vivo* using serial multiphoton imaging in new mouse models with fluorescent lineage tags. *Nat. Med.* 19 (12), 1661–1666. doi:10.1038/nm.3405

Hickmann, L., Steglich, A., Gerlach, M., Al-Mekhlafi, M., Sradnick, J., Lachmann, P., et al. (2017). Persistent and inducible neogenesis repopulates progenitor renin lineage cells in the kidney. *Kidney Int.* 92 (6), 1419–1432. doi:10.1016/j.kint.2017.04.014

Hohne, M., Ising, C., Hagmann, H., Volker, L. A., Brahler, S., Schermer, B., et al. (2013). Light microscopic visualization of podocyte ultrastructure demonstrates oscillating glomerular contractions. *Am. J. Pathol.* 182 (2), 332–338. doi:10.1016/j.ajpath.2012.11.002

Ikeda, M., Wakasaki, R., Schenning, K. J., Swide, T., Lee, J. H., Miller, M. B., et al. (2017). Determination of renal function and injury using near-infrared fluorimetry in experimental cardiorenal syndrome. *Am. J. Physiol. Ren. Physiol.* 312 (4), F629–F39. doi:10.1152/ajprenal.00573.2016

Kaverina, N. V., Kadoya, H., Eng, D. G., Rusiniak, M. E., Sequeira-Lopez, M. L. S., Gomez, R. A., et al. (2017). Tracking the stochastic fate of cells of the renin lineage after podocyte depletion using multicolor reporters and intravital imaging. *PLOS ONE* 12 (3), e0173891. doi:10.1371/journal.pone.0173891

Khitrin, A. K., Petruccelli, J. C., and Model, M. A. (2017). Bright-field microscopy of transparent objects: A ray tracing approach. *Microsc. Microanal.* 23 (6), 1116–1120. doi:10.1017/S1431927617012624

Klingberg, A., Hasenberg, A., Ludwig-Portugall, I., Medyukhina, A., Mann, L., Brenzel, A., et al. (2017). Fully automated evaluation of total glomerular number and capillary tuft size in nephritic kidneys using lightsheet microscopy. *J. Am. Soc. Nephrol.* 28 (2), 452–459. doi:10.1681/ASN.2016020232

Kostenko, A., Batenburg, K. J., Suhonen, H., Offerman, S. E., and van Vliet, L. J. (2013). Phase retrieval in in-line x-ray phase contrast imaging based on total variation minimization. *Opt. Express* 21 (1), 710–723. doi:10.1364/OE.21.000710

Matsushita, K., Golgotiu, K., Orton, D. J., Smith, R. D., Rodland, K. D., Piehowski, P. D., et al. (2018). Micropuncture of bowman's space in mice facilitated by 2 photon microscopy. *J. Vis. Exp.* 140, e58206. doi:10.3791/58206

Oliver, J. A., Maarouf, O., Cheema, F. H., Martens, T. P., and Al-Awqati, Q. (2004). The renal papilla is a niche for adult kidney stem cells. *J. Clin. Invest.* 114 (6), 795–804. doi:10.1172/JCI20921

Pippin, J. W., Kaverina, N. V., Eng, D. G., Krofft, R. D., Glenn, S. T., Duffield, J. S., et al. (2015). Cells of renin lineage are adult pluripotent progenitors in experimental glomerular disease. *Am. J. Physiol. Ren. Physiol.* 309 (4), F341–F358. doi:10.1152/ajprenal.00438.2014

Pippin, J. W., Sparks, M. A., Glenn, S. T., Buitrago, S., Coffman, T. M., Duffield, J. S., et al. (2013). Cells of renin lineage are progenitors of podocytes and parietal epithelial cells in experimental glomerular disease. *Am. J. Pathol.* 183 (2), 542–557. doi:10.1016/j.ajpath.2013.04.024

Renier, N., Wu, Z., Simon, D. J., Yang, J., Ariel, P., and Tessier-Lavigne, M. (2014). iDISCO: a simple, rapid method to immunolabel large tissue samples for volume imaging. *Cell.* 159 (4), 896–910. doi:10.1016/j.cell.2014.10.010

Ruhnke, L., Sradnick, J., Al-Mekhlafi, M., Gerlach, M., Gembardt, F., Hohenstein, B., et al. (2018). Progenitor Renin Lineage Cells are not involved in the regeneration of glomerular endothelial cells during experimental renal thrombotic microangiopathy. *PLoS One* 13 (5), e0196752. doi:10.1371/journal.pone.0196752

Sarhan, M., Land, W. G., Tonnus, W., Hugo, C. P., and Linkermann, A. (2018). Origin and consequences of necroinflammation. *Physiol. Rev.* 98 (2), 727–780. doi:10.1152/physrev.00041.2016

Saxena, V., Gao, H., Arregui, S., Zollman, A., Kamocka, M. M., Xuei, X., et al. (2021). Kidney intercalated cells are phagocytic and acidify internalized uropathogenic *Escherichia coli*. *Nat. Commun.* 12 (1), 2405. doi:10.1038/s41467-021-22672-5

Schiessl, I. M., Bardehle, S., and Castrop, H. (2013). Superficial nephrons in BALB/c and C57BL/6 mice facilitate *in vivo* multiphoton microscopy of the kidney. *PLoS One* 8 (1), e52499. doi:10.1371/journal.pone.0052499

Schiessl, I. M., Fremter, K., Burford, J. L., Castrop, H., and Peti-Peterdi, J. (2020). Long-term cell fate tracking of individual renal cells using serial intravital microscopy. *Methods Mol. Biol.* 2150, 25–44. doi:10.1007/7651_2019_232

Sequeira Lopez, M. L., and Gomez, R. A. (2011). Development of the renal arterioles. *J. Am. Soc. Nephrol.* 22 (12), 2156–2165. doi:10.1681/ASN.2011080818

Sequeira-Lopez, M. L. S., and Gomez, R. A. (2021). Renin cells, the kidney, and hypertension. *Circ. Res.* 128 (7), 887–907. doi:10.1161/CIRCRESAHA.121.318064

Starke, C., Betz, H., Hickmann, L., Lachmann, P., Neubauer, B., Kopp, J. B., et al. (2015). Renin lineage cells repopulate the glomerular mesangium after injury. *J. Am. Soc. Nephrol.* 26 (1), 48–54. doi:10.1681/ASN.2014030265

Steglich, A., Hickmann, L., Linkermann, A., Bornstein, S., Hugo, C., and Todorov, V. T. (2020). in *Reviews of Physiology, biochemistry and pharmacology*. Editor S. H. F. Pedersen (Cham: Springer International Publishing), 53–81.

Steglich, A., Kessel, F., Hickmann, L., Gerlach, M., Lachmann, P., Gembardt, F., et al. (2019). Renin cells with defective Gsα/cAMP signaling contribute to renal endothelial damage. *Pflugers Arch.* 471 (9), 1205–1217. doi:10.1007/s00424-019-02298-9

Thurau, K., and Schnermann, J. (1965). Die Natriumkonzentration an den Macula densa-Zellen als regulierender Faktor für das Glomerulumfiltrat (Mikropunktionsversuche). *Klin. Wochenschr.* 43 (8), 410–413. doi:10.1007/BF01483845

Zhang, K., Chen, S., Sun, H., Wang, L., Li, H., Zhao, J., et al. (2020). *In vivo* two-photon microscopy reveals the contribution of Sox9(+) cell to kidney regeneration in a mouse model with extracellular vesicle treatment. *J. Biol. Chem.* 295 (34), 12203–12213. doi:10.1074/jbc.RA120.012732

frontiers | Frontiers in Physiology

TYPE Original Research
PUBLISHED 12 October 2022
DOI 10.3389/fphys.2022.984362

OPEN ACCESS

EDITED BY
Ignacio Gimenez,
University of Zaragoza, Spain

REVIEWED BY
Shaolin Shi,
Nanjing University, China
Alvaro Conrado Ucero,
Universidad Complutense de Madrid, Spain

*CORRESPONDENCE
Alexander Paliege,
alexander.paliege@ukdd.de

SPECIALTY SECTION
This article was submitted to Renal Physiology and Pathophysiology, a section of the journal Frontiers in Physiology

RECEIVED 01 July 2022
ACCEPTED 23 September 2022
PUBLISHED 12 October 2022

CITATION
Labes R, Dong L, Mrowka R, Bachmann S, von Vietinghoff S and Paliege A (2022), Annexin A1 exerts renoprotective effects in experimental crescentic glomerulonephritis. *Front. Physiol.* 13:984362. doi: 10.3389/fphys.2022.984362

Annexin A1 exerts renoprotective effects in experimental crescentic glomerulonephritis

Robert Labes[1], Lei Dong[2], Ralf Mrowka[3], Sebastian Bachmann[1], Sibylle von Vietinghoff[4] and Alexander Paliege[5,6]*

[1]Department of Anatomy, Charité-Universitätsmedizin Berlin, Berlin, Germany, [2]Nephrology Department, Tongji Hospital, Tongji College, Huazhong University of Science and Technology, Wuhan, China, [3]Klinik für Innere Medizin III, AG Experimentelle Nephrologie, Universitätsklinikum Jena, Jena, Germany, [4]Nephrology Section, First Medical Clinic, University Clinic and Rheinische Friedrich-Wilhelms Universität Bonn, Bonn, Germany, [5]Division of Nephrology, Department of Internal Medicine III, Technische Universität Dresden, Dresden, Germany, [6]Berlin Institute of Health (BIH), Berlin, Germany

Non-resolving inflammation plays a critical role during the transition from renal injury towards end-stage renal disease. The glucocorticoid-inducible protein annexin A1 has been shown to function as key regulator in the resolution phase of inflammation, but its role in immune-mediated crescentic glomerulonephritis has not been studied so far.

Methods: Acute crescentic glomerulonephritis was induced in annexin A1-deficient and wildtype mice using a sheep serum against rat glomerular basement membrane constituents. Animals were sacrificed at d5 and d10 after nephritis induction. Renal leukocyte abundance was studied by immunofluorescence and flow cytometry. Alterations in gene expression were determined by RNA-Seq and gene ontology analysis. Renal levels of eicosanoids and related lipid products were measured using lipid mass spectrometry.

Results: Histological analysis revealed an increased number of sclerotic glomeruli and aggravated tubulointerstitial damage in the kidneys of annexin A1-deficient mice compared to the wildtype controls. Flow cytometry analysis confirmed an increased number of $CD45^+$ leukocytes and neutrophil granulocytes in the absence of annexin A1. Lipid mass spectrometry showed elevated levels of prostaglandins PGE2 and PGD2 and reduced levels of antiinflammatory epoxydocosapentaenoic acid regioisomers. RNA-Seq with subsequent gene ontology analysis revealed induction of gene products related to leukocyte activation and chemotaxis as well as regulation of cytokine production and secretion.

Conclusion: Intrinsic annexin A1 reduces proinflammatory signals and infiltration of neutrophil granulocytes and thereby protects the kidney during crescentic glomerulonephritis. The annexin A1 signaling cascade may therefore provide novel targets for the treatment of inflammatory kidney disease.

KEYWORDS

annexin A1 (AnxA1), nephrotoxic serum nephritis, crescentic glomerulonephritis, renal fibrosis, neutrophil granulocyte (PMN), prostaglandin E2 (PGE2), resolution of inflammation, epoxydocosapentaenoic acids (EDPs)

Introduction

Intense inflammation, necrotic destruction of the glomerular tuft and the subsequent formation of crescentic scars (crescentic glomerulonephritis, cGN) are defining features of rapidly progressive glomerulonephritis. The natural course of this condition is characterized by an acute onset of renal dysfunction with marked glomerular hematuria, proteinuria, and a rapid loss of excretory kidney function. Despite the utilization of harsh immunosuppressive treatment, cGN frequently causes chronic, progressive kidney injury and remains a common cause of end stage renal disease (Saran et al., 2019; Trimarchi, 2021), therefore highlighting the need for novel renoprotective therapeutic strategies (Kidney Disease: Improving Global Outcomes (KDIGO) Glomerular Diseases Work Group, 2021).

Previous studies have identified a variety of intrinsic mediators which are activated during the resolution phase of acute inflammation and exert antiinflammatory effects (Ortega-Gomez et al., 2013). The calcium- and phospholipid-binding protein annexin A1 (AnxA1) inhibits leukocyte recruitment and adhesion to endothelial cells (Brancaleone et al., 2011), promotes apoptosis of neutrophils in the inflamed tissue (Vago et al., 2012) and suppresses the synthesis of essential proinflammatory cytokines (Pupjalis et al., 2011; Sugimoto et al., 2016) and eicosanoid species (Herbert et al., 2007; Wang et al., 2011; Seidel et al., 2012). AnxA1 was therefore proposed to play a central role in the resolution of inflammation (Gobbetti and Cooray, 2016). In addition, AnxA1 can be released by damaged and dying cells to act as a "find me" and "eat me" signal for phagocytes. Thereby, AnxA1 may contribute to the effective clearance of apoptotic and necrotic cells and thus help to avoid secondary damage and autoimmunity (Scannell et al., 2007; Blume et al., 2012). AnxA1 is abundantly expressed in the kidney but may also be introduced to the site of damage by infiltrating leukocytes and fibroblasts (McKanna et al., 1992; Dreier et al., 1998; Seidel et al., 2012; Neymeyer et al., 2015; Wang et al., 2022). Evidence for a significant contribution of leukocyte species to the overall tissue abundance of AnxA1 in the diseased kidney is also provided by recent single cell RNA-seq data which show a high abundance of AnxA1 mRNA in fibroblasts, monocytes and other leukocyte subspecies (https://www.kpmp.org).

Renoprotective effects of AnxA1 have been demonstrated for a variety of not primarily immune-mediated conditions including diabetic nephropathy (Wu et al., 2021), ischemia/reperfusion injury (Facio et al., 2011; Suliman et al., 2021) and calcineurin inhibitor toxicity (Araujo et al., 2010; Araujo et al., 2012). Protective mechanisms include antiinflammatory and antifibrotic effects *via* formyl peptide receptor 2 signaling, alteration of MAP kinase signaling and inhibition of TGF-β and NF-kB (Neymeyer et al., 2015; Purvis et al., 2018; Wu et al., 2021).

The regulation of AnxA1 during the course of acute cGN and its effects on renal inflammation and fibrosis in this setting have not been studied. Using the nephrotoxic serum nephritis model of cGN in wildtype (WT) and AnxA1-deficient mice, we here show that AnxA1 protein abundance is increased at d10 after nephritis induction in WT mice. Localization studies revealed an accumulation of AnxA1 immunoreactive protein in regions with damaged glomeruli and nephron segments, corresponding to inflammatory infiltrates and fibrotic scar tissue. At this point in time, proteinuria, morphological damage markers, leukocyte infiltration, expression of proinflammatory cytokines and fibrotic markers were all increased in AnxA1-deficient mice compared to the WT mice. Our data demonstrate a protective role of intrinsic AnxA1 in this model for acute cGN and provide a rational for further studies exploring AnxA1-based pharmacological treatment strategies in inflammatory diseases of the kidney.

Materials and methods

Animal studies and tissue preservation

Animal studies were approved by the Berlin Council on Animal Care (permission no. G0251/14) and performed according the NIH Guide for the Care and Use of Laboratory Animals. AnxA1-deficient mice were originally generated by (Hannon et al., 2003) and bred in the Charité animal facility maintaining a C57Bl/6 genetic background. AnxA1-deficient and WT mice were derived from heterozygous breeder pairs and maintained in homozygous colonies under identical environmental conditions.

cGN was induced by intraperitoneal injection of 400 µl of a sheep serum raised against rat glomerular basement membrane constituents (PTX-001S; PROBETEX, San Antonio, United States). The dose was chosen based on published data (Moll et al., 2018; Ougaard et al., 2018) and on preliminary studies in which this dose showed a robust nephritic response without excessive mortality of AnxA1-deficient mice. The same batch of serum was used throughout the study to avoid variations in composition and activity. Control mice for both genotypes received an injection with normal sheep serum (Dianova, Hamburg, Germany). 18 h urine samples were collected on

day 4 and 9, and the experiment was terminated at d5 or d10 after nephritis induction.

Kidneys for morphological and immunofluorescence analysis were perfusion-fixed *via* the abdominal aorta using 3% paraformaldehyde in PBS and processed for paraffin or cryostat sectioning as previously described (Paliege et al., 2012). Kidneys for biochemical analysis and flow cytometry were flushed with phosphate buffer (4.3 g/l NaH2PO4 and 14.8 g/l Na2HPO4) (Andrews and Coffey, 1984) to remove blood cells and plasma constituents and either processed immediately for flow cytometry or snap frozen in liquid nitrogen and stored at -80°C.

Laboratory parameters

Urinary creatinine and albumin concentrations were measured in the Clinical Chemistry Department at the University Hospital Dresden using standard procedures.

Quantitative real time PCR

Generation of cDNA and subsequent PCR analysis were performed following established methodology (Seidel et al., 2012). In brief, total mRNA from whole kidneys was extracted using the TRIzol™ chloroform extraction method (5Prime, Hamburg, Germany). cDNA was generated by reverse transcription using a kit (Bioline, Luckenwalde, Germany). Expression levels of AnxA1 and Col1A1 were assessed using TaqMan® real time RT-PCR with GAPDH serving as loading control. Probes (AnxA1 #4331182, Col1A1 #4331182, murine GAPDH 4352339E-1108037), and master mix (#4369016) were purchased from Applied Biosystems™ (Darmstadt, Germany). Data were analyzed according to the $2^{-\Delta\Delta CT}$ method, and mRNA levels expressed as x-fold of control (Livak and Schmittgen, 2001).

Histology and morphometric analysis

Paraffin sections (4 µm) were deparaffinized in Xylol and rehydrated in ethanol and PBS. Periodic acid-Schiff (PAS) staining and Sirius Red staining were performed using established methodology (Junqueira et al., 1979). Stained sections were imaged using a Leica DMRB light microscope equipped with a Zeiss AxioCam MRc digital camera and AxioVision software (Zeiss, Jena, Germany). Quantification of glomerular damage was performed in a blinded manner by counting glomeruli displaying signs of necrosis in the glomerular tuft, crescent formation or global sclerosis. Numbers of glomeruli with crescents and global sclerosis were added and normalized to the total number of glomeruli in the section. Tubulointerstitial damage was determined on blinded sections by visual assessment of the area with interstitial fibrosis and tubular atrophy (Farris et al., 2011). Quantification of Sirius Red signal was performed in an automated image analysis approach using the Fiji distribution of ImageJ (Schindelin et al., 2012). To this end, 6 to 8 adjacent 200 x color images from the kidney cortex were acquired using constant illumination and camera settings. Images were converted to red, green and blue. Sirius Red signal was segmented with a color threshold (HUE min = 232, max = 255; saturation min = 132, max = 255; brightness min = 0, max = 255). The resulting black-and-white image was used to calculate the total signal area and to generate a mask for the measurement of integrated signal intensity with built-in Fiji tool kit.

Immunofluorescence staining

Four-µm paraffin sections were deparaffinized in xylene and rehydrated in ethanol and PBS. Sections were subsequently boiled in 0.1 M citrate buffer to improve antigen presentation. Cryostat sections were incubated with 0.5% Triton™ X-100 (Sigma-Aldrich, Saint Louis, United States) in PBS for 30 min at room temperature to improve antibody penetration. Unspecific protein binding sites were blocked with 5% skim milk in PBS for 30 min at room temperature. Primary antibodies (Supplementary Table S1) were diluted in milk and incubated overnight at 4 °C. Bound antibodies were detected with Cy2-or Cy3-labeled secondary antibodies (Jackson Laboratories, Bar Harbor, United States). Image acquisition was performed with a Zeiss LSM5 Exciter confocal microscope and ZEN imaging software (Zeiss, Jena, Germany).

Immunoblotting

Tissue samples were homogenized in liquid nitrogen and dissolved in buffer containing 250 mM sucrose, 10 mM triethanolamine, protease inhibitor (cOmplete™; Roche) as previously described (Seidel et al., 2012; Neymeyer et al., 2015). Samples were sonicated and nuclei removed by centrifugation (1,000 ×*g* for 10 min). Postnuclear supernatants were separated on 10% polyacrylamide mini-gels. Proteins were transferred to nitrocellulose membranes. Unspecific binding sites were blocked with 5% skim milk in PBS for 1 h at room temperature. Antibodies were diluted in milk as detailed in Supplementary Table S1 and applied overnight at 4°C. The abundance of α-tubulin was determined in parallel and served as loading control. Detection of bound primary antibodies was performed by incubation with horseradish peroxidase-conjugated secondary antibodies (Agilent Technologies, Santa Clara, United States) diluted in milk. Signals were generated by incubation with ECL solution (Western Blotting Detection

Reagents, GE Healthcare). Image acquisition and signal quantification were performed using an Intas ECL ChemoCam Imager HR 3.2/6.0 (Intas Science Imaging Instruments, Göttingen, Germany).

Flow cytometry

Fresh kidney samples were prepared for enzymatic digestion as previously described (Ge et al., 2013). In brief, kidneys were dissected in digestion buffer containing 450 U/ml collagenase type I, 250 U/ml collagenase type XI, 120 U/ml hyaluronidase type I-s and 120 U/ml DNAse 1 (all Sigma-Aldrich, Saint Louis, United States) and subsequently incubated for 1 h at 37°C and 150 RPM. The tissue suspension was passed through a cell strainer (mesh size = 70 µm; Corning, New York, United States) to produce a single cell suspension. Staining was performed by mixing the cell suspensions with a cocktail containing the appropriate antibodies (Supplementary Table S1). Yellow and near-infrared LIVE/DEAD™ Fixable Dead Cell Stain Kit (Invitrogen, Carlsbad, CA) was used according to the manufacturer's instructions. Flow cytometry analysis was performed using a Becton-Dickinson FACSCanto™ II flow cytometer (BD Biosciences, Heidelberg, Germany). Cells were gated for live $CD45^+$ cells and normalized to the number of total events to determine the leukocyte abundance in relation to all renal cells. Data analysis was performed using FlowJo™ software (TreeStar Inc., Ashland, OR). The gating strategy is depicted in the Supplementary Figures S1–S3.

In situ hybridization

mRNA *in situ* hybridization for collagen 1 was performed using a probe covering nucleotides 2,256–2,468 of rat collagen 1a2 cDNA (NM_053356). Bound RNA was visualized using 4-nitroblue tetrazolium chloride as described previously (Skogstrand et al., 2013). Stained sections were evaluated using the Leica DMRB microscope.

Quantification of renal eicosanoid levels

Free tissue levels of eicosanoids and related lipid mediators were determined by mass spectrometry as previously described (Boldt et al., 2016). In brief, kidney samples were finely ground in liquid nitrogen and dissolved in a 50/50 vol/vol mixture of water and methanol supplemented with 0.01% butylhydroxytoluol. Samples were subsequently mixed with 10 µl internal standard solution (0.5 µg/ml) and 2 ml SPE-buffer (0.1 mol/l aqueous sodium acetate solution, pH 6). Solid-phase extraction was performed using a Bond-ElutCertify-II-Column (Phenomenex, Torrance, CA) following the instructions of the manufacturer. Eicosanoids were eluted with 2 ml n-hexane/ethylacetate (25/75 vol/vol) with 1% acetic acid. The solvent was evaporated and residues were resuspended in 100 µl methanol/water mixture. Liquid chromatography-mass spectrometry (LC-MS/MS) was performed at the mass spectrometry facility of Lipidomix (Lipidomix, Berlin, Germany). Values were normalized to the protein content of the sample.

Gene expression analysis

Transcriptome analysis was performed using Illumina Next Generation Sequencing with an Illumina HiSeq 4000 System and HiSeq Cluster Kit v4 and HiSeq SBS Kit v4 according to the manufacturer's protocol (Illumina Inc. San Diego, United States). Data from 5 mice per group were obtained and evaluated using the web-based Gene SeT AnaLysis Toolkit (WebGestalt) (Wang et al., 2017). All differentially regulated genes with $p < 0.05$ were included in the analysis. Pathway analysis was conducted using the Gene Ontology Biological processes database (Ashburner et al., 2000). The top 20 pathways sorted by the adjusted p-value for down- and upregulated genes are shown.

Statistical analysis

All statistical analyses were performed using GraphPad Prism 5 software (GraphPad Software, Inc., La Jolla, United States). Differences between survival curves were analyzed using Mantel-Cox log-rank test. Outliers were identified using the ROUT method with Q = 1%. Student's t-test was used for comparisons of renal lipid levels at d10 after nephritis induction; ANOVA with Sidak´s post-hoc test was applied for the comparison of multiple groups as indicated. $p < 0.05$ was considered to be statistically significant.

Results

AnxA1 biosynthesis is increased during cGN

Acute cGN was induced in WT and AnxA1-deficient mice by intraperitoneal injection of sheep nephrotoxic serum (Figure 1A). In the first set of experiments, we studied WT mice to determine the effects of nephrotoxic serum injection on renal AnxA1 mRNA expression and protein abundance. Specificity of the AnxA1 antibody was confirmed in AnxA1-deficient mice (Supplementary Figure S4). Quantification of renal AnxA1 mRNA by TaqMan® real time RT-PCR showed a non-significant trend towards higher levels at d5 (272 ± 58% of controls, p = n. s) and significantly elevated levels at d10 (373 ± 94% of controls, $p < 0.05$) after nephritis induction

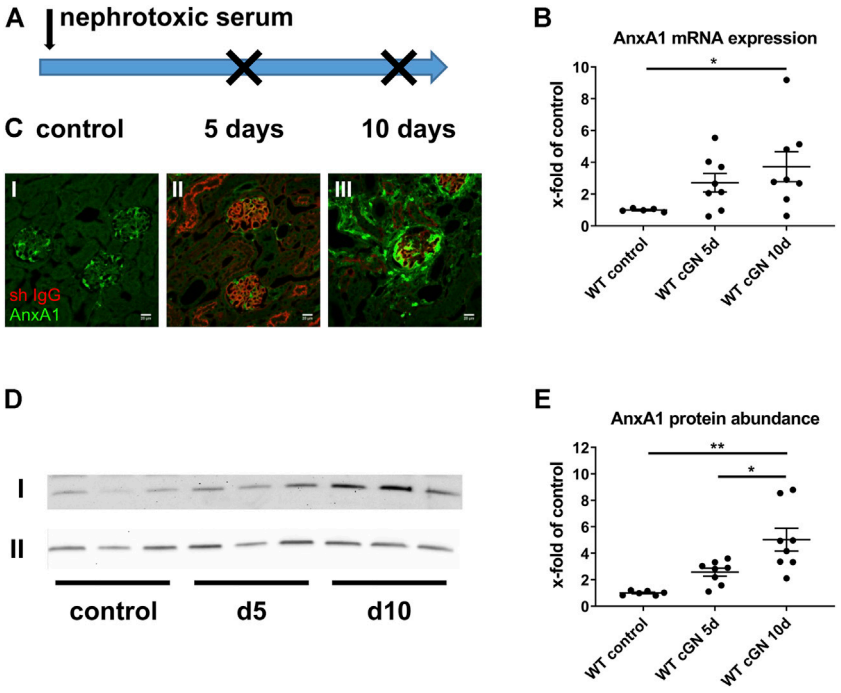

FIGURE 1
Regulation of annexin A1 during experimental crescentic GN. **(A)** Schematic of experimental setup. Crescentic glomerulonephritis (cGN) was induced at d0 in wildtype (WT) and annexin A1 (AnxA1)-deficient mice by intraperitoneal injection of sheep nephrotoxic serum; animals after injection of normal sheep serum served as controls. Kidneys were harvested at d5 and d10 after cGN induction. **(B)** TaqMan® real time RT-PCR quantification of AnxA1 mRNA abundance in WT mice. **(C)** Representative micrographs showing immunofluorescence staining for AnxA1 (green) and sheep IgG (red) in controls (I) and in mice at 5 (d5; II) and 10 (d10; III) after cGN induction. Scale bar = 20 µm. **(D)** Representative images of Western blots of WT mice treated with control or nephrotoxic serum for 5 (d5) and 10 days (d10). The β-actin content of the tissue homogenates was determined in parallel and served as loading control (lane II). **(E)** Densitometric analysis of the signals in **(D)**. Quantitative data in B and D is shown as x-fold changes in relation to controls. Dots represent measurements from individual mice; horizontal lines indicate mean values and error bars represent the SEM. Statistical significance of changes was calculated using one-way ANOVA and indicated by * for $p < 0.05$ and ** for $p < 0.01$; $n = 5–8$ per group.

(Figure 1B). Renal localization of AnxA1 signals and deposition of sheep IgG were studied by double-labeling immunofluorescence (Figure 1C). In WT controls, AnxA1 signal was strong in podocytes and weaker in parietal epithelial cells and peritubular fibroblasts, confirming earlier results (McKanna et al., 1992; Seidel et al., 2012). Staining for sheep IgG was absent in the control mice treated with normal sheep serum (Figure 1C, Image I). At d5 after nephrotoxic serum injection, direct immunofluorescence for sheep IgG showed strong linear staining along the glomerular basement membrane, while peritubular capillaries were weakly positive. Immunoreactive signal was further detected in proximal tubular cells, likely representing IgG reabsorbed from the tubular fluid. The glomerular AnxA1 signal was greatly reduced, whereas the tubulointerstitial signal was unchanged (Figure 1C, Image II). At d10, glomerular staining for sheep IgG had decreased which may reflect partial clearance of the antigen. By contrast, AnxA1 immunoreactive signals in the glomeruli and the tubulointerstitium were now markedly increased (Figure 1C, Image III). Immunoblotting for AnxA1 revealed a non-significant trend towards higher protein levels at d5 (257 ± 31% of controls, p = n. s.) and, more so, at d10 (503 ± 86% of controls, $p < 0.01$; 196 ± 34% of d5, $p < 0.05$) which agreed with the mRNA levels. As expected, AnxA1 KO mice showed no immunofluorescence signal, thus confirming the specificity of the antibody (Supplementary Figure S4).

In summary, these data show a time-dependent increase of renal AnxA1 abundance during the course of experimental cGN.

AnxA1 deficiency has no effect on survival but increases proteinuria

Next, we determined the effect of AnxA1 deficiency on survival and albuminuria. All mice treated with the control serum survived until the end of the study. Survival data from the nephrotoxic serum groups showed no significant differences

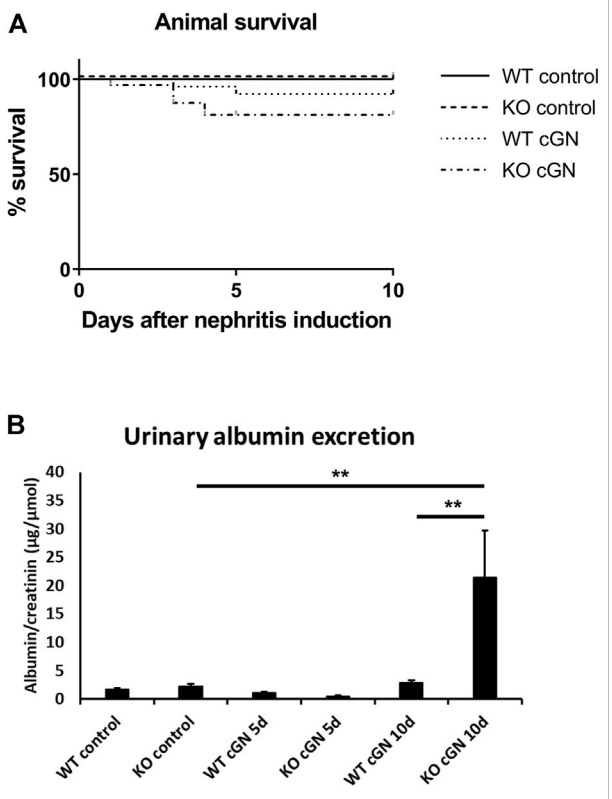

FIGURE 2
Survival and proteinuria. **(A)** Kaplan-Meier curves showing survival of wildtype (WT) and annexin A1-deficient (KO) mice after induction of crescentic glomerulonephritis (cGN) or after injection of normal sheep serum (control). **(B)** Quantification of urinary albumin-to-creatinine ratio in control mice and at d5 and d10 after cGN induction. Statistical analysis of differences between survival curves was performed using Mantel-Cox log-rank test; proteinuria data was analyzed using two-way ANOVA; n = 5–8 per group.

between WT (11%) and AnxA1-deficient mice (19%). In all cases, death occurred between d1 and d5 after nephritis induction (Figure 2A).

Urinary albumin excretion was determined in 18 h-collection samples and normalized to creatinine concentration. Control mice and mice at d5 after nephritis induction showed low levels of albuminuria, irrespective of genotype. At d10, albuminuria showed a marked 6.6-fold increase in AnxA1-deficient compared to WT mice (+659% ± 288%, $p < 0.01$; Figure 2B).

Deficiency of AnxA1 aggravates renal damage

Glomerular necrosis, crescent formation, and extent of tubulointerstitial damage were estimated in PAS-stained paraffin sections. Glomeruli from WT and AnxA1-deficient mice frequently showed segmental or global fibrinoid necrosis along with the formation of tip lesions at d5 after nephritis induction. Parietal epithelial cells were activated displaying enlarged nuclei and polygonal cell bodies. Scattered tubular profiles filled with protein precipitates reflected the proteinuria (Figure 3A). Tubular structure was otherwise normal and the tubulointerstitium showed only mild, focal expansion. Morphology in the control mice was normal. Quantification of necrotic glomeruli at d5 after nephritis induction showed significantly increased numbers in nephritic WT (32.2 ± 4.7%, $p < 0.01$) and AnxA1-deficient mice (31.4 ± 5.4%, $p < 0.01$) without significant differences between both genotypes (Figure 3C). The extent of tubulointerstitial damage, expressed by the estimated area with tubular atrophy and interstitial fibrosis, was also similar between WT and AnxA1-deficient mice. At d10, kidneys showed signs of advanced glomerular damage with crescent formation or global sclerosis. Tubulointerstitial damage was increased as well with focal accumulation of leukocytes and fibroblasts in the periglomerular space and around damaged tubules and blood vessels (Figure 3B). Quantification of glomerular profiles with crescents or global sclerosis revealed a significantly increased number of damaged glomeruli in the nephritic WT (23.8 ± 4.2%, $p < 0.01$) and, more severely, in AnxA1-deficient mice (42.1 ± 5.6%, $p < 0.01$). The difference between the nephritic WT and AnxA1-deficient mice was statistically significant (177 ± 24%, $p < 0.01$; Figure 3D).

The tubulointerstitial damage was increased in parallel to the glomerular damage in nephritic WT (10 ± 0%, $p < 0.01$) and AnxA1-deficient mice (33 ± 2%, $p < 0.01$). Again, damage was more severe in the AnxA1-deficient mice (330 ± 20% of WT, $p < 0.01$; Figure 3E).

In summary, these results show a marked aggravation of renal damage in the AnxA1-deficient mice 10 days after nephritis induction.

AnxA1 deficiency aggravates renal inflammation

To determine the effect of AnxA1 on leukocyte infiltration during cGN, we performed flow cytometry of total kidney single cell suspensions. Accumulation of PMN, macrophages, and T-lymphocytes was further studied using immunofluorescence. Injection of nephrotoxic serum caused renal infiltration of $CD45^+$ leukocytes in mice of both genotypes. At d5, numbers were increased 10-fold in WT (1,006 ± 132%, $p < 0.01$) and 12-fold in the AnxA1-deficient mice (1,207 ± 206%, $p < 0.01$); changes were not statistically different between genotypes. At d10, numbers of $CD45^+$ cells were increased 12.5-fold in WT (1,248 ± 253%, $p < 0.01$) and 31.5-fold (3,149 ± 687%, $p < 0.01$) in the AnxA1-deficient mice, and changes were significantly different between genotypes (206 ± 4.5%, $p < 0.01$; Figure 4A).

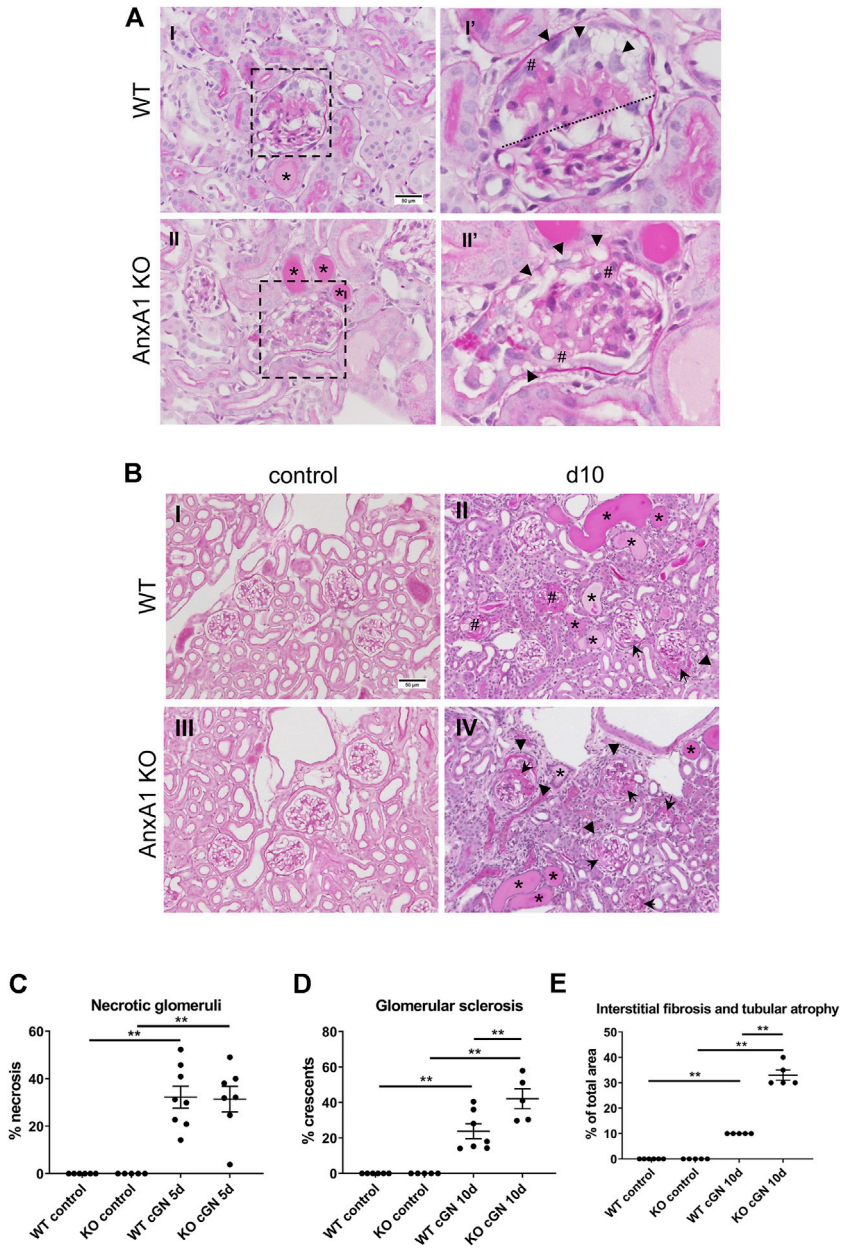

FIGURE 3
Deficiency of annexin A1 has no effect at d5 but aggravates renal damage at d10. **(A)** Representative micrographs of PAS-stained kidney sections from wildtype (WT; I,I′) and annexin A1 (AnxA1)-deficient mice (KO; II,II′) at d5 after induction of crescentic glomerulonephritis (cGN). Low power micrographs (I,II) show glomeruli with signs of necrosis, tubular profiles filled with protein casts (*) and mild focal interstitial expansion. Magnification of the glomerular profiles boxed in I and II (I′, II′) show segmental (above dotted line in I′) and global necrosis (II′) as well as several tip lesions with attachment of the glomerular tuft to the Bowman capsule (#). Parietal epithelial cells show typical signs of activation with enlarged nuclei and polygonal cell bodies (arrowheads in I′ and II′). Scale bar = 50 µm in I + II. **(B)** Representative micrographs of PAS-stained kidney sections from wildtype (WT; I,II) and annexin A1 (AnxA1)-deficient mice (KO; III,IV) at d10 after injection of normal sheep serum (control; I,III) or induction of cGN (II,IV). Control mice of both genotypes show normal renal morphology. At d10 after cGN induction, glomeruli in mice of both genotypes show morphological hallmarks of extracapillary proliferative glomerulonephritis with crescent formation (arrowheads), global sclerosis (#), and periglomerular fibrosis (arrows). The interstitial space is expanded with an increased number of leukocytes and fibroblasts. Numerous tubular profiles are filled with protein casts (*). Scale bar = 50 µm in I-IV. **(C)** Quantification of glomerular profiles with morphological signs of necrosis at d5 after cGN induction. **(D)** Quantification of glomerular profiles with crescents or global sclerosis at d10 after cGN induction. **(E)** Quantification of areas with tubular atrophy and interstitial fibrosis at d10 after cGN induction. Dots represent values from individual animals; horizontal lines indicate mean values and error bars represent the SEM. Statistical significance of changes was calculated using one-way ANOVA; n = 5–8 per group.

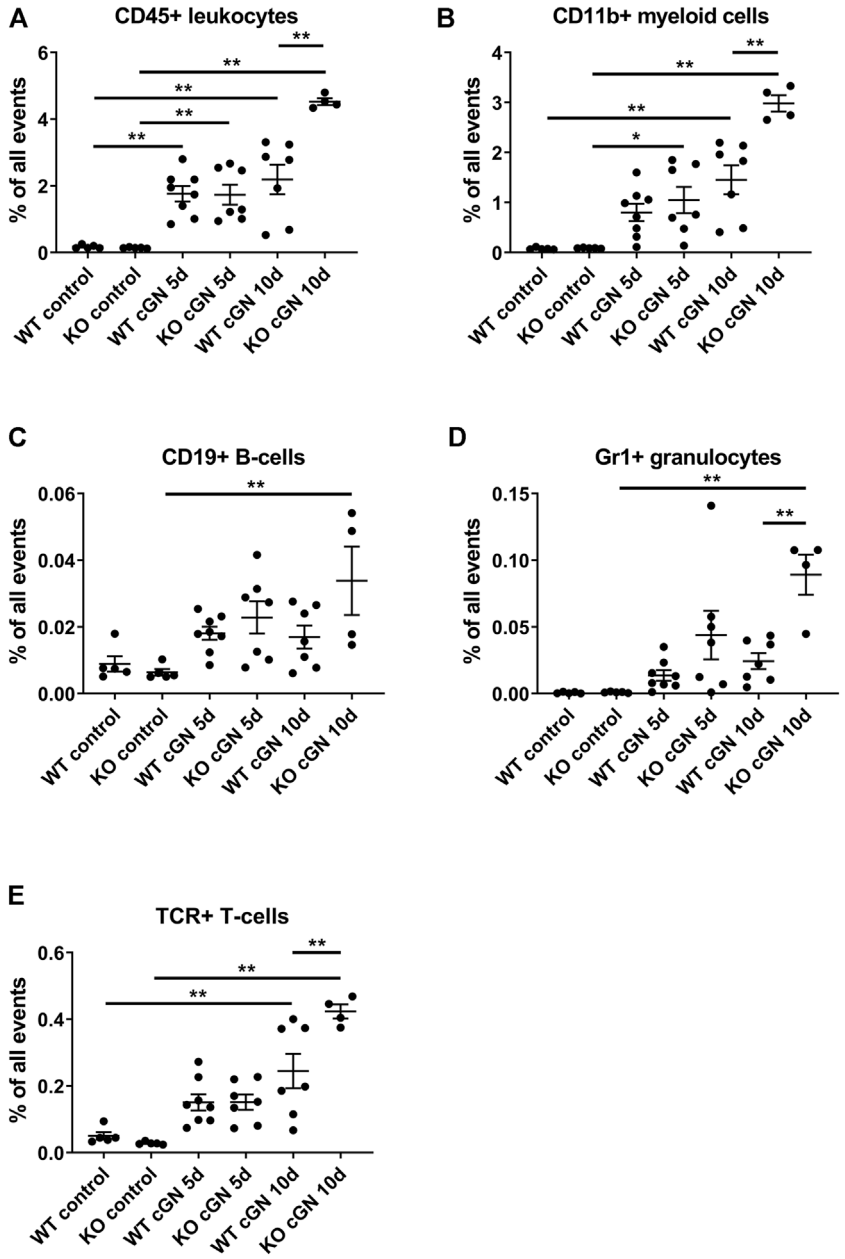

FIGURE 4
Deficiency of annexin A1 aggravates renal inflammation Flow cytometry quantification of renal CD45$^+$ leukocytes **(A)**, CD11b$^+$ myeloid cells **(B)**, CD19$^+$ B-lymphocytes **(C),** neutrophils defined as live CD45$^+$/GR1^{HIGH} cells **(D)** and T-lymphocytes defined as live CD45+/β-TCR$^+$ cells **(E)** in wildtype (WT) and annexin A1 (AnxA1)-deficient mice (KO) at d5 and d10 after injection of normal sheep serum (control) or induction of crescentic glomerulonephritis (cGN). Dots represent values from individual animals; horizontal lines indicate mean values and error bars represent the SEM. Statistical significance of changes was calculated using one-way ANOVA; *$p < 0.05$; **$p < 0.01$; $n = 5–8$ per group.

Quantification of CD11b$^+$ myeloid cells at d5 revealed a numerical increase in WT (1,038 ± 224%, p = n.s.) and a significant, 11.6-fold increase in the AnxA1-deficient mice (1,164 ± 291%, $p < 0.05$). There was no statistical difference between the genotypes. At d10, the number of CD11b$^+$ cells was increased 19-fold in WT (1886 ± 375%, $p < 0.01$) and 33-fold (3,310 ± 185%, $p < 0.01$) in the AnxA1-deficient mice. The difference between the genotypes at d10 was statistically significant (205 ± 11%, $p < 0.01$; Figure 4B).

Renal CD19$^+$ B-lymphocytes showed a marked, 5-fold increase (529 ± 160%, $p < 0.01$) in the AnxA1-deficient mice at d10 after nephritis induction, despite inter-animal variations,

10.3389/fphys.2022.984362

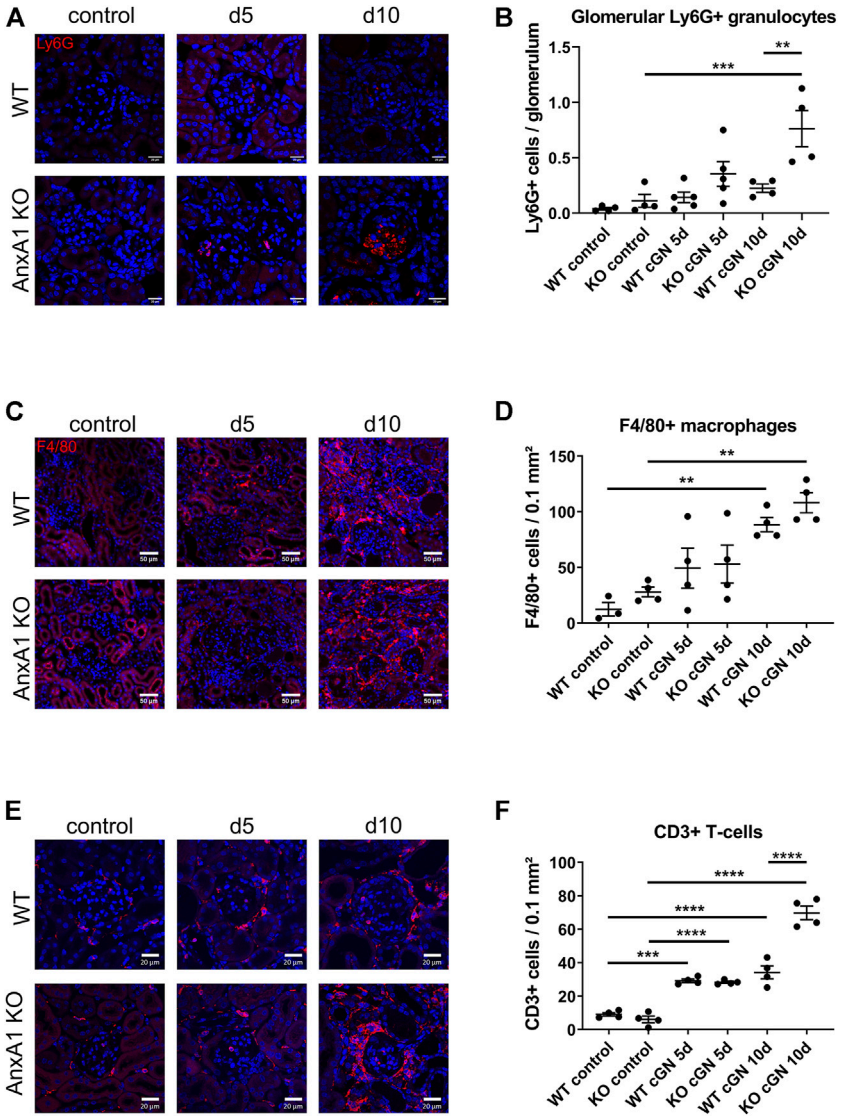

FIGURE 5
Deficiency of annexin A1 increases the renal abundance of neutrophils, T-lymphocytes and macrophages. **(A)** Representative images of kidney sections from control wildtype (WT) and annexin A1 (AnxA1)-deficient mice (KO) and from mice at d5 and d10 after injection of normal sheep serum (control) or induction of crescentic glomerulonephritis (cGN). Sections were stained for Ly6G as marker for neutrophil granulocytes (red). **(B)** Quantification of glomerular granulocytes shows an increased abundance of Ly6G-positive cells in KO mice at d10 after cGN induction as compared to the nephritic WT mice. **(C)** Representative images of kidney sections from control WT and KO mice and from animals at d5 and d10 after cGN induction. Sections were stained for F4/80 as marker for macrophages (red). F4/80 positive cells accumulate in the renal interstitium of WT and KO animals at d10 after cGN induction. **(D)** Quantification of renal macrophages shows an increased abundance of F4/80 positive cells at d10 after cGN induction without difference between the genotypes. **(E)** Representative images of kidney sections from control WT and KO mice and from animals at d5 and d10 after cGN induction. Sections were stained for CD3 as marker for T-lymphocytes (red). **(F)** Quantification of renal T-lymphocytes shows a significantly increased abundance of CD3-positive cells in the AnxA1-deficient mice at d10 after cGN induction as compared to the nephritic WT mice. Scale bar = 20 μm in A,E and 50 μm in C, blue signal marks DAPI-stained nuclei. Dots in B,D, and F represent values from individual mice; horizontal lines indicate mean values and error bars represent the SEM. Statistical significance of changes was calculated using one-way ANOVA; $*p < 0.05$; $**p < 0.01$; $***p < 0.001$; $n = 3–5$ per group.

as compared to AnxA1-deficient control mice. Changes in the abundance of $CD19^+$ cells in nephritic WT mice were not significant (Figure 5C).

Analysis of $GR1^+$ neutrophils revealed a numerical increase at d5 and a significant 9-fold increase at d10 after nephritis induction in AnxA1-deficient mice as compared to the AnxA1-

deficient controls (8,804 ± 1,481%, $p < 0.01$). In contrast, renal abundance of GR1$^+$ neutrophils was not significantly altered in the WT mice. At d10, renal abundance of Gr1$^+$ neutrophils was significantly higher in the AnxA1-deficient mice as compared to the nephritic WT mice (367 ± 62%, $p < 0.01$; Figure 4D).

Quantification of TCR$^+$ lymphocyte abundance revealed a numerical increase of positive cells at d5 after nephritis induction without significant genotype-dependent differences. At d10, the number of positive cells was increased 4.8-fold in WT (480 ± 101%, $p < 0.01$) and 15-fold in the AnxA1-defcient mice (1,495 ± 74%, $p < 0.01$). Now the difference between the genotypes was significant (173 ± 9%, $p < 0.01$; Figure 4E).

To localize renal neutrophils, macrophages and T-lymphocytes during nephrotoxic serum nephritis, we performed immunofluorescence staining for Ly6G, F4/80, and, CD3, respectively (Figure 5). Glomeruli of control animals of both genotypes and nephritic WT mice showed only few glomerular profiles with Ly6G$^+$ cells without significant differences between the two time points. In contrast, glomeruli in the AnxA1-deficient mice displayed large accumulations of Ly6G$^+$ cells at d5 and d10 after nephritis induction. Quantification of glomerular Ly6G$^+$ cells in AnxA1-deficient mice revealed a non-significant increase at d5 (320 ± 100%, p = n.s) and a significant 7-fold increase at d10 (688 ± 148%, $p < 0.001$). Comparison of both genotypes at this time point revealed significantly higher numbers of glomerular Ly6G$^+$ cells in the AnxA1-deficient mice (338 ± 72%, $p < 0.01$; Figure 5B). Localization studies for F4/80$^+$ macrophages in the control mice revealed only very few scattered immunoreactive cells throughout the tubulointerstitium and the perivascular region. Quantification of F4/80$^+$ macrophages revealed a non-significant trend towards higher numbers in the AnxA1-deficient mice as compared to WT controls. After nephritis induction, the number of F4/80$^+$ immunoreactive cells showed a numerical increase in both, WT and Anxa1-deficient mice at d5 and a further marked increase at d10. Immunoreactive cells were predominantly localized in the tubulointerstitium of the damaged areas whereas glomeruli were generally devoid of F4/80$^+$ immunoreactive cells. Quantification of positive cells at d10 after nephritis induction showed a significant 7-fold increase in WT (713 ± 52%, $p < 0.01$) and a 3.8-fold increase in AnxA1-deficient mice (387 ± 32%, $p < 0.01$) relative to the respective control animals (Figure 5D). However, there was no significant difference between the genotypes for both time points.

CD3 immunofluorescence staining in control animals of both genotypes showed few scattered cells in glomeruli, periglomerular region and in the tubulointerstitial space. At d5 after nephritis induction, the overall number of CD3 immunoreactive cells was markedly increased with focal accumulation in the periglomerular space of damaged glomeruli. There was no genotype-dependent difference in the quantity and distribution pattern of the cells. At d10 after nephritis induction, numbers of immunoreactive cells were further increased in the wildtype mice and more dramatically in the AnxA1-deficient mice. Again, immunoreactive cells accumulated in the periglomerular region of the damaged glomeruli and in the tubulointerstitial space of the corresponding nephrons (Figure 5E).

Quantification of CD3$^+$ cells in AnxA1-deficient mice revealed a non-significant increase at d5 (320 ± 100%, p = n.s) and a significant 7-fold increase at d10 (688 ± 148%, $p < 0.001$). Comparison of both genotypes at this time point revealed significantly higher numbers of glomerular CD3$^+$ cells in the AnxA1-deficient mice (338 ± 72%, $p < 0.01$; Figure 5F).

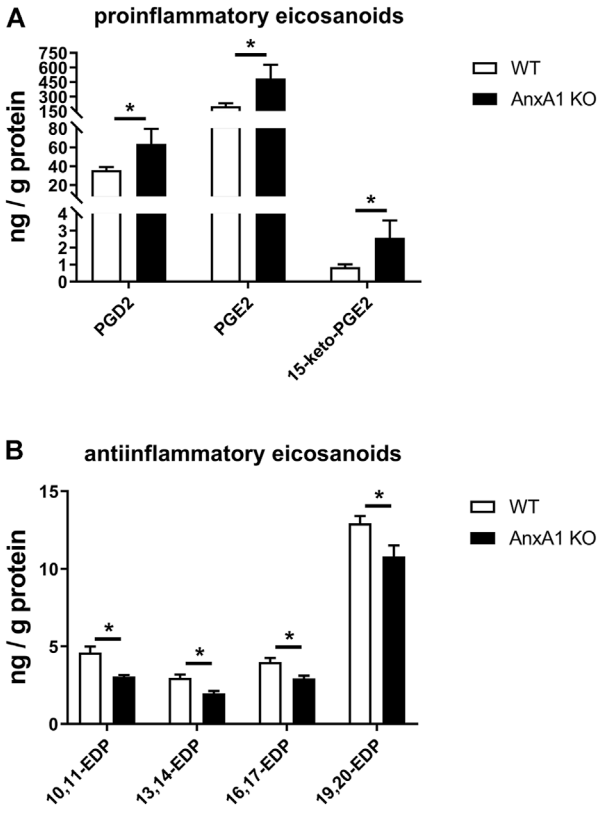

FIGURE 6
Deficiency of annexin A1 regulates the abundance of proinflammatory and antiinflammatory eicosanoids. **(A)** Lipidomics analysis of proinflammatory renal eicosanoid species in wildtype (WT) and annexin A1 (AnxA1)-deficient mice (AnxA1 KO) at d10 after induction of crescentic glomerulonephritis shows significantly higher tissue levels for prostaglandin D2 (PGD2), prostaglandin E2 (PGE2) and of the principal PGE2 metabolite 15-keto-PGE2 in the AnxA1-KO mice as compared to nephritic WT mice. **(B)** Analysis of antiinflammatory epoxydocosapentaenoic acid (EDP) regioisomers shows significantly lower tissue levels for 10,11-EDP, 13,14-EDP, 16,17-EDP, and 19,20-EDP in AnxA1-KO mice at d10 after induction of crescentic glomerulonephritis as compared to nephritic WT mice. Statistical significance of changes was calculated using Student`s t-test; *$p < 0.05$; $n = 5$ per group.

10.3389/fphys.2022.984362

TABLE 1 Functional enrichment of negatively regulated genes annexin A1 deficient mice compared to wildtype mice at d10 of experimental crescentic GN. Regulated gene products corresponding to the individual in pathways are listed in Supplementary Table S2.

Pathway name	O	C	E	R	adjP
Cofactor metabolic process	154	488	55.75	2.76	<9.99E-15
Purine-containing compound metabolic process	132	481	54.95	2.40	<9.99E-15
Ribose phosphate metabolic process	131	443	50.61	2.59	<9.99E-15
Mitochondrion organization	125	434	49.58	2.52	<9.99E-15
Generation of precursor metabolites and energy	118	389	44.44	2.66	<9.99E-15
Small molecule catabolic process	107	328	37.47	2.86	<9.99E-15
Nucleoside monophosphate metabolic process	85	279	31.87	2.67	<9.99E-15
Nucleoside triphosphate metabolic process	83	270	30.85	2.69	<9.99E-15
Cellular amino acid metabolic process	85	260	29.70	2.86	<9.99E-15
Sulfur compound metabolic process	78	275	31.42	2.48	6.58E-13
Dicarboxylic acid metabolic process	41	99	11.31	3.63	1.61E-12
NADH dehydrogenase complex assembly	25	42	4.80	5.21	5.80E-12
Pyridine-containing compound metabolic process	51	150	17.14	2.98	1.17E-11
Organic acid biosynthetic process	85	349	39.87	2.13	3.17E-10
Nucleoside bisphosphate metabolic process	38	106	12.11	3.14	2.00E-09
Cellular ketone metabolic process	53	182	20.79	2.55	2.91E-09
Cellular aldehyde metabolic process	29	70	8.00	3.63	6.61E-09
Tricarboxylic acid metabolic process	20	36	4.11	4.86	6.90E-09
Mitochondrial transport	49	166	18.96	2.58	7.70E-09
Organophosphate biosynthetic process	102	484	55.29	1.84	1.57E-08

O, the number of genes in the gene set and also in the category.
C, the number of reference genes in the category.
E, the expected number in the category.
R, ratio of enrichment.
adjP, p value adjusted by the multiple test adjustment.

In the aggregate, these data demonstrate a phenotype of severe progressive inflammation in nephritic AnxA1-deficient mice.

Deficiency of AnxA1 causes coordinated alterations of renal lipid levels at d10 of experimental cGN

Renal tissue levels of eicosanoids and related lipid mediators were measured by mass-spectrometry lipidomics analysis in WT and AnxA1-deficient mice at d10 after nephritis induction. AnxA1-deficient mice displayed increased levels of proinflammatory lipid mediators including PGD2 (178 ± 45%; $p < 0.05$), PGE2 (240 ± 71%; $p < 0.05$) and its degradation product 15-keto-PGE2 (300 ± 120%; $p < 0.05$; Figure 6A). Concomitantly, the abundance of several antiinflammatory epoxydocosapentaenoic acid regioisomers was reduced (10,11-EDP: 66 ± 2%, $p < 0.05$; 13,14-EDP: 66 ± 5%, $p < 0.05$; 16,17-EDP: 74 ± 5%, $p < 0.05$; 19,20-EDP: 84 ± 5%, $p < 0.05$; Figure 6B). Despite extensive efforts, we were unable to detect significant amounts of the canonical proresolving lipid mediators lipoxin A4, resolvins, protectins and maresins in the kidney samples of our experimental animals. A complete list of the lipidomics analysis is presented in Supplementary Table S2.

Deficiency of AnxA1 causes broad alterations of the renal transcriptome

To assess the influence of AnxA1 on the renal transcriptome in the setting of nephrotoxic serum nephritis, we performed NGS followed by pathway analysis on WT and AnxA1-deficient mice at d10 after nephritis induction. AnxA1 deficiency resulted in differential expression of 1937 genes with downregulation of 1,027 and upregulation of 910 gene products. Pathway analysis of downregulated genes revealed enrichment in pathways relevant for epithelial cell metabolism and function (Table 1). Upregulated genes were enriched in pathways related to leukocyte activation, regulation of cytokine production and secretion as well as leukocyte chemotaxis (Table 2). A comprehensive list of the regulated gene products corresponding to the individual pathways are presented in Supplementary Tables S3, S4.

TABLE 2 Functional enrichment of positively regulated genes annexin A1 deficient mice compared to wildtype mice at d10 of experimental crescentic GN. Regulated gene products corresponding to the individual in pathways are listed in Supplementary Table S3.

Pathway name	O	C	E	R	adjP
Regulation of leukocyte activation	136	482	56.31	2.42	<9.99E-15
T cell activation	123	458	53.51	2.30	<9.99E-15
Negative regulation of immune system process	125	431	50.35	2.48	<9.99E-15
Positive regulation of cytokine production	118	404	47.20	2.50	<9.99E-15
Adaptive immune response	116	397	46.38	2.50	<9.99E-15
Regulation of cell-cell adhesion	106	369	43.11	2.46	<9.99E-15
Activation of immune response	111	368	42.99	2.58	<9.99E-15
Positive regulation of defense response	99	341	39.84	2.48	<9.99E-15
Leukocyte migration	97	315	36.80	2.64	<9.99E-15
Immune response-regulating signaling pathway	99	310	36.22	2.73	<9.99E-15
Positive regulation of cell activation	89	306	35.75	2.49	<9.99E-15
Leukocyte cell-cell adhesion	91	301	35.17	2.59	<9.99E-15
Cell chemotaxis	84	280	32.71	2.57	<9.99E-15
Regulation of innate immune response	82	267	31.19	2.63	<9.99E-15
Cytokine secretion	71	213	24.88	2.85	<9.99E-15
Myeloid leukocyte activation	70	194	22.67	3.09	<9.99E-15
Cytokine-mediated signaling pathway	97	360	42.06	2.31	3.18E-14
Interleukin-6 production	54	144	16.82	3.21	3.51E-14
Regulation of inflammatory response	88	313	36.57	2.41	4.74E-14
Negative regulation of cell activation	61	180	21.03	2.90	1.08E-13

O, the number of genes in the gene set and also in the category.
C, the number of reference genes in the category.
E, the expected number in the category.
R, ratio of enrichment.
adjP, p value adjusted by the multiple test adjustment.

Deficiency of AnxA1 increases markers of renal fibrosis

Fibrotic scar formation is a consequence of nephron loss during cGN. To assess the extent of renal scarring, we performed *in-situ* hybridization and TaqMan® real time RT-PCR for Col1A1. In addition, the abundance of extracellular collagen fibers was visualized and quantified by Sirius Red Stain with subsequent measurement of the integrated signal intensity. As shown in Figure 7A, Col1A1 mRNA was localized in fibroblasts in the periglomerular region of damaged glomeruli and the perivascular space of arcuate arteries in kidneys of mice at d10 after nephritis induction. Col1A1 mRNA signal abundance was increased in AnxA1-deficient mice compared to their WT counterparts. Quantitative real time RT-PCR revealed a 11.5-fold increase of renal Col1A1 mRNA abundance in WT (1,054 ± 188%, $p < 0.01$) and a 11.7-fold increase in AnxA1-deficient mice (1,169 ± 113%, $p < 0.01$) at d10 after nephritis induction (Figure 7B). Comparison of both genotypes showed a significant higher Col1A1 mRNA expression in kidneys of the AnxA1-deficient mice (189 ± 18%, $p < 0.01$). Under control conditions, Sirius Red-positive extracellular collagen fibers were predominantly located in the vicinity of Bowman's capsule and in the perivascular space (Figure 7C). 10 days after nephritis induction, Sirius Red-positive collagen fibers accumulated in areas with glomerular and tubulointerstitial damage as well as in the perivascular space of interlobular arteries. At d10 after nephritis induction, quantification of Sirius Red signal demonstrated only a numerical increase in the signal density in WT (165 ± 47%, p = n.s.) and a significant 13-fold increase (1,285 ± 321%, $p < 0.01$) in AnxA1-deficient mice as compared to the respective controls. Comparison of both genotypes at this time point revealed significantly higher Sirius Red signal intensity in the AnxA1-deficient mice (230 ± 57%, $p < 0.05$; Figure 7D).

Discussion

We hereby show that AnxA1 mRNA expression and protein abundance are increased at d10 after induction of nephrotoxic serum nephritis. Both intrinsic renal cells and infiltrating leukocytes contribute to these elevated levels. Functionally, AnxA1-deficient mice display a phenotype of severe non-resolving inflammation as indicated by elevated tissue levels of leukocytes and proinflammatory mediators including

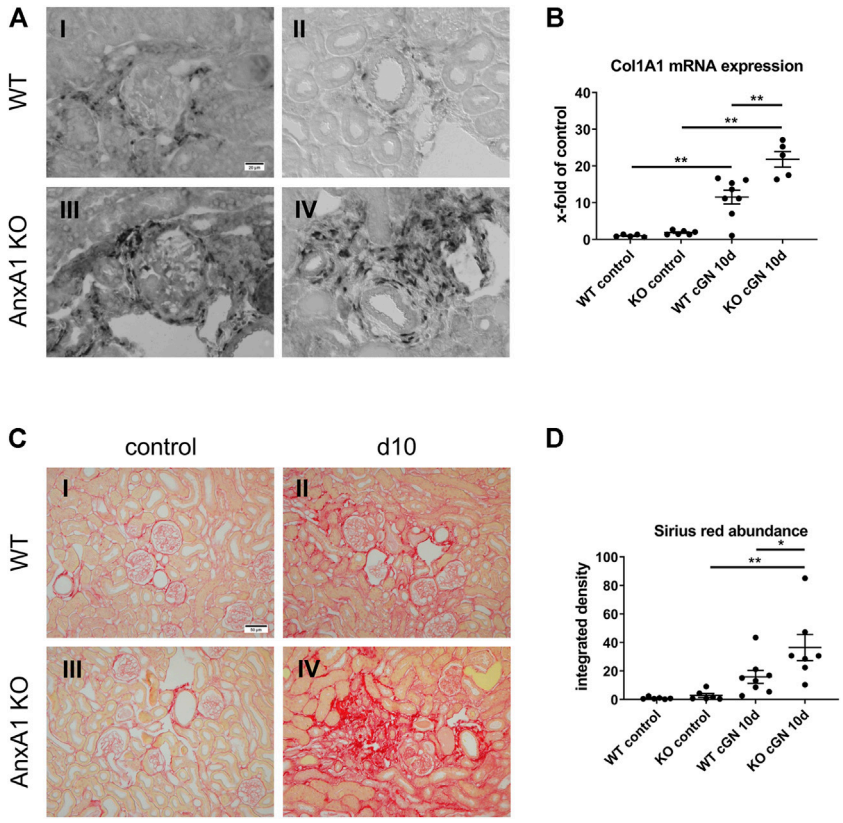

FIGURE 7
Deficiency of annexin A1 aggravates renal fibrosis. **(A)** Representative images of alpha-1 type 1 collagen (Col1A1) mRNA *in situ* hybridization performed on kidney sections from wildtype (WT; I, II) and annexin A1 (AnxA1)-deficient mice (KO; III,IV) at d10 after injection of normal sheep serum (control) or induction of crescentic glomerulonephritis (cGN). Col1A1 mRNA signal is localized to fibroblasts in the periglomerular region of damaged glomeruli (I,III) and the perivascular space of arcuate arteries (II,IV). **(B)** TaqMan® real time RT-PCR quantification of Col1A1 mRNA abundance in WT and KO mice at d10 after cGN induction. **(C)** Representative images of Sirius Red-stained kidney sections from WT (I,II) and KO (III,IV) mice at d10 after cGN induction in control- (I, III), or cGN mice (II,IV). **(D)** Quantification of renal cortical Sirius Red signal by automated image analysis shows an increased abundance in the KO cGN mice as compared to the nephritic WT mice. Scale bar = 20 µm in A and 50 µm in **(C)**. Dots in B and D represent values from individual mice; horizontal lines indicate mean values and error bars represent the SEM. Statistical significance of changes was calculated using two-way ANOVA; $*p < 0.05$; $**p < 0.01$; $n = 6–8$ per group.

prostaglandins D2 and E2 as well as aggravated glomerular crescent formation, tubulointerstitial damage and severe proteinuria.

Renal expression of AnxA1 and its regulation in kidney disease have been studied in considerable detail (McKanna et al., 1992; Ka et al., 2014; Neymeyer et al., 2015; Wu et al., 2021). In a model of Adriamycin-induced nephropathy, the authors observed a time-dependent increase in glomerular AnxA1 expression with maximum levels in podocytes and parietal epithelial cells at d7 and d14 after induction. Elevated expression at these sites was further reported in biopsies from patients with diabetic kidney disease, cGN and proliferative lupus nephritis (Ka et al., 2014; Wu et al., 2021). Our localization studies recapitulate these findings, thus suggesting that upregulation of AnxA1 in podocytes and parietal epithelial cells may be part of a universal response to glomerular injury. Since AnxA1 is involved in membrane homeostasis (Babiychuk et al., 2011; Potez et al., 2011) and the stabilization of intracellular calcium levels during phases of energy depletion and acidosis (Vais et al., 2020), elevated AnxA1 levels may increase the resilience of these cells against further insults.

A pronounced accumulation of AnxA1 was also observed in the tubulointerstitial space corresponding to inflammatory infiltrates and fibrotic areas. These findings are in line with previous localization studies by us and others (Neymeyer et al., 2015; Wu et al., 2021) and with data from single cell RNA sequencing studies (https://kpmp.org/). Prominent expression of AnxA1 in neutrophils and macrophages underlines the importance of these cells for the generation of pro-resolving signals in the inflamed tissue (Sugimoto et al., 2016).

In a detailed analysis of renal leukocyte species by flow cytometry and immunohistology, we found no difference in the extent of renal leukocyte infiltration between wildtype and AnxA1-deficient mice at d5 after induction of nephrotoxic serum nephritis. In addition, the evaluation of glomerular profiles at this time point revealed a similar damage pattern without significant differences between genotypes. These findings argue against a major protective role of AnxA1 during the initiation phase of nephrotoxic serum nephritis. In contrast, at d10 after nephritis induction, we observed higher numbers of infiltrating leukocytes along with increased glomerular and tubulointerstitial damage in the AnxA1-deficient mice as compared to the WT controls. Analysis of leukocyte populations by flow cytometry and immunofluorescence revealed an increased abundance of lymphocytes, macrophages and neutrophil granulocytes. To further corroborate these findings, we performed RNAseq gene expression analysis which revealed increased mRNA levels of gene products involved in neutrophil activation and chemotaxis as well as macrophage activation. Reduced mRNA levels of gene products involved in metabolic processes likely reflect the loss of transporting nephron epithelia. These findings therefore present hallmark features of non-resolving inflammation and the associated progressive destruction of functional renal tissue.

A central result of our study is the highly increased abundance of neutrophils in the glomeruli and in the tubulointerstitium of AnxA1-deficient mice at d10 after nephritis induction. Typically, neutrophils are among the first leukocytes to arrive in the glomerulus after induction of nephrotoxic serum nephritis (Kuligowski et al., 2006) where they contribute to glomerular damage by generating neutrophil extracellular traps (NET) (Westhorpe et al., 2017) and by initiating the respiratory burst reaction (Suzuki et al., 2003; Xiao et al., 2005; Kurts et al., 2013; Antonelou et al., 2022). Neutrophil recruitment may either occur *via* direct Fcγ receptor/Mac-1-mediated binding of antibodies on the glomerular basement membrane (Suzuki et al., 2003) or in a mechanism depending on platelet-derived P-selectin (Kuligowski et al., 2006). In resolution-competent animals these neutrophils are rapidly cleared during the first 72 h after nephritis induction (Wu et al., 1996; Devi, 2013 #44). In line with this timeframe, we found only few neutrophils in glomeruli of the wildtype mice at d5 and d10 after nephritis induction. Mechanisms of neutrophil clearance in the setting of nephrotoxic serum nephritis-induced cGN have not been determined. However, our finding of increased numbers of neutrophils in the kidneys of AnxA1-deficient mice suggests an essential role for AnxA1 during this process.

Importantly, neutrophils themselves are an essential source for AnxA1 in the inflammatory microenvironment (Vergnolle et al., 1995). In neutrophils, AnxA1 is localized in gelatinase granules and in the cytosol (Perretti et al., 2000) and is released during degranulation and NETosis. After externalization, AnxA1 is subject to proteolytic cleavage by neutrophil elastase and proteinase 3 which results in the release of bioactive, soluble N-terminal protein fragments (Oliani et al., 2001; Rescher et al., 2006; Vong et al., 2007). Both full-length AnxA1 and its fragments have been shown to contribute to the antiinflammatory actions of the protein (Walther et al., 2000; Bode et al., 2019). Multiple effects of AnxA1 on neutrophil function have been described (Sugimoto et al., 2016). AnxA1 reduces neutrophil adhesion to endothelial cells by promoting the shedding of L-selectins and by counteracting the activation and clustering of essential integrins (Solito et al., 2003; Drechsler et al., 2015). In the inflamed tissue, AnxA1 induces neutrophil apoptosis in a calcium and FPR2-dependent mechanism (Solito et al., 2003; Dalli et al., 2013). The apoptotic bodies arising from this process are important mediators of the resolution phase of acute inflammation since they function as decoy receptors for proinflammatory cytokines (Jones et al., 2016). Efferocytosis of neutrophil-derived apoptotic bodies by macrophages induces a pro-resolving phenotype with increased phagocytic activity and expression of antiinflammatory cytokines including IL-10, TGF-β (Sugimoto et al., 2016). In addition, AnxA1 reduces platelet P-selectin levels (Vital et al., 2020) which may be of particular relevance for the suppression of glomerular neutrophil infiltration during nephrotoxic serum nephritis.

Various components of the adaptive immune system have been implicated in the pathogenesis of cGN (Artinger et al., 2017; Chen et al., 2018). In particular, gamma delta T cells and their principal cytokine, interleukin 17, have been shown to be instrumental for neutrophil recruitment and the development of renal injury in nephrotoxic serum-induced cGN (Turner et al., 2012; Disteldorf et al., 2015).

Studies addressing the role of AnxA1 in models of Th17-dependent autoimmune diseases have produced conflicting results with protective effects reported in mouse models of retinal inflammation (Yazid et al., 2015), collagen-induced arthritis, contact dermatitis (Yang et al., 2013) and in patients with multiple sclerosis (Colamatteo et al., 2019). In contrast, in mouse models of allergic airway inflammation and experimental autoimmune encephalomyelitis AnxA1-deficient mice showed decreased Th1/Th17 polarization of T cells and reduced disease activity, suggesting proinflammatory effects of AnxA1 (D'Acquisto et al., 2007; Paschalidis et al., 2009).

In the present study, we observed increased numbers of Th17-expressing T cells at d5 which decreased at d10, thus confirming previous reports regarding the kinetics of Th17 T-cells in the nephrotoxic serum nephritis model (Turner et al., 2012). Unexpectedly, we found no genotype-dependent differences in the number of Th17-expressing T cells for both points in time. Furthermore, RNAseq gene expression analysis showed no genotype-dependent difference in the mRNA levels of IL-17 family members and their putative receptors at d10 after nephritis induction. The mRNA abundance

of the principal effector cytokines of TH17 cells, CXCL1, and CXCL5 remained unchanged as well (data not shown). In aggregate, these findings therefore argue against an important contribution of Th17 T-cells to the excessive inflammation and tissue destruction observed in the AnxA1-deficient mice. However, further studies are needed to fully elucidate the effects of AnxA1 on Th17 T-cell generation and function.

Prostaglandins and related lipid mediators control important aspects of kidney function and inflammation in cGN (Takahashi et al., 1990; Kvirkvelia et al., 2013). Since AnxA1 has been shown to inhibit renal prostaglandin synthesis by interfering with phospholipase A2 and cyclooxygenase 2, the two rate-limiting enzymes involved in the generation of PGE2, we measured renal levels of PGE2 and other polyunsaturated fatty acids metabolites. Using an unbiased state-of-the-art lipidomics approach, we found markedly elevated levels of PGE2 and its predominant metabolite 15-keto-PGE2 in the kidney homogenates of the AnxA1-deficient mice at d10 after nephritis induction. This finding is in line with the well-established inhibitory effect of AnxA1 on renal PGE2 synthesis and thus confirms previous studies (Seidel et al., 2012). The functional consequences of these elevated PGE2 levels are not well understood and may involve proinflammatory effects due to increased Cxcl-5 expression (Aringer et al., 2018) on the one hand and tissue-protective and repair-promoting effects on the other (Kvirkvelia et al., 2013). However, since PGE2 has been shown to cause glomerular hyperfiltration in the setting of cGN (Takahashi et al., 1990), we speculate that these hemodynamic effects are also present in our animals. In fact, glomerular hyperfiltration due to PGE2-mediated dilatation of the afferent arteriole may explain the severe proteinuria and excessive glomerular damage in these animals.

An unexpected finding of the lipidomics analysis was the marked reduction of renal epoxydocosapentaenoic acid levels. These compounds are produced from docosahexaenoic acid in a cytochrome P450 epoxygenase-dependent manner and subject to inactivation by soluble epoxide hydrolase (Spector and Kim, 2015). Their biological functions include potent antihypertensive, antiinflammatory, antifibrotic, and antiangiogenetic effects (Spector and Kim, 2015; Sharma et al., 2016; Schunck et al., 2018). Reduced levels of these compounds in the nephritic AnxA1-deficient mice may therefore contribute to the aggravated damage. However, further studies are needed to elucidate the effects of AnxA1 on the metabolism of these compounds and their interaction with AnxA1 on the functional level.

Of note, we were unable to detect relevant levels of the canonical pro-resolving lipid mediators lipoxin A4, resolvin, and maresin, while other metabolites of their parent molecules were readily detectable. Technical reasons may be responsible for this finding. The characterization of SPM biosynthesis has typically relied on analyses of exudates from mouse models of resolving inflammation but measurement of tissue levels of these compounds is not routinely performed. Thus, the relevance of these mediators during the resolution process of cGN remains to be determined.

The final fundamental result of our study is the accelerated development of glomerulosclerosis and tubulointerstitial fibrosis in the nephritic AnxA1-deficient mice. Renal fibrosis is the final common pathway mediating the transition from injury to chronic renal failure irrespective of the underlying disease (Humphreys, 2018; Moeller et al., 2021). Since the excessive deposition of extracellular matrix components and the resulting rarefication of the renal microvasculature cause tissue hypoxia, fibrosis by itself has been suggested to contribute to the development of renal damage.

Numerous studies have demonstrated an antifibrotic effect of AnxA1 in different models of tissue fibrosis (Damazo et al., 2011; Locatelli et al., 2014; Wu et al., 2021; Gadipudi et al., 2022). In addition to its antiinflammatory and tissueprotective activity, AnxA1 directly counteracts the effects of TGF-β on renal fibroblasts (Neymeyer et al., 2015) and blocks the profibrotic effects of NF-kB (Wu et al., 2021). These findings suggest that, in addition to the aggravation of renal inflammation, tissue damage and increased proteinuria, lack of AnxA1 may also directly contribute to the accelerated kidney fibrosis observed in the AnxA1-deficient mice. Further studies are needed to elucidate the relative contributions of the different mechanisms to the development of renal fibrosis in cGN.

Conclusion

In conclusion, we have shown that AnxA1-deficient mice show a severely aggravated course of nephrotoxic serum nephritis with increased glomerular and tubulointerstitial damage as well as proteinuria. Renal damage was accompanied by non-resolving inflammation with elevated expression of pro-inflammatory cytokines and an increased abundance of neutrophil granulocytes and other leukocyte species. These data therefore demonstrate a non-redundant role of AnxA1 during the resolution phase of renal immune-mediated inflammatory disease and provide the rational for the development of AnxA1-based therapeutic strategies for these conditions.

Data availability statement

The datasets presented in this study can be found in online repositories. The names of the repository/repositories and accession number(s) can be found below: https://www.ncbi.nlm.nih.gov/, GSE204873.

Ethics statement

The animal study was reviewed and approved by Berlin Council on Animal Care.

Author contributions

Conceptualization: AP, SB; funding acquisition: AP, SB; performed experiments: RL, LD, SvV, and AP; data analysis: RL, RM, SvV, and AP; writing: RL, SvV, SB, and AP. All authors have read and agreed to the published version of the manuscript.

Funding

The work was supported by a grant from the Deutsche Forschungsgemeinschaft (Research Unit 1368 to AP and SB). AP was supported by the Charite Clinical Scientist Program (Charite-Universitatsmedizin Berlin and the Berlin Institute of Health).

Acknowledgments

We thank F. Grams and K. Riskowsky for their expert technical assistance and A. Drobbe for editorial support.

Conflict of interest

The authors declare that the research was conducted in the absence of any commercial or financial relationships that could be construed as a potential conflict of interest.

Publisher's note

Supplementary material

The Supplementary Material for this article can be found online at: https://www.frontiersin.org/articles/10.3389/fphys.2022.984362/full#supplementary-material.

References

Andrews, P. M., and Coffey, A. K. (1984). A technique to reduce fixation artifacts to kidney proximal tubules. *Kidney Int.* 25, 964–968. doi:10.1038/ki.1984.118

Antonelou, M., Evans, R. D. R., Henderson, S. R., and Salama, A. D. (2022). Neutrophils are key mediators in crescentic glomerulonephritis and targets for new therapeutic approaches. *Nephrol. Dial. Transpl.* 37, 230–238. doi:10.1093/ndt/gfaa206

Araujo, L. P., Truzzi, R. R., Mendes, G. E., Luz, M. A., Burdmann, E. A., and Oliani, S. M. (2012). Annexin A1 protein attenuates cyclosporine-induced renal hemodynamics changes and macrophage infiltration in rats. *Inflamm. Res.* 61, 189–196. doi:10.1007/s00011-011-0400-z

Araujo, L. P., Truzzi, R. R., Mendes, G. E., Luz, M. A., Burdmann, E. A., and Oliani, S. M. (2010). Interaction of the anti-inflammatory annexin A1 protein and tacrolimus immunosuppressant in the renal function of rats. *Am. J. Nephrol.* 31, 527–533. doi:10.1159/000309756

Aringer, I., Artinger, K., Kirsch, A. H., Schabhüttl, C., Jandl, K., Bärnthaler, T., et al. (2018). Blockade of prostaglandin E(2) receptor 4 ameliorates nephrotoxic serum nephritis. *Am. J. Physiol. Ren. Physiol.* 315, F1869–F1880. doi:10.1152/ajprenal.00113.2018

Artinger, K., Kirsch, A. H., Aringer, I., Moschovaki-Filippidou, F., Eller, P., Rosenkranz, A. R., et al. (2017). Innate and adaptive immunity in experimental glomerulonephritis: A pathfinder tale. *Pediatr. Nephrol.* 32, 943–947. doi:10.1007/s00467-016-3404-7

Ashburner, M., Ball, C. A., Blake, J. A., Botstein, D., Butler, H., Cherry, J. M., et al. (2000). Gene ontology: Tool for the unification of biology. The gene ontology consortium. *Nat. Genet.* 25, 25–29. doi:10.1038/75556

Babiychuk, E. B., Monastyrskaya, K., Potez, S., and Draeger, A. (2011). Blebbing confers resistance against cell lysis. *Cell. Death Differ.* 18, 80–89. doi:10.1038/cdd.2010.81

Blume, K. E., Soeroes, S., Keppeler, H., Stevanovic, S., Kretschmer, D., Rautenberg, M., et al. (2012). Cleavage of annexin A1 by ADAM10 during secondary necrosis generates a monocytic "find-me" signal. *J. Immunol.* 188, 135–145. doi:10.4049/jimmunol.1004073

Bode, K., Bujupi, F., Link, C., Hein, T., Zimmermann, S., Peiris, D., et al. (2019). Dectin-1 binding to annexins on apoptotic cells induces peripheral immune tolerance via NADPH oxidase-2. *Cell. Rep.* 29, 4435–4446. e4439. doi:10.1016/j.celrep.2019.11.086

Boldt, C., Röschel, T., Himmerkus, N., Plain, A., Bleich, M., Labes, R., et al. (2016). Vasopressin lowers renal epoxyeicosatrienoic acid levels by activating soluble epoxide hydrolase. *Am. J. Physiol. Ren. Physiol.* 311, F1198–F1210. doi:10.1152/ajprenal.00062.2016

Brancaleone, V., Dalli, J., Bena, S., Flower, R. J., Cirino, G., and Perretti, M. (2011). Evidence for an anti-inflammatory loop centered on polymorphonuclear leukocyte formyl peptide receptor 2/lipoxin A4 receptor and operative in the inflamed microvasculature. *J. Immunol.* 186, 4905–4914. doi:10.4049/jimmunol.1003145

Chen, A., Lee, K., D'agati, V. D., Wei, C., Fu, J., Guan, T. J., et al. (2018). Bowman's capsule provides a protective niche for podocytes from cytotoxic CD8+ T cells. *J. Clin. Invest.* 128, 3413–3424. doi:10.1172/JCI97879

Colamatteo, A., Maggioli, E., Azevedo Loiola, R., Hamid Sheikh, M., Calì, G., Bruzzese, D., et al. (2019). Reduced annexin A1 expression associates with disease severity and inflammation in multiple sclerosis patients. *J. Immunol.* 203, 1753–1765. doi:10.4049/jimmunol.1801683

D'Acquisto, F., Paschalidis, N., Sampaio, A. L., Merghani, A., Flower, R. J., and Perretti, M. (2007). Impaired T cell activation and increased Th2 lineage commitment in Annexin-1-deficient T cells. *Eur. J. Immunol.* 37, 3131–3142. doi:10.1002/eji.200636792

Dalli, J., Consalvo, A. P., Ray, V., Di Filippo, C., D'amico, M., Mehta, N., et al. (2013). Proresolving and tissue-protective actions of annexin A1-based cleavage-resistant peptides are mediated by formyl peptide receptor 2/lipoxin A4 receptor. *J. Immunol.* 190, 6478–6487. doi:10.4049/jimmunol.1203000

Damazo, A. S., Sampaio, A. L., Nakata, C. M., Flower, R. J., Perretti, M., and Oliani, S. M. (2011). Endogenous annexin A1 counter-regulates bleomycin-induced lung fibrosis. *BMC Immunol.* 12, 59. doi:10.1186/1471-2172-12-59

Devi, S., Li, A., Westhorpe, C. L., Lo, C. Y., Abeynaike, L. D., Snelgrove, S. L., et al. (2012). Multiphoton imaging reveals a new leukocyte recruitment paradigm in the glomerulus. *Nat. Med.* 19 (1), 107–112. doi:10.1038/nm.3024

Disteldorf, E. M., Krebs, C. F., Paust, H. J., Turner, J. E., Nouailles, G., Tittel, A., et al. (2015). CXCL5 drives neutrophil recruitment in TH17-mediated GN. *J. Am. Soc. Nephrol.* 26, 55–66. doi:10.1681/ASN.2013101061

Drechsler, M., De Jong, R., Rossaint, J., Viola, J. R., Leoni, G., Wang, J. M., et al. (2015). Annexin A1 counteracts chemokine-induced arterial myeloid cell recruitment. *Circ. Res.* 116, 827–835. doi:10.1161/CIRCRESAHA.116.305825

Dreier, R., Schmid, K. W., Gerke, V., and Riehemann, K. (1998). Differential expression of annexins I, II and IV in human tissues: An immunohistochemical study. *Histochem. Cell. Biol.* 110, 137–148. doi:10.1007/s004180050275

Facio, F. N., Jr., Sena, A. A., Araújo, L. P., Mendes, G. E., Castro, I., Luz, M. A., et al. (2011). Annexin 1 mimetic peptide protects against renal ischemia/reperfusion injury in rats. *J. Mol. Med.* 89, 51–63. doi:10.1007/s00109-010-0684-4

Farris, A. B., Adams, C. D., Brousaides, N., Della Pelle, P. A., Collins, A. B., Moradi, E., et al. (2011). Morphometric and visual evaluation of fibrosis in renal biopsies. *J. Am. Soc. Nephrol.* 22, 176–186. doi:10.1681/ASN.2009091005

Gadipudi, L. L., Ramavath, N. N., Provera, A., Reutelingsperger, C., Albano, E., Perretti, M., et al. (2022). Annexin A1 treatment prevents the evolution to fibrosis of experimental nonalcoholic steatohepatitis. *Clin. Sci.* 136, 643–656. doi:10.1042/CS20211122

Ge, S., Hertel, B., Koltsova, E. K., Sörensen-Zender, I., Kielstein, J. T., Ley, K., et al. (2013). Increased atherosclerotic lesion formation and vascular leukocyte accumulation in renal impairment are mediated by interleukin-17A. *Circ. Res.* 113, 965–974. doi:10.1161/CIRCRESAHA.113.301934

Gene Ontology Consortium (2021). The gene ontology resource: Enriching a GOld mine. *Nucleic Acids Res.* 49, D325–d334. doi:10.1093/nar/gkaa1113

Gobbetti, T., and Cooray, S. N. (2016). Annexin A1 and resolution of inflammation: Tissue repairing properties and signalling signature. *Biol. Chem.* 397, 981–993. doi:10.1515/hsz-2016-0200

Hannon, R., Croxtall, J. D., Getting, S. J., Roviezzo, F., Yona, S., Paul-Clark, M. J., et al. (2003). Aberrant inflammation and resistance to glucocorticoids in annexin 1-/- mouse. *Faseb J.* 17, 253–255. doi:10.1096/fj.02-0239fje

Herbert, S. P., Odell, A. F., Ponnambalam, S., and Walker, J. H. (2007). The confluence-dependent interaction of cytosolic phospholipase A2-alpha with annexin A1 regulates endothelial cell prostaglandin E2 generation. *J. Biol. Chem.* 282, 34468–34478. doi:10.1074/jbc.M701541200

Humphreys, B. D. (2018). Mechanisms of renal fibrosis. *Annu. Rev. Physiol.* 80, 309–326. doi:10.1146/annurev-physiol-022516-034227

Jones, H. R., Robb, C. T., Perretti, M., and Rossi, A. G. (2016). The role of neutrophils in inflammation resolution. *Semin. Immunol.* 28, 137–145. doi:10.1016/j.smim.2016.03.007

Junqueira, L. C., Bignolas, G., and Brentani, R. R. (1979). Picrosirius staining plus polarization microscopy, a specific method for collagen detection in tissue sections. *Histochem. J.* 11, 447–455. doi:10.1007/BF01002772

Ka, S. M., Tsai, P. Y., Chao, T. K., Yang, S. M., Hung, Y. J., Chen, J. S., et al. (2014). Urine annexin A1 as an index for glomerular injury in patients. *Dis. Markers* 2014, 854163. doi:10.1155/2014/854163

Kidney Disease: Improving Global Outcomes (KDIGO) Glomerular Diseases Work Group (2021). KDIGO 2021 clinical practice guideline for the management of glomerular diseases. *Kidney Int.* 100, S1–S276. doi:10.1016/j.kint.2021.05.021

Kuligowski, M. P., Kitching, A. R., and Hickey, M. J. (2006). Leukocyte recruitment to the inflamed glomerulus: A critical role for platelet-derived P-selectin in the absence of rolling. *J. Immunol.* 176, 6991–6999. doi:10.4049/jimmunol.176.11.6991

Kurts, C., Panzer, U., Anders, H. J., and Rees, A. J. (2013). The immune system and kidney disease: Basic concepts and clinical implications. *Nat. Rev. Immunol.* 13, 738–753. doi:10.1038/nri3523

Kvirkvelia, N., Mcmenamin, M., Chaudhary, K., Bartoli, M., and Madaio, M. P. (2013). Prostaglandin E2 promotes cellular recovery from established nephrotoxic serum nephritis in mice, prosurvival, and regenerative effects on glomerular cells. *Am. J. Physiol. Ren. Physiol.* 304, F463–F470. doi:10.1152/ajprenal.00575.2012

Livak, K. J., and Schmittgen, T. D. (2001). Analysis of relative gene expression data using real-time quantitative PCR and the 2(-Delta Delta C(T)) Method. *Methods* 25, 402–408. doi:10.1006/meth.2001.1262

Locatelli, I., Sutti, S., Jindal, A., Vacchiano, M., Bozzola, C., Reutelingsperger, C., et al. (2014). Endogenous annexin A1 is a novel protective determinant in nonalcoholic steatohepatitis in mice. *Hepatology* 60, 531–544. doi:10.1002/hep.27141

McKanna, J. A., Chuncharunee, A., Munger, K. A., Breyer, J. A., Cohen, S., and Harris, R. C. (1992). Localization of p35 (annexin I, lipocortin I) in normal adult rat kidney and during recovery from ischemia. *J. Cell. Physiol.* 153, 467–476. doi:10.1002/jcp.1041530305

Moeller, M. J., Kramann, R., Lammers, T., Hoppe, B., Latz, E., Ludwig-Portugall, I., et al. (2021). New aspects of kidney fibrosis-from mechanisms of injury to modulation of disease. *Front. Med.* 8, 814497. doi:10.3389/fmed.2021.814497

Moll, S., Yasui, Y., Abed, A., Murata, T., Shimada, H., Maeda, A., et al. (2018). Selective pharmacological inhibition of DDR1 prevents experimentally-induced glomerulonephritis in prevention and therapeutic regime. *J. Transl. Med.* 16, 148. doi:10.1186/s12967-018-1524-5

Neymeyer, H., Labes, R., Reverte, V., Saez, F., Stroh, T., Dathe, C., et al. (2015). Activation of annexin A1 signalling in renal fibroblasts exerts antifibrotic effects. *Acta Physiol.* 215, 144–158. doi:10.1111/apha.12586

Oliani, S. M., Paul-Clark, M. J., Christian, H. C., Flower, R. J., and Perretti, M. (2001). Neutrophil interaction with inflamed postcapillary venule endothelium alters annexin 1 expression. *Am. J. Pathol.* 158, 603–615. doi:10.1016/S0002-9440(10)64002-3

Ortega-Gómez, A., Perretti, M., and Soehnlein, O. (2013). Resolution of inflammation: An integrated view. *EMBO Mol. Med.* 5 (5), 661–674. doi:10.1002/emmm.201202382

Ougaard, M. K. E., Kvist, P. H., Jensen, H. E., Hess, C., Rune, I., and Søndergaard, H. (2018). Murine nephrotoxic nephritis as a model of chronic kidney disease. *Int. J. Nephrol.* 2018, 8424502. doi:10.1155/2018/8424502

Paliege, A., Roeschel, T., Neymeyer, H., Seidel, S., Kahl, T., Daigeler, A. L., et al. (2012). Group VIA phospholipase A2 is a target for vasopressin signaling in the thick ascending limb. *Am. J. Physiol. Renal. Physiol.* 302 (7), F865–F874. doi:10.1152/ajprenal.00222.2011

Paschalidis, N., Iqbal, A. J., Maione, F., Wood, E. G., Perretti, M., Flower, R. J., et al. (2009). Modulation of experimental autoimmune encephalomyelitis by endogenous annexin A1. *J. Neuroinflammation* 6, 33. doi:10.1186/1742-2094-6-33

Perretti, M., Christian, H., Wheller, S. K., Aiello, I., Mugridge, K. G., Morris, J. F., et al. (2000). Annexin I is stored within gelatinase granules of human neutrophil and mobilized on the cell surface upon adhesion but not phagocytosis. *Cell. Biol. Int.* 24, 163–174. doi:10.1006/cbir.1999.0468

Potez, S., Luginbühl, M., Monastyrskaya, K., Hostettler, A., Draeger, A., and Babiychuk, E. B. (2011). Tailored protection against plasmalemmal injury by annexins with different Ca2+ sensitivities. *J. Biol. Chem.* 286, 17982–17991. doi:10.1074/jbc.M110.187625

Pupjalis, D., Goetsch, J., Kottas, D. J., Gerke, V., and Rescher, U. (2011). Annexin A1 released from apoptotic cells acts through formyl peptide receptors to dampen inflammatory monocyte activation via JAK/STAT/SOCS signalling. *EMBO Mol. Med.* 3, 102–114. doi:10.1002/emmm.201000113

Purvis, G. S. D., Chiazza, F., Chen, J., Azevedo-Loiola, R., Martin, L., Kusters, D. H. M., et al. (2018). Annexin A1 attenuates microvascular complications through restoration of Akt signalling in a murine model of type 1 diabetes. *Diabetologia* 61, 482–495. doi:10.1007/s00125-017-4469-y

Rescher, U., Goebeler, V., Wilbers, A., and Gerke, V. (2006). Proteolytic cleavage of annexin 1 by human leukocyte elastase. *Biochim. Biophys. Acta* 1763, 1320–1324. doi:10.1016/j.bbamcr.2006.08.041

Saran, R., Robinson, B., Abbott, K. C., Bragg-Gresham, J., Chen, X., Gipson, D., et al. (2019). US renal data system 2019 annual data report: Epidemiology of kidney disease in the United States. *Am. J. Kidney Dis.* 75, A6–A7. doi:10.1053/j.ajkd.2019.09.003

Scannell, M., Flanagan, M. B., Destefani, A., Wynne, K. J., Cagney, G., Godson, C., et al. (2007). Annexin-1 and peptide derivatives are released by apoptotic cells and stimulate phagocytosis of apoptotic neutrophils by macrophages. *J. Immunol.* 178, 4595–4605. doi:10.4049/jimmunol.178.7.4595

Schindelin, J., Arganda-Carreras, I., Frise, E., Kaynig, V., Longair, M., Pietzsch, T., et al. (2012). Fiji: An open-source platform for biological-image analysis. *Nat. Methods* 9, 676–682. doi:10.1038/nmeth.2019

Schunck, W. H., Konkel, A., Fischer, R., and Weylandt, K. H. (2018). Therapeutic potential of omega-3 fatty acid-derived epoxyeicosanoids in cardiovascular and inflammatory diseases. *Pharmacol. Ther.* 183, 177–204. doi:10.1016/j.pharmthera.2017.10.016

Seidel, S., Neymeyer, H., Kahl, T., Röschel, T., Mutig, K., Flower, R., et al. (2012). Annexin A1 modulates macula densa function by inhibiting cyclooxygenase 2. *Am. J. Physiol. Ren. Physiol.* 303, F845–F854. doi:10.1152/ajprenal.00704.2011

Sharma, A., Hye Khan, M. A., Levick, S. P., Lee, K. S., Hammock, B. D., and Imig, J. D. (2016). Novel omega-3 fatty acid epoxygenase metabolite reduces kidney fibrosis. *Int. J. Mol. Sci.* 17, E751. doi:10.3390/ijms17050751

Skogstrand, T., Leh, S., Paliege, A., Reed, R. K., Vikse, B. E., Bachmann, S., et al. (2013). Arterial damage precedes the development of interstitial damage in the nonclipped kidney of two-kidney, one-clip hypertensive rats. *J. Hypertens.* 31, 152–159. doi:10.1097/HJH.0b013e32835a5d4e

Solito, E., Kamal, A., Russo-Marie, F., Buckingham, J. C., Marullo, S., and Perretti, M. (2003). A novel calcium-dependent proapoptotic effect of annexin 1 on human neutrophils. *Faseb J.* 17, 1544–1546. doi:10.1096/fj.02-0941fje

Spector, A. A., and Kim, H. Y. (2015). Cytochrome P450 epoxygenase pathway of polyunsaturated fatty acid metabolism. *Biochim. Biophys. Acta* 1851, 356–365. doi:10.1016/j.bbalip.2014.07.020

Sugimoto, M. A., Vago, J. P., Teixeira, M. M., and Sousa, L. P. (2016). Annexin A1 and the resolution of inflammation: Modulation of neutrophil recruitment, apoptosis, and clearance. *J. Immunol. Res.* 2016, 8239258. doi:10.1155/2016/8239258

Suliman, H., Ma, Q., Zhang, Z., Ren, J., Morris, B. T., Crowley, S. D., et al. (2021). Annexin A1 tripeptide mimetic increases sirtuin-3 and augments mitochondrial function to limit ischemic kidney injury. *Front. Physiol.* 12, 683098. doi:10.3389/fphys.2021.683098

Suzuki, Y., Gómez-Guerrero, C., Shirato, I., López-Franco, O., Gallego-Delgado, J., Sanjuán, G., et al. (2003). Pre-existing glomerular immune complexes induce polymorphonuclear cell recruitment through an fc receptor-dependent respiratory burst: Potential role in the perpetuation of immune nephritis. *J. Immunol.* 170, 3243–3253. doi:10.4049/jimmunol.170.6.3243

Takahashi, K., Schreiner, G. F., Yamashita, K., Christman, B. W., Blair, I., and Badr, K. F. (1990). Predominant functional roles for thromboxane A2 and prostaglandin E2 during late nephrotoxic serum glomerulonephritis in the rat. *J. Clin. Invest.* 85, 1974–1982. doi:10.1172/JCI114661

Trimarchi, H. (2021). Crescents in primary glomerulonephritis: A pattern of injury with dissimilar actors. A pathophysiologic perspective. *Pediatr. Nephrol.* 37, 1205–1214. doi:10.1007/s00467-021-05199-1

Turner, J. E., Krebs, C., Tittel, A. P., Paust, H. J., Meyer-Schwesinger, C., Bennstein, S. B., et al. (2012). IL-17A production by renal γδ T cells promotes kidney injury in crescentic GN. *J. Am. Soc. Nephrol.* 23, 1486–1495. doi:10.1681/ASN.2012010040

Vago, J. P., Nogueira, C. R., Tavares, L. P., Soriani, F. M., Lopes, F., Russo, R. C., et al. (2012). Annexin A1 modulates natural and glucocorticoid-induced resolution of inflammation by enhancing neutrophil apoptosis. *J. Leukoc. Biol.* 92, 249–258. doi:10.1189/jlb.0112008

Vais, H., Wang, M., Mallilankaraman, K., Payne, R., Mckennan, C., Lock, J. T., et al. (2020). ER-luminal [Ca(2+)] regulation of InsP(3) receptor gating mediated by an ER-luminal peripheral Ca(2+)-binding protein. *Elife* 9, e53531. doi:10.7554/eLife.53531

Vergnolle, N., Coméra, C., and Buéno, L. (1995). Annexin 1 is overexpressed and specifically secreted during experimentally induced colitis in rats. *Eur. J. Biochem.* 232, 603–610. doi:10.1111/j.1432-1033.1995.tb20850.x

Vital, S. A., Senchenkova, E. Y., Ansari, J., and Gavins, F. N. E. (2020). Targeting AnxA1/formyl peptide receptor 2 pathway affords protection against pathological thrombo-inflammation. *Cells* 9 (11), 2473. doi:10.3390/cells9112473

Vong, L., D'acquisto, F., Pederzoli-Ribeil, M., Lavagno, L., Flower, R. J., Witko-Sarsat, V., et al. (2007). Annexin 1 cleavage in activated neutrophils: A pivotal role for proteinase 3. *J. Biol. Chem.* 282, 29998–30004. doi:10.1074/jbc.M702876200

Walther, A., Riehemann, K., and Gerke, V. (2000). A novel ligand of the formyl peptide receptor: annexin I regulates neutrophil extravasation by interacting with the FPR. *Mol. Cell.* 5, 831–840. doi:10.1016/s1097-2765(00)80323-8

Wang, L. M., Li, W. H., Xu, Y. C., Wei, Q., Zhao, H., and Jiang, X. F. (2011). Annexin 1-derived peptide Ac2-26 inhibits eosinophil recruitment *in vivo* via decreasing prostaglandin D_2. *Int. Arch. Allergy Immunol.* 154, 137–148. doi:10.1159/000320228

Wang, J., Vasaikar, S., Shi, Z., Greer, M., and Zhang, B. (2017). WebGestalt 2017: A more comprehensive, powerful, flexible and interactive gene set enrichment analysis toolkit. *Nucleic Acids Res.* 45, W130–W137. doi:10.1093/nar/gkx356

Wang, R. X., Wu, L., Chen, S. F., Li, Z. Y., Zhao, M. H., and Chen, M. (2022). Renal expression of annexin A1 is associated with the severity of renal injury in antineutrophil cytoplasmic autoantibody-associated vasculitis. *Front. Med.* 9, 769813. doi:10.3389/fmed.2022.769813

Westhorpe, C. L., Bayard, J. E., O'sullivan, K. M., Hall, P., Cheng, Q., Kitching, A. R., et al. (2017). *In vivo* imaging of inflamed glomeruli reveals dynamics of neutrophil extracellular trap formation in glomerular capillaries. *Am. J. Pathol.* 187, 318–331. doi:10.1016/j.ajpath.2016.10.008

Wu, L., Liu, C., Chang, D. Y., Zhan, R., Sun, J., Cui, S. H., et al. (2021). Annexin A1 alleviates kidney injury by promoting the resolution of inflammation in diabetic nephropathy. *Kidney Int.* 100, 107–121. doi:10.1016/j.kint.2021.02.025

Wu, X., Tiwari, A. K., Issekutz, T. B., and Lefkowith, J. B. (1996). Differing roles of CD18 and VLA-4 in leukocyte migration/activation during anti-GBM nephritis. *Kidney Int.* 50, 462–472. doi:10.1038/ki.1996.337

Xiao, H., Heeringa, P., Liu, Z., Huugen, D., Hu, P., Maeda, N., et al. (2005). The role of neutrophils in the induction of glomerulonephritis by anti-myeloperoxidase antibodies. *Am. J. Pathol.* 167, 39–45. doi:10.1016/S0002-9440(10)62951-3

Yang, Y. H., Song, W., Deane, J. A., Kao, W., Ooi, J. D., Ngo, D., et al. (2013). Deficiency of annexin A1 in CD4+ T cells exacerbates T cell-dependent inflammation. *J. Immunol.* 190, 997–1007. doi:10.4049/jimmunol.1202236

Yazid, S., Gardner, P. J., Carvalho, L., Chu, C. J., Flower, R. J., Solito, E., et al. (2015). Annexin-A1 restricts Th17 cells and attenuates the severity of autoimmune disease. *J. Autoimmun.* 58, 1–11. doi:10.1016/j.jaut.2014.12.004

frontiers | Frontiers in Physiology

TYPE Mini Review
PUBLISHED 07 December 2022
DOI 10.3389/fphys.2022.1048738

OPEN ACCESS

EDITED BY
Nuria M. Pastor-Soler,
University of Southern California,
United States

REVIEWED BY
Biagio Saitta,
University of Southern California,
United States
Mariela Mendez,
Henry Ford Hospital, United States

*CORRESPONDENCE
Ignacio Giménez,
igimenez@unizar.es

SPECIALTY SECTION
This article was submitted to Renal Physiology and Pathophysiology, a section of the journal Frontiers in Physiology

RECEIVED 19 September 2022
ACCEPTED 31 October 2022
PUBLISHED 07 December 2022

CITATION
Lacueva-Aparicio A, Lindoso RS, Mihăilă SM and Giménez I (2022), Role of extracellular matrix components and structure in new renal models *in vitro*. *Front. Physiol.* 13:1048738. doi: 10.3389/fphys.2022.1048738

Role of extracellular matrix components and structure in new renal models *in vitro*

Alodia Lacueva-Aparicio[1,2], Rafael Soares Lindoso[3], Silvia M. Mihăilă[4] and Ignacio Giménez[1,5,6]*

[1]Renal and Cardiovascular Physiopathology (FISIOPREN), Aragon's Health Sciences Institute, Zaragoza, Spain, [2]Tissue Microenvironment Lab (TME Lab), I3A, University of Zaragoza, Zaragoza, Spain, [3]Carlos Chagas Institute of Biophysics, Federal University of Rio de Janeiro, Rio de Janeiro, Brazil, [4]Division of Pharmacology, Utrecht Institute for Pharmaceutical Sciences, Utrecht University, Utrecht, Netherlands, [5]Institute for Health Research Aragon (IIS Aragon), Zaragoza, Spain, [6]School of Medicine, University of Zaragoza, Zaragoza, Spain

The extracellular matrix (ECM), a complex set of fibrillar proteins and proteoglycans, supports the renal parenchyma and provides biomechanical and biochemical cues critical for spatial-temporal patterning of cell development and acquisition of specialized functions. As *in vitro* models progress towards biomimicry, more attention is paid to reproducing ECM-mediated stimuli. ECM's role in *in vitro* models of renal function and disease used to investigate kidney injury and regeneration is discussed. Availability, affordability, and lot-to-lot consistency are the main factors determining the selection of materials to recreate ECM *in vitro*. While simpler components can be synthesized *in vitro*, others must be isolated from animal or human tissues, either as single isolated components or as complex mixtures, such as Matrigel or decellularized formulations. Synthetic polymeric materials with dynamic and instructive capacities are also being explored for cell mechanical support to overcome the issues with natural products. ECM components can be used as simple 2D coatings or complex 3D scaffolds combining natural and synthetic materials. The goal is to recreate the biochemical signals provided by glycosaminoglycans and other signaling molecules, together with the stiffness, elasticity, segmentation, and dimensionality of the original kidney tissue, to support the specialized functions of glomerular, tubular, and vascular compartments. ECM mimicking also plays a central role in recent developments aiming to reproduce renal tissue *in vitro* or even in therapeutical strategies to regenerate renal function. Bioprinting of renal tubules, recellularization of kidney ECM scaffolds, and development of kidney organoids are examples. Future solutions will probably combine these technologies.

KEYWORDS

extracellular matrix, matrigel, kidney, bioprinting, scaffolds, microfluidics, organoids

Introduction

Extracellular matrix components provide critical cues for renal cell and tissue functions

The extracellular matrix (ECM) is a biological scaffold holding all cellular tissue components together (Supplementary Figure 1). The main components of kidney ECM are collagen I, proteoglycans, and glycosaminoglycans. The basal membrane (BM) surrounding the renal tubules contains collagen IV, laminins, and fibronectin (Theocharis et al., 2016). ECM composition and dimensionality establish biomechanical and biochemical signals essential for kidney's development (Clause and Barker, 2013; Loganathan et al., 2020), tissue growth, differentiation (Muncie and Weaver, 2018), and function (Frantz et al., 2010; Manninen, 2015; Loganathan et al., 2020).

The stiffness of the ECM influences organ or tissue differentiation and morphogenesis. ECM stiffness is determined by the material's elasticity, as measured by the Young's elastic modulus. Conventional plastic cell culture containers (10^9 Pa) are stiffer than bone (15–20 10^6 Pa) and the kidney (5–10 10^3 Pa). The substrate mechanical properties affect cell adhesion, migration, proliferation, and differentiation (Chen et al., 2014; Melica et al., 2019). Topography and dimensionality, which identify ECM forms, features, and distribution, are linked to cell polarization, actin bundle alignment, cell adhesion, orientation, migration, and morphology (Nur-E-Kamal et al., 2006; Kim et al., 2014; Sciancalepore et al., 2016; Hulshof et al., 2018; Bosch-Fortea et al., 2019) and renal progenitors' fate (Nur-E-Kamal et al., 2006; Kim et al., 2014; Bosch-Fortea et al., 2019; Walma and Yamada, 2020). Microfabrication methods can reproduce ECM mechanical and physical properties and architectural features, but resolution and complexity are still rudimentary (Le Digabel et al., 2010). Engineered ECM can be tailored to meet cell or tissue-specific needs (Beamish et al., 2017).

ECM components, particularly glycosaminoglycans (GAGs), provide biochemical signals that regulate cell functions and the organization of the ECM itself (Weber et al., 2017) (Table 1). Hyaluronan, the most abundant GAG (Iozzo and Schaefer, 2015; Theocharis et al., 2016), heparan sulphate or chondroitin sulphate (Lelongt and Ronco, 2003) are involved in tissue development, by displaying growth factors spatial-temporal distribution during epithelial branching (Nigam and Bush, 2014). ECM-renal cells interact through ECM-binding transmembrane receptors such as integrins (Chen et al., 2004; Clause and Barker, 2013; Handorf et al., 2015; Bülow and Boor, 2019) or polycystins (Nickel et al., 2002) that translate ECM biomechanical features into intracellular signals (Hagelaars et al., 2022). In diabetic nephropathy (Kolset et al., 2012) or autosomal dominant polycystic kidney disease (ADPKD) (Zhang et al., 2020), ECM disruptions result in alterations in kidney function. Changes in ECM synthesis and turnover of laminin, heparan sulphate, and chondroitin sulphate proteoglycans contribute to disease pathogenesis (Zhang et al., 2020). Unresolved renal parenchyma damage causes scarring by abnormal deposition of ECM. Chronic damage or excessive scarring leads to fibrosis, a hallmark of chronic kidney disease (Clause and Barker, 2013; Bülow and Boor, 2019). Any *in vitro* model aiming to accurately represent kidney function, damage, and regeneration should incorporate the ECM compartment. We review ECM's role in *in vitro* kidney models. Established models are briefly discussed to better understand the advantages of new methodological developments.

Extracellular matrix sources for *in vitro* models

In vivo, stromal cells (fibroblasts) produce ECM, and renal epithelial cells contribute themselves to BM synthesis, which can be exploited in *in vitro* models (Satyam et al., 2020). Simple ECM proteins like laminins are commercially available as recombinant proteins with proven utility for *in vitro* kidney models (Karamessinis et al., 2002; Chung et al., 2008; Zhang et al., 2009; Sebinger et al., 2013; Homan et al., 2019; Adelfio et al., 2020). However, most *in vitro* research uses ECM extracts from animal tissues because it is difficult to make complex macromolecular GAGs and large proteoglycans (Petkau-Milroy and Brunsveld, 2013; Aisenbrey and Murphy, 2020; Xing et al., 2020). Stroma-rich tissues like bone or cartilage can yield large quantities of pure ECM components. Commercial sources for human and animal collagen in various isoforms, hyaluronic acid, and fibronectin are available.

The biochemical complexity present in the original tissue is required to induce or maintain a specific phenotype. Here it is best to use complex, unfractionated tissue extracts containing a complex mix of glycosaminoglycans and other signaling molecules. Several commercial products, the best known being Matrigel (Kleinman and Martin, 2005; Passaniti et al., 2021), are readily available in different formulations (e.g., reduced growth factors). There are many examples of *in vitro* renal models employing such extracts (Zhang et al., 2009; Lam et al., 2014; Takasato et al., 2015; Figliuzzi et al., 2017; King et al., 2017; Hiraki et al., 2018; Howden et al., 2019; Otero et al., 2020) (Supplementary Table S1). Matrigel complexity (contains laminin, collagen IV, entactin, heparan sulfate proteoglycan and bound growth factors) yields better results than gelatin, collagen I, poly-L-lysine, and laminin alone (Hughes et al., 2010; Gao et al., 2011; Passaniti et al., 2021).

Matrigel-like products are expensive, batch-variable, ethically questionable (made from tumors grown in animals) and cannot be employed in human cell-therapy downstream applications. To solve recent availability and ethics-related issues, JellaGel, made from jellyfish Collagen 0 isolates, has recently

TABLE 1 Role of ECM in *in vitro* models of renal function and disease.

2D models

Culture architecture	ECM surrogate	Cells	Biological structure	Application	References
Coated PS plates	Fibronectin, laminin, collagen type IV and Matrigel	hESCs	Differentiated PT-like cells monolayer	Induced Differentiation to PT	Narayanan et al. (2013)
Coated glass plates and electrospun PCL-BU membranes	PCL-BU vs Collagens, laminin, MG, L-Dopa	HK-2, RPTEC	Differentiated PT-like cells monolayer	Synthetic membrane for BAK	van Gaal et al. (2021)
Coated PES/PVP/PSF-FC membranes	Collagen I, collagen IV, Laminin, L-DOPA	HPTCs, HK-2	Differentiated PT-like cells monolayer	Synthetic membrane for BAK	Ni et al. (2011)
Coated PS- and PES-microstructured substrates	L-DOPA, collagen IV	ciPTEC	Monolayer of differentiated PT-like cells	Synthetic membrane for BAK	Hulshof et al. (2018)
Coated microPES hollow fiber membrane	L-DOPA, collagen IV	ciPTEC	Monolayer of differentiated PT-like cells	Synthetic membrane for BAK	Jansen et al. (2015)
Coated PE and PES-50 transwell membrane	L-DOPA, collagen IV	ciPTEC	Monolayer of differentiated PT-like cells	Synthetic membrane for BAK	Schophuizen et al. (2015)
Hydrogel bioprinted onto polyester Transwell membrane	Organovo's NovoGel Bio-Ink	RPTEC Renal fibroblasts and HUVEC	RPTEC monolayer on top of hydrogel with HUVEC and fibroblasts	Differentiation CTX Fibrosis	King et al. (2017)
Coated Polycarbonate porous membrane within a microchip	Matrigel	RPTECs	Monolayer of differentiated PT-like cells	Synthetic membrane for BAK	Gao et al. (2011)

2.5D Models

Culture architecture	ECM surrogate	Cells	Biological structure	Application	References
Coated Micropatterned Silicon-PDMS surfaces	Fibronectin, laminin, matrigel. Matrigel in medium	MDCK, RPTEC, LLC-PK1	Cysts and tubules (PT)	Morphogenesis Nephrotoxicity	Bosch-Fortea et al. (2019)
Hydrogels Coated PS plates	Matrigel	HPTCs	Tubules (PT)	Morphogenesis	Zhang et al. (2011)

3D Models

Culture architecture	ECM surrogate	Cells	Biological structure	Application	References
Hydrogel	20% Growth factor-depleted Matrigel 80% Collagen I	Mouse embryonic UB and BSN primary cells mIMCD3	Cysts and tubules (UB)	Tubulogenesis Development	Sakurai et al. (1997)
Hydrogel	Matrigel	Primary baby mouse kidney epithelial cells	Tubules	Tubulogenesis	Taub et al. (1990)
Hydrogel	Rat tail collagen type I	Primary murine renal cells	Tubule- and glomerulus-like structures	Morphogenesis	Joraku et al. (2009)
0.4 μm Polyester Transwell membranes	Matrigel and collagen I (1:1)	RPTEC	Tubules (PT)	Tubulogenesis	Miya et al. (2011)
0.4 μm polycarbonate Transwell membranes	Matrigel and rat tail collagen I (1:1)	NKi-2	Tubules	Morphogenesis Nephrotoxicity	DesRochers et al. (2013)
Hydrogel	Collagen	MDCK co-cultured with Swiss 3T3	Tubules (Distal nephron)	Morphogenesis	Montesano et al. (1991a)
Hydrogel	Collagen	MDCK and co-cultured with MRC-5	Tubules (Distal nephron)	Morphogenesis	Montesano et al. (1991b)
Hydrogel	Collagen	HK-2	Tubules (PT)	Morphogenesis	Kher et al. (2011)
Hydrogel	Matrigel	Mouse renal tubule fragments	Cysts and tubules (Collecting Duct)	Genetic disease (ADPKD)	Dixon et al. (2020)
Hydrogel	Growth factor reduced, phenol red-free Matrigel	RPTEC/TERT1	Tubules (PT)	Nephrotoxicity	Secker et al. (2018)
Casting molds in 12-well plate	Collagen-Matrigel	Neonatal rat renal cells	Tubule- and glomerulus-like structures	Morphogenesis	Lü et al. (2012)

(Continued on following page)

TABLE 1 (*Continued*) Role of ECM in *in vitro* models of renal function and disease.

3D Models

Culture architecture	ECM surrogate	Cells	Biological structure	Application	References
Round bottom microwell plate	GFR-Matrigel	MDCK	Tubules (distal nephron)	Morphogenesis	Hirashima et al. (2017)
Hydrogel	Collagen I, GRF-Matrigel	RPTEC, renal fibroblasts and HUVEC	Tubules (PT) and endothelial unit	Tubulo-vascular interactions	Wang et al. (2020)
Printed silicon gasket	Gelatin, Fibrinogen	PTECT-TERT1, GMECs	Tubules (PT) and endothelial unit	Epithelial transport Tubulo-vascular interactions	Lin et al. (2019)
Hydrogel	Collagen I	HKC-8 and WS-1	HKC-8 monolayer on top of WS-1 embeded hydrogel	Fibrosis Nephrotoxicity	Moll et al. (2013)
Polystyrene multiwell plate	Covalent polymer networks of heparin and/or starPEG	HK-2	Tubules (PT)	Tubulogenesis	Weber et al. (2017)
PEGDA Hydrogel	HA	Mouse proximal tubule cells	Tubules (PT)	Nephrotoxicity	Astashkina et al. (2012); Astashkina et al. (2014)
Hydrogel	HA Matrigel	Embryonic rat UB	Tubules (UB)	Morphogenesis	Rosines et al. (2007)
PEG hydrogel	PEG functionalized with RGD peptide, laminin-1	MDCK	Cysts	Epithelial morphogenesis	Chung et al. (2008)
Scaffold	Silk	hiPSCs	Organoids	Development Differentiation	Gupta et al. (2019)
Scaffold	Thiol-ene crosslinked alginate	hiPSCs	Organoids	Development Differentiation	Geuens et al. (2021); Ruiter et al. (2022)
Scaffold	PLA Matrigel-Geltrex	HRECs	Monolayer-	ECM biomechanical properties	Love et al. (2019)
Hydrogel	PEG-4-MAL	MDCK	Cysts	ECM biomechanical properties	Enemchukwu et al. (2016)
PCLdi (u-UPy) electro-spun HFM	Collagen I, IV, fibronectin, laminin	hRPTECs	Monolayer	Bioactive membranes for BAKs	Dankers et al. (2011)
Electrospun transwell membrane	1:1 dKECM-PLC	hRPCs HUVEC	Monolayer	Differentiation Tubule-Vascular unit Nephrotoxicity	Sobreiro-Almeida et al. (2019); Sobreiro-Almeida et al. (2020)
Melt-electrowritten tubular scaffold	PCL	ciPTEC HUVEC	Monolayer Self-produced ECM	Tubule-Vascular unit Bioactive membranes for BAKs	van Genderen et al. (2021)
Silk-based porous scaffold	Matrigel and Collagen-Matrigel	MEK	Tubules and cysts	Genetic disease (ADPKD)	Subramanian et al. (2010)
Silk-based porous scaffold	Collagen type I and Matrigel (1:1)	mIMCD	Cysts	Genetic disease (ADPKD)	Subramanian et al. (2012)
Hollow tubes insidehydrogel	Collagen I	MDCK Primary PCT from transgenic mice	Tubules	Genetic disease (ADPKD)	Myram et al. (2021)
Extruded topographic hollow fiber (h- FIBER)	RGD-conjugated alginate	Podocytes and endothelial cells	Tubules Glomerulus-like structure	Glomerular filtration studies	Xie et al. (2020)
EDC hollow fibers	Collagen IV	HK-2	Tubules (PT)	Bioengineering renal tubules	Shen et al. (2015)
MicroPES HFM	Collagen IV and L-DOPA	ciPTEC	Tubules (PT)	Bioactive membranes for BAKs	Chevtchik et al. (2016)

(Continued on following page)

TABLE 1 (*Continued*) Role of ECM in *in vitro* models of renal function and disease.

3D Models

Culture architecture	ECM surrogate	Cells	Biological structure	Application	References
PCL tubular nanofiber scaffold	Collagen IV and L-DOPA	ciPTEC-OAT1	Tubules (PT)	Bioactive membranes for BAKs Nephrotoxicity	Jansen et al. (2019)

Bioprinted Scaffolds

Culture architecture	ECM surrogate	Cells	Biological structure	Application	References
Bioprinted renal constructs	dKECMMA	Human primary kidney cells	Tubular Glomerular-like structures	Tissue bioengineering	Ali et al. (2019)
Bioprinted renal construct	dKECM Gelatin	hRPCs HUVEC, podocytes	3D glomerular model	Regenerative medicine	Sobreiro-Almeida et al. (2021)
Bioprinted hollow tubules	dECM and alginate	RPTEC, HUVEC, hBMMSCs	Perfused Tubules and capillaries	Regenerative medicine	Singh et al. (2020)
Bioprinted hollow tubules	Gelatin-fibrin hydrogel	RPTEC/TERT1, GMECs	Perfused Tubules and capillaries	Tubule-Vascular unit Nephrotoxicity	Homan et al. (2016); Lin et al. (2019); Aceves et al. (2022)
Hydrogel-sandwiched, bioprinted tubular structure	Collagen I, Matrigel, Fibrin	RPTEC/TERT1, iRECs	Perfused Tubules	Bioengineering renal tubules	Tröndle et al. (2021)

Natural polymers: HA: hyaluronic acid, FMB: fibrin microbreads, dKECMMA: photo-crosslinable kidney ECM-derived bioink.
Synthetic polymers: EDC: 1-ethyl-3-(3- (dimethylamino)propyl) carbodiimide hydrochloride, PA: polyacrylamide.
Cell lines: HUTECs: Primary human tubular epithelial cells, HK-2: Human kidney-2, HPTCs: Human primary renal proximal tubule cells, RPTECs: renal proximal tubular epithelial cells, hESCs: embryonic stem cells, HUVEC: human umbilical vein endothelial cells, NKi-2: human renal epithelial cells, MDCK: Madin-Darby canine kidney, MRC-5: human fibroblasts, MEK: mouse embryonic kidney, HK-2: human immortalized proximal tubule epithelial cells, ciPTECs: Conditionally immortalized proximal tubule epithelial cells, HRECs: Human renal epithelial cells, LLC-PK1: pig kidney epithelial cells, 3T3: fibroblasts, UB: ureteric bud,HEK-293: Human embryonic kidney cell line, CaKi-1: human renal cancer cells, mIMCD: mouse inner medullary collecting duct, GMECs: glomerular microvascular endothelial cells, HKC-8: human proximal tubular epithelial cells, WS-1: human dermal fibroblasts, hBMMSCs: human bone marrow-derived mesenchymal stem cells, GMECs: glomerular microvascular endothelial cells, iRECs: induced renal tubular epithelial cells.

become available. However, this formulation does not fully mimic the kidney ECM's specific proteomic signature. ECM extracts from decellularized human kidneys can capture this specificity (Figliuzzi et al., 2017; Hiraki et al., 2018).

In recent years, artificial ECMs have been designed to replace natural ECM for renal epithelium scaffolding to reduce batch variability and degradation. This alternative allows more control over biochemical and mechanical properties and functionalization with instructive biomolecular tags to enhance cell attachment, proliferation, and differentiation (Aisenbrey and Murphy, 2020). Synthetic ECMs can be formed as hydrogels (Minuth et al., 2004; Chung et al., 2008; Astashkina et al., 2012) or hollow fibers (Dankers et al., 2011; Jansen et al., 2015; Shen et al., 2015; Chevtchik et al., 2016; Jansen et al., 2019; Xie et al., 2020; Myram et al., 2021) (Supplementary Table S1). The goal is to obtain a material whose composition can be tailored to control physiochemical matrix properties such as elasticity (Love et al., 2019), density, and stiffness, while ensuring low degradation under specific conditions (Petkau-Milroy and Brunsveld, 2013; Cruz-Acuña et al., 2019).

Conventional models of kidney function and disease

Two-dimensional renal cell culture on extracellular matrix-Coated surfaces

In the simplest culture configuration, renal cells grew directly on plastic surfaces as two-dimensional (2D) epithelial monolayers (Figure 1A). Adsorbing (coating) ECM components on plastic surfaces enhances renal cell adhesion, proliferation, and differentiation (Narayanan et al., 2013; van Gaal et al., 2021). Matrigel's complex set of biochemical signals is used when cell differentiation is the goal (Narayanan et al., 2013). ECM coatings are also used to functionalize synthetic scaffolds (Chung et al., 2008; Ni et al., 2011). Relevant examples of 2D *in vitro* kidney models are provided in Table 1. However, lack of complex cell interactions can lead to undesired effects, such as epithelial-to-mesenchymal transition (EMT) (Forino et al., 2006).

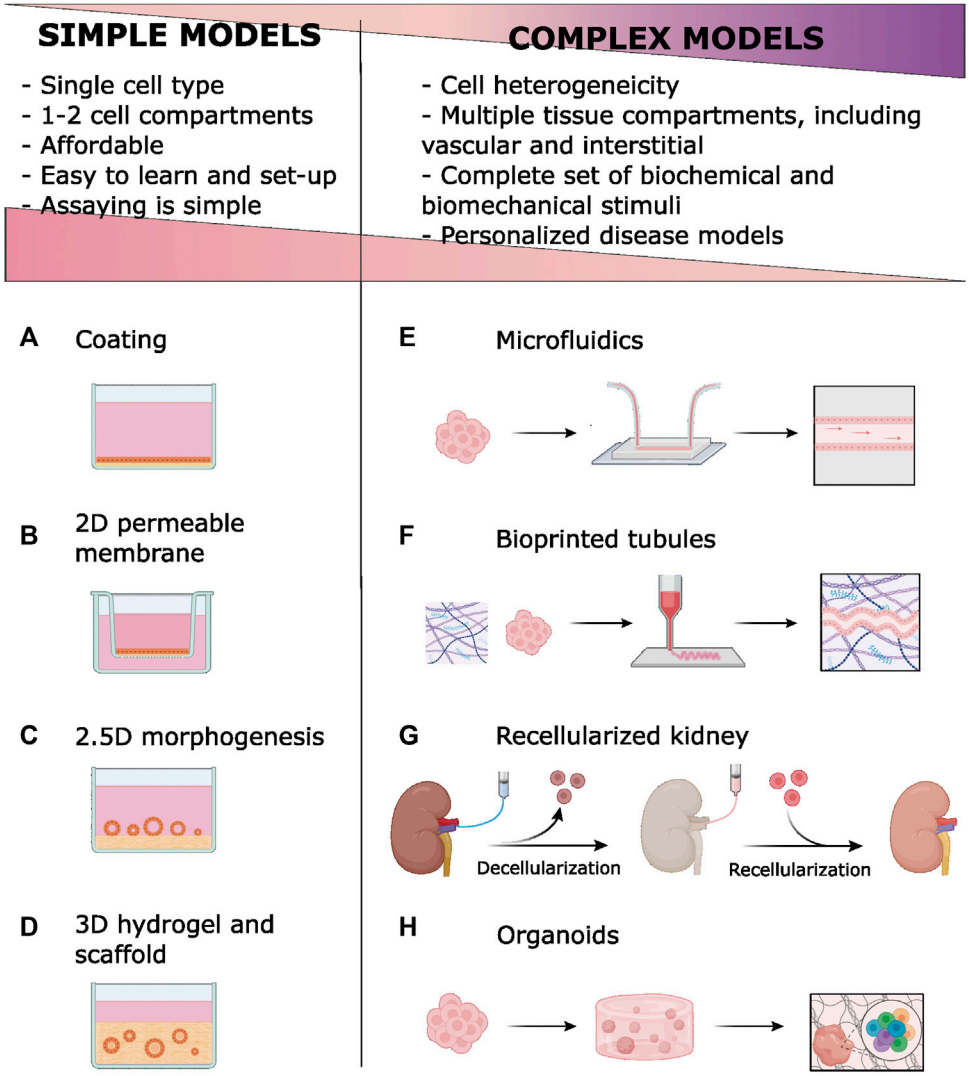

FIGURE 1
Simple models *in vitro* of renal epithelia employ ECM components of basal membrane (BM) and extracellular matrix (ECM) Coatings are simply ECM materials, usually collagen, adsorbed to the plastic **(A)** or permeable membrane **(B)**. Permeable membranes and scaffold-based models improve epithelial polarity by offering two fluid compartments. Tubulogenesis is stimulated by growing renal epithelial cells onto **(C)** or within **(D)** hydrogels. New technologies [microfluidics **(E)**, bioprinting **(F)**, ECM decellularization **(G)** and organoids development **(H)**] enable complex models that introduce cell heterogeneity, vascular and interstitial compartments, and biomechanical stimuli. Compared to simpler, conventional models, these models have disadvantages related to their complexity. However, complex models allow for more faithful modeling of kidney function and disease. A licensed version of BioRender was used to prepare this figure.

Epithelial 2D monolayers are frequently grown on permeable supports, like the Transwell system, to promote cell polarization (Gao et al., 2011; Ni et al., 2011; Shamir and Ewald, 2014; Schophuizen et al., 2015; Hulshof et al., 2018) (Figure 1B). Porous membranes can be coated with ECM (Ni et al., 2011; Shamir and Ewald, 2014) or used as scaffolds for thin hydrogels to improve mechanical properties (Shamir and Ewald, 2014) (Table 1). This configuration also facilitates co-culture with other kidney-relevant components (King et al., 2017).

When grown on top of hydrogels, kidney primary cells (Zhang et al., 2011) and most renal cell lines form tubular structures (tubulogenesis; termed 2.5D architecture; Figure 1C). Formation of tubules requires adding Matrigel to the hydrogel and/or to the medium, stressing the need for specific ECM chemical signals (Shamir and Ewald, 2014; Bosch-Fortea et al., 2019). Tubulogenesis studies on the MDCK cell line have been instrumental for understanding molecular the processes involved in epithelial differentiation and polarization (Bosch-Fortea et al., 2019). Hagelaars et al.

have recently used this model to show cellular differences in how matrix stiffness affects integrin-mediated cell-ECM attachment and cell polarization (Hagelaars et al., 2022). Better differentiation can happen when the tubule is fully embedded in the ECM (3D architecture, discussed below), however, direct exposure to culture medium in 2.5D structures facilitates imaging and biochemical treatments and assays.

Three-dimensional renal cell culture in hydrogel and scaffolds

Primary or continuous renal cell lines grown within collagen I or Matrigel hydrogels spontaneously form tubule-like structures (Taub et al., 1990; Sakurai et al., 1997; Zegers et al., 2003; Joraku et al., 2009; Schlüter and Margolis, 2009) (Figure 1D). Dissociated cells are mixed with biocompatible hydrogels in liquid form and allowed to polymerize (Miya et al., 2011; DesRochers et al., 2013). Alternatively, cells can be sandwiched between two ECM layers (Montesano et al., 1991a; Montesano et al., 1991b; Kher et al., 2011; Secker et al., 2018; Dixon et al., 2020) In the presence of appropriate factors, cells form hollow cysts (Zegers et al., 2003; Schlüter and Margolis, 2009) and continue to differentiate by elongation (Joraku et al., 2009) and tubule branching. Different nephron segments, including the glomerulus, have been modeled in 3D hydrogels (Joraku et al., 2009; Lü et al., 2012; Hirashima et al., 2017).

3D-culture allows co-culturing of different renal cell lineages, introducing complexity in kidney models (Montesano et al., 1991a; Montesano et al., 1991b; Secker et al., 2018). Wang et al. showed that using a sandwich 3D co-culture model is possible to recreate *in vitro* the tubule-interstitial-vascular unit, with more tubular cell polarity and enhanced functional gene expression (Wang et al., 2020). Gelatin-fibrin hydrogels outperformed conventional Transwell co-culture in modeling the proximal tubule-vascular unit *in vitro* (Lin et al., 2019). Tubulointerstitial fibrosis, a common feature in chronic kidney disease, has been modeled in 3D co-cultures (Moll et al., 2013).

Collagen I and Matrigel-like ECM extracts are often used, alone, mixed, or combined with other ECM components like collagen IV, fibronectin, or laminins (Weber et al., 2017). Functionality depends on the 3D hydrogel's composition, protein concentration, and stiffness (Shamir and Ewald, 2014; Hirashima et al., 2017; Hiraki et al., 2018). Hyaluronic acid is an interesting alternative to tissue extracts because it provides good mechanical and biochemical stimuli. 3D organoids containing proximal tubule structures were generated from mouse kidney explants by prolonged (6 weeks) culture in hyaluronic acid hydrogels resembling *in vivo* environment (Astashkina et al., 2012). This model has been successfully employed in the preclinical evaluation of nanoparticle nephrotoxicity (Astashkina et al., 2014). Hyaluronic acid modulated ureteric bud branching and promoted mesenchymal-to-epithelial transition (Rosines et al., 2007). The polarity of tubular structures obtained by growing human renal cells (HK-2, ciPTEC, and primary proximal tubule cells) in glycosaminoglycan-based hydrogels was found to depend on sulphated GAGs (Weber et al., 2017). Matrix stiffness strongly affects tubulogenesis in MDCK cells (Hirashima et al., 2017). Such studies (Table 1) exemplify how morphogenesis and function can be modulated by adjusting hydrogel degradability, growth factor signaling, and mechanics.

ECM-derived hydrogels have low resistance to mechanical stress, partly a consequence of active cell remodeling, limiting their use. A potential solution is to exploit the mechanical properties of natural (silk, alginate) or synthetic (PEG, PCL, PLA) polymers to complement natural ECM components (Chung et al., 2008; Enemchukwu et al., 2016; Gupta et al., 2019) (Supplementary Table S2). Plastic materials are easily deposited in 2D or 3D structures by electrospinning or printing techniques (Dankers et al., 2011; Sobreiro-Almeida et al., 2020; van Genderen et al., 2021). Murine PKD1 knockout renal tubular cells seeded in silk-scaffolds filled with Matrigel and collagen hydrogels has been shown to reproduce morphological and functional abnormalities present in Autosomal Dominant Polycystic Kidney disease (ADPKD) (Subramanian et al., 2010; Subramanian et al., 2012).

Recently, 3D models have gained momentum with microfabrication techniques. The organ-on-a-chip technology aims to mimic *in vivo* tissue architecture by providing independent but connected compartments (Rayner et al., 2018) (Figure 1E). Models based on microfabricated devices recapitulate intercellular and cell-ECM interactions at the microscale. Microfluidics integration adds flow-mediated shear stress, a critical mechanical stimulus for the renal tubule (Jang et al., 2013). Mimetas Organoplate allows for a high throughput culture and analysis of 3D tissue units under fluidic stimulus (Schutgens et al., 2019) and it has proven useful in modeling nephrotoxicity (Vormann et al., 2021) and acute kidney injury (Vormann et al., 2022). Commercial organ-on-chip solutions are listed in Supplementary Table S2.

3D models of tubulogenesis have been instrumental in defining chemical and mechanical stimuli involved in ECM-cell interactions and their role in kidney development and function. Lumen access, high-resolution imaging, biochemical studies, and manipulation for functional or nephrotoxicity assays are, however, limited in their architecture.

New strategies in *in vitro* modeling of kidney function and disease

Bioprinted scaffolds

Bioprinting has recently emerged as a tool for building complex tissue structures. Biocompatible polymers (bioinks) are layered to create 3D structures (Figure 1F). Cells are seeded on these 3D scaffolds or directly mixed in the bioink. Bioprinting offers unprecedented flexibility and versatility to recreate *in vivo* environments at the microscale

through stereotaxic control of bioink deposition (Fransen et al., 2021).

Bioinks are chosen for their rheological properties and printing device compatibility. As technology evolves, the use of bioinks derived from native tissue like collagen and decellularized ECM is favored (Garreta et al., 2017; Ali et al., 2019; Dzobo et al., 2019; Sobreiro-Almeida et al., 2021). This enhances kidney-specific gene expression by providing tissue-specific biochemical cues (Singh et al., 2020). However, because ECM bioinks exhibit poor mechanical stability, they are often combined with other polymers like methacrylate (Ali et al., 2019).

Using bioprinting, perfused renal tubules have been successfully made. Lewis's group used fugitive ink to cast tubular conduits within hydrogels, which they populated with proximal tubule cells or endothelial cells and perfused in a closed circuit for days. These tubular-vascular units expressed differentiated phenotypes, and their response to pathogenic insults mimicked those observed in native human tissues (Homan et al., 2016; Lin et al., 2019; Aceves et al., 2022). Tröndle et al. recently reported a modified 3D sandwich model in which renal cells were bioprinted as clusters at a controlled topography on a collagen and Matrigel substrate gel. Cell clusters formed lumen-containing spheroids, which coalesced into tubular structures that could be connected to fluidic systems (Tröndle et al., 2021). Both strategies use fibrin polymers to improve hydrogel biomechanics. A third strategy used a proprietary bioprinting technology (the Organovo 3D printing platform) to sequentially print epithelial tubule, fibroblast-containing ECM, and endothelial vessels (King et al., 2017). A glomerular functional unit was successfully recreated by printing hollow tubules from a functional hybrid bioink (alginate plus decellularized ECM) (Singh et al., 2020).

Bioprinting's flexibility and automatization capabilities make it a promising method for *in vitro* modeling of the kidney's basic functional unit. An immediate challenge is to make it affordable for the general laboratory.

Decellularized kidney as a tissue-specific scaffold

Regenerative medicine has long sought to fabricate a functional kidney using a donor's decellularized ECM scaffold repopulated with host cells to mitigate the shortage of organs available for transplant (Sullivan et al., 2012). The technique involves perfusing whole kidneys with detergent solutions to remove cells and preserve ECM microscopic architecture and tissue-specific ECM components like collagens and laminins, as well as basement membranes (Song et al., 2013) (Figure 1G). Conservation of signaling molecules, namely glycosaminoglycans, requires proper detergent composition and perfusion rates and timing (Caralt et al., 2015; Poornejad et al., 2016; He et al., 2017; Kajbafzadeh et al., 2019; Zhou et al., 2020; Shahraki et al., 2022). Decellularization can be successfully applied to stored frozen tissues (Chani et al., 2017). Decellularized scaffolds have been successfully repopulated with pluripotent, progenitor, epithelial, or endothelial cells. When implanted in animal models, this bioengineered tissue integrates with host structures and shows some kidney functions (Bonandrini et al., 2014; Caralt et al., 2015; Figliuzzi et al., 2017; Ciampi et al., 2019; Han et al., 2019; Zhang et al., 2019) or helps to revert EMT and fibrosis (Hu et al., 2020).

Regenerating a fully functional organ from a decellularized scaffold is a formidable challenge because of the kidney's high structural and functional complexity. Nevertheless, studies on kidney decellularization have provided valuable information on cell-ECM interactions, supporting GAGs' critical role (Louzao-Martinez et al., 2019; Ullah et al., 2020). Moreover, decellularized scaffolds are useful for *in vitro* method development. Decellularized kidney sections serve as scaffolds for growing renal cells in nephrotoxicity models (Fedecostante et al., 2018). These scaffolds allow for the investigation of cell-ECM interactions in specific organ or tissue microdomains. For example, the fate of pluripotent or progenitor cells in a recellularized scaffold can be followed to learn about specific cell differentiation determinants (Du et al., 2016; Bombelli et al., 2018; Zhang et al., 2019; Bombelli et al., 2020; Ullah et al., 2020).

An acid hydrolysate of decellularized kidney scaffolds, termed dKECM, can be used as a source of tissue-specific ECM materials for surface coating and hydrogel fabrication (Hiraki et al., 2018; Zhou et al., 2020; Shen et al., 2021; Lee et al., 2022). Combining dKECM with other natural or synthetic compounds can enhance their rheological or biophysical properties (Lih et al., 2019; Sobreiro-Almeida et al., 2019; Sobreiro-Almeida et al., 2020; Geng et al., 2021; Ko et al., 2021; Sobreiro-Almeida et al., 2021). Accordingly, dKECM is becoming a favorite bioink in bioprinting applications (Ali et al., 2019; Han et al., 2019). The undesired effects observed when growing human glomerular endothelial cells within hydrogels made of porcine dKECM (Su et al., 2018) illustrates the remarkable specificity of biochemical signals delivered by ECM.

Role of ECM in kidney organoids development

Two strategies are currently used to develop 3D renal structures from progenitor or pluripotent cells by exploiting kidney development programs. Tubuloids are generated from primary cells and kidney organoids from pluripotent stem cells. Both situations require ECM components. Tubuloid culture is a refined version of 3D culture in Matrigel hydrogels where specific biochemical factors are added to stimulate progenitor cell proliferation and differentiation (Schutgens et al., 2019; Wiraja et al., 2021). Human tubuloid culture allows for long-term propagation of donor-specific primary kidney epithelium without requiring immortalization or genetic modification. A recent study comparing the polarization of tubuloid-derived cells and MDCK cells in response to substrate stiffness demonstrated tubuloid-derived cells appear to have different requirements and

use different polarization mechanisms (Hagelaars et al., 2022). Unlike tubuloids, immortalized, well-established cell lines have been selected to grow on plastic substrates. By skipping the phase of culture on a stiff substrate, tubuloids might retain more of their physiological responses to ECM. This makes them a simple and affordable alternative cell source for *in vitro* models.

In the organoid technique (Figure 1H), Matrigel (Xia et al., 2013; Kang and Han, 2014; Takasato et al., 2015; Takasato and Little, 2017; Howden et al., 2019; Low et al., 2019) or Geltrex (Lam et al., 2014; Morizane et al., 2015; Morizane and Bonventre, 2017) coatings or hydrogels are used in feeder-free culture of stem cells or at several differentiation steps. For instance, Taguchi et al. used a 50% Matrigel culture medium to stimulate branching morphogenesis in ureteric buds and to induce interactions with nephron progenitors (Taguchi and Nishinakamura, 2017). Freedman et al. induced epiblast spheroids differentiation by sandwiching hPSC between two layers of diluted Matrigel (Freedman et al., 2015). Under the appropriate concentration and timing of specific biochemical inducers, complex self-organized 3D structures develop.

Organoids contain kidney parenchyma and stroma components, and the synthesis of ECM has been observed (Lam et al., 2014; Takasato et al., 2015; Howden et al., 2019). Given the complexity and animal origin of Matrigel and similar products, there have been efforts to replace it with recombinant ECM proteins, such as laminins (Howden et al., 2019; Mae et al., 2020) or vitronectin (van den Berg et al., 2018), or synthetic products like Synthemax (Toyohara et al., 2015). Recently, Geunes et al. cultured kidney organoids in thiol-ene cross-linked alginate hydrogels and showed a reduction in the onset of aberrant ECM expression and off-target cell populations (Geuens et al., 2021). By engineering gel mechanics and dynamics, ECM deposition and organoid maturation could be tuned, highlighting the role of engineered matrices in stirring organoid commitment (Ruiter et al., 2022).

Incomplete maturation and lack of vascularization are unsolved issues in organoid development where a proper selection and use of ECM components could help. Garreta et al. demonstrated that ECM biophysical properties modulate hPSC proliferation and differentiation (Garreta et al., 2019). Soft hydrogels with stiffness in the physiological range better mimic the early stages of embryonic development. Vascular compartment expression improved when organoids were grown in hydrogels made from decellularized human kidney extracellular matrix (Kim et al., 2022). Bioprinting cellular bioinks allows for precise and reproducible manipulation of organoid size and more differentiated cells (Howden et al., 2019; Lawlor et al., 2021). Perfusion of organoids in microfluidic devices induces higher expression of vascular and podocyte compartments (Homan et al., 2016; Lee et al., 2021). High levels of structural and functional complexity in bioprinted, perfused organoids model more faithfully renal function and disease, as shown recently for APKD (Howden et al., 2021; Hiratsuka et al., 2022).

Relevance of ECM-based *in vitro* models of renal disease for studies of renoprotection and kidney regeneration

Increasing rates of chronic kidney disease (CKD) represent a major burden for social and healthcare systems worldwide. Fighting underlying causes (diabetes, obesity, cardiovascular disease, etc.) is key. But it is equally important to prevent, slow down, or reverse CKD progression, which very often results from maladaptive responses to acute kidney injury.

Shortcomings of traditional preclinical models (animal experimentation and conventional cell culture) have fueled the development of sophisticated *in vitro* kidney models that take advantage of recent technological advances (Morizane et al., 2015). Only through such complex models is it possible, for instance, to recreate the delicate glomerular filtration barrier, allowing for the investigation of the varied glomerulopathies (Lü et al., 2012; Du et al., 2016; Xie et al., 2020). Sophisticated models, such as organoids, are already being used successfully to study genetic (e.g., ADPKD (Subramanian et al., 2010; Freedman et al., 2015; Dixon et al., 2020; Zhang et al., 2020; Howden et al., 2021; Myram et al., 2021; Hiratsuka et al., 2022)) or metabolic tubulopathies (Fabry's disease (Kim et al., 2022)). Investigating the mechanisms of drug-related nephrotoxicity and discovering ways to prevent it is frequently the goal behind model design or validation (Astashkina et al., 2012; DesRochers et al., 2013; King et al., 2017; Fedecostante et al., 2018; Vormann et al., 2021; Tröndle et al., 2022). Research on common mechanisms underlying CKD progression, irrespective of its cause, such as epithelial-to-mesenchymal transition (Forino et al., 2006) or fibrosis (Moll et al., 2013; Hu et al., 2020; Li et al., 2022), requires the presence of all participants in such complex processes. Studying tubulogenesis or cell-repair mechanisms in complex *in vitro* models helps identification of signals needed for kidney regeneration (Miya et al., 2011). These processes, which involve multiple actors from distinct compartments, cannot be studied adequately with conventional *in vitro* models. Some bioengineering strategies are originally aimed at fabricating tissue-like structures for regenerative techniques, based on the concept of regenerating an entire organ from a decellularized scaffold (Song et al., 2013; Du et al., 2016; Figliuzzi et al., 2017; Ciampi et al., 2019) or by stimulating regeneration *in vivo via* cell or tissue implants (Lih et al., 2019; Ko et al., 2021; van den Berg et al., 2018; Garreta et al., 2019; Kim et al., 2022).

We have summarized the essential roles of ECM in *in vitro* kidney function and disease modeling. ECM provides the biochemical and mechanical stimuli required for promoting and maintaining cell differentiation. A proper 3D architecture also permits cell-cell interactions and facilitates the presence of all necessary compartments, including fluid convection, to faithfully mimic *in vivo* kidney function. More efforts are needed to make the technical skills required simpler and to lower the costs associated with using such models, which would increase their adoption in kidney translational research.

Author contributions

All authors: conceptual design, data adquisition and interpretation, critical revision, final approval of the version to be published.

Funding

Publication of this review has been made possible through funds provided by the Government of Spain (RTI2018-0099946-B-100 to I.G.) and a "2017 Research Fellowship" from Sociedad Española de Nefrología.

Acknowledgments

We would like to thank all the excellent technical assistance provided by the people at our institutions that make possible working with complex and sophisticated cell culture models.

Conflict of interest

The authors declare that the research was conducted in the absence of any commercial or financial relationships that could be construed as a potential conflict of interest.

Publisher's note

All claims expressed in this article are solely those of the authors and do not necessarily represent those of their affiliated organizations, or those of the publisher, the editors and the reviewers. Any product that may be evaluated in this article, or claim that may be made by its manufacturer, is not guaranteed or endorsed by the publisher.

Supplementary material

The Supplementary Material for this article can be found online at: https://www.frontiersin.org/articles/10.3389/fphys.2022.1048738/full#supplementary-material

References

Aceves, J. O., Heja, S., Kobayashi, K., Robinson, S. S., Miyoshi, T., Matsumoto, T., et al. (2022). 3D proximal tubule-on-chip model derived from kidney organoids with improved drug uptake. *Sci. Rep.* 12 (1), 14997. doi:10.1038/s41598-022-19293-3

Adelfio, M., Szymkowiak, S., and Kaplan, D. L. (2020). Matrigel-free laminin-entactin matrix to induce human renal proximal tubule structure formation *in vitro*. *ACS Biomater. Sci. Eng.* 6 (12), 6618–6625. doi:10.1021/acsbiomaterials.0c01385

Aisenbrey, E. A., and Murphy, W. L. (2020). Synthetic alternatives to matrigel. *Nat. Rev. Mat.* 5 (7), 539–551. doi:10.1038/s41578-020-0199-8

Ali, M., Pr, A. K., Yoo, J. J., Zahran, F., Atala, A., and Lee, S. J. (2019). A photo-crosslinkable kidney ECM-derived bioink accelerates renal tissue formation. *Adv. Healthc. Mat.* 8 (7), e1800992. doi:10.1002/adhm.201800992

Astashkina, A. I., Jones, C. F., Thiagarajan, G., Kurtzeborn, K., Ghandehari, H., Brooks, B. D., et al. (2014). Nanoparticle toxicity assessment using an invitro 3-D kidney organoid culture model. *Biomaterials* 35 (24), 6323–6331. doi:10.1016/j.biomaterials.2014.04.060

Astashkina, A. I., Mann, B. K., Prestwich, G. D., and Grainger, D. W. (2012). A 3-D organoid kidney culture model engineered for high-throughput nephrotoxicity assays. *Biomaterials* 33 (18), 4700–4711. doi:10.1016/j.biomaterials.2012.02.063

Beamish, J. A., Chen, E., and Putnam, A. J. (2017). Engineered extracellular matrices with controlled mechanics modulate renal proximal tubular cell epithelialization. *PLoS One* 12 (7), e0181085. doi:10.1371/journal.pone.0181085

Bombelli, S., Meregalli, C., Grasselli, C., Bolognesi, M. M., Bruno, A., Eriani, S., et al. (2020). PKHhigh/CD133+/CD24- renal stem-like cells isolated from human nephrospheres exhibit *in vitro* multipotency. *Cells* 9 (8), E1805. doi:10.3390/cells9081805

Bombelli, S., Meregalli, C., Scalia, C., Bovo, G., Torsello, B., De Marco, S., et al. (2018). Nephrosphere-derived cells are induced to multilineage differentiation when cultured on human decellularized kidney scaffolds. *Am. J. Pathol.* 188 (1), 184–195. doi:10.1016/j.ajpath.2017.09.012

Bonandrini, B., Figliuzzi, M., Papadimou, E., Morigi, M., Perico, N., Casiraghi, F., et al. (2014). Recellularization of well-preserved acellular kidney scaffold using embryonic stem cells. *Tissue Eng. Part A* 20 (9–10), 1486–1498. doi:10.1089/ten.TEA.2013.0269

Bosch-Fortea, M., Rodriguez-Fraticelli, A. E., Herranz, G., Hachimi, M., Barea, M. D., Young, J., et al. (2019). Micropattern-based platform as a physiologically relevant model to study epithelial morphogenesis and nephrotoxicity. *Biomaterials* 218, 119339. doi:10.1016/j.biomaterials.2019.119339

Bülow, R. D., and Boor, P. (2019). Extracellular matrix in kidney fibrosis: More than just a scaffold. *J. Histochem. Cytochem.* 67 (9), 643–661. doi:10.1369/0022155419849388

Caralt, M., Uzarski, J. S., Iacob, S., Obergfell, K. P., Berg, N., Bijonowski, B. M., et al. (2015). Optimization and critical evaluation of decellularization strategies to develop renal extracellular matrix scaffolds as biological templates for organ engineering and transplantation. *Am. J. Transpl.* 15 (1), 64–75. doi:10.1111/ajt.12999

Chani, B., Puri, V., Sobti, R. C., Jha, V., and Puri, S. (2017). Decellularized scaffold of cryopreserved rat kidney retains its recellularization potential. *PLoS One* 12 (3), 01730400–e173120. doi:10.1371/journal.pone.0173040

Chen, D., Roberts, R., Pohl, M., Nigam, S., Kreidberg, J., Wang, Z., et al. (2004). Differential expression of collagen- and laminin-binding integrins mediates ureteric bud and inner medullary collecting duct cell tubulogenesis. *Am. J. Physiol. Ren. Physiol.* 287 (4 56-4), 602–611. doi:10.1152/ajprenal.00015.2004

Chen, W. C., Lin, H. H., and Tang, M. J. (2014). Regulation of proximal tubular cell differentiation and proliferation in primary culture by matrix stiffness and ECM components. *Am. J. Physiol. Ren. Physiol.* 307 (6), F695–F707. doi:10.1152/ajprenal.00684.2013

Chevtchik, N. V., Fedecostante, M., Jansen, J., Mihajlovic, M., Wilmer, M., Rüth, M., et al. (2016). Upscaling of a living membrane for bioartificial kidney device. *Eur. J. Pharmacol.* 790, 28–35. doi:10.1016/j.ejphar.2016.07.009

Chung, I. M., Enemchukwu, N. O., Khaja, S. D., Murthy, N., Mantalaris, A., and García, A. J. (2008). Bioadhesive hydrogel microenvironments to modulate epithelial morphogenesis. *Biomaterials* 29 (17), 2637–2645. doi:10.1016/j.biomaterials.2008.03.008

Ciampi, O., Bonandrini, B., Derosas, M., Conti, S., Rizzo, P., Benedetti, V., et al. (2019). Engineering the vasculature of decellularized rat kidney scaffolds using human induced pluripotent stem cell-derived endothelial cells. *Sci. Rep.* 9 (1), 8001. doi:10.1038/s41598-019-44393-y

Clause, K. C., and Barker, T. H. (2013). Extracellular matrix signaling in morphogenesis and repair. *Curr. Opin. Biotechnol.* 24 (5), 830–833. doi:10.1016/j.copbio.2013.04.011

Cruz-Acuña, R., Mulero-Russe, A., Clark, A. Y., Zent, R., and García, A. J. (2019). Identification of matrix physicochemical properties required for renal epithelial cell tubulogenesis by using synthetic hydrogels. *J. Cell Sci.* 132 (20), jcs226639. doi:10.1242/jcs.226639

Dankers, P. Y. W., Boomker, J. M., Huizinga-van der Vlag, A., Wisse, E., Appel, W. P. J., Smedts, F. M. M., et al. (2011). Bioengineering of living renal membranes

consisting of hierarchical, bioactive supramolecular meshes and human tubular cells. *Biomaterials* 32 (3), 723–733. doi:10.1016/j.biomaterials.2010.09.020

DesRochers, T. M., Suter, L., Roth, A., and Kaplan, D. L. (2013). Bioengineered 3D human kidney tissue, a platform for the determination of nephrotoxicity. *PLoS One* 8 (3), e59219. doi:10.1371/journal.pone.0059219

Dixon, E. E., Maxim, D. S., Halperin Kuhns, V. L., Lane-Harris, A. C., Outeda, P., Ewald, A. J., et al. (2020). GDNF drives rapid tubule morphogenesis in a novel 3D *in vitro* model for ADPKD. *J. Cell Sci.* 133 (14), jcs249557. doi:10.1242/jcs.249557

Du, C., Narayanan, K., Leong, M. F., Ibrahim, M. S., Chua, Y. P., Khoo, V. M. H., et al. (2016). Functional kidney bioengineering with pluripotent stem-cell-derived renal progenitor cells and decellularized kidney scaffolds. *Adv. Healthc. Mat.* 5 (16), 2080–2091. doi:10.1002/adhm.201600120

Dzobo, K., Motaung, K. S. C. M., and Adesida, A. (2019). Recent trends in decellularized extracellular matrix bioinks for 3D printing: An updated review. *Int. J. Mol. Sci.* 20 (18), E4628. doi:10.3390/ijms20184628

Enemchukwu, N. O., Cruz-Acuña, R., Bongiorno, T., Johnson, C. T., García, J. R., Sulchek, T., et al. (2016). Synthetic matrices reveal contributions of ECM biophysical and biochemical properties to epithelial morphogenesis. *J. Cell Biol.* 212 (1), 113–124. doi:10.1083/jcb.201506055

Fedecostante, M., Westphal, K. G. C., Buono, M. F., Romero, N. S., Wilmer, M. J., Kerkering, J., et al. (2018). Recellularized native kidney scaffolds as a novel tool in nephrotoxicity screening. *Drug Metab. Dispos.* 46 (9), 1338–1350. doi:10.1124/dmd.118.080721

Figliuzzi, M., Bonandrini, B., and Remuzzi, A. (2017). Decellularized kidney matrix as functional material for whole organ tissue engineering. *J. Appl. Biomater. Funct. Mat.* 15 (4), e326–e333. doi:10.5301/jabfm.5000393

Forino, M., Torregrossa, R., Ceol, M., Murer, L., Della Vella, M., Del Prete, D., et al. (2006). TGFbeta1 induces epithelial-mesenchymal transition, but not myofibroblast transdifferentiation of human kidney tubular epithelial cells in primary culture. *Int. J. Exp. Pathol.* 87 (3), 197–208. doi:10.1111/j.1365-2613.2006.00479.x

Fransen, M. F. J., Addario, G., Bouten, C. V. C., Halary, F., Moroni, L., and Mota, C. (2021). Bioprinting of kidney *in vitro* models: Cells, biomaterials, and manufacturing techniques. *Essays Biochem.* 65 (3), 587–602. doi:10.1042/EBC20200158

Frantz, C., Stewart, K. M., and Weaver, V. M. (2010). The extracellular matrix at a glance. *J. Cell Sci.* 123 (24), 4195–4200. doi:10.1242/jcs.023820

Freedman, B. S., Brooks, C. R., Lam, A. Q., Fu, H., Morizane, R., Agrawal, V., et al. (2015). Modelling kidney disease with CRISPR-mutant kidney organoids derived from human pluripotent epiblast spheroids. *Nat. Commun.* 6, 8715. doi:10.1038/ncomms9715

Gao, X., Tanaka, Y., Sugii, Y., Mawatari, K., and Kitamori, T. (2011). Basic structure and cell culture condition of a bioartificial renal tubule on chip towards a cell-based separation microdevice. *Anal. Sci.* 27 (9), 907–912. doi:10.2116/analsci.27.907

Garreta, E., Oria, R., Tarantino, C., Pla-Roca, M., Prado, P., Fernández-Avilés, F., et al. (2017). Tissue engineering by decellularization and 3D bioprinting. *Mat. TodayKidlingt.* 20 (4), 166–178. doi:10.1016/j.mattod.2016.12.005

Garreta, E., Prado, P., Tarantino, C., Oria, R., Fanlo, L., Martí, E., et al. (2019). Fine tuning the extracellular environment accelerates the derivation of kidney organoids from human pluripotent stem cells. *Nat. Mat.* 18 (4), 397–405. doi:10.1038/s41563-019-0287-6

Geng, G., Xiao, Y., Shang, Y., Zhang, Y., Zhu, F., Tang, L., et al. (2021). Naphthalenephenylalanine-phenylalanine-glycine-arginine-glycine-aspartic promotes self-assembly of nephron progenitor cells in decellularized scaffolds to construct bioengineered kidneys. *Biomater. Adv.* 134, 112590. doi:10.1016/j.msec.2021.112590

Geuens, T., Ruiter, F. A. A., Schumacher, A., Morgan, F. L. C., Rademakers, T., Wiersma, L. E., et al. (2021). Thiol-ene cross-linked alginate hydrogel encapsulation modulates the extracellular matrix of kidney organoids by reducing abnormal type 1a1 collagen deposition. *Biomaterials* 275, 120976. doi:10.1016/j.biomaterials.2021.120976

Gupta, A. K., Coburn, J. M., Davis-Knowlton, J., Kimmerling, E., Kaplan, D. L., and Oxburgh, L. (2019). Scaffolding kidney organoids on silk. *J. Tissue Eng. Regen. Med.* 13 (5), 812–822. doi:10.1002/term.2830

Hagelaars, M. J., Yousef Yengej, F. A., Verhaar, M. C., Rookmaaker, M. B., Loerakker, S., and Bouten, C. V. C. (2022). Substrate stiffness determines the establishment of apical-basal polarization in renal epithelial cells but not in tubuloid-derived cells. *Front. Bioeng. Biotechnol.* 10, 820930. doi:10.3389/fbioe.2022.820930

Han, W., Singh, N. K., Kim, J. J., Kim, H., Kim, B. S., Park, J. Y., et al. (2019). Directed differential behaviors of multipotent adult stem cells from decellularized tissue/organ extracellular matrix bioinks. *Biomaterials* 224, 119496. doi:10.1016/j.biomaterials.2019.119496

Handorf, A. M., Zhou, Y., Halanski, M. A., and Li, W. J. (2015). Tissue stiffness dictates development, homeostasis, and disease progression. *Organogenesis*, 11 (1), 1–15. doi:10.1080/15476278.2015.1019687

He, M., Callanan, A., Lagaras, K., Steele, J. A. M., and Stevens, M. M. (2017). Optimization of SDS exposure on preservation of ECM characteristics in whole organ decellularization of rat kidneys. *J. Biomed. Mat. Res. B Appl. Biomater.* 105 (6), 1352–1360. doi:10.1002/jbm.b.33668

Hiraki, H. L., Nagao, R. J., Himmelfarb, J., and Zheng, Y. (2018). Fabricating a kidney cortex extracellular matrix-derived hydrogel. *J. Vis. Exp.* 140, e58314. doi:10.3791/58314

Hirashima, T., Hoshuyama, M., and Adachi, T. (2017). *In vitro* tubulogenesis of Madin–Darby canine kidney (MDCK) spheroids occurs depending on constituent cell number and scaffold gel concentration. *J. Theor. Biol.* 435, 110–115. doi:10.1016/j.jtbi.2017.09.009

Hiratsuka, K., Miyoshi, T., Kroll, K. T., Gupta, N. R., Valerius, M. T., Ferrante, T., et al. (2022). Organoid-on-a-chip model of human ARPKD reveals mechanosensing pathomechanisms for drug discovery. *Sci. Adv.* 8 (38), eabq0866. doi:10.1126/sciadv.abq0866

Homan, K. A., Gupta, N., Kroll, K. T., Kolesky, D. B., Skylar-Scott, M., Miyoshi, T., et al. (2019). Flow-enhanced vascularization and maturation of kidney organoids *in vitro*. *Nat. Methods* 16 (3), 255–262. doi:10.1038/s41592-019-0325-y

Homan, K. A., Kolesky, D. B., Skylar-Scott, M. A., Herrmann, J., Obuobi, H., Moisan, A., et al. (2016). Bioprinting of 3D convoluted renal proximal tubules on perfusable chips. *Sci. Rep.* 6, 34845. doi:10.1038/srep34845

Howden, S. E., Vanslambrouck, J. M., Wilson, S. B., Tan, K. S., and Little, M. H. (2019). Reporter-based fate mapping in human kidney organoids confirms nephron lineage relationships and reveals synchronous nephron formation. *EMBO Rep.* 20 (4), 474833–e47513. doi:10.15252/embr.201847483

Howden, S. E., Wilson, S. B., Groenewegen, E., Starks, L., Forbes, T. A., Tan, K. S., et al. (2021). Plasticity of distal nephron epithelia from human kidney organoids enables the induction of ureteric tip and stalk. *Cell Stem Cell* 28 (4), 671–684.e6. e6. doi:10.1016/j.stem.2020.12.001

Hu, D., Zhang, D., Liu, B., Liu, Y., Zhou, Y., Yu, Y., et al. (2020). Human ucMSCs seeded in a decellularized kidney scaffold attenuate renal fibrosis by reducing epithelial-mesenchymal transition via the TGF-β/Smad signaling pathway. *Pediatr. Res.* 88 (2), 192–201. doi:10.1038/s41390-019-0736-6

Hughes, C. S., Postovit, L. M., and Lajoie, G. A. (2010). Matrigel: A complex protein mixture required for optimal growth of cell culture. *Proteomics* 10 (9), 1886–1890. doi:10.1002/pmic.200900758

Hulshof, F., Schophuizen, C., Mihajlovic, M., van Blitterswijk, C., Masereeuw, R., de Boer, J., et al. (2018). New insights into the effects of biomaterial chemistry and topography on the morphology of kidney epithelial cells. *J. Tissue Eng. Regen. Med.* 12 (2), e817–e827. doi:10.1002/term.2387

Iozzo, R. V., and Schaefer, L. (2015). Matrix biology. *Proteoglycan Funct. A Compr. Nomencl. proteoglycans* 42, 11–55.

Jang, K. J., Mehr, A. P., Hamilton, G. A., McPartlin, L. A., Chung, S., Suh, K. Y., et al. (2013). Human kidney proximal tubule-on-a-chip for drug transport and nephrotoxicity assessment. *Integr. Biol.* 5 (9), 1119–1129. doi:10.1039/c3ib40049b

Jansen, J., De Napoli, I. E., Fedecostante, M., Schophuizen, C. M. S., Chevtchik, N. V., Wilmer, M. J., et al. (2015). Human proximal tubule epithelial cells cultured on hollow fibers: Living membranes that actively transport organic cations. *Sci. Rep.* 5 (1), 16702. doi:10.1038/srep16702

Jansen, K., Castilho, M., Aarts, S., Kaminski, M. M., Lienkamp, S. S., Pichler, R., et al. (2019). Fabrication of kidney proximal tubule grafts using biofunctionalized electrospun polymer scaffolds. *Macromol. Biosci.* 19 (2), e1800412–e1800419. doi:10.1002/mabi.201800412

Joraku, A., Stern, K. A., Atala, A., and Yoo, J. J. (2009). *In vitro* generation of three-dimensional renal structures. *Methods* 47 (2), 129–133. doi:10.1016/j.ymeth.2008.09.005

Kajbafzadeh, A. M., Khorramirouz, R., Nabavizadeh, B., Ladi Seyedian, S. S., Akbarzadeh, A., Heidari, R., et al. (2019). Whole organ sheep kidney tissue engineering and *in vivo* transplantation: Effects of perfusion-based decellularization on vascular integrity. *Mat. Sci. Eng. C Mat. Biol. Appl.* 98, 392–400. doi:10.1016/j.msec.2019.01.018

Kang, M., and Han, Y. M. (2014). Differentiation of human pluripotent stem cells into nephron progenitor cells in a serum and feeder free system. *PLoS One* 9 (4), e94888. doi:10.1371/journal.pone.0094888

Karamessinis, P. M., Tzinia, A. K., Kitsiou, P. V., Stetler-Stevenson, W. G., Michael, A. F., Fan, W-W., et al. (2002). Proximal tubular epithelial cell integrins respond to high glucose by altered cell-matrix interactions and differentially regulate matrixin expression. *Lab. Invest.* 82 (8), 1081–1093. doi:10.1097/01.lab.0000022224.86237.31

Kher, R., Sha, E. C., Escobar, M. R., Andreoli, E. M., Wang, P., Xu, W. M., et al. (2011). Ectopic expression of cadherin 8 is sufficient to cause cyst formation in a novel 3D collagen matrix renal tubule culture. *Am. J. Physiol. Cell Physiol.* 301 (1), C99–C105. doi:10.1152/ajpcell.00151.2010

Kim, J. W., Nam, S. A., Yi, J., Kim, J. Y., Lee, J. Y., Park, S. Y., et al. (2022). Kidney decellularized extracellular matrix enhanced the vascularization and maturation of human kidney organoids. *Adv. Sci.* 9 (15), e2103526. doi:10.1002/advs.202103526

Kim, M-H., Sawada, Y., Taya, M., and Kino-Oka, M. (2014). Influence of surface topography on the human epithelial cell response to micropatterned substrates with convex and concave architectures. *J. Biol. Eng.* 8 (1), 13. doi:10.1186/1754-1611-8-13

King, S. M., Higgins, J. W., Nino, C. R., Smith, T. R., Paffenroth, E. H., Fairbairn, C. E., et al. (2017). 3D proximal tubule tissues recapitulate key aspects of renal physiology to enable nephrotoxicity testing. *Front. Physiol.* 8 (MAR), 123. doi:10.3389/fphys.2017.00123

Kleinman, H. K., and Martin, G. R. (2005). Matrigel: Basement membrane matrix with biological activity. *Semin. Cancer Biol.* 15 (5), 378–386. doi:10.1016/j.semcancer.2005.05.004

Ko, K. W., Park, S. Y., Lee, E. H., Yoo, Y. I., Kim, D. S., Kim, J. Y., et al. (2021). Integrated bioactive scaffold with polydeoxyribonucleotide and stem-cell-derived extracellular vesicles for kidney regeneration. *ACS Nano* 15 (4), 7575–7585. doi:10.1021/acsnano.1c01098

Kolset, S. O., Reinholt, F. P., and Jenssen, T. (2012). Diabetic nephropathy and extracellular matrix. *J. Histochem. Cytochem.* 60 (12), 976–986. doi:10.1369/0022155412465073

Lam, A. Q., Freedman, B. S., Morizane, R., Lerou, P. H., Valerius, M. T., and Bonventre, J. V. (2014). Rapid and efficient differentiation of human pluripotent stem cells into intermediate mesoderm that forms tubules expressing kidney proximal tubular markers. *J. Am. Soc. Nephrol.* 25 (6), 1211–1225. doi:10.1681/ASN.2013080831

Lawlor, K. T., Vanslambrouck, J. M., Higgins, J. W., Chambon, A., Bishard, K., Arndt, D., et al. (2021). Cellular extrusion bioprinting improves kidney organoid reproducibility and conformation. *Nat. Mat.* 20 (2), 260–271. doi:10.1038/s41563-020-00853-9

Le Digabel, J., Ghibaudo, M., Trichet, L., Richert, A., and Ladoux, B. (2010). Microfabricated substrates as a tool to study cell mechanotransduction. *Med. Biol. Eng. Comput.* 48 (10), 965–976. doi:10.1007/s11517-010-0619-9

Lee, E. H., Chun, S. Y., Yoon, B. H., Kim, H. T., Chung, J-W., Lee, J. N., et al. (2022). Application of porcine kidney-derived extracellular matrix as coating, hydrogel, and scaffold material for renal proximal tubular epithelial cell. *Biomed. Res. Int.* 2022, 2220641. doi:10.1155/2022/2220641

Lee, H. N., Choi, Y. Y., Kim, J. W., Lee, Y. S., Choi, J. W., Kang, T., et al. (2021). Effect of biochemical and biomechanical factors on vascularization of kidney organoid-on-a-chip. *Nano Converg.* 8 (1), 35. doi:10.1186/s40580-021-00285-4

Lelongt, B., and Ronco, P. (2003). Role of extracellular matrix in kidney development and repair. *Pediatr. Nephrol.* 18, 731–742. doi:10.1007/s00467-003-1153-x

Li, L., Fu, H., and Liu, Y. (2022). The fibrogenic niche in kidney fibrosis: Components and mechanisms. *Nat. Rev. Nephrol.* 18 (9), 545–557. doi:10.1038/s41581-022-00590-z

Lih, E., Park, W., Park, K. W., Chun, S. Y., Kim, H., Joung, Y. K., et al. (2019). A bioinspired scaffold with anti-inflammatory magnesium hydroxide and decellularized extracellular matrix for renal tissue regeneration. *ACS Cent. Sci.* 5 (3), 458–467. doi:10.1021/acscentsci.8b00812

Lin, N. Y. C., Homan, K. A., Robinson, S. S., Kolesky, D. B., Duarte, N., Moisan, A., et al. (2019). Renal reabsorption in 3D vascularized proximal tubule models. *Proc. Natl. Acad. Sci. U. S. A.* 116 (12), 5399–5404. doi:10.1073/pnas.1815208116

Loganathan, R., Little, C. D., and Rongish, B. J. (2020). Extracellular matrix dynamics in tubulogenesis. *Cell. Signal.* 72, 109619. doi:10.1016/j.cellsig.2020.109619

Louzao-Martinez, L., van Dijk, C. G. M., Xu, Y. J., Korn, A., Bekker, N. J., Brouwhuis, R., et al. (2019). A proteome comparison between human fetal and mature renal extracellular matrix identifies EMILIN1 as a regulator of renal epithelial cell adhesion. *Matrix Biol. Plus* 4, 100011. doi:10.1016/j.mbplus.2019.100011

Love, H. D., Ao, M., Jorgensen, S., Swearingen, L., Ferrell, N., Evans, R., et al. (2019). Substrate elasticity governs differentiation of renal tubule cells in prolonged culture. *Tissue Eng. Part A* 25 (13–14), 1013–1022. doi:10.1089/ten.TEA.2018.0182

Low, J. H., Li, P., Chew, E. G. Y., Zhou, B., Suzuki, K., Zhang, T., et al. (2019). Generation of human PSC-derived kidney organoids with patterned nephron segments and a de novo vascular network. *Cell Stem Cell* 25 (3), 373–387. e9. doi:10.1016/j.stem.2019.06.009

Lü, S. H., Lin, Q., Liu, Y. N., Gao, Q., Hao, T., Wang, Y., et al. (2012). Self-assembly of renal cells into engineered renal tissues in collagen/Matrigel scaffold *in vitro*. *J. Tissue Eng. Regen. Med.* 6 (10), 786–792. doi:10.1002/term.484

Mae, S-I., Ryosaka, M., Sakamoto, S., Matsuse, K., Nozaki, A., Igami, M., et al. (2020). Expansion of human iPSC-derived ureteric bud organoids with repeated branching potential. *Cell Rep.* 32 (4), 107963. doi:10.1016/j.celrep.2020.107963

Manninen, A. (2015). Epithelial polarity - generating and integrating signals from the ECM with integrins. *Exp. Cell Res.* 334 (2), 337–349. doi:10.1016/j.yexcr.2015.01.003

Melica, M. E., La Regina, G. L., Parri, M., Peired, A. J., Romagnani, P., and Lasagni, L. (2019). Substrate stiffness modulates renal progenitor cell properties via a ROCK-mediated mechanotransduction mechanism. *Cells* 8 (12), E1561. doi:10.3390/cells8121561

Minuth, W. W., Sorokin, L., and Schumacher, K. (2004). Generation of renal tubules at the interface of an artificial interstitium. *Cell. Physiol. biochem.* 14 (4–6), 387–394. doi:10.1159/000080348

Miya, M., Maeshima, A., Mishima, K., Sakurai, N., Ikeuchi, H., Kuroiwa, T., et al. (2011). Enhancement of *in vitro* human tubulogenesis by endothelial cell-derived factors: Implications for *in vivo* tubular regeneration after injury. *Am. J. Physiol. Ren. Physiol.* 301 (2), 387–395. doi:10.1152/ajprenal.00619.2010

Moll, S., Ebeling, M., Weibel, F., Farina, A., Araujo Del Rosario, A., Hoflack, J. C., et al. (2013). Epithelial cells as active player in fibrosis: Findings from an *in vitro* model. *PLoS One* 8 (2), e56575. doi:10.1371/journal.pone.0056575

Montesano, R., Matsumoto, K., Nakamura, T., and Orci, L. (1991). Identification of a fibroblast-derived epithelial morphogen as hepatocyte growth factor. *Cell* 67 (5), 901–908. doi:10.1016/0092-8674(91)90363-4

Montesano, R., Schaller, G., and Orci, L. (1991). Induction of epithelial tubular morphogenesis *in vitro* by fibroblast-derived soluble factors. *Cell* 66 (4), 697–711. doi:10.1016/0092-8674(91)90115-f

Morizane, R., and Bonventre, J. V. (2017). Generation of nephron progenitor cells and kidney organoids from human pluripotent stem cells. *Nat. Protoc.* 12 (1), 195–207. doi:10.1038/nprot.2016.170

Morizane, R., Lam, A. Q., Freedman, B. S., Kishi, S., Valerius, M. T., and Bonventre, J. V. (2015). Nephron organoids derived from human pluripotent stem cells model kidney development and injury. *Nat. Biotechnol.* 33 (11), 1193–1200. doi:10.1038/nbt.3392

Muncie, J. M., and Weaver, V. M. (2018). The physical and biochemical properties of the extracellular matrix regulate cell fate. *Curr. Top. Dev. Biol.* 130, 1–37. doi:10.1016/bs.ctdb.2018.02.002

Myram, S., Venzac, B., Lapin, B., Battistella, A., Cayrac, F., Cinquin, B., et al. (2021). A multitubular kidney-on-chip to decipher pathophysiological mechanisms in renal cystic diseases. *Front. Bioeng. Biotechnol.* 9, 624553. doi:10.3389/fbioe.2021.624553

Narayanan, K., Schumacher, K. M., Tasnim, F., Kandasamy, K., Schumacher, A., Ni, M., et al. (2013). Human embryonic stem cells differentiate into functional renal proximal tubular-like cells. *Kidney Int.* 83 (4), 593–603. doi:10.1038/ki.2012.442

Ni, M., Teo, J. C. M., Ibrahim, M. S., Zhang, K., Tasnim, F., Chow, P-Y., et al. (2011). Characterization of membrane materials and membrane coatings for bioreactor units of bioartificial kidneys. *Biomaterials* 32 (6), 1465–1476. doi:10.1016/j.biomaterials.2010.10.061

Nickel, C., Benzing, T., Sellin, L., Gerke, P., Karihaloo, A., Liu, Z-X., et al. (2002). The polycystin-1 C-terminal fragment triggers branching morphogenesis and migration of tubular kidney epithelial cells. *J. Clin. Invest.* 109 (4), 481–489. doi:10.1172/JCI12867

Nigam, S. K., and Bush, K. T. (2014). Growth factor-heparan sulfate "switches" regulating stages of branching morphogenesis. *Pediatr. Nephrol.* 29 (4), 727–735. doi:10.1007/s00467-013-2725-z

Nur-E-Kamal, A., Ahmed, I., Kamal, J., Schindler, M., and Meiners, S. (2006). Three-dimensional nanofibrillar surfaces promote self-renewal in mouse embryonic stem cells. *Stem Cells* 24 (2), 426–433. doi:10.1634/stemcells.2005-0170

Otero, J., Navajas, D., and Alcaraz, J. (2020). Characterization of the elastic properties of extracellular matrix models by atomic force microscopy. *Methods Cell Biol.* 156, 59–83. doi:10.1016/bs.mcb.2019.11.016

Passaniti, A., Kleinman, H. K., and Martin, G. R. (2021). Matrigel: History/background, uses, and future applications. *J. Cell Commun. Signal.* doi:10.1007/s12079-021-00643-1

Petkau-Milroy, K., and Brunsveld, L. (2013). Supramolecular chemical biology; bioactive synthetic self-assemblies. *Org. Biomol. Chem.* 11 (2), 219–232. doi:10.1039/c2ob26790j

Poornejad, N., Schaumann, L. B., Buckmiller, E. M., Momtahan, N., Gassman, J. R., Ma, H. H., et al. (2016). The impact of decellularization agents on renal tissue extracellular matrix. *J. Biomater. Appl.* 31 (4), 521–533. doi:10.1177/0885328216656099

Rayner, S. G., Phong, K. T., Xue, J., Lih, D., Shankland, S. J., Kelly, E. J., et al. (2018). Reconstructing the human renal vascular–tubular unit *in vitro*. *Adv. Healthc. Mat.* 7 (23), e1801120. doi:10.1002/adhm.201801120

Rosines, E., Schmidt, H. J., and Nigam, S. K. (2007). The effect of hyaluronic acid size and concentration on branching morphogenesis and tubule differentiation in developing kidney culture systems: Potential applications to engineering of renal tissues. *Biomaterials* 28 (32), 4806–4817. doi:10.1016/j.biomaterials.2007.07.034

Ruiter, F. A. A., Morgan, F. L. C., Roumans, N., Schumacher, A., Slaats, G. G., Moroni, L., et al. (2022). Soft, dynamic hydrogel confinement improves kidney organoid lumen morphology and reduces epithelial-mesenchymal transition in culture. *Adv. Sci.* 9 (20), e2200543. doi:10.1002/advs.202200543

Sakurai, H., Barros, E. J., Tsukamoto, T., Barasch, J., and Nigam, S. K. (1997). An *in vitro* tubulogenesis system using cell lines derived from the embryonic kidney shows dependence on multiple soluble growth factors. *Proc. Natl. Acad. Sci. U. S. A.* 94 (12), 6279–6284. doi:10.1073/pnas.94.12.6279

Satyam, A., Tsokos, M. G., Tresback, J. S., Zeugolis, D. I., and Tsokos, G. C. (2020). Cell derived extracellular matrix-rich biomimetic substrate supports podocyte proliferation, differentiation and maintenance of native phenotype. *Adv. Funct. Mat.* 30 (44), 1908752. doi:10.1002/adfm.201908752

Schlüter, M. A., and Margolis, B. (2009). Apical lumen formation in renal epithelia. *J. Am. Soc. Nephrol.* 20 (7), 1444–1452. doi:10.1681/ASN.2008090949

Schophuizen, C. M. S., De Napoli, I. E., Jansen, J., Teixeira, S., Wilmer, M. J., Hoenderop, J. G. J., et al. (2015). Development of a living membrane comprising a functional human renal proximal tubule cell monolayer on polyethersulfone polymeric membrane. *Acta Biomater.* 14, 22–32. doi:10.1016/j.actbio.2014.12.002

Schutgens, F., Rookmaaker, M. B., Margaritis, T., Rios, A., Ammerlaan, C., Jansen, J., et al. (2019). Tubuloids derived from human adult kidney and urine for personalized disease modeling. *Nat. Biotechnol.* 37 (3), 303–313. doi:10.1038/s41587-019-0048-8

Sciancalepore, A. G., Portone, A., Moffa, M., Persano, L., De Luca, M., Paiano, A., et al. (2016). Micropatterning control of tubular commitment in human adult renal stem cells. *Biomaterials* 94, 57–69. doi:10.1016/j.biomaterials.2016.03.042

Sebinger, D. D. R., Ofenbauer, A., Gruber, P., Malik, S., and Werner, C. (2013). ECM modulated early kidney development in embryonic organ culture. *Biomaterials* 34 (28), 6670–6682. doi:10.1016/j.biomaterials.2013.05.031

Secker, P. F., Luks, L., Schlichenmaier, N., and Dietrich, D. R. (2018). RPTEC/TERT1 cells form highly differentiated tubules when cultured in a 3D matrix. *ALTEX* 35 (2), 223–234. doi:10.14573/altex.1710181

Shahraki, S., Bideskan, A. E., Aslzare, M., Tavakkoli, M., Bahrami, A. R., Hosseinian, S., et al. (2022). Decellularization with triton X-100 provides a suitable model for human kidney bioengineering using human mesenchymal stem cells. *Life Sci.* 295, 120167. doi:10.1016/j.lfs.2021.120167

Shamir, E. R., and Ewald, A. J. (2014). Three-dimensional organotypic culture: Experimental models of mammalian biology and disease. *Nat. Rev. Mol. Cell Biol.* 15 (10), 647–664. doi:10.1038/nrm3873

Shen, C., Zhang, G., Wang, Q., and Meng, Q. (2015). Fabrication of collagen gel hollow fibers by covalent cross-linking for construction of bioengineering renal tubules. *ACS Appl. Mat. Interfaces* 7 (35), 19789–19797. doi:10.1021/acsami.5b05809

Shen, L., Song, X., Xu, Y., Tian, R., Wang, Y., Li, P., et al. (2021). Patterned vascularization in a directional ice-templated scaffold of decellularized matrix. *Eng. Life Sci.* 21 (10), 683–692. doi:10.1002/elsc.202100034

Singh, N. K., Han, W., Nam, S. A., Kim, J. W., Kim, J. Y., Kim, Y. K., et al. (2020201911973). Three-dimensional cell-printing of advanced renal tubular tissue analogue. *Biomaterials* 232, 119734. doi:10.1016/j.biomaterials.2019.119734

Sobreiro-Almeida, R., Fonseca, D. R., and Neves, N. M. (2019). Extracellular matrix electrospun membranes for mimicking natural renal filtration barriers. *Mat. Sci. Eng. C Mat. Biol. Appl.* 103, 109866. doi:10.1016/j.msec.2019.109866

Sobreiro-Almeida, R., Gómez-Florit, M., Quinteira, R., Reis, R. L., Gomes, M. E., and Neves, N. M. (2021). Decellularized kidney extracellular matrix bioinks recapitulate renal 3D microenvironment *in vitro*. *Biofabrication* 13 (4), 045006. doi:10.1088/1758-5090/ac0fca

Sobreiro-Almeida, R., Melica, M. E., Lasagni, L., Romagnani, P., and Neves, N. M. (2020). Co-cultures of renal progenitors and endothelial cells on kidney decellularized matrices replicate the renal tubular environment *in vitro*. *Acta Physiol.* 230 (1), e13491. doi:10.1111/apha.13491

Song, J. J., Guyette, J. P., Gilpin, S. E., Gonzalez, G., Vacanti, J. P., and Ott, H. C. (2013). Regeneration and experimental orthotopic transplantation of a bioengineered kidney. *Nat. Med.* 19 (5), 646–651. doi:10.1038/nm.3154

Su, J., Satchell, S. C., Shah, R. N., and Wertheim, J. A. (2018). Kidney decellularized extracellular matrix hydrogels: Rheological characterization and human glomerular endothelial cell response to encapsulation. *J. Biomed. Mat. Res. A* 106 (9), 2448–2462. doi:10.1002/jbm.a.36439

Subramanian, B., Ko, W. C., Yadav, V., DesRochers, T. M., Perrone, R. D., Zhou, J., et al. (2012). The regulation of cystogenesis in a tissue engineered kidney disease system by abnormal matrix interactions. *Biomaterials* 33 (33), 8383–8394. doi:10.1016/j.biomaterials.2012.08.020

Subramanian, B., Rudym, D., Cannizzaro, C., Perrone, R., Zhou, J., and Kaplan, D. L. (2010). Tissue-engineered three-dimensional *in vitro* models for normal and diseased kidney. *Tissue Eng. Part A* 16 (9), 2821–2831. doi:10.1089/ten.tea.2009.0595

Sullivan, D. C., Mirmalek-Sani, S. H., Deegan, D. B., Baptista, P. M., Aboushwareb, T., Atala, A., et al. (2012). Decellularization methods of porcine kidneys for whole organ engineering using a high-throughput system. *Biomaterials* 33 (31), 7756–7764. doi:10.1016/j.biomaterials.2012.07.023

Taguchi, A., and Nishinakamura, R. (2017). Higher-order kidney organogenesis from pluripotent stem cells. *Cell Stem Cell* 21 (6), 730–746. e6. doi:10.1016/j.stem.2017.10.011

Takasato, M., Er, P. X., Chiu, H. S., Maier, B., Baillie, G. J., Ferguson, C., et al. (2015). Kidney organoids from human iPS cells contain multiple lineages and model human nephrogenesis. *Nature* 526 (7574), 564–568. doi:10.1038/nature15695

Takasato, M., and Little, M. H. (2017). Making a kidney organoid using the directed differentiation of human pluripotent stem cells. *Methods Mol. Biol.* 1597, 195–206. doi:10.1007/978-1-4939-6949-4_14

Taub, M., Wang, Y., Szczesny, T. M., and Kleinman, H. K. (1990). Epidermal growth factor or transforming growth factor α is required for kidney tubulogenesis in matrigel cultures in serum-free medium. *Proc. Natl. Acad. Sci. U. S. A.* 87 (10), 4002–4006. doi:10.1073/pnas.87.10.4002

Theocharis, A. D., Skandalis, S. S., Gialeli, C., and Karamanos, N. K. (2016). Extracellular matrix structure. *Adv. Drug Deliv. Rev.* 97, 4–27. doi:10.1016/j.addr.2015.11.001

Toyohara, T., Mae, S-I., Sueta, S-I., Inoue, T., Yamagishi, Y., Kawamoto, T., et al. (2015). Cell therapy using human induced pluripotent stem cell-derived renal progenitors ameliorates acute kidney injury in mice. *Stem Cells Transl. Med.* 4 (9), 980–992. doi:10.5966/sctm.2014-0219

Tröndle, K., Miotto, G., Rizzo, L., Pichler, R., Koch, F., Koltay, P., et al. (2022). Deep learning-assisted nephrotoxicity testing with bioprinted renal spheroids. *Int. J. Bioprint.* 8 (2), 528. doi:10.18063/ijb.v8i2.528

Tröndle, K., Rizzo, L., Pichler, R., Koch, F., Itani, A., Zengerle, R., et al. (2021). Scalable fabrication of renal spheroids and nephron-like tubules by bioprinting and controlled self-assembly of epithelial cells. *Biofabrication* 13 (3), 035019. doi:10.1088/1758-5090/abe185

Ullah, I., Busch, J. F., Rabien, A., Ergün, B., Stamm, C., Knosalla, C., et al. (2020). Adult tissue extracellular matrix determines tissue specification of human iPSC-derived embryonic stage mesodermal precursor cells. *Adv. Sci.* 7 (5), 1901198. doi:10.1002/advs.201901198

van den Berg, C. W., Ritsma, L., Avramut, M. C., Wiersma, L. E., van den Berg, B. M., Leuning, D. G., et al. (2018). Renal subcapsular transplantation of PSC-derived kidney organoids induces neo-vasculogenesis and significant glomerular and tubular maturation *in vivo*. *Stem Cell Rep.* 10 (3), 751–765. doi:10.1016/j.stemcr.2018.01.041

van Gaal, R. C., Vrehen, A. F., van Sprang, J. F., Fransen, P-P. K. H., van Turnhout, M. C., and Dankers, P. Y. W. (2021). Biomaterial screening of protein coatings and peptide additives: Towards a simple synthetic mimic of a complex natural coating for a bio-artificial kidney. *Biomater. Sci.* 9 (6), 2209–2220. doi:10.1039/d0bm01930e

van Genderen, A. M., Jansen, K., Kristen, M., van Duijn, J., Li, Y., Schuurmans, C. C. L., et al. (2021). Topographic guidance in melt-electrowritten tubular scaffolds enhances engineered kidney tubule performance. *Front. Bioeng. Biotechnol.* 8, 617364. doi:10.3389/fbioe.2020.617364

Vormann, M. K., Tool, L. M., Ohbuchi, M., Gijzen, L., van Vught, R., Hankemeier, T., et al. (2022). Modelling and prevention of acute kidney injury through ischemia and reperfusion in a combined human renal proximal tubule/blood vessel-on-a-chip. *Kidney360* 3 (2), 217–231. doi:10.34067/KID.0003622021

Vormann, M. K., Vriend, J., Lanz, H. L., Gijzen, L., van den Heuvel, A., Hutter, S., et al. (2021). Implementation of a human renal proximal tubule on a chip for nephrotoxicity and drug interaction studies. *J. Pharm. Sci.* 110 (4), 1601–1614. doi:10.1016/j.xphs.2021.01.028

Walma, D. A. C., and Yamada, K. M. (2020). The extracellular matrix in development. *Development* 147 (10), dev175596–9. doi:10.1242/dev.175596

Wang, X., Guo, C., Chen, Y., Tozzi, L., Szymkowiak, S., Li, C., et al. (2020). Developing a self-organized tubulogenesis model of human renal proximal tubular epithelial cells *in vitro*. *J. Biomed. Mat. Res. A* 108 (3), 795–804. doi:10.1002/jbm.a.36858

Weber, H. M., Tsurkan, M. V., Magno, V., Freudenberg, U., and Werner, C. (2017). Heparin-based hydrogels induce human renal tubulogenesis *in vitro*. *Acta Biomater.* 57, 59–69. doi:10.1016/j.actbio.2017.05.035

Wiraja, C., Mori, Y., Ichimura, T., Hwang, J., Xu, C., and Bonventre, J. V. (2021). Nephrotoxicity assessment with human kidney tubuloids using spherical nucleic acid-based mRNA nanoflares. *Nano Lett.* 21 (13), 5850–5858. doi:10.1021/acs.nanolett.1c01840

Xia, Y., Nivet, E., Sancho-Martinez, I., Gallegos, T., Suzuki, K., Okamura, D., et al. (2013). Directed differentiation of human pluripotent cells to ureteric bud kidney progenitor-like cells. *Nat. Cell Biol.* 15 (12), 1507–1515. doi:10.1038/ncb2872

Xie, R., Korolj, A., Liu, C., Song, X., Lu, R. X. Z., Zhang, B., et al. (2020). h-FIBER: Microfluidic topographical hollow fiber for studies of glomerular filtration barrier. *ACS Cent. Sci.* 6 (6), 903–912. doi:10.1021/acscentsci.9b01097

Xing, H., Lee, H., Luo, L., and Kyriakides, T. R. (2020). Extracellular matrix-derived biomaterials in engineering cell function. *Biotechnol. Adv.* 42, 107421. doi:10.1016/j.biotechadv.2019.107421

Zegers, M. M. P., O'Brien, L. E., Yu, W., Datta, A., and Mostov, K. E. (2003). Epithelial polarity and tubulogenesis *in vitro*. *Trends Cell Biol.* 13 (4), 169–176. doi:10.1016/s0962-8924(03)00036-9

Zhang, H., Lau, S. F-T., Heng, B. F., Teo, P. Y., Alahakoon, P. K. D. T., Ni, M., et al. (2011). Generation of easily accessible human kidney tubules on two-dimensional surfaces *in vitro*. *J. Cell. Mol. Med.* 15 (6), 1287–1298. doi:10.1111/j.1582-4934.2010.01113.x

Zhang, H., Tasnim, F., Ying, J. Y., and Zink, D. (2009). The impact of extracellular matrix coatings on the performance of human renal cells applied in bioartificial kidneys. *Biomaterials* 30 (15), 2899–2911. doi:10.1016/j.biomaterials.2009.01.046

Zhang, J., Li, K., Kong, F., Sun, C., Zhang, D., Yu, X., et al. (2019). Induced intermediate mesoderm combined with decellularized kidney scaffolds for functional engineering kidney. *Tissue Eng. Regen. Med.* 16 (5), 501–512. doi:10.1007/s13770-019-00197-9

Zhang, Y., Reif, G., and Wallace, D. P. (2020). Extracellular matrix, integrins, and focal adhesion signaling in polycystic kidney disease. *Cell. Signal.* 72, 109646. doi:10.1016/j.cellsig.2020.109646

Zhou, C., Zhou, L., Liu, J., Xu, L., Xu, Z., Chen, Z., et al. (2020). Kidney extracellular matrix hydrogel enhances therapeutic potential of adipose-derived mesenchymal stem cells for renal ischemia reperfusion injury. *Acta Biomater.* 115, 250–263. doi:10.1016/j.actbio.2020.07.056

frontiers | Frontiers in Physiology

TYPE Original Research
PUBLISHED 08 February 2023
DOI 10.3389/fphys.2023.1024238

OPEN ACCESS

EDITED BY
Christian Hugo,
University Hospital Carl Gustav Carus, Germany

REVIEWED BY
Rossana Franzin,
University of Bari Aldo Moro, Italy
Thierry Hauet,
University of Poitiers, France

*CORRESPONDENCE
Peter R. Corridon,
peter.corridon@ku.ac.ae

SPECIALTY SECTION
This article was submitted to Renal Physiology and Pathophysiology, a section of the journal Frontiers in Physiology

RECEIVED 21 August 2022
ACCEPTED 30 January 2023
PUBLISHED 08 February 2023

CITATION
Corridon PR (2023), Enhancing the expression of a key mitochondrial enzyme at the inception of ischemia-reperfusion injury can boost recovery and halt the progression of acute kidney injury. *Front. Physiol.* 14:1024238. doi: 10.3389/fphys.2023.1024238

Enhancing the expression of a key mitochondrial enzyme at the inception of ischemia-reperfusion injury can boost recovery and halt the progression of acute kidney injury

Peter R. Corridon [1,2,3]*

[1]Department of Immunology and Physiology, College of Medicine and Health Sciences, Khalifa University, Abu Dhabi, United Arab Emirates, [2]Healthcare Engineering Innovation Center, Khalifa University, Abu Dhabi, United Arab Emirates, [3]Center for Biotechnology, Khalifa University, Abu Dhabi, United Arab Emirates, [4]Indiana Center for Biological Microscopy, Indiana University School of Medicine, Indianapolis, IN, United States

Hydrodynamic fluid delivery has shown promise in influencing renal function in disease models. This technique provided pre-conditioned protection in acute injury models by upregulating the mitochondrial adaptation, while hydrodynamic injections of saline alone have improved microvascular perfusion. Accordingly, hydrodynamic mitochondrial gene delivery was applied to investigate the ability to halt progressive or persistent renal function impairment following episodes of ischemia-reperfusion injuries known to induce acute kidney injury (AKI). The rate of transgene expression was approximately 33% and 30% in rats with prerenal AKI that received treatments 1 (T_{1hr}) and 24 (T_{24hr}) hours after the injury was established, respectively. The resulting mitochondrial adaptation *via* exogenous IDH2 (isocitrate dehydrogenase 2 (NADP+) and mitochondrial) significantly blunted the effects of injury within 24 h of administration: decreased serum creatinine (≈60%, $p < 0.05$ at T_{1hr}; ≈50%, $p < 0.05$ at T_{24hr}) and blood urea nitrogen (≈50%, $p < 0.05$ at T_{1hr}; ≈35%, $p < 0.05$ at T_{24hr}) levels, and increased urine output (≈40%, $p < 0.05$ at T_{1hr}; ≈26%, $p < 0.05$ at T_{24hr}) and mitochondrial membrane potential, $\Delta\psi_m$, (≈ by a factor of 13, $p < 0.001$ at T_{1hr}; ≈ by a factor of 11, $p < 0.001$ at T_{24hr}), despite elevated histology injury score (26%, $p < 0.05$ at $T1_{hr}$; 47%, $p < 0.05$ at T_{24hr}). Therefore, this study identifies an approach that can boost recovery and halt the progression of AKI at its inception.

KEYWORDS

IDH2 [isocitrate dehydrogenase 2 (NADP+) and mitochondrial], gene delivery, acute kidney injury, hydrodynamic injections, ischemia-reperfusion injury (I/R), hydrodynamic gene delivery

1 Introduction

Maintaining kidney health for its multitude of essential regulatory functions remains a significant global clinical challenge (Ferguson et al., 2008; Corridon et al., 2017; Corridon, 2021; Pantic et al., 2022b). As a result, renal dysfunction is both a common and progressive problem, threatening the lives of millions daily. This complex disorder can stem from prerenal, renal, and postrenal conditions and generally results from renal trauma, blood loss, and the accumulation of various toxins, such as broad-spectrum antibiotics, chemotherapeutic drugs, and

radiocontrast agents (Nagase et al., 1977; Thadhani et al., 1996; Bellomo et al., 2004; Cerda et al., 2008; Himmelfarb et al., 2008; Hingorani et al., 2009; Lattanzio and Kopyt, 2009; Kinsey and Okusa, 2011a). Such dysfunction can be gradual or sudden, and it is imperative to address these issues and minimize secondary organ damage, which can occur primarily as a consequence of an acute disorder.

Acute kidney injury (AKI) management depends on identifying and treating its underlying cause(s) (Palevsky et al., 2008; Basu et al., 2012). Fortunately, in some instances, sudden impairment, which is the focus of this work, can be reversed within several weeks to months if the underlying cause has been treated. Yet, beyond certain thresholds, these disorders induce persistent cell death and progressing degrees of atrophy that drive the progression of AKI (Holderied et al., 2020). At this stage, current treatment regimens, which comprise fluid, electrolyte, and acid-base balance management, are still mainly supportive and unable to halt the progression of the illness (Kinsey and Okusa, 2011b; Rostami et al., 2022). As a result, gene therapy has been proposed as an alternative to treat and prevent the underlying causes and progression of AKI (Humes et al., 1997; Torras et al., 2008; Molitoris et al., 2009).

The first human gene therapy trial in 1990 laid the foundation for a new medical paradigm (Imai, 2003). However, since then, gene therapy has undergone more than thirty years of trials and tribulations with unexpected side effects dampening the enthusiasm for this form of treatment (Imai, 2003; Davis and Park, 2019). Fortunately, in the past few years, however, gene therapy has enjoyed a renaissance with recent successes in lymphoma treatment (Nogrady, 2018), retinal degeneration (Leroy et al., 2022), and neuromuscular atrophy (Ali et al., 2021), using a variety of viral and non-viral vector-based applications. With these successes, continued efforts are being employed using a broad spectrum of vectors for proof-of-concept and therapeutic approaches in nearly every organ system in the body, including the kidney. However, the progress in the development of direct gene transfer methods in the kidney has been limited compared with other organs due in part to our lack of knowledge about the biological factors needed to promote efficient vector entry into the cell and the complex anatomical structure of the kidney (Davis and Park, 2019).

Numerous methods have been proposed to deliver exogenous genes to mammalian cells to study and treat human disease (Friedmann and Roblin, 1972; Amiel et al., 2000; Niidome and Huang, 2002; Chen et al., 2003; Appledorn et al., 2008; Miyazaki et al., 2009; Corridon et al., 2013; Collins and Thrasher, 2015; Hitchman et al., 2017; Kolb et al., 2018; Shen et al., 2018; Peek and Wilson, 2022). With specific regard to the kidney, attempts have been made to protect and repair renal function by targeting single genetic loci (Lien and Lai, 1997). Such approaches have utilized purified protein products, plasmids, and viruses encoding peptides and proteins. Historically, recombinant growth factors have been used in experimental and clinical AKI settings to preserve renal function and accelerate tissue repair. For instance, these studies have suggested that hepatocyte growth factor (HGF) may have a significant role in the management of AKI. HGF has been shown to have diverse functions in kidney repair following acute injury, as it can act as both a renotropic and anti-fibrotic agent (Dai et al., 2002; Yazawa et al., 2004). Parallel studies have shown that HGF may prevent cyclosporin-induced tubulointerstitial fibrosis, indicating its additional renoprotective capacity (Yazawa et al., 2004).

Similarly, other investigations have shown that exogenous vascular endothelial growth factor (VEGF) enhances renal microvascular integrity and function following acute and chronic injuries (Corridon et al., 2006; Leonard et al., 2008; Engel et al., 2019; Gao et al., 2020). The therapeutic potential of recombinant interleukin binding protein (IL-18 Bp) was also investigated in established ischemia AKI rodent models. Intravenous injections of IL-18 Bp improved renal function and tubule morphology and reduced tubular necrosis and apoptosis (Wang et al., 2012). More recently, inhibition of IL-18 by peritoneal doses of IL-18 Bp has been shown to reduce renal fibrosis following IRI (Liang et al., 2018). Recombinant uteroglobin treatment prevented glomerulonephritis by reducing proteinuria and cellular pathogenic globulin-glomerular biding (Lee et al., 2004). However, several factors may limit the clinical benefit of this therapy. Such factors include the relatively short half-life of recombinant proteins and the prohibitive costs and recurrent doses required for treatments (Mizui et al., 2004; Yazawa et al., 2004). Altogether, these factors outline a basis for generating adverse side effects that can result from administering supraphysiologic doses of recombinant proteins.

In contrast, vector-based gene transfer procedures can be more straightforward, safer, and cheaper, requiring less frequent dosing (Mizui et al., 2004). For instance, researchers have utilized adenoviral, adeno-associated viral, and lentiviral vectors for gene transfer. Previous studies have identified the ability to robustly elicit targeted gene transfer with adenoviral vectors using pressurized renal vein injection techniuqes (Corridon et al., 2013; Corridon et al., 2021). This type of research has also identified the possibility of improving renal transplant outcomes in clinically relevant models of acute rejection using immunomodulating genes like interleukin-13 (a known potent anti-inflammatory agent) (Sandovici et al., 2007) and 2,3-indoleamine dioxygenase (a stimulator of regulatory T cell production) (Vavrincova-Yaghi et al., 2011) using an adenovirus-based approach *via* intrarenal and renal arterial injections, respectively. These findings are significant since ischemic and toxic renal injuries repair critically depends on regulating a redundant, interactive network of cytokine and growth factors (Wang et al., 2012).

Recent studies have highlighted the benefits and drawbacks of adeno-associated viruses and lentiviruses (Rubin et al., 2019). For example, retrograde ureteral and subcapsular adeno-associated injections have been used to transduce the kidney. However, viral particles leaked from the organ during these processes and mediated substantial off-target gene transfer. Analogously, similar results were observed with lentiviral vectors, which also effectively transduced kidney cells, albeit with less off-target tissue transduction. Thus, it would be of value to devise a system that can modulate gene expression levels in a therapeutic manner capable of reinstating renal function without inducing harmful viral-derived toxicity. However, viral vectors may ultimately be confined to experimental gene therapy applications unless we overcome the obstacles that limit their widespread use (DeYoung and Dichek, 1998; Kay et al., 2001).

Comparatively, one of the simplest forms of DNA transfection involves transfer without a specific vector or carrier molecule. Studies dating back roughly two decades have shown how plasmid DNA can be transferred using only a solvent intravenously (Liu et al., 1999). Plasmid-based vector treatments have confirmed the renotherapeutic potential of HGF as it mediated tissue regeneration and protected tubular epithelial cells from injury and apoptosis during acute renal failure. These results were obtained using single intravenous injections

of plasmids encoding HGF (Dai et al., 2002). One major issue related to this intravenous approach was the offsite nature of delivery to the liver. To enhance the delivery to other tissues, namely the kidney, a form of pressurized injection (hydrodynamic-based delivery) was coupled with DNA polyplexation techniques to improve the effectiveness of the technique (Tros de Ilarduya et al., 2010). Even though these tools increased transfection efficiency compared to naked DNA transfections (Hayat et al., 2019), this process could not limit offsite genetic alterations (Rubin and Barry, 2020). Nevertheless, the original hydrodynamic injections technique showed great promise in advancing an ability to aid effective renal gene transfer. Altogether, these studies highlight the generational issues related to combining the appropriate vector with the delivery technique to provide efficient and targeted renal gene therapy.

In particular, hydrodynamic-based delivery increases the permeability of endothelial (Suda and Liu, 2007) and epithelial (Wang et al., 2000) junctions by non-adversely enhancing poration in plasma membranes. This transient process facilitates the cellular internalization of macromolecules of interest (Herweijer and Wolff, 2007). It has also been shown that the unique renal anatomy provides various innate delivery paths (renal artery, renal vein, and ureter) that may be ideal for hydrodynamic gene delivery (Xing et al., 2009), recalling the ability to facilitate efficient exogenous protein expression *in vivo* using plasmid reporter vectors (Corridon et al., 2013; Corridon et al., 2021). Based on these tenets, our group devised ways to examine the ability to alter functional protein activity with plasmid-based vectors by adapting the injection process to include a brief period of vascular cross-clamping. This adaptation focused on limiting or eliminating offsite genetic alterations, resulting in efficacious and targeted exogenous protein expression (Corridon et al., 2013).

After that, we aimed to alter functional protein activity that can be clinically significant to AKI. Specifically, this approach was formulated to induce benefits from ischemic pre-conditioning, which renders tissues resistant to subsequent deleterious effects of prolonged ischemia after previous exposure to vascular occlusion (Ishida et al., 1997). This pre-conditioning effect is linked to an innate organ-derived ability to withstand additional ischemic events after a non-lethal event (Murry et al., 1986). We have previously shown, using proteomic screens, that this non-lethal approach facilitates the upregulation of key mitochondrial proteins, including NADP + -dependent isocitrate dehydrogenase 2 (IDH2) (Kolb et al., 2018). IDH2 is the primary enzyme responsible for generating the mitochondrial NADPH pool critical for maintaining the mitochondrial antioxidant system (Lee et al., 2017). This system helps protect cells from potentially harmful reactive oxygen species. These results, in turn, provided a potential genetic target of clinical significance that may be used to alter proteomic expression using hydrodynamic-based approaches for therapeutic purposes.

Moreover, prior research has shown that rodents deficient in IDH2 observed a unique acceleration of renal senescence and substantial deterioration in structure and function *via* disruptions to redox status that promoted oxidative damage and apoptosis (Lee et al., 2017). Similar reductions in redox status are well-established consequences of ischemia-reperfusion injury (IRI), leading to AKI (Zhang et al., 2021). Yet, from a therapeutic point of view, we have previously altered the mitochondrial proteome *via* hydrodynamic IDH2 plasmid delivery. Such alterations have significantly upregulated IDH2 renal expression and conferred organ-wide protection against subsequent IRI in live rats in a manner that mimics IPC. Such focus on elucidating IDH2's protective role in that study also helped uncover how hydrodynamic IDH2-mediated exogenous expression increased the mitochondria membrane potential ($\Delta\psi_m$), maximal respiratory capacity, and intracellular ATP levels. Based on the success of these results, it is of value to extend the utility of hydrodynamic renal gene therapy by determining whether upregulating the expression of this key mitochondrial enzyme could boost recovery and halt the progression of AKI at the inception of such injury. Thus, herein, prerenal AKI was induced in rats using an IRI model, which is widely applied for both fundamental and therapeutic intervention studies of AKI (Le Clef et al., 2016), to help examine the associated therapeutic potential of hydrodynamic-based delivery known to elicit efficacious and targeted genetic alterations.

2 Materials and methods

2.1 Prerenal acute kidney injury

Male Sprague Dawley rats, 200–250 gm, were obtained from Harlan Laboratories (Indianapolis, IN, United States) and allowed free access to food and water. After anesthetization by intraperitoneal injections of sodium pentobarbital (50 mg/kg body weight), each animal was placed on heating pads to maintain normal physiological temperature. Midline incisions were performed to expose the renal hila. In this study, rats were subjected to a sham injury or either of two forms of AKI: mild and moderate. First, to induce a mild injury, the micro-serrefine clamps with delicate, atraumatic serrations (Fine Science Tools, Foster City, CA, United States) were used to bilaterally clamp the renal pedicles for 10–15 min to induce a mild injury. Second, the clamping period was 30–45 min to generate a moderate injury. The clamps were removed at the end of each injury induction period to reinstate renal blood flow and generate IRI. Last, animals in the sham (control) group underwent the same procedures without having their renal pedicle clamped. It should be noted that during the actual or sham clamping periods, the midline incisions were temporarily closed to prevent infection and support homeostasis. A schematic of the experimental workflow is presented in Figure 1.

2.2 Ischemic pre-conditioning

Similar to the induction of AKI, rats were again anesthetized in the manner described above and subjected to bilateral pedicle clamps to occlude renal blood flow for 30–45 min for IPC. The incisions were again temporarily closed during ischemia. The animals were then allowed to recover for 14 days, after which *in vivo* mitochondrial activity was examined. For such studies, kidneys were collected and analyzed for adaptations in mitochondrial activity and compared to control rats using immunoblotting techniques.

2.3 Serum creatinine and blood urea nitrogen measurements

Blood samples were collected from the rats in 1 mL Eppendorf heparin-treated tubes after making small incisions on their tails. These samples were centrifuged at 100,000–130,000 rpm for 10 min. The supernatants were then stored at 4°C. Quantitative determination of

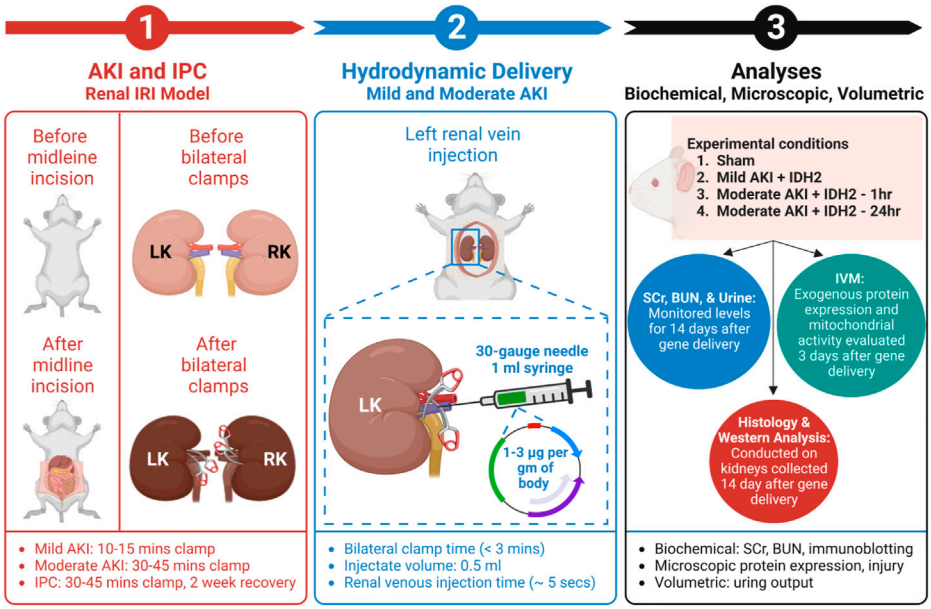

FIGURE 1
An outline of the experimental workflow. (1) This experimental approach began by subjecting animals to different degrees of IRI to induce AKI *via* bilateral renal pedicle clamps for periods to induce mild (occluded blood flow for 10–15 min) and moderate (occluded blood flow for 30–45 min) injuries, and IPC (occluded blood flow for 30–45 min). (Corridon et al., 2013) (2) The next step included hydrodynamic gene delivery for four experimental conditions by conducting rapid retrograde injections using vascular cross-clamping into the renal vein. The experimental conditions were sham injury, mild injury followed by hydrodynamic gene delivery 1 h after reperfusion (Mild AKI + IDH2—1h), moderate injury followed by hydrodynamic gene delivery 1 h after reperfusion (Moderate AKI + IDH2—1h), and moderate injury followed by hydrodynamic gene delivery 24 h after reperfusion (Moderate AKI + IDH2—24 h). The injections took approximately 5 s to deliver 1–3 µg per Gram of plasmid DNA per body weight suspended in 0.5 mL saline (Engel et al., 2019). (3) The last phase experiment relied on a series of biochemical, microscopic, and volumetric analyses to examine whether hydrodynamic gene delivery could upregulate IDH2 expression in the mammalian kidney and what effects altering the mitochondrial proteome in this manner could have on serum creatinine (SCr), blood urea nitrogen (BUN), and urine output levels, as well as the renal mitochondrial membrane potential ($\Delta\psi_m$) and renal microarchitecture. LK, left kidney; RK, right kidney; IVM, intravital microscopy; and IDH2, isocitrate dehydrogenase [NADP], mitochondrial.

creatine kinase activity in serum was then estimated with Pointe Scientific CK (Liquid) Reagents (Point Scientific, Inc., Canton, MI, USA). Serum creatinine (SCr) measurements were performed with a Beckman Creatinine Analyzer 2 (Beckman Instruments, Brea, CA, USA) according to the manufacturer's specifications and reported in milligrams per deciliter (mg/dL). Sera blood urea nitrogen (BUN) measurements were made using the Liquid Urea Nitrogen Reagent Set (Pointe Scientific, Canton, MI, United States), whereby the working reagent was prepared by mixing five parts of the enzyme reagent (R1) with 1 part of coenzyme (R2) reagent. Approximately 10 µL of each serum sample was added to the working reagent (1,000 µL), and the absorbance was immediately measured using a microplate reader. The levels of these metabolites were measured before all forms of IRI were induced and monitored across the subsequent 14 days to investigate the effect of IDH2 hydrodynamic-based injections.

2.4 Urine output measurements

Rats were also housed separately in metabolic cages (Fisher Scientific, Hampton, NH, USA) to allow standard volumetric measurements of individual urine outputs collected daily in falcon tubes without intervention. The animal committee approved the studies using the metabolic cages, and the animals were checked daily and independently by the researcher and the animal housing staff for signs of stress; if any adverse conditions were identified, they would have been excluded from the study.

2.5 Intravital multiphoton fluorescence microscopy

Intravital microscopy (IVM) and its fundamentals are well outlined in the literature (Burne-Taney et al., 2005; Molitoris and Sandoval, 2005; Tanner et al., 2005; Ashworth et al., 2007; Dunn et al., 2007; Corridon et al., 2013; Hall et al., 2013; Corridon et al., 2021; Cai et al., 2022; Corridon, 2022a; Shaya et al., 2022). However, briefly, after sedation, vertical flank incisions externalized each rat's left kidney, which was then placed inside a glass bottom dish containing saline. This imaging dish was set above a X60 water immersion objective which supported the acquisition of fluorescent micrographs from an inverted Olympus FV 1000-MPE microscope equipped with a Spectra-Physics MaiTai Deep See laser tuned to an 800–850 nm excitation wavelength (Olympus, Tokyo, Japan). The system was connected to external detectors for multiphoton imaging, and dichroic mirrors for the collection of blue, green, and red emissions.

2.6 Hydrodynamic injections

In this study, the following four experimental groups of rats were subjected to hydrodynamic injections performed with vascular cross-clamping: sham injury; mild injury followed by hydrodynamic gene delivery 1 h after reperfusion; moderate injury followed by hydrodynamic gene delivery 1 h after reperfusion; and moderate injury followed by hydrodynamic gene delivery 24 h after reperfusion. For this injection process, midline incisions allowed the isolation of the left renal vein, with a 4–0 silk loop, in each sedated rat. The renal artery was occluded first and followed by the renal vein, using the micro-serrefine clamps. The vein was then gently elevated, and 0.5 mL infusates were rapidly injected distal to the clamp using a 30-gauge needle within roughly 5 s. Pressure was then applied to the injection site for approximately 3 min to induce hemostasis. The venous clamp was removed, followed by the arterial clamp, and the animal was prepared for recovery.

The various infusates were prepared as follows. For the toluidine blue infusates, stock solutions were prepared by dissolving 50 mg of tolonium chloride dye (Toluidine Blue O, Electron Microscopy Sciences, Fort Washington, PA, United States) in 5 mL of 0.9% saline, of which 0.5 mL was used for each injection. This infusate was used to examine whether this targeted injection process could support exogenous macromolecular confinement to the injected kidney.

Infusates of fluorescent dextrans comprised of 0.5 mL saline containing 4 kDa (low molecular weight) fluorescein isothiocyanate, FITC, and 150 kDa (large molecular weight) Tetramethylrhodamine-isothiocyanate, TRITC, dextrans (TdB Consultancy, Uppsala, Sweden), and 30 µL of Hoechst 33,342 (Invitrogen, Carlsbad, CA, United States), which was applied to identify cellular nuclei within the tubular epithelium). These infusates were used to investigate the subcellular incorporation of the exogenous macromolecules into the renal epithelium, as well as renal structure and function in the injury models.

Fluorescent plasmid DNA infusates were used to investigate live and subcellular incorporation of the exogenous macromolecular and renal structure and function in the injury models. These fluorescent infusates were prepared by suspensions in saline using Qiagen Maxi Prep systems (Qiagen, Chatsworth, CA, United States). These plasmids encoded enhanced green fluorescent protein (EGFP)-actin (Clontech Laboratories, Inc., Mountain View, CA, United States). This pAcGFP1-actin vector expressed the Aequorea coerulescens GFP(AcGFP1)-actin fusion protein in mammalian cells. The protein is incorporated into growing actin filaments and allows for the visualization of actin-containing subcellular structures. Likewise, non-fluorescently labeled plasmid vectors that encode mitochondrial enzymes isocitrate dehydrogenase [NADP], mitochondrial, IDH2, (OriGene Technologies, Inc., Rockville, MD, United States) were also used in this study. The IDH2 vector was a Myc-DDK-tagged ORF clone of *Homo sapiens* isocitrate dehydrogenase 2 (NADP+), mitochondrial (IDH2), nuclear gene encoding mitochondrial protein as transfection-ready DNA. Moreover, each transgene solution was prepared by suspending 1–3 µg of plasmid DNA per Gram of body weight of either plasmid vectors in 0.5 mL of saline, as outlined in previous related studies (Corridon et al., 2013; Collett et al., 2017; Kolb et al., 2018; Corridon et al., 2021).

2.7 *In vivo* estimations of exogenous gene expression

In order to estimate the degree of transgene expression that resulted from the pressurized injection process, intravital micrographs were used to determine the proportion of renal segments that expressed the transgenes. For this process, micrographs were acquired from three adjacent intravital fields and were randomly chosen from each live kidney within a given experimental group. A segment was considered transfected if at least one of its cells expressed the EGFP-actin plasmid vector. Using ImageJ software (National Institute of Mental Health, NIH, Bethesda, MD, United States), transgene fluorescence signals were identified with intensities at least double those of autofluorescent signals. With this criterion, the percentage of segments that expressed the reporter transgenes within fields acquired with the X60 objective was calculated as the average percentage of transfected segments within the randomly chosen nephron cross-sections.

2.8 *In Vivo* estimations of the renal mitochondrial membrane potential

To study *in vivo* mitochondrial activity, a stock solution of tetramethyl rhodamine methyl ester, TMRM (Invitrogen Molecular probes, Eugene, OR, United States) was prepared by suspending 5 µg of the dye in 2 mL of saline. An incision was made to expose the jugular vein. The vein was isolated with two 3–0 or 4–0 silk loops. The superior loop was tied and clamped with a pair of hemostats to stiffen and elevate this vein. A PE-50 polyethylene catheter tubing (Clay Adams, Division of Becton, Dickson and Company, Parsippany, NJ, USA) was attached to a 1 mL syringe containing the TMRM injectate was inserted into a minor incision in the jugular vein. The other silk loop was used to anchor the catheter in the vein. The plasma membrane-permeant TMRM dye was slowly infused into the vein, and intravital imaging was performed once a steady state was established to estimate the renal mitochondrial membrane potential ($\Delta\psi_m$). To estimate renal mitochondrial membrane potential ($\Delta\psi_m$), mean fluorescent intensities from TMRM-labelled mitochondria were computed from each tubule within three adjacent intravital fields randomly chosen from each live kidney within a given experimental group using ImageJ software.

2.9 Histological assessments

After fixation with 4% paraformaldehyde for 24 h at 4°C, the kidney samples were immersed in formalin, which was phosphate-buffered, for 24 h. The samples were kept at room temperature and then rinsed with distilled H_2O. After washing, they were stored in 70% ethanol at room temperature and then subjected to dehydration *via* a gradation of ethanol solutions that ranged from 70%–100%, with increments of 10%. Clearing with xylene and infiltration with paraffin (four paraffin changes under vacuum at 59°C for 45 min each) followed. The samples were then embedded in fresh paraffin for sectioning to produce around 5 µm thick sections with a Reichert-Jung 820 microtome (Depew, NY, United States). These sections were counterstained with hematoxylin

and eosin (H&E) and imaged with an X60 objective mounted on a Nikon Microphot SA Upright Microscope (Nikon, Tokyo, Japan). The degree of injury associated with each treatment condition was estimated as a percentage of the injured cells within the micrographs collected. Specifically, these percentages were computed as ratios of cells with disrupted/adversely altered plasma membranes to the total number of cells in a micrograph and averaged across three randomly chosen micrographs for each animal.

2.10 Western blot analysis

Whole kidneys were collected from anesthetized rats and cryofixed in liquid nitrogen. Post cryofixation, transverse sections of roughly 300 mg, extending from the cortex to the pedicle, were obtained and homogenized in 300 µL RIPA buffer using Dounce homogenizer on ice and the lysate was spun at 13,000 g for 20 min in a 4°C pre-cooled centrifuge. Bicinchoninic acid assays were then performed to determine the protein concentration, and denatured protein samples were acquired by adding equal volumes of 2X Laemmli Sample Buffer at 70°C for 5 min. After which 5 ug of each protein sample was loaded on 10% SDS-PAGE gel, along with molecular weight markers, and ran for 50 min at 240 V. Protein samples were then transferred from the gel to the membrane for approximately 30 min at 24 V, which preceded overnight membrane blocking that occurred the at 4°C using TBS blocking solution with 3% FBS.

The next day, the membrane was incubated with 1:1,000 dilution of primary antibody (Rabbit PolyAb Anti-IDH2 (Novus Biologicals, Littleton, CO, United States) in TBS blocking solution with 0.3% FBS for 1 h at room temperature and washed then three times with TBS for 5 min. The membrane was then incubated with 1:40,000 dilution of the secondary antibody HRP D&R in TBS blocking buffer with 0.3% FBS at room temperature for 1 h, and the gel was washed three times with TBS. Finally, the blots were incubated in the enhanced chemiluminescence (ECL) reagents, SuperSignalTM West Pico Chemiluminescent Substrate (Thermo Fisher Scientific, Waltham, MA, United States), to facilitate image acquisition.

2.11 Statistical analysis of data

The Kruskal–Wallis one-way analysis of variance (ANOVA) with the *post hoc* pairwise Dunn's test was applied as appropriate to examine levels of exogenous gene expression, SCr, BUN, urine output, $\Delta\psi_m$, and cellular injury. These analyses were conducted at a $p < 0.05$ level of significance and the data are presented as the mean ± SD.

3 Results

3.1 Hydrodynamic renal fine needle injections support widespread and targeted delivery of exogenous probes in rats with mild and moderate AKI

Whole kidneys were extracted from euthanized rats after they received hydrodynamic delivery of 0.5 mL of toluidine blue dye. These kidneys were harvested and sectioned within 20 min of injections, revealing substantial and localized dye uptake in all four examined conditions:

- sham injury;
- mild injury followed by delivery 1 h after reperfusion;
- moderate injury followed by delivery 1 h after reperfusion; and
- moderate injury followed by delivery 24 h after reperfusion.

In each case, the dye appeared throughout the cortex and medulla of the left kidneys and was absent in the contralateral kidneys, as shown in various digital photographs (Figure 2). These results illustrate the ability to facilitate localized delivery to the kidney using hydrodynamic-based delivery with vascular cross-clamping in rats with sham and mild injuries and in animals with substantially greater degrees of injury.

3.2 Retrograde hydrodynamic injections facilitate the delivery of large and low molecular weight dextrans in rats with mild and moderate AKI

Compared to the macroscopic (visible) evidence provided in the previous section, intravital micrographs obtained from sham injured rats (Figure 3A) approximately 20 min after hydrodynamic infusions of infusates with dextrans and Hoechst stains also illustrated the robust uptake of each fluorescent tag. These images were obtained after this period to allow for homeostasis after the injection process. Intense TRITC-derived signals (red-based fluorescence) from the large molecular weight dextran were confined to the vasculature, which is consistent with normal/minimally altered function (Dunn et al., 2003; Molitoris and Sandoval, 2005; Dunn et al., 2007). At the same time, FITC-conjugated low molecular weight dextran molecules lined brush borders. These green, fluorescent molecules appeared as internalized puncta within the proximal tubule epithelium and concentrated within the distal tubular lumen (seen as a substantial degree of the green fluorescence that filled the lumen of this nephron segment). These observations provide evidence of widespread delivery of exogenous materials in the sham group and intact structural and functional renal capacities.

Similarly, there was clear evidence of widespread renal delivery of the exogenous probes observed in animals with mild and moderate forms of injury. For instance, in the mildly injured rats, there was evidence of impaired filtrative capacities based on the simultaneous presence of both FITC and TRITC dyes in the lumens of proximal and distal tubules (Figure 3B), as well as the reduced intensity of the large molecular weight TRITC dextran within the peritubular vasculature. Additionally, the reduced levels of the low molecular weight FITC dextran molecules that normally line the proximal tubule's brush border highlighted alterations to this epithelium's innate endocytic capacities. There was also evidence of cellular injury outlined by the low level of Hoechst-labelled nuclei within tubular lumens.

As expected, the injury levels escalated with moderate IRI-derived injuries. There was still a substantial and widespread presence of the FITC and TRITC dyes, yet their localization differed from the sham and mild conditions. In particular, there was a far greater degree of inhomogeneous and composite TRITC and FITC fluorescent-based signals emanating from the peritubular vasculature and lumens illustrated by the reduced levels of fluorescence in the vasculature seen in the fields obtained from the moderately injured rats, 1 h post-reperfusion, and the presence of intense of yellow-based fluorescence, blebs, and cellular nuclei within the lumens (Figure 3C). Likewise,

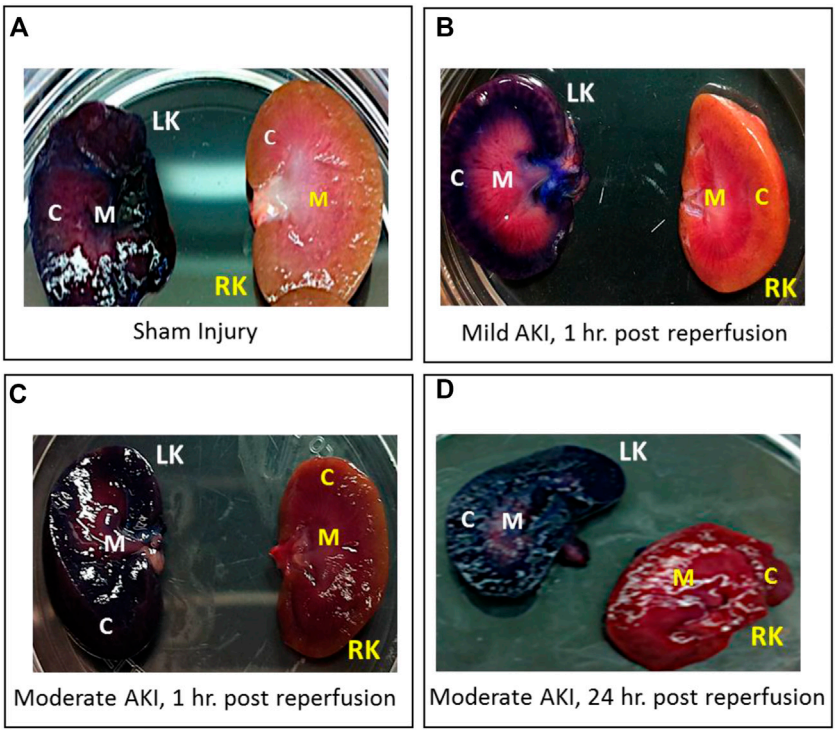

FIGURE 2
Digital photographs were used to illustrate the localized and widespread delivery resulting from renal vein hydrodynamic injections performed in **(A)** Sham injured rats and those with **(B)** mild AKI (injections performed 1 h after inducing AKI), **(C)** moderate AKI (injections performed 1 h after inducing AKI), and **(D)** moderate AKI (injections performed 24 h after inducing AKI). These kidneys were harvested and sectioned within 20 min of performing the injections. The dye appeared throughout the cortex and medulla of the left kidneys and was absent in the contralateral kidneys. LK = left kidney, RK = right kidney, C = cortex, and M = medulla.

atypical, brown-based fluorescence lined the peritubular vasculature of the moderately injured rats that received hydrodynamic-based injections 24 h post-reperfusion (Figure 3D). The tubular lumens also contained higher levels of TRITC and FITC dye composites and detached nuclei. Such deformation of tubular epithelial nuclei and their atypical presence in the lumen are hallmarks of IRI-induced AKI (Corridon et al., 2021). Again, additional signs of impaired filtration are presented and depicted by the reduced concentrations of FITC molecules and blebs within distal tubule lumens known to stem from IRI (Hall and Molitoris, 2014). Beyond the aspects mentioned above related to injury, it was essential to observe signs of the incorporation of the TRITC dextran molecules in the tubular epithelia. As a result, these images provided evidence that this injection technique can effectively deliver various macromolecules across the nephron in the various injury models.

3.3 Intravital microscopy and Western blot analysis demonstrate that hydrodynamic gene delivery induces exogenous renal protein expression and upregulates IDH2 activity in rats with mild and moderate AKI

It should also be noted that the intravital investigations were limited to proximal and distal tubular compartments, as these segments are easily accessible within the IVM system's 100–200 µm imaging depth, while the superficial glomeruli are rare in the strain of rat. Multiphoton micrographs presented in Figure 4 reveal enhanced EGFP-actin-derived fluorescence signals within proximal and distal tubule epithelia from the sham and AKI model rats 3 days after gene delivery. This time point was chosen based on previous characterizations that outline the potential to induce stable exogenous gene expression as early as this period after gene transfer (Corridon et al., 2013). At that time, distinctive fluorescent patterns were observed along proximal tubule brush borders and within distal tubular epithelial cells of sham (Figure 3E) and mildly injured (Figure 3F) animals. In comparison, these patterns were absent in the renal compartments of rats subjected to moderate IRI. As anticipated, moderate AKI induced substantial disruptions to the typical renal architecture, which provides clear means to differentiate proximal ad distal tubular segments in the strain of rats used for this study. Nevertheless, IRI-derived injury made it challenging to make routine morphological distinctions between proximal and distal segments.

Additionally, the different rates of transgene expression in live renal segments were determined from the percentage of renal segments within a microscopic field that expressed the transgenes (Figure 4I). Again, a segment was considered transfected if at least one of its cells expressed the EGFP fluorescent transgenes. These estimations provided approximately 30%–40% transfection efficiency rates in the superficial cortex accessible by intravital multiphoton microscopy in rats that received moderate IRI (32.8% in the rats that received hydrodynamic gene delivery 1 h after reperfusion and 30.4% in the rats that received hydrodynamic gene delivery 24 h after reperfusion). These estimated efficiencies were lower than those obtained for sham (51.4%) and mildly injured (43.0%)

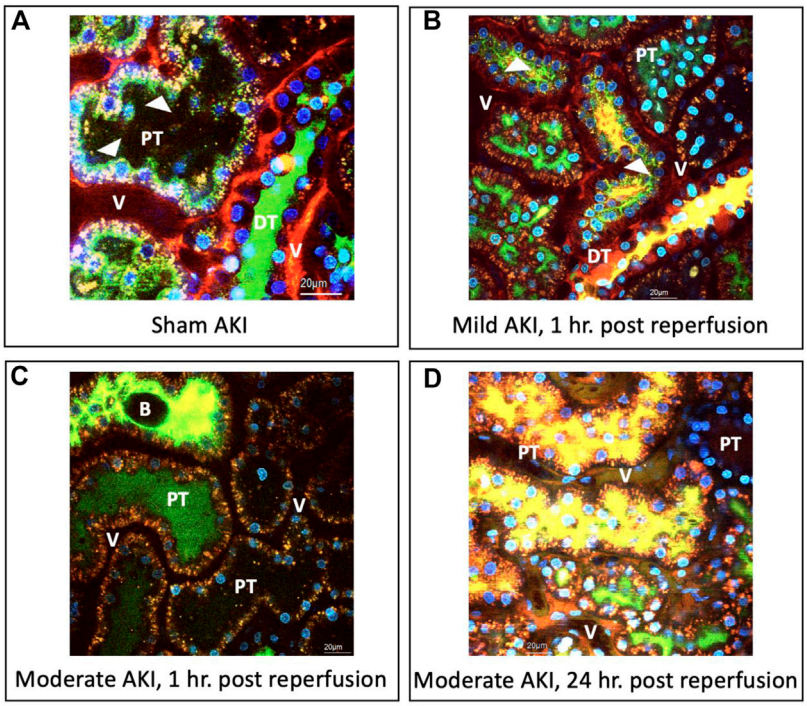

FIGURE 3
Intravital micrographs illustrate the incorporation of macromolecules by various renal compartments resulting from renal vein hydrodynamic injections performed in **(A)** sham injured rats and those with **(B)** mild AKI (injections performed 1 h after inducing AKI), **(C)** moderate AKI (injections performed 1 h after inducing AKI), and **(D)** moderate AKI (injections performed 24 h after inducing AKI). These micrographs were acquired from live rats within 20 min of receiving hydrodynamic infusions of 0.5 mL saline containing 4 kDa FITC and 150 kDa TRITC dextrans, and Hoechst 33,342 (this image A was acquired with 1.5X digital zoom to illustrate better the dynamic events outlined). The arrowheads highlight regions where the fluorescent dextran molecules appear to bound brush borders or endocytosed puncta within tubular epithelial cells. All images were taken using a blend of the red-, green-, and blue-pseudo-color channels. DT, distal tubule; PT, proximal tubule; and V, vasculature; and B, bleb, observed within the tubular lumen.

rats, whose transgene expression rates were roughly 50%. However, no significant difference (p = 0.392) was detected in the levels of transgene expression among the groups, indicating the potential of this technique to induce genetic alterations throughout the diseased kidney.

Western blot analyses were performed to examine further genetic alterations that could have resulted from hydrodynamic-gene delivery and IPC. These blots are presented in Figure 4J. Control data obtained from the Western analyses illustrate the consistent and intense levels of actin expression in regions that correspond to the molecular weight of actin (≈42 kDa) molecules in all groups. These results are consistent with the innate presence of actin within the kidney. In comparison, such analyses also revealed enhanced and distant bands in regions corresponding to the molecular weight of IDH2 (≈47 kDa) molecules, indicating the upregulation of IDH2 expression in kidneys 3 days after receiving hydrodynamic delivery and 14 days after IPC compared to the levels of IDH2 expression detected in control (sham) kidneys.

3.4 Enhanced mitochondrial activity observed in rats treated with IDH2 plasmid DNA and ischemic-preconditioning

In order to gain physiological insight into the effects of IDH2 upregulation in these injury models, mitochondrial activity was investigated in various groups of live rats 3 days after hydrodynamic gene delivery of IDH2 and 14 days after IPC. Intravital measurements of the mean fluorescent intensities were obtained approximately 20 min after the jugular infusion of the mitochondrial membrane potential-dependent dye, TMRM. These investigations revealed substantial elevations in TMRM-based fluorescence signals obtained from kidneys that received IDH2 gene transfer (5C through 5E) and IPC (Figure 5B), compared to the sham group (Figure 5A). Specifically, enhancements in mitochondrial activity exceeded factors of 13 ($p < 0.001$ at T_{1hr}) and 11 ($p < 0.001$ at T_{24hr}) when IDH2 hydrodynamic-based treatments were applied to 1h and 24 h after inducing moderate AKI.

Such results illustrate a potential increase in mitochondrial activity related to the upregulation of the mitochondrial enzymes facilitated by hydrodynamic-derived gene delivery and ischemic pre-conditioning, which are consistent with the previous studies (Kolb et al., 2018). This upregulation in mitochondrial enzyme activity was confirmed using Western analysis (Figure 4J). Moreover, the combination of Hoechst 33342-based and TMRM-based staining was used to further examine alterations to the innate renal ultrastructure. The probes highlighted cellular sloughing from the tubular epithelium, cast formation within the tubular lumen, and collapsed tubules. Interestingly, such enhancements to the mitochondrial proteome occurred despite substantial deformation to the renal microarchitecture. As anticipated, lower degrees of injury were observed in the animals subjected to sham and mild injuries.

Furthermore, non-parametric statistical analyses using the Kruskal-Wallis ($p < 0.001$) revealed significant differences among these TMRM-based fluorescent intensities. At the same time, Dunn's *ad hoc* test only indicated significant differences between the means of sham injured rats

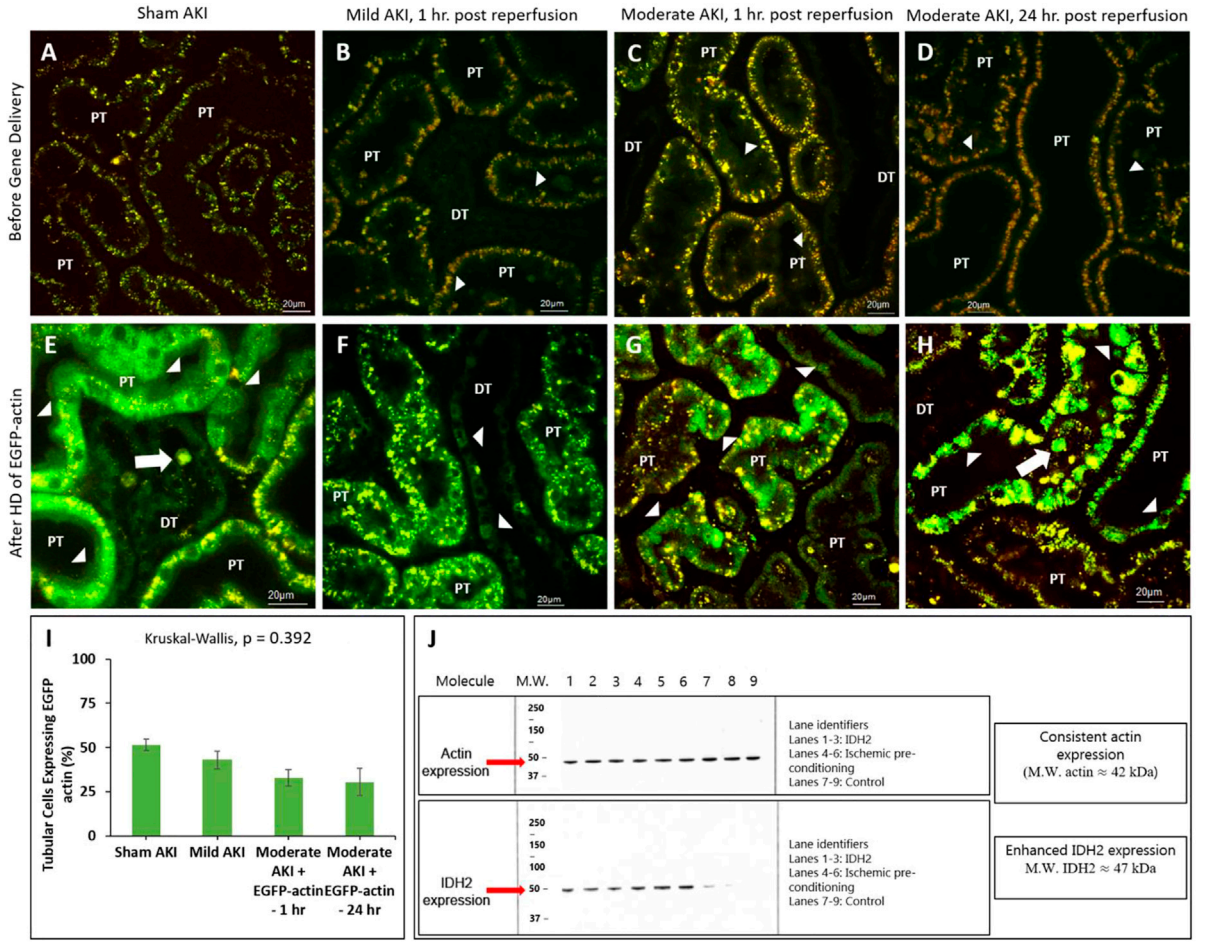

FIGURE 4
Hydrodynamic injection derived fluorescent actin expression. Intravital micrographs illustrate the hydrodynamic delivery-based expression of EGFP-actin in various settings. In sham rats **(A)** before and **(E)** after gene delivery. In rats subjected to mild AKI (injections performed 1 h after inducing AKI), **(B)** before and **(F)** after gene delivery. In rats subjected to moderate AKI (injections performed 1 h after inducing AKI), **(C)** before and **(G)** after gene delivery. In rats subjected to moderate AKI (injections performed 24 h after inducing AKI), **(D)** before and **(H)** after gene delivery. The arrowheads highlight regions where the fluorescent actin expression is highlighted along the brush border and within cuboidal distal tubule cells. The arrows pinpoint fluorescent casts/debris within the tubular lumen. Image E was acquired with 1.5X digital zoom to highlight these details further. All micrographs were taken 3 days after gene delivery using a blend of the red- and green-pseudo-color channels to distinguish the true presence of EGFP-based fluorescence. **(I)** Comparison of the levels of exogenous gene expression induced by the hydrodynamic technique determined from IVM data. **(J)** Western blots illustrate the enhanced expression of IDH2 in kidney tissues harvested from rats 3 days after hydrodynamic injections of the IDH2 plasmids (lanes 1 through 3) and IPC (lanes 4 through 6) compared to the control group that received sham injections (lanes 7 through 9). n = 3 for all groups. DT, distal tubule and PT, proximal tubule.

and rats with mild injuries followed by hydrodynamic gene delivery 1 h after reperfusion (Mild AKI + IDH2—1 h), $p < 0.001$, rats with moderate injuries followed by hydrodynamic gene delivery 1 h after reperfusion (Moderate AKI + IDH2—1 h), $p < 0.001$, and rats with moderate injuries followed by hydrodynamic gene delivery 24 h after reperfusion (Moderate AKI + IDH2—1 h), $p = 0.001$ (Figure 5F).

3.5 SCr, BUN, and urine output indicate that hydrodynamic injections of IDH2 plasmids boost recovery and halt the functional progression of AKI despite increased levels of structural damage

Biochemical (Figures 6A, B) and volumetric (Figure 6C) analyses demonstrated the restorative effect that upregulated IDH2 expression provided since, on average, SCr levels (≈60%, $p < 0.05$ at T_{1hr}; ≈50%, $p < 0.05$ at T_{24hr}) and blood urea nitrogen (≈50%, $p < 0.05$ at T_{1hr}; ≈35%, $p < 0.05$ at T_{24hr}) were decreased. Furthermore, SCr and BUN measurements show how hydrodynamic IDH2 plasmid delivery 1 and 24 h after inducing moderate IRI in live rats significantly blunted the normal elevated injury response. Strikingly, hydrodynamic plasmids injections administered at the 24-h mark resulted in faster returns to normal baseline levels. This return to baseline occurred as early as 3 days after the initial insult, compared to 7 days in the groups that did not receive hydrodynamic injections of the key mitochondrial enzyme, IDH2. Additionally, providing these injections at the 1-h mark after inducing moderate AKI lowered the variations in these biomarkers significantly and halted the injury's effect, and creatine and BUN values stayed within the normal range. The data presented an analogous effect on urine output as pairwise comparisons revealed an average increased urine output (≈40%, $p < 0.05$ at T_{1hr}; ≈26%, $p <$

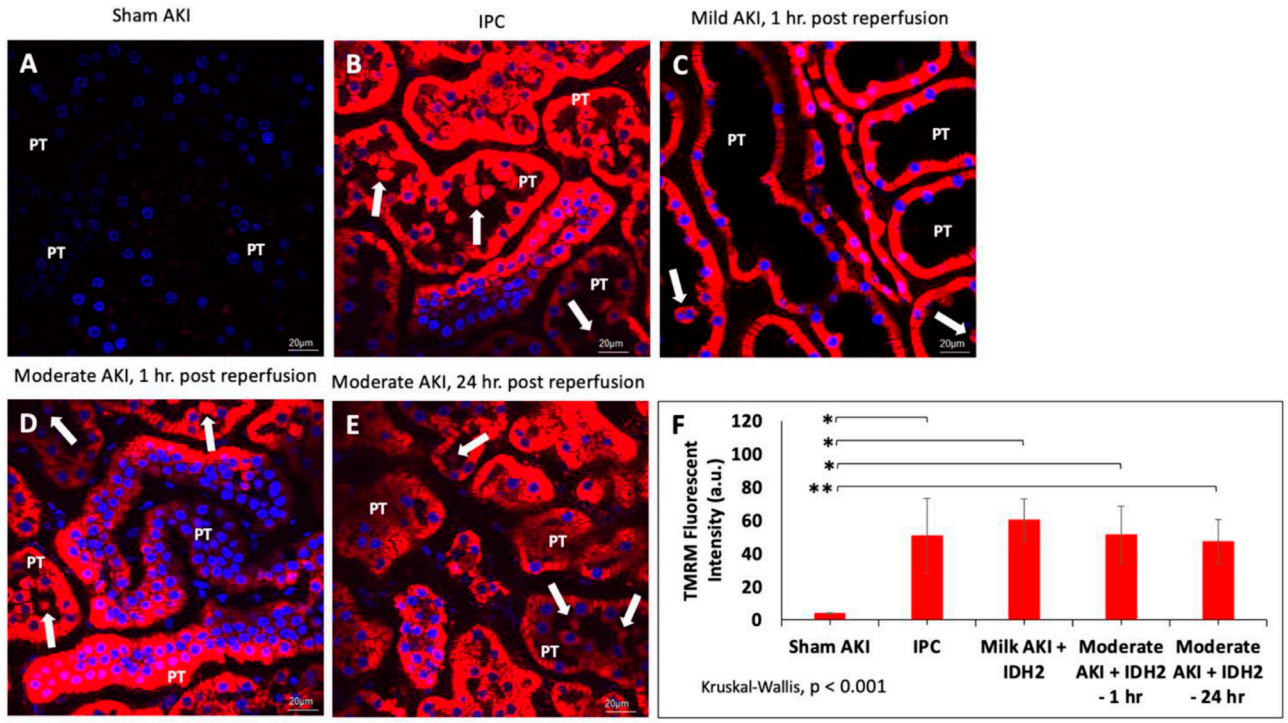

FIGURE 5
Mitochondrial membrane potential activity was examined in nephron segments of various live rats *via* TMRM-labeled signaling in **(A)** sham animals; **(B)** IPC animals; **(C)** animals with mild AKI that received hydrodynamic injections of IDH2 1 h after inducing IRI for 10–15 min; and **(D)** animals with moderate AKI that received hydrodynamic injections of IDH2 1 h after inducing IRI for 30–35 min; and animals with moderate AKI that received hydrodynamic injections of IDH2 24 h after inducing IRI for 30–35 min. **(E)** The mean TMRM -based fluorescent intensity from each experimental condition (n = 10 tubules per rat). The arrows pinpoint fluorescent casts/cellular debris within the tubular lumen. PT, proximal tubule. **(F)** Mean TMRM fluorescent intensities that were recorded from the various experimental groups. Scale bar, 20 μm, * represents $p < 0.001$, and ** represents $p = 0.001$.

0.05 at T_{24hr}). The volumetric data appeared to support the urinalysis directly.

Conversely, histological assessments provided further insight into the damage that resulted from these experimental conditions (Figure 7; Table 1). Mild degrees of morphological injury were observed in the Sham AKI (Figure 7A) and mild AKI (Figure 7B) groups. Interestingly, comparable injuries were observed with each corresponding case that accompanied hydrodynamic delivery of IDH2 plasmid vectors, i.e., there were no significant differences between the levels of injury observed between the AKI and AKI + IDH2 groups ($p \not< 0.05$), and the mild AKI and mild AKI + IDH2 groups ($p \not< 0.05$). Whereas more substantial levels of structural damage were detected in the animals subjected to moderate forms of injury (Figure 7C). Again, analogous injury levels were also detected between the moderate AKI group and the moderate AKI group that received hydrodynamic IDH2 plasmid injections 1 h ($p \not< 0.05$) and 24 h ($p \not< 0.05$) after inducing IRI.

Previous characterizations of the injection process performed with vascular cross-clamping have outlined that the hydrodynamic forces and brief ischemia-reperfusion injury generated from this 3-min process are associated with a minor level of injury, far lower than that what is derived from the mild form of AKI, which was induced with 10–15 min of IRI (Corridon et al., 2013). Also, the concentration of the plasmid vectors used in this study is not known to induce appreciable pathogenicity and toxicity. As a result, comparisons made among these groups of animals could be used to demonstrate that the injection process or the transgene expression did not adversely affect morphology. Notably, the degrees of structural damage observed in the sham, mild, and moderate experimental conditions (with and without IDH2 treatments) are consistent with these forms of injury. Thus, it can be inferred, in combination with the SCr and BUN analyses, that no further substantial degree of injury could have resulted from the injection process.

Yet, extensive disruptions to proximal tubular brush border integrity and distal tubular and glomerular deformation produced significantly elevated average histology injury scores (≈40%, $p < 0.05$ at T_{1hr}; ≈40%, $p < 0.05$ at T_{24hr}). These results coincide with the fact that renal IRI is a dynamic process characterized by endothelial and epithelial cellular injury, inflammation, and hemodynamic alterations (Bonventre and Yang, 2011). Within proximal nephron segments, several essential and high energy demand ATP-dependent transport processes are eliminated by this form of injury (Vormann et al., 2022). Typically, the proximal tubule is the main site of injury in renal IRI, and the injuries observed herein coincide with reductions in oxygen associated with diminished renal blood flow. While this segment contains a high density of mitochondria, it lacks anaerobic ATP-generating capacity and is thus quite vulnerable to such oxygen supply disruptions (Hall and Molitoris, 2014).

Even though IRI is widely associated with tubular damage, this form of injury also induces significant podocyte effacements and disruptions of slit diaphragms (Wagner et al., 2008), which can lead to atypical filtrative capacities observed in these intravital

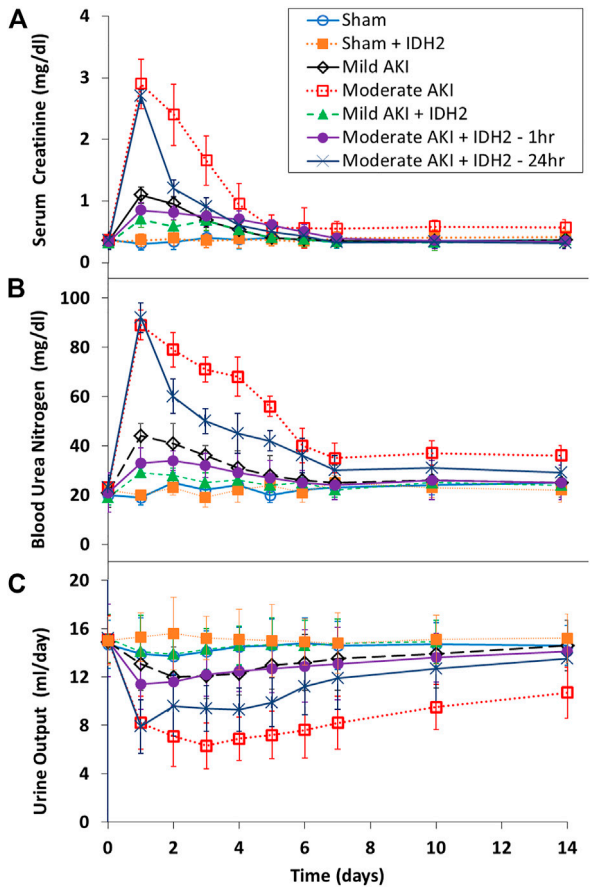

FIGURE 6
Blood biochemical and urine volumetric analyses. A comparative view of the restorative effects of upregulating IDH2 renal expression *via* hydrodynamic injections on **(A)** serum creatinine, **(B)** blood urea nitrogen, and **(C)** urine across the 14-day measurement period compared to characteristic injury responses. n = 3 for all groups.

studies. On the other hand, distal tubules have far greater glycolytic capacities than their proximal counterparts, which supports their ability better to maintain the $\Delta\psi_m$ and mitochondrial structure during ischemia (Hall et al., 2009). Likewise, prerenal flow reductions can also reduce GFR by limiting glomerular perfusion and increasing tubular obstruction due to necrotic and sloughed tubular epithelial cells (Burek et al., 2020), as observed in the intravital micrographs (Figure 3 through Figure 5).

4 Discussion

AKI is a severe medical condition that results in approximately 1.7 million deaths worldwide each year (Vormann et al., 2022). Treatments that can rapidly restore renal function are attractive options to help reduce the global burden of kidney diseases. Current AKI treatment regimens are mainly supportive and cannot halt the illness's progression into chronic and end-stage conditions. Thus, there is a need for alternative treatments, like gene therapy (Pantic et al., 2022a; Wang et al., 2023; Pantic et al., 2023a; Khan et al., 2023). This form of therapy provides a means to treat and prevent the root cause of a given condition. Over the years, several methods have been proposed to elicit efficient gene transfer in various settings (Corridon, 2022b; Corridon et al., 2022; Davidovic et al., 2022; Wang et al., 2022a; Wang et al., 2022b; Corridon, 2023; Pantic et al., 2023b; Shakeel and Corridon, 2023). However, progress in the development of direct gene transfer methods in the kidney has been limited compared with other organs. This issue is partly due to the need to understand better the biological factors needed to promote efficient vector entry into the cell and the complex anatomical structure of the kidney (Davis and Park, 2019).

Recently, plasmid-based hydrodynamic gene delivery has shown promise in overcoming this issue (Corridon, 2023). Therefore, this study aimed to demonstrate the potential of hydrodynamic-based gene delivery to halt progressive or persistent renal function impairment following episodes of ischemia-reperfusion injuries. The approach presented in this manuscript is based on the transfer of an essential enzyme *via* a plasmid vector at the inception of IRI-based injuries to boost renal recovery. In this first instance, it was essential to identify whether this rapid injection technique, augmented with vascular cross-clamping, could provide widespread and targeted renal vector delivery.

In order to achieve this goal, various attempts were made to examine the possibility of extending previous successful applications using this delivery technique to upregulate the level of mitochondrial enzymatic activity. From a mechanistic perspective, hydrodynamic injections of 0.5 mL of tolonium chloride solutions revealed robust distributions of this pigment across the injected kidney and no visible traces within the right contralateral kidney. Additionally, the localization of the large molecular weight dextran molecules within the damaged tubular epithelium, illustrated the potential to facilitate the cellular internalization of exogenous plasmids of comparable size using this technique (Corridon et al., 2013; Nishi et al., 2017). These macroscopic and microscopic evaluations provided sufficient evidence that the injection process could facilitate widespread and targeted delivery of the vector to the kidney.

The next phase of the study focused on the actual delivery of plasmid vectors and their resulting expression rates, using EGFP-actin reporter plasmids. IVM also allowed the *in vivo* visualization of the reporter transgene expression, and it was reassuring to detect significant and comparable rates of fluorescent protein expression in the injury models, especially for the moderate forms of AKI. From the estimated transfection rates in the injured rats, it is conceivable that ischemia-reperfusion injury, which is known to promote vasculature and cellular permeability, may have afforded an increased passage of exogenous material across denatured membranes. This phenomenon may have also directly enhanced the internalization of plasmids/exogenous probes in the possible absence or reduction of innate endocytic capacities and supports a similar rationale for the transgene expression observed in rats with injured glomeruli using viral vectors (Kelley and Sukhatme, 1999).

Earlier on, hydrodynamic gene delivery was initially conducted on mice. However, there is a clear advantage in performing renal-targeted hydrodynamic gene delivery in rats compared to mice due to the relative ease in executing intricate intravascular injections in rats and inducing hemostasis post-injection without inducing further bouts of ischemic injury and damage to the smaller and more delicate mouse renal vein. Moreover, a growing body of evidence suggests that gender differences exist in cardiovascular responses to significant alterations to normal circulatory conditions, including vascular occlusive cases and hypertension

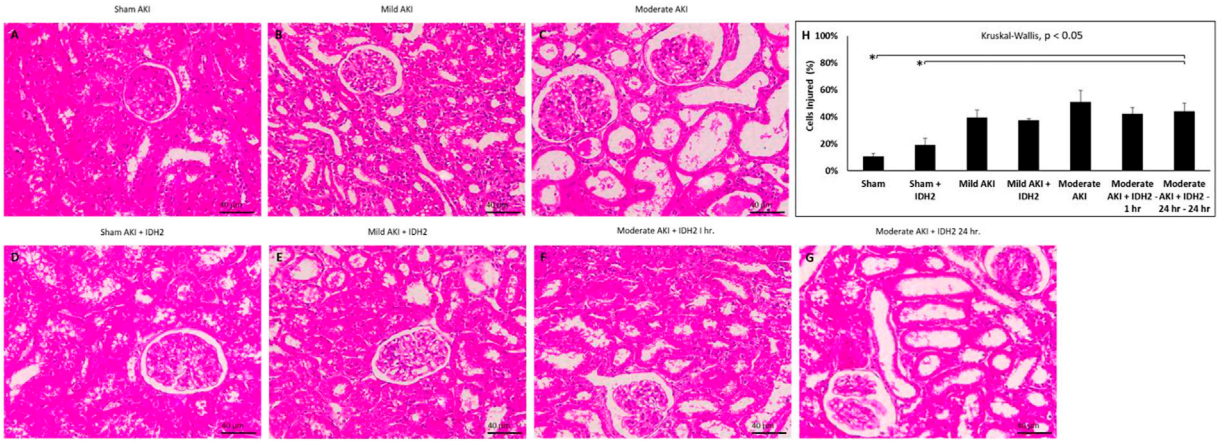

FIGURE 7
Histological assessments. X60 brightfield images of cortical sections from **(A)** sham AKI, **(B)** mild AKI, **(C)** moderate AKI, **(D)** Sham AKI + IDH2, **(E)** mild AKI + IDH2 (HD 1-h post-reperfusion), **(F)** moderate AKI + IDH2 (HD 1-h post-reperfusion) **(G)** moderate AKI + IDH2 (HD 24-h post-reperfusion). **(H)** Comparison of the injury levels observed in tubular cells from all the above groups. $n = 3$ for all groups. Scale bar, 40 μm *represents significant differences between groups at a level of $p < 0.001$.

TABLE 1 Histological assessments for each experimental condition.

Experimental condition	Average total cell counts	Average number of damaged cells	% Damaged cells
Sham	433	42	9.76
Sham + IDH2	450	62	13.78
Mild AKI	860	328	38.28
Mild AKI + IDH2	450	148	33.22
Moderate AKI	466	265	57.99
Moderate AKI + IDH2–1 h	463	194	42.26
Moderate AKI + IDH2–24 h–24 h	517	156	30.45

(Lü et al., 2005; Gao et al., 2019). While the underlying mechanism(s) related to these gender differences remain to be elucidated, the author believed that it was essential to conduct this study using male rats to provide a proper comparison for previous work that led to the design of this investigation.

Also, it is well known that AKI is strongly associated with damage to the proximal tubule and that the dysfunction or death of proximal tubule cells is often the main consequence of AKI (Corridon et al., 2021). Cells within this epithelium often undergo programmed cell death or necrosis depending on the severity of the injury, while in some very mild AKI cases, such cellular dysfunction is barely noticeable and reversible without intervention (Corridon et al., 2013). This investigation captured the intrinsic nature of this form of injury, as the real-time effects of cellular damage led to the effacement and loss of brush border in the proximal tubule, detachment of tubular epithelial cells from associated basement membranes, and cellular sloughing, which resulted in the formation of fluorescent casts with tubular lumens (Basile et al., 2012; Corridon et al., 2021). Besides, prerenal injury generates immediate and marked rises in the nicotinamide adenine dinucleotide (NADH) signal in tubular cells, which then decrease again upon restoration of renal blood flow and imply rapid transitions that occur in tubular cellular mitochondria activity stemming from IRI. This conversion can lead to decreased respiratory chain activity and a shift of the NADH pool into a reduced state (Hall and Molitoris, 2014), thereby adversely reducing the energy carrier capacity within the nephron.

At this stage, examining the therapeutic potential of upregulating IDH2 activity in these injury models was necessary. The impacts of such genetic alterations on renal function were evaluated using various biochemical, microscopic, and volumetric analyses. Western blot analyses confirmed enhanced expression of this crucial mitochondrial enzyme after hydrodynamic gene transfer. Likewise, before any injury, serum creatinine (SCr), blood urea nitrogen (BUN), and urine output aligned with respective typical ranges of 0.4–0.8 mg/dl[90], 15–22 mg/dL (Thammitiyagodage et al., 2020), and 10–15 mL/day (Kurien et al., 2004). Conversely, with AKI, sudden and significant spikes in SCr and BUN were observed and known to usually occur within 24 h of the inception of the injury, whereas these levels gradually returned to baseline (Zhou et al., 2006; O'Kane et al., 2018).

Remarkably, the major finding in this study is that the hydrodynamic-based mitochondrial IDH2 gene delivery led to recovery and halt of the progression of AKI by decreases in serum creatinine and blood urea nitrogen levels, and increases in urine output and mitochondrial membrane potential. In contrast, the introduction of IRI produced representative and inverse effects on urine production (Wei et al., 2019) and mitochondrial activity (Hato et al., 2018). Although the metabolic cage is commonly used for such studies, it has been recognized as constituting a unique stressor that could affect behavior and the measurements presented (Kalliokoski et al., 2013; Whittaker et al., 2016). This effect is a possible limitation of the study that can be examined in future research by comparing the results obtained in this study with conventional housed rats. Recognizing this issue and after receiving approval for such studies, the animals were checked daily by the researcher and facility staff for signs of stress, and if any adverse conditions were identified in a given animal, it would have been excluded from the study.

Recalling that mitochondrial impairment resulting from IRI represents an early step in the pathogenesis of renal injury, harnessing the therapeutic effects observed in IPC may be the key to recovery. Specifically, from a molecular perspective, mitochondrial isocitrate dehydrogenases catalyze the oxidative decarboxylation of isocitrate. These enzymes are integral to cellular mechanisms that have evolved to shield cells from oxidative damage (Zhang et al., 2013) and the unique acceleration of renal senescence due to IDH2 depletion (Lee et al., 2017). Such effects are partly mediated by preserving mitochondria function in response to IRI by preserving cellular ATP levels, reducing reactive oxygen species (ROS) production, and inhibiting cell death pathways (Jassem et al., 2002; Kolb et al., 2018). We had already shown that gene delivery of IDH2 before injury attenuated surges in serum creatinine and amplified the mitochondria membrane potential, maximal respiratory capacity, and intracellular ATP levels (Kolb et al., 2018). Furthermore, this delivery process has also been shown to improve microvascular perfusion by eliminating rouleaux to reduce peritubular capillary erythrocyte congestion and the accumulation of renal leukocytes (Collett et al., 2017). Therefore, it is reasonable to attribute comparable mechanistic responses generated by cellular pathways that supported renal recovery amidst substantial morphological damage.

5 Conclusion

Traditionally, the development of renal gene therapy has lagged other organ-directed gene therapies due to low renal gene transfer efficiencies and difficulty targeting specific kidney cell types. Nevertheless, hydrodynamic delivery appears to overcome this problem in the setting of mild and moderate acute disorders. This possibility may benefit the outcome of AKIs, characterized by sudden losses of renal function, subsequent rises in creatinine and BUN, and reductions in urine output, as current treatments are mainly supportive. It is possible to arrive at this conclusion from the data presented in this report, as this relatively simple technique could be used to generate efficient transgene expression in live renal segments, namely tubular epithelial cells, which are major sites of damage in AKI (Molitoris, 2004; Chevalier, 2016; Corridon et al., 2021). Interestingly, substantial levels of transgene expression were observed in mammalian kidneys with AKI during both the initial phase of injury and at the maximal point of damage, albeit in a limited sample size.

Based on this, it is necessary to consider the state of the cells expressing the transgenes. There is a high probability that injured, and functional cell populations would express transgenes in some undefined ratio. Naturally, it would be of interest to shift this ratio to benefit injured cells. Nevertheless, due to the nature of AKI and proximal tubule function, it would be of interest to target functional cells in an attempt to protect them from irreversible damage and foster their proliferation to compensate for terminally injured cells (Kume et al., 2012). Hence, the results presented herein may be used to further investigate the delivery of clinically relevant transgenes in an attempt to provide further therapeutic, yet transient genetic modifications in live mammalian kidneys. Such approaches can improve the current understanding of and ways to combat AKI by boosting recovery and halting progression at its inception. Although gene therapy for kidney disease remains a major challenge, new and evolving technologies may actualize treatment for AKI (Peek and Wilson, 2022). Continued and complimentary research to identify new key structural and functional genetic targets, and better examine existing ones while improving gene delivery, will further enhance the utility of genetic medicine as we aim to envision its promise.

Finally, the versatility and ease of use of the CRISPR gene editing system also suggest its potential for renal gene therapy. CRISPR has been shown to work in mammalian (including human) cells, underlining the possibility of using this technique for clinically driven gene editing and gene targeting applications (Cruz and Freedman, 2018; Aulicino et al., 2022). As with previous rodent studies, systemic delivery (*via* the tail vein) of CRISPR editing tools provided evidence of genetic variations limited to the liver (Liang et al., 2022). Thus, as with other vectors, significant challenges remain, including how to effectively deliver CRISPR to kidneys and control gene editing events within the genome (Cruz and Freedman, 2018). Future studies could be devised for the combination of retrograde renal hydrodynamic fluid delivery and CRSPR to devise preclinical models that forge its safe and efficacious translation into therapies.

Data availability statement

The original contributions presented in the study are included in the article/supplementary materials, further inquiries can be directed to the corresponding author.

Ethics statement

The experiments were performed in accordance with approved guidelines. All animal experiments were performed in accordance with the Animal Research Oversight Committee at Khalifa University, Abu Dhabi, UAE, and the Institutional Animal Care and Use Committee at Indiana University, IN, Uinted States.

Author contributions

PC conceived and designed research, performed experiments, analyzed data, interpreted results of experiments, and prepared the manuscript.

Funding

Khalifa University of Science and Technology supported this project, Grant Numbers: FSU-2020-25 and RC2-2018-022 (HEIC), and the College of Medicine and Health Sciences. Funding was also provided by an NIH P-30 O'Brien Center award (DK 079312).

Acknowledgments

The author would like to thank Ms. Raheem Khan for her support in preparing data for analysis and Mr. Abdulhamid Mustafa Abdi for reviewing the manuscript.

Conflict of interest

The authors declare that the research was conducted in the absence of any commercial or financial relationships that could be construed as a potential conflict of interest.

Publisher's note

References

Ali, H. G., Ibrahim, K., Elsaid, M. F., Mohamed, R. B., Abeidah, M. I. A., Al Rawwas, A. O., et al. (2021). Gene therapy for spinal muscular atrophy: The Qatari experience. *Gene Ther.* 28, 676–680. doi:10.1038/s41434-021-00273-7

Amiel, G. E., Yoo, J. J., and Atala, A. (2000). Renal therapy using tissue-engineered constructs and gene delivery. *World J. Urol.* 18, 71–79. doi:10.1007/s003450050013

Appledorn, D. M., Seregin, S., and Amalfitano, A. (2008). Adenovirus vectors for renal-targeted gene delivery. *Contrib. Nephrol.* 159, 47–62. doi:10.1159/000125581

Ashworth, S. L., Sandoval, R. M., Tanner, G. A., and Molitoris, B. A. (2007). Two-photon microscopy: Visualization of kidney dynamics. *Kidney Int.* 72, 416–421. doi:10.1038/sj.ki.5002315

Aulicino, F., Pelosse, M., Toelzer, C., Capin, J., Ilegems, E., Meysami, P., et al. (2022). Highly efficient CRISPR-mediated large DNA docking and multiplexed prime editing using a single baculovirus. *Nucleic Acids Res.* 50, 7783–7799. doi:10.1093/nar/gkac587

Basile, D. P., Anderson, M. D., and Sutton, T. A. (2012). Pathophysiology of acute kidney injury. *Compr. Physiol.* 2, 1303–1353. doi:10.1002/cphy.c110041

Basu, R. K., Chawla, L. S., Wheeler, D. S., and Goldstein, S. L. (2012). Renal angina: An emerging paradigm to identify children at risk for acute kidney injury. *Pediatr. Nephrol.* 27, 1067–1078. doi:10.1007/s00467-011-2024-5

Bellomo, R., Ronco, C., Kellum, J. A., Mehta, R. L., and Palevsky, P.Acute Dialysis Quality Initiative workgroup (2004). Acute renal failure - definition, outcome measures, animal models, fluid therapy and information technology needs: The second international consensus conference of the acute dialysis quality initiative (ADQI) group. *Crit. Care* 8, R204–R212. doi:10.1186/cc2872

Bonventre, J. V., and Yang, L. (2011). Cellular pathophysiology of ischemic acute kidney injury. *J. Clin. Invest.* 121, 4210–4221. doi:10.1172/JCI45161

Burek, M., Burmester, S., Salvador, E., Moller-Ehrlich, K., Schneider, R., Roewer, N., et al. (2020). Kidney ischemia/reperfusion injury induces changes in the drug transporter expression at the blood–brain barrier *in vivo* and *in vitro*. *Front. Physiology* 11, 569881. doi:10.3389/fphys.2020.569881

Burne-Taney, M. J., Yokota, N., and Rabb, H. (2005). Persistent renal and extrarenal immune changes after severe ischemic injury. *Kidney Int.* 67, 1002–1009. doi:10.1111/j.1523-1755.2005.00163.x

Cai, N., Alvin, C. K. L., Kin, L., Peter, R. C., David, J. G., Vincent, C., et al. (2022). Recent advances in fluorescence recovery after photobleaching for decoupling transport and kinetics of biomacromolecules in cellular Physiology. *Polym. (Basel)* 14, 1913. doi:10.3390/polym14091913

Cerda, J., Lameire, N., Eggers, P., Pannu, N., Uchino, S., Wang, H., et al. (2008). Epidemiology of acute kidney injury. *Clin. J. Am. Soc. Nephrol.* 3, 881–886. doi:10.2215/CJN.04961107

Chen, S., Agarwal, A., Glushakova, O. Y., Jorgensen, M. S., Salgar, S. K., Poirier, A., et al. (2003). Gene delivery in renal tubular epithelial cells using recombinant adeno-associated viral vectors. *J. Am. Soc. Nephrol.* 14, 947–958. doi:10.1097/01.asn.0000057858.45649.f7

Chevalier, R. L. (2016). The proximal tubule is the primary target of injury and progression of kidney disease: Role of the glomerulotubular junction. *Am. J. Physiol. Ren. Physiol.* 311, F145–F161. doi:10.1152/ajprenal.00164.2016

Collett, J. A., Corridon, P. R., Mehrotra, P., Kolb, A. L., Rhodes, G. J., Miller, C. A., et al. (2017). Hydrodynamic isotonic fluid delivery ameliorates moderate-to-severe ischemia-reperfusion injury in rat kidneys. *J. Am. Soc. Nephrol.* 28, 2081–2092. doi:10.1681/ASN.2016040404

Collins, M., and Thrasher, A. (2015). Gene therapy: Progress and predictions. *Proc. Biol. Sci.* 282, 20143003. doi:10.1098/rspb.2014.3003

Corridon, P. R. (2022a). Capturing effects of blood flow on the transplanted decellularized nephron with intravital microscopy. *bioRxiv*. 2021.2002.2010.430561.

Corridon, P. R. (2022b). Intravital microscopy datasets examining key nephron segments of transplanted decellularized kidneys. *Sci Data* 9, 561.

Corridon, P. R. (2021). *In vitro* investigation of the impact of pulsatile blood flow on the vascular architecture of decellularized porcine kidneys. *Sci. Rep.* 11, 16965. doi:10.1038/s41598-021-95924-5

Corridon, P. (2023). Still finding ways to augment the existing management of acute and chronic kidney diseases with targeted gene and cell therapies: Opportunities and hurdles. Preprints 2023010447. doi:10.20944/preprints202301.0447.v1

Corridon, P. R., Wang, X., Shakeel, A., and Chan, V. (2022). Digital technologies: Advancing individualized treatments through gene and cell therapies, pharmacogenetics, and disease detection and diagnostics. *Biomedicines* 10 (10), 2445.

Corridon, P. R., Karam, S. H., Khraibi, A. A., Khan, A. A., and Alhashmi, M. A. (2021). Intravital imaging of real-time endogenous actin dysregulation in proximal and distal tubules at the onset of severe ischemia-reperfusion injury. *Sci. Rep.* 11, 8280. doi:10.1038/s41598-021-87807-6

Corridon, P. R., Ko, I. K., Yoo, J. J., and Atala, A. (2017). Bioartificial kidneys. *Curr. Stem Cell Rep.* 3, 68–76. doi:10.1007/s40778-017-0079-3

Corridon, P. R., Rhodes, G. J., Leonard, E. C., Basile, D. P., Gattone, V. H., Bacallao, R. L., et al. (2013). A method to facilitate and monitor expression of exogenous genes in the rat kidney using plasmid and viral vectors. *Am. J. Physiol. Ren. Physiol.* 304, F1217–F1229. doi:10.1152/ajprenal.00070.2013

Corridon, P., Ascázubi, R., Krest, C., and Wilke, I. (2006). "Time-domain terahertz spectroscopy of artificial skin," in Advanced Biomedical and Clinical Diagnostic Systems IV Proc. SPIE 6080, 608007.

Cruz, N. M., and Freedman, B. S. (2018). CRISPR gene editing in the kidney. *Am. J. Kidney Dis.* 71, 874–883. doi:10.1053/j.ajkd.2018.02.347

Dai, C., Yang, J., and Liu, Y. (2002). Single injection of naked plasmid encoding hepatocyte growth factor prevents cell death and ameliorates acute renal failure in mice. *J. Am. Soc. Nephrol.* 13, 411–422. doi:10.1681/ASN.V132411

Davis, L., and Park, F. (2019). Gene therapy research for kidney diseases. *Physiol. Genomics* 51, 449–461. doi:10.1152/physiolgenomics.00052.2019

Davidovic, L. M., Cumic, J., Dugalic, S., Vicentic, S., Sevarac, Z., Petroianu, G., et al. (2022). Gray-level co-occurrence matrix analysis for the detection of discrete, ethanol-induced, structural changes in cell nuclei: An artificial intelligence approach. *Microsc. Microanal.* 28, 265–271.

DeYoung, M. B., and Dichek, D. A. (1998). Gene therapy for restenosis: Are we ready? *Circ. Res.* 82, 306–313. doi:10.1161/01.res.82.3.306

Dunn, K. W., Sandoval, R. M., and Molitoris, B. A. (2003). Intravital imaging of the kidney using multiparameter multiphoton microscopy. *Nephron Exp. Nephrol.* 94, e7–e11. doi:10.1159/000070813

Dunn, K. W., Sutton, T. A., and Sandoval, R. M. (2007). Live-animal imaging of renal function by multiphoton microscopy. *Curr. Protoc. Cytom.* Chapter 12, Unit12 19, 12.9.1–12.9.25. doi:10.1002/0471142956.cy1209s41

Engel, J. E., Williams, E., Williams, M. L., Bidwell, G. L., 3rd, and Chade, A. R. (2019). Targeted VEGF (vascular endothelial growth factor) therapy induces long-term renal recovery in chronic kidney disease via macrophage polarization. *Hypertension* 74, 1113–1123. doi:10.1161/HYPERTENSIONAHA.119.13469

Ferguson, M. A., Vaidya, V. S., and Bonventre, J. V. (2008). Biomarkers of nephrotoxic acute kidney injury. *Toxicology* 245, 182–193. doi:10.1016/j.tox.2007.12.024

Friedmann, T., and Roblin, R. (1972). Gene therapy for human genetic disease? *Science* 175, 949–955. doi:10.1126/science.175.4025.949

Gao, L., Zhong, X., Jin, J., Li, J., and Meng, X.-M. (2020). Potential targeted therapy and diagnosis based on novel insight into growth factors, receptors, and downstream effectors in acute kidney injury and acute kidney injury-chronic kidney disease progression. *Signal Transduct. Target. Ther.* 5, 9. doi:10.1038/s41392-020-0106-1

Gao, Z., Chen, Z., Sun, A., and Deng, X. (2019). Gender differences in cardiovascular disease. *Med. Nov. Technol. Devices* 4, 100025. doi:10.1016/j.medntd.2019.100025

Hall, A. M., and Molitoris, B. A. (2014). Dynamic multiphoton microscopy: Focusing light on acute kidney injury. *Physiol. (Bethesda)* 29, 334–342. doi:10.1152/physiol.00010.2014

Hall, A. M., Rhodes, G. J., Sandoval, R. M., Corridon, P. R., and Molitoris, B. A. (2013). *In vivo* multiphoton imaging of mitochondrial structure and function during acute kidney injury. *Kidney Int.* 83, 72–83. doi:10.1038/ki.2012.328

Hall, A. M., Unwin, R. J., Parker, N., and Duchen, M. R. (2009). Multiphoton imaging reveals differences in mitochondrial function between nephron segments. *J. Am. Soc. Nephrol.* 20, 1293–1302. doi:10.1681/ASN.2008070759

Hato, T., Winfree, S., and Dagher, P. C. (2018). Kidney imaging: Intravital microscopy. *Methods Mol. Biol.* 1763, 129–136. doi:10.1007/978-1-4939-7762-8_12

Hayat, S. M. G., Farahani, N., Safdarian, E., Roointan, A., and Sahebkar, A. (2019). Gene delivery using lipoplexes and polyplexes: Principles, limitations and solutions. *Crit. Rev. Eukaryot. Gene Expr.* 29, 29–36. doi:10.1615/CritRevEukaryotGeneExpr.2018025132

Herweijer, H., and Wolff, J. A. (2007). Gene therapy progress and prospects: Hydrodynamic gene delivery. *Gene Ther.* 14, 99–107. doi:10.1038/sj.gt.3302891

Himmelfarb, J., Joannidis, M., Molitoris, B., Schietz, M., Okusa, M. D., Warnock, D., et al. (2008). Evaluation and initial management of acute kidney injury. *Clin. J. Am. Soc. Nephrol.* 3, 962–967. doi:10.2215/CJN.04971107

Hingorani, S., Molitoris, B. A., and Himmelfarb, J. (2009). Ironing out the pathogenesis of acute kidney injury. *Am. J. Kidney Dis.* 53, 569–571. doi:10.1053/j.ajkd.2009.01.002

Hitchman, E., Hitchman, R. B., and King, L. A. (2017). BacMam delivery of a protective gene to reduce renal ischemia-reperfusion injury. *Hum. Gene Ther.* 28, 747–756. doi:10.1089/hum.2016.100

Holderied, A., Kraft, F., Marschner, J. A., Weidenbusch, M., and Anders, H. J. (2020). Point of no return" in unilateral renal ischemia reperfusion injury in mice. *J. Biomed. Sci.* 27, 34. doi:10.1186/s12929-020-0623-9

Humes, H. D., MacKay, S. M., Funke, A. J., and Buffington, D. A. (1997). Acute renal failure: Growth factors, cell therapy, and gene therapy. *Proc. Assoc. Am. Physicians* 109, 547–557.

Imai, E. (2003). Gene therapy for renal diseases: Its potential and limitation. *J. Am. Soc. Nephrol.* 14, 1102–1104. doi:10.1097/01.asn.0000067655.48829.d5

Ishida, T., Yarimizu, K., Gute, D. C., and Korthuis, R. J. (1997). Mechanisms of ischemic preconditioning. *Shock* 8, 86–94. doi:10.1097/00024382-199708000-00003

Jassem, W., Fuggle, S. V., Rela, M., Koo, D. D., and Heaton, N. D. (2002). The role of mitochondria in ischemia/reperfusion injury. *Transplantation* 73, 493–499. doi:10.1097/00007890-200202270-00001

Kalliokoski, O., Jacobsen, K. R., Darusman, H. S., Henriksen, T., Weimann, A., Poulsen, H. E., et al. (2013). Mice do not habituate to metabolism cage housing--a three week study of male BALB/c mice. *PLoS One* 8, e58460. doi:10.1371/journal.pone.0058460

Kay, M. A., Glorioso, J. C., and Naldini, L. (2001). Viral vectors for gene therapy: The art of turning infectious agents into vehicles of therapeutics. *Nat. Med.* 7, 33–40. doi:10.1038/83324

Kelley, V. R., and Sukhatme, V. P. (1999). Gene transfer in the kidney. *Am. J. Physiol.* 276, F1–F9. doi:10.1152/ajprenal.1999.276.1.F1

Khan, R. L., Khraibi, A. A., Dumée, L. F., and Corridon, P. R. (2023). From waste to wealth: Repurposing slaughterhouse waste for xenotransplantation. *Front. Bioeng. Biotechnol.*, 11.

Kinsey, G. R., and Okusa, M. D. (2011). Pathogenesis of acute kidney injury: Foundation for clinical practice. *Am. J. Kidney Dis.* 58, 291–301. doi:10.1053/j.ajkd.2011.02.385

Kinsey, G. R., and Okusa, M. D. (2011). Pathogenesis of acute kidney injury: Foundation for clinical practice. *Am. J. Kidney Dis. Official J. Natl. Kidney Found.* 58, 291–301. doi:10.1053/j.ajkd.2011.02.385

Kolb, A. L., Corridon, P. R., Zhang, S., Xu, W., Witzmann, F. A., Collett, J. A., et al. (2018). Exogenous gene transmission of isocitrate dehydrogenase 2 mimics ischemic preconditioning protection. *J. Am. Soc. Nephrol.* 29, 1154–1164. doi:10.1681/ASN.2017060675

Kume, S., Thomas, M. C., and Koya, D. (2012). Nutrient sensing, autophagy, and diabetic nephropathy. *Diabetes* 61, 23–29. doi:10.2337/db11-0555

Kurien, B. T., Everds, N. E., and Scofield, R. H. (2004). Experimental animal urine collection: A review. *Lab. Anim.* 38, 333–361. doi:10.1258/0023677041958945

Lattanzio, M. R., and Kopyt, N. P. (2009). Acute kidney injury: New concepts in definition, diagnosis, pathophysiology, and treatment. *J. Am. Osteopath Assoc.* 109, 13–19.

Le Clef, N., Verhulst, A., D'Haese, P. C., and Vervaet, B. A. (2016). Unilateral renal ischemia-reperfusion as a robust model for acute to chronic kidney injury in mice. *PLoS One* 11, e0152153. doi:10.1371/journal.pone.0152153

Lee, D. S., Yang, S. H., Kim, H. L., Joo, K. W., Lim, C. S., Chae, D. W., et al. (2004). Recombinant uteroglobin prevents the experimental crescentic glomerulonephritis. *Kidney Int.* 66, 1061–1067. doi:10.1111/j.1523-1755.2004.00855.x

Lee, S. J., Cha, H., Lee, S., Kim, H., Ku, H. J., Kim, S. H., et al. (2017). Idh2 deficiency accelerates renal dysfunction in aged mice. *Biochem. Biophysical Res. Commun.* 493, 34–39. doi:10.1016/j.bbrc.2017.09.082

Leonard, E. C., Friedrich, J. L., and Basile, D. P. (2008). VEGF-121 preserves renal microvessel structure and ameliorates secondary renal disease following acute kidney injury. *Am. J. Physiol. Ren. Physiol.* 295, F1648–F1657. doi:10.1152/ajprenal.00099.2008

Leroy, B. P., Fischer, M. D., Flannery, J. G., MacLaren, R. E., Dalkara, D., Scholl, H. P. N., et al. (2022). Gene therapy for inherited retinal disease: Long-term durability of effect. *Ophthalmic Res.* 179–196 doi:10.1159/000526317

Liang, H., Xu, F., Zhang, T., Huang, J., Guan, Q., Wang, H., et al. (2018). Inhibition of IL-18 reduces renal fibrosis after ischemia-reperfusion. *Biomed. Pharmacother.* 106, 879–889. doi:10.1016/j.biopha.2018.07.031

Liang, S.-Q., Liu, P., Smith, J. L., Mintzer, E., Maitland, S., Dong, X., et al. (2022). Genome-wide detection of CRISPR editing *in vivo* using GUIDE-tag. *Nat. Commun.* 13, 437. doi:10.1038/s41467-022-28135-9

Lien, Y. H., and Lai, L. W. (1997). Gene therapy for renal diseases. *Kidney Int.* 61, S85–S88.

Liu, F., Song, Y. K., and Liu, D. (1999). Hydrodynamics-based transfection in animals by systemic administration of plasmid DNA. *Gene Ther.* 6, 1258–1266. doi:10.1038/sj.gt.3300947

Lü, P., Liu, F., Wang, C. Y., Chen, D. D., Yao, Z., Tian, Y., et al. (2005). Gender differences in hepatic ischemic reperfusion injury in rats are associated with endothelial cell nitric oxide synthase-derived nitric oxide. *World J. Gastroenterol.* 11, 3441–3445. doi:10.3748/wjg.v11.i22.3441

Miyazaki, M., Yamashita, T., Miyazaki, T., Taira, H., and Suzuki, A. (2009). Gene delivery to renal tubular epithelial cells using adeno-associated virus vector in domestic cats. *Res. Vet. Sci.* 87, 408–412. doi:10.1016/j.rvsc.2009.03.016

Mizui, M., Isaka, Y., Takabatake, Y., Mizuno, S., Nakamura, T., Ito, T., et al. (2004). Electroporation-mediated HGF gene transfer ameliorated cyclosporine nephrotoxicity. *Kidney Int.* 65, 2041–2053. doi:10.1111/j.1523-1755.2004.00625.x

Molitoris, B. A. (2004). Actin cytoskeleton in ischemic acute renal failure. *Kidney Int.* 66, 871–883. doi:10.1111/j.1523-1755.2004.00818.x

Molitoris, B. A., Dagher, P. C., Sandoval, R. M., Campos, S. B., Ashush, H., Fridman, E., et al. (2009). siRNA targeted to p53 attenuates ischemic and cisplatin-induced acute kidney injury. *J. Am. Soc. Nephrol.* 20, 1754–1764. doi:10.1681/ASN.2008111204

Molitoris, B. A., and Sandoval, R. M. (2005). Intravital multiphoton microscopy of dynamic renal processes. *Am. J. Physiol. Ren. Physiol.* 288, F1084–F1089. doi:10.1152/ajprenal.00473.2004

Murry, C. E., Jennings, R. B., and Reimer, K. A. (1986). Preconditioning with ischemia: A delay of lethal cell injury in ischemic myocardium. *Circulation* 74, 1124–1136. doi:10.1161/01.cir.74.5.1124

Nagase, M., Aisawa, T., Honda, N., and Nihei, H. (1977). Renal pathophysiology of hemorrhagic hypotension, acute ischemic renal failure, and obstructive nephropathy (author's transl). *Nihon Jinzo Gakkai shi* 19, 254–261.

Niidome, T., and Huang, L. (2002). Gene therapy progress and prospects: Nonviral vectors. *Gene Ther.* 9, 1647–1652. doi:10.1038/sj.gt.3301923

Nishi, S., Yamamoto, C., Yoneda, S., and Sueda, S. (2017). Labeling of cytoskeletal proteins in living cells using biotin ligase carrying a fluorescent protein. *Anal. Sci.* 33, 897–902. doi:10.2116/analsci.33.897

Nogrady, B. (2018). Genetically modified T cells target lymphoma. *Nature* 563, S42–S43. doi:10.1038/d41586-018-07361-6

O'Kane, D., Gibson, L., May, C. N., du Plessis, J., Shulkes, A., Baldwin, G. S., et al. (2018). Zinc preconditioning protects against renal ischaemia reperfusion injury in a preclinical sheep large animal model. *BioMetals* 31, 821–834. doi:10.1007/s10534-018-0125-3

Palevsky, P. M., Zhang, J. H., O'Connor, T. Z., Chertow, G. M., Crowley, S. T., Choudhury, D., et al. (2008). Intensity of renal support in critically ill patients with acute kidney injury. *N. Engl. J. Med.* 359, 7–20. doi:10.1056/NEJMoa0802639

Pantic, I., Cumic, J., Dugalic, S., and Petroianu, G. A. (2022a). Gray level co-occurrence matrix and wavelet analyses reveal discrete changes in proximal tubule cell nuclei after mild acute kidney injury. *Res. Sq.* Preprint. doi:10.21203/rs.3.rs-1762202/v1

Pantic, I. V., Shakeel, A., Petroianu, G. A., and Corridon, P. R. (2022b). Analysis of vascular architecture and parenchymal damage generated by reduced blood perfusion in decellularized porcine kidneys using a gray level Co-occurrence matrix. *Front. Cardiovasc. Med.* 9, 797283. doi:10.3389/fcvm.2022.797283

Pantic, I., Cumic, J., Valjarevic, S., Shakeel, A., Wang, X., Vurivi, H., et al. (2023a). Computational approaches for evaluating morphological changes in the corneal stroma associated with decellularizationComputational approaches for evaluating morphological

changes in the corneal stroma associated with decellularization. *Res. Sq.* Preprint. doi:10.21203/rs.3.rs-2480023/v1

Pantic, I., Paunovic, J., Cumic, J., Valjarevic, S., Petroianu, G. A., and Corridon, P. R. (2023b). Artificial neural networks in contemporary toxicology research. *Chem. Biol. Interact.* 369, 110269.

Peek, J. L., and Wilson, M. H. (2022). Gene therapy for kidney disease: Targeting cystinuria. *Curr. Opin. Nephrol. Hypertens.* 31, 175–179. doi:10.1097/MNH.0000000000000768

Rostami, Z., Mastrangelo, G., Einollahi, B., Nemati, E., Shafiee, S., Ebrahimi, M., et al. (2022). A prospective study on risk factors for acute kidney injury and all-cause mortality in hospitalized COVID-19 patients from tehran (Iran). *Front. Immunol.* 13, 874426. doi:10.3389/fimmu.2022.874426

Rubin, J. D., and Barry, M. A. (2020). Improving molecular therapy in the kidney. *Mol. Diagn Ther.* 24, 375–396. doi:10.1007/s40291-020-00467-6

Rubin, J. D., Nguyen, T. V., Allen, K. L., Ayasoufi, K., and Barry, M. A. (2019). Comparison of gene delivery to the kidney by adenovirus, adeno-associated virus, and lentiviral vectors after intravenous and direct kidney injections. *Hum. Gene Ther.* 30, 1559–1571. doi:10.1089/hum.2019.127

Sandovici, M., Deelman, L. E., van Goor, H., Helfrich, W., de Zeeuw, D., and Henning, R. H. (2007). Adenovirus-mediated interleukin-13 gene therapy attenuates acute kidney allograft injury. *J. Gene Med.* 9, 1024–1032. doi:10.1002/jgm.1106

Shakeel, A., and Corridon, P. R. (2023). Mitigating challenges and expanding the future of vascular tissue engineering–are we there yet? *Front. Physiol.* 13, 1079421.

Shaya, J., Corridon, P. R., Al-Omari, B., Aoudi, A., Shunnar, A., Mohideen, M. I. H., et al. (2022). Design, photophysical properties, and applications of fluorene-based fluorophores in two-photon fluorescence bioimaging: A review. *J. Photochem. Photobiol. C Photochem. Rev.* 52, 100529. doi:10.1016/j.jphotochemrev.2022.100529

Shen, X., Xu, Y., Bai, Z., Ma, D., Niu, Q., Meng, J., et al. (2018). Transparenchymal renal pelvis injection of recombinant adeno-associated virus serotype 9 vectors is a practical approach for gene delivery in the kidney. *Hum. Gene Ther. Methods* 29, 251–258. doi:10.1089/hgtb.2018.148

Suda, T., and Liu, D. (2007). Hydrodynamic gene delivery: Its principles and applications. *Mol. Ther.* 15, 2063–2069. doi:10.1038/sj.mt.6300314

Tanner, G. A., Sandoval, R. M., Molitoris, B. A., Bamburg, J. R., and Ashworth, S. L. (2005). Micropuncture gene delivery and intravital two-photon visualization of protein expression in rat kidney. *Am. J. Physiol. Ren. Physiol.* 289, F638–F643. doi:10.1152/ajprenal.00059.2005

Thadhani, R., Pascual, M., and Bonventre, J. V. (1996). Acute renal failure. *N. Engl. J. Med.* 334, 1448–1460. doi:10.1056/NEJM199605303342207

Thammitiyagodage, M. G., de Silva, N. R., Rathnayake, C., KaRunakaRan, R., Wgss, K., Gunatillka, M. M., et al. (2020). Biochemical and histopathological changes in Wistar rats after consumption of boiled and un-boiled water from high and low disease prevalent areas for chronic kidney disease of unknown etiology (CKDu) in north Central Province (NCP) and its comparison with low disease prevalent Colombo, Sri Lanka. *BMC Nephrol.* 21, 38. doi:10.1186/s12882-020-1693-3

Torras, J., Cruzado, J. M., Herrero-Fresneda, I., and Grinyo, J. M. (2008). Gene therapy for acute renal failure. *Contrib. Nephrol.* 159, 96–108. doi:10.1159/000125614

Tros de Ilarduya, C., Sun, Y., and Düzgüneş, N. (2010). Gene delivery by lipoplexes and polyplexes. *Eur. J. Pharm. Sci.* 40, 159–170. doi:10.1016/j.ejps.2010.03.019

Vavrincova-Yaghi, D., Deelman, L. E., Goor, H., Seelen, M., Kema, I. P., Smit-van Oosten, A., et al. (2011). Gene therapy with adenovirus-delivered indoleamine 2,3-dioxygenase improves renal function and morphology following allogeneic kidney transplantation in rat. *J. Gene Med.* 13, 373–381. doi:10.1002/jgm.1584

Vormann, M. K., Tool, L. M., Ohbuchi, M., Gijzen, L., van Vught, R., Hankemeier, T., et al. (2022). Modelling and prevention of acute kidney injury through ischemia and reperfusion in a combined human renal proximal tubule/blood vessel-on-a-chip. *Kidney360* 3, 217–231. doi:10.34067/KID.0003622021

Wagner, M. C., Rhodes, G., Wang, E., Pruthi, V., Arif, E., Saleem, M. A., et al. (2008). Ischemic injury to kidney induces glomerular podocyte effacement and dissociation of slit diaphragm proteins Neph1 and ZO-1. *J. Biol. Chem.* 283, 35579–35589. doi:10.1074/jbc.M805507200

Wang, G., Zabner, J., Deering, C., Launspach, J., Shao, J., Bodner, M., et al. (2000). Increasing epithelial junction permeability enhances gene transfer to airway epithelia *in vivo*. *Am. J. Respir. Cell Mol. Biol.* 22, 129–138. doi:10.1165/ajrcmb.22.2.3938

Wang, J., Long, Q., Zhang, W., and Chen, N. (2012). Protective effects of exogenous interleukin 18-binding protein in a rat model of acute renal ischemia-reperfusion injury. *Shock* 37, 333–340. doi:10.1097/SHK.0b013e318240bdc8

Wang, X., Chan, V., and Corridon, P. R. (2022a). Acellular tissue-engineered vascular grafts from polymers: Methods, achievements, characterization, and challenges. *Polymers (Basel)* 14, 4285.

Wang, X., Chan, V., and Corridon, P. R. (2022b). Decellularized blood vessel development: Current state-of-the-art and future directions. *Front. Bioeng. Biotechnol.* 10, 951644.

Wang, X., Shakeel, A., Salih, A. E., Vurivi, H., Dauod, S., Desidery, L., et al. (2023). A scalable corneal xenograft platform: Simultaneous opportunities for tissue engineering and circular economic sustainability by repurposing slaughterhouse waste. *Res. Sq.* Preprint. doi:10.21203/rs.3.rs2480068/v1

Wei, J., Wang, Y., Zhang, J., Wang, L., Fu, L., Cha, B. J., et al. (2019). A mouse model of renal ischemia-reperfusion injury solely induced by cold ischemia. *Am. J. Physiol. Ren. Physiol.* 317, F616–F622. doi:10.1152/ajprenal.00533.2018

Whittaker, A. L., Lymn, K. A., and Howarth, G. S. (2016). Effects of metabolic cage housing on rat behavior and performance in the social interaction test. *J. Appl. Anim. Welf. Sci.* 19, 363–374. doi:10.1080/10888705.2016.1164048

Xing, Y., Pua, E. C., Lu, X., and Zhong, P. (2009). Low-amplitude ultrasound enhances hydrodynamic-based gene delivery to rat kidney. *Biochem. Biophys. Res. Commun.* 386, 217–222. doi:10.1016/j.bbrc.2009.06.020

Yazawa, K., Isaka, Y., Takahara, S., Imai, E., Ichimaru, N., Shi, Y., et al. (2004). Direct transfer of hepatocyte growth factor gene into kidney suppresses cyclosporin A nephrotoxicity in rats. *Nephrol. Dial. Transpl.* 19, 812–816. doi:10.1093/ndt/gfh064

Zhang, G., Han, H., Zhuge, Z., Dong, F., Jiang, S., Wang, W., et al. (2021). Renovascular effects of inorganic nitrate following ischemia-reperfusion of the kidney. *Redox Biol.* 39, 101836. doi:10.1016/j.redox.2020.101836

Zhang, Y., and Rowley, J. D. (2013). "Chapter 75 - leukemias, lymphomas, and other related disorders," in *Emery and rimoin's principles and practice of medical genetics*. Editors D. Rimoin, R. Pyeritz, and B. Korf Sixth Edition (Oxford: Academic Press), 1–44.

Zhou, H., PisiTkun, T., Aponte, A., Yuen, P. S. T., Hoffert, J. D., Yasuda, H., et al. (2006). Exosomal fetuin-A identified by proteomics: A novel urinary biomarker for detecting acute kidney injury. *Kidney Int.* 70, 1847–1857. doi:10.1038/sj.ki.5001874

Frontiers in Physiology

Understanding how an organism's components work together to maintain a healthy state

The second most-cited physiology journal, promoting a multidisciplinary approach to the physiology of living systems - from the subcellular and molecular domains to the intact organism and its interaction with the environment.

Discover the latest Research Topics

See more →

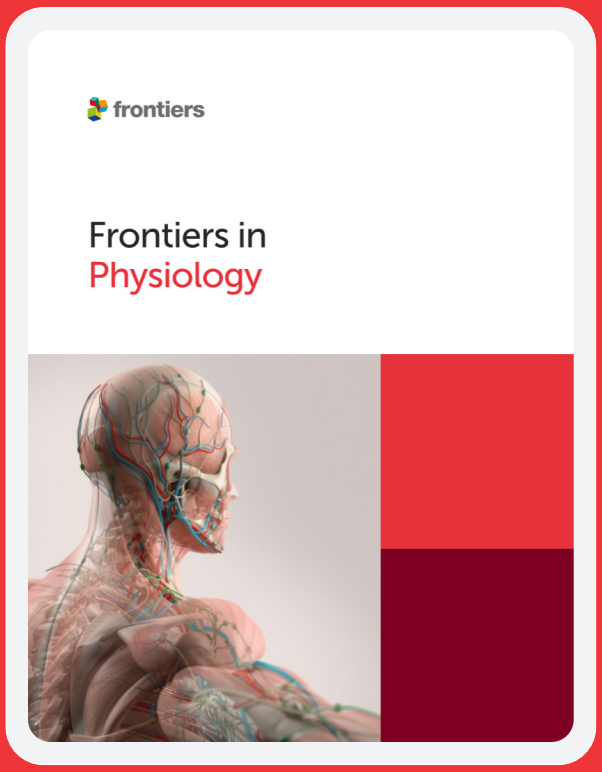

Frontiers

Avenue du Tribunal-Fédéral 34
1005 Lausanne, Switzerland
frontiersin.org

Contact us

+41 (0)21 510 17 00
frontiersin.org/about/contact